Title

Exploring Polymer and Liposomal Carriers for Optimized Drug Delivery

Permalink

https://escholarship.org/uc/item/2qm497bh

Author

Ferguson, Heidi M

Publication Date

2012

Exploring Polymer and Liposomal Carriers for Optimized Drug Delivery

by

Heidi M. Kieler-Ferguson

A dissertation submitted in partial satisfaction of the

requirements for the degree of

Doctor of Philosophy

in

Chemistry

in the

Graduate Division

of the

University of California, Berkeley

Committee in charge:

Professor Jean M. J. Fréchet, Chair

Professor Matthew B. Francis

Professor Jhih-Wei Chu

Fall 2012

Exploring Polymer and Liposomal Carriers for Optimized Drug Delivery

Copyright 2012

by

Heidi M. Kieler-Ferguson

Abstract

Exploring Polymer and Liposomal Carriers for Optimized Drug Delivery

by

Heidi M. Kieler-Ferguson

Doctor of Philosophy in Chemistry

University of California, Berkeley

Professor Jean M. J. Fréchet, Chair

The efficacy of chemotherapy drugs is often hampered by poor molecule properties, such as solubility, rapid excretion, indiscriminate toxicity, and lack of targeting to tumor tissue. Macromolecular carriers have been explored for their potential to modulate drug pharmacokinetics and increase tumor uptake through passive targeting. In this work, I examined the design of delivery systems to optimize the delivery of chemotherapeutics. An introduction to polymer and liposomal drug delivery vehicles is presented in Chapter 1. The benefits and challenges with each delivery scaffold, as opposed to conventional chemotherapies, are discussed. The remainder of the chapter will focus on camptothecin and platinum (II) drug delivery in the context of combination therapies and controlled release.

In Chapter 2, the design of camptothecin pro-drugs for pH sensitive release through a hydrazone bond is explored. I describe the synthesis of a poly-lysine dendrimer, to which camptothecin is conjugated. The synthesis of a new, more synthetically accessible PEGylated ester amide dendrimer is presented. The dendrimer was appended with both camptothecin and doxorubicin to investigate drug synergy for a dual-drug delivery system.

In Chapters 3 and 4, polymer Pt (II) drug delivery is explored in collaboration with Dr. Derek van der Poll. A PEGylated ester amide dendrimer is modified with a variety of amino acid inspired chelators to study how platinum release is correlated with cytotoxicity and efficacy. Both a fast and slow releasing chelator were evaluated *in vivo*. Next, a series of ketone containing bidentate Pt (II) drugs were synthesized. Increasingly cytotoxic complexes could be designed by cross coupling additional aromatic ligands, exploring electronic considerations, and modifying platinum ring sizes. Although Pt content was substantially increased in tumors, this did not translate to increased efficacy in the C26 murine colon carcinoma tumor model.

Chapter 5, in collaboration with Aditya Kohli and Darren Chan, presents an introduction to the utility of sterol modified lipids (SML). The bilayer properties of liposomes composed of SMLs were characterized using fluorescence anisotropy measurements and content release assays. The influence of the acyl chain length in the SML on contents release is discussed. A

pharmacokinetic study indicated that changes in the SML used to form the liposome controlled the release of the liposome contents but did not influence the circulation time of the liposome. This finding highlights one of the advantages of the SMLs for creating a circulating reservoir of drug which could be advantages for tumor targeting.

In Chapter 6, liposomes composed of SMLs or traditional lipids are prepared to control the release of cisplatin over a range of release rates. I investigated a variety of procedures for encapsulating cisplatin in the liposome and selected the ethanol loading procedure as the best one to obtain good Pt encapsulation with retention of activity. These were used to test the hypothesis that liposomal cisplatin formulations with an intermediate release rate would have improved anti-tumor properties compared to liposomes with slow release rates; however non-leaky formulations had a better anti-tumor efficacy. In an attempt to understand why this was the case, I measured both the distribution of platinum in the tumor using X-ray fluorescence spectroscopy as well as the formation of Pt-DNA adducts in the tumor for free and liposomal cisplatin. All formulations had substantially more Pt in the tumors and a greater amount of Pt-DNA adducts formed than the free cisplatin. Thus, the reason for why liposomal cisplatin formulations do not provide a substantially better anti-tumor effect than the free compound remains elusive.

Table of Contents

Acknowledgments

I would like to take the opportunity to thank all of the people who have made this work possible. First, I would like to thank Professor Fréchet for his mentorship, discernment, and desire to create strong, independent scientists. Secondly, I would like to thank Professor Szoka for his mentorship and for giving me the opportunity to explore a new facet of drug delivery. I do not think any other groups could have given me the breadth of opportunities I experienced.

I would like to thank all of the excellent scientists I have had the pleasure of working with during my time here, especially the drug delivery and particle teams. In particular, I appreciate Steve Guillaudeu's mentorship my first year, as well as Megan Fox teaching me everything I know about cells and mice. Derek van der Poll has been an amazing collaborator and I will miss working with him. Tripp Floyd, dragon slayer extraordinaire, not only made every day fun but could be counted on to think outside the box. Piper Klemm always gave me a fresh perspective on science and reminded me to never forget my goals. Getting to work in the Szoka lab has been a wonderful experience and I value all of the knowledge that has been shared with me. I could not have done any of the *in vivo* experiments without the expertise of our technicians Katherine Jerger and Darren Chan. Charles Noble and Mark Hayes of ZoneOnePharma are excellent liposome scientists and I appreciate the help they gave me with my many liposome challenges. Last but not least, thanks to my classmates John Weinstein, Jessica Wood, and Leah Witus for our friendship both in and out of lab.

I would like to thank Dr. McGaff for encouraging me to dream big and making my undergraduate research a truly enjoyable experience. I will always carry with me fond memories of Elvis Costello, new crystal structures on the door, old coffee cups in lab, and great discussions about everything under the sun.

I would like to thank my parents for all of their love and support. You both have made me the person I am today. And to my best friend and sister Ashley, for being my creative partner in crime.

And last, but certainly not least, my husband Jeff for your support, patience, love, advice, and endless late night trips to lab.

Chapter 1
Introduction to Dendrimer and Liposome Delivery

ABSTRACT

For the past 40 years, liposomal and polymeric delivery vehicles have been studied as systems capable of controlling the cytotoxicity of small molecule chemotherapeutics, increasing survival times, and improving drug targeting. Although a number of macromolecular-drug conjugates have progressed to clinical trials, tuning drug release to maintain efficacy in conjunction with controlling drug toxicity has prevented the adoption of many vehicles. In this chapter, the motivations for and approaches to PEGylated dendrimer and liposomal delivery with regards to camptothecin and cisplatin delivery are discussed.

INTRODUCTION
Limitations of Small Molecule Chemotherapeutics

The efficacy of chemotherapeutics is often attenuated by drawbacks such as poor solubility, bioavailability, and indiscriminant toxicity. Once injected, small molecule drugs pass through the liver and undergo metabolism by Cytochrome P450 and other enzymes.[1] This first-pass metabolism often targets important moieties installed for target specificity and solubility, rendering drugs inactive or with modified toxicity and bioavailability profiles. With half-lives on the order of minutes, drugs are rapidly excreted from the body, thus requiring large doses and lengthy infusion to overcome solubility challenges. Organs responsible for drug clearance are easily damaged; for example, cisplatin causes severe nephrotoxicity (kidney toxicity)[2] and camptothecin regains activity in the acidic environment of the bladder to induce toxicity.[3] Likewise, other cells in active growth such as bone marrow and digestive tissues are affected, causing most of the side effects associated with chemotherapy. In general, changing salt forms or formulation conditions as well as synthetic modifications to the drug can address these challenges; however, some drugs can incur additional toxicities or diminished activity.[4,5]

Alternatively, delivery platforms such as polymers, liposomes, and nanoparticles are being explored as effective methods to modulate drug activity.[6–10] Macromolecular carriers shuttle drugs to the site of action, thereby limiting metabolism and toxicity. Carriers should possess a number of favorable features including water solubility, lack of toxicity and immunogenicity, long circulation times with half-lives ranging from hours to days, the capacity for high drug loading, and ideally the potential to degrade into non-toxic components. Because the pharmacokinetics of the drug are dictated by the carrier, important factors such as drug release rates and blood circulation time can be modulated by changes to the delivery system. Furthermore, there is the potential for significantly higher tumor accumulation as compared to the small molecule drug due to the passive targeting phenomenon known as the Enhanced Permeation and Retention (EPR) effect.[11] The rapid growth and high nutritional demands of tumor tissue result in poorly formed vasculature with loose junctions between the endothelial cells near the tumor, and little to no lymphatic system (Figure 1.1). Macromolecules in the blood stream can more easily access the interstitial space in tumor tissue and accumulate due to the lack of lymphatic drainage. Normal tissue contains tight junctions between the blood capillary cells, preventing macromolecules but not small molecules from entering normal tissue. The distribution of small molecules throughout the body leads to poor tumor targeting and systemic toxicities.
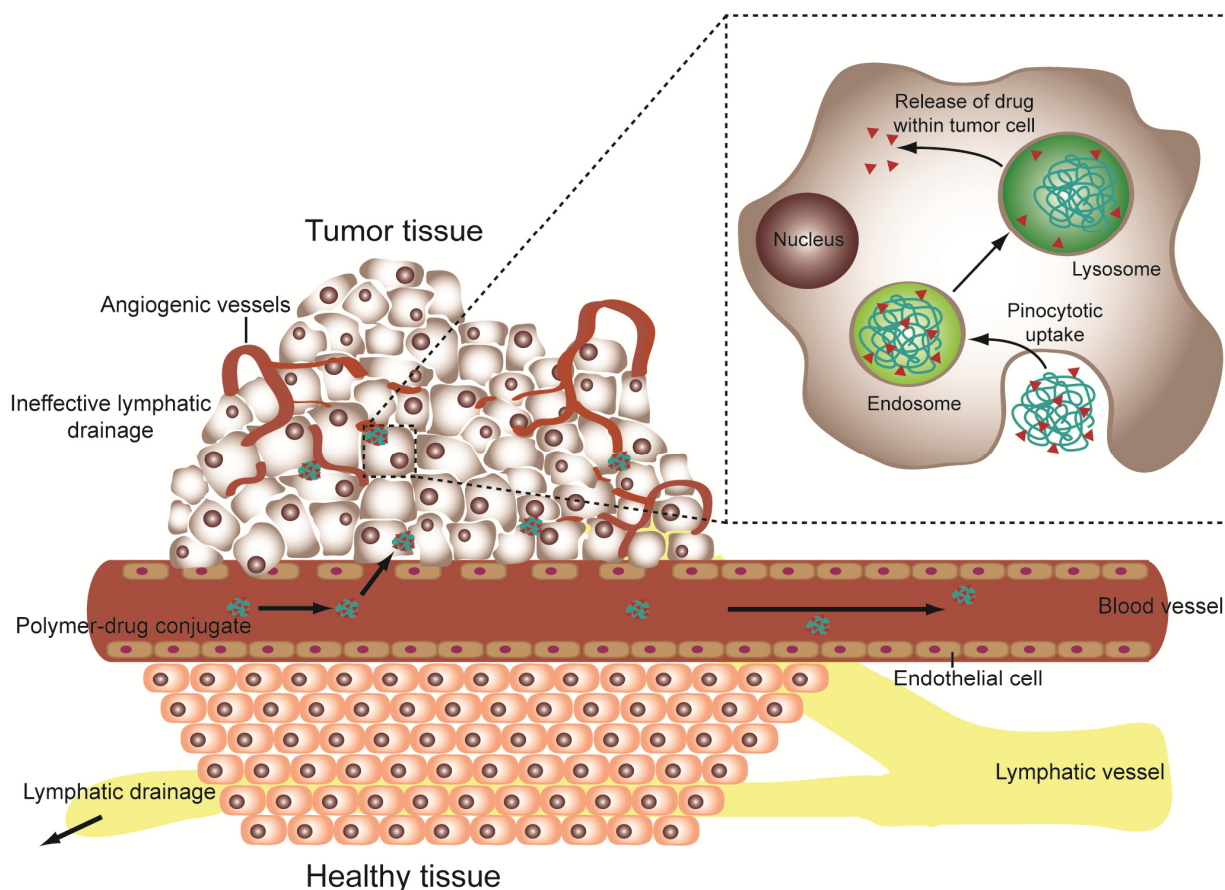
Figure 1.1. Increased uptake of macromolecular carriers in tumor tissue as compared to healthy tissue due to the EPR effect. Adapted from reference 10.

Macromolecular delivery

In this thesis, one focus is on the application of polymers, specifically PEGylated dendrimers, for drug delivery. Dendrimers are synthesized in a strict, stepwise approach which precisely controls the number of branches, giving a well defined molecular weight and polydispersity (Figure 1.2). Polyethylene glycol (PEG) is often conjugated to dendrimers to efficiently increase the molecular weight above the renal threshold and keep the number of synthetic steps low. The availability of PEG in a wide variety of sizes allows dendrimer properties, such as M_w and circulation time, to be tuned to the *in vivo* needs of the drug.[12] PEGylation also provides a water soluble, protective shell for the dendrimer core, sequestering drugs away from other circulating biomolecules. The more hydrophobic core is useful for solubizing important compounds and the periphery can be de-symmetrized with multiple functional handles to allow for the attachment of PEG, drug molecules, imaging agents, or targeting groups. The versatility of the dendrimer structure allows drugs to be conjugated through a variety of linkages including esters, hydrazones, thiols, chelators, and bonds susceptible to enzymatic degradation.[13,14]

Although dendrimers require a more time intensive synthesis than other polymers, this allows for a reproducible polymer which is important for *in vivo* applications and FDA approval. Structural changes can influence size, rate of excretion, and tissue uptake;[10] therefore batch diversity can be detrimental to sample analysis. Likewise, the often limited number of drug attachment points can lead to low drug weight loading. Dendrimer carriers generally have a

higher maximum tolerated dose, which coupled with the increased tumor accumulation can help to circumvent this shortcoming. However, tuning drug release to achieve high tumoral concentrations and efficacy can be a challenge.
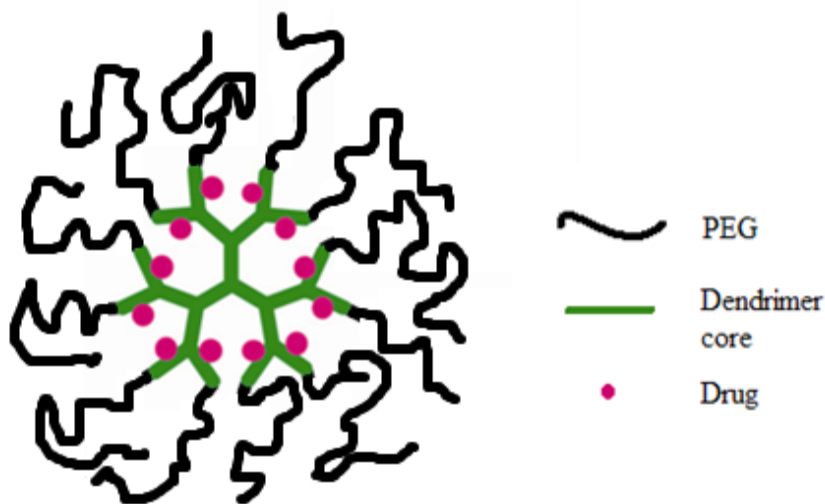

Figure 1.2. Schematic core-shell architecture of PEGylated dendrimer loaded with a drug in the interior.

A second system of interest for drug delivery is liposomes. Composed of a phospholipid bilayer, the structural properties of liposomes are easily manipulated to meet the needs of the encapsulated species. Naturally occurring phospholipids can be used to make relatively non-toxic and non-immunogenic liposomes, while the incorporation of PEGylated lipids stabilizes the bilayer, limits degradation, and creates long circulating "Stealth" liposomes to improve efficacy (Figure 1.3).[15,16] The addition of cholesterol in the bilayer provides further stabilization.[17–19] The ease in generating new formulations by altering the molar ratios of lipids makes liposomes a versatile carrier for the delivery of small molecules, proteins, and genetic material. Liposome size can be closely controlled by sonication and extrusion to limit uptake by the mononuclear phagocyte system primarily located in the spleen and liver, and improve tissue targeting.[16] The aqueous interior is favorable for encapsulation of water soluble drugs, while hydrophobic drugs partition into the bilayer.

Weakly basic drugs, such as Doxorubicin, can be loaded with high encapsulation efficiencies through the design of a pH gradient and subsequent salt formation;[20,21] however, many drugs are not amenable to this type of encapsulation method and suffer from either inadequate loading or poor stability. Modifications to the lipid formulation or the synthesis of prodrugs can circumvent some of these problems, as the camptothecin prodrug Irinotecan can be encapsulated while the active drug SN-38 cannot.[22] As with polymer systems, achieving appropriate drug release can be a challenge. Furthermore, liposomes are more sensitive to degradation and aggregation upon long term storage.
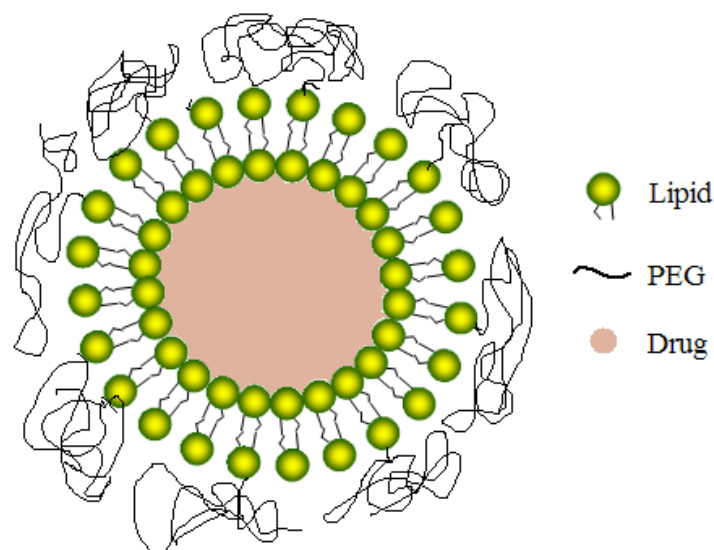
Figure 1.3. Graphic of PEGylated liposome with drug encapsulated in aqueous inner compartment.

Delivery of Camptothecin

  Camptothecin is a highly potent alkaloid isolated from the plant *Camptotheca acuminata*, which suffers from poor stability and solubility.[23] Upon administration, an equilibrium forms between the active lactone species and the inactive carboxylate form, which is driven by the carboxylate form preferentially binding to serum albumin, resulting in poor bioavailability and efficacy.[24] The lactone reforms in the acidic environment of the bladder causing severe toxicity and, coupled with the poor solubility, rendering this drug unusable. A number of water soluble derivatives have been synthesized (Figure 1.4) with only two gaining FDA approval.[25] Irinotecan and Topotecan are used to treat colon and ovarian cancer, respectively, but severe side effects limit their use.[26,27] The camptothecins target Topoisomerase I, an enzyme responsible for relieving tension in DNA during replication, transcription, and recombination, by creating and then repairing single strand breaks.[28] The DNA-Topo I complex is stabilized by CPT, preventing DNA re-ligation and ultimately causing cell death. To expand the utility of these drugs, a number of delivery systems are being explored clinically, although at this time none have been approved for clinical use.
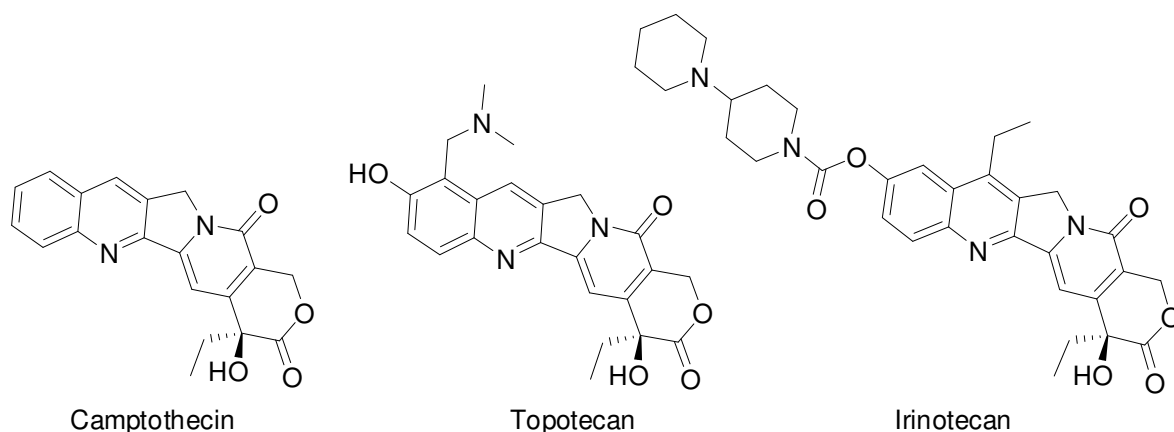
Figure 1.4. Structure of camptothecin and approved water soluble derivatives.

Camptothecin has been conjugated to a number of different polymers including HPMA, PEG, and poly-glutamic acid (Table 1.1). MAG-CPT has camptothecin conjugated to HPMA and had a favorable pharmacokinetic profile in Phase I studies, but had no improved tumor accumulation or reduction in bladder toxicity.[29–32] Clinical development was discontinued due to the toxicity concerns. PEG-CPT (EZ-246) gave mild to moderate bladder toxicity, but having only two CPT molecules per PEG limited efficacy and it was discontinued from further study.[33] CT-2106, a poly-L glutamate carrier, showed an improved toxicity profile compared to free CPT with a limited patient response, but Cell Therapeutics is focusing on other more promising drug conjugates and no further studies have been planned.[34] CPT conjugated to β-cyclodextrin (CRLX101) gave a stable response in patients and has just entered Phase II clinical trials.[35] XMT-101 is a poly-acetal polymer and has just started Phase I studies.[36]

Table 1.1. Camptothecin compounds in clinical trials

Compound	Polymer	%wt loading	M_w	Circulation $t_{1/2}$	Maximum Dose
MAG-CPT[29-32]	HPMA	10	20 kDa	100 hr	68-80 mg/m^2
EZ-246[33]	PEG	1.7	40 kDa	77 hr	7000 mg/m^2
CT-2106[34]	Poly-L-Glutamate	30	30-50 kDa	40 hr	25 mg/m^2
CRLX101[35]	β -cyclodextrin	8	60-100 kDa	39 hr	15 mg/m^2
XMT-1001[36]	Poly-acetal, PFH	5-7	70kDa	NA	113 mg/m^2

Despite the advances made in camptothecin delivery, dose limiting toxicity is still a limitation in the work described above. Previous work by our group has utilized the pH sensitive hydrazone linkage to successfully deliver chemotherapeutics with a variety of PEGylated dendrimers.[37–41] Having delivered a tubulysin analogue appended with a ketone functionality, we proceeded to design a camptothecin prodrug for delivery via the hydrazone linkage, as described in Chapter 2. Chemotherapy drugs are often used in combination, so co-delivery of polymeric camptothecin

5

and doxorubicin is also discussed. Combination therapy is necessary to improve treatment efficacy, reduce toxicity, and limit drug resistance; however, it is difficult to translate the specific drug ratios and treatment schedules identified in cell toxicity assays to *in vivo* synergistic therapies.[42–48] Differing rates of clearance and bioavailability of small molecule drugs create significant challenges in maintaining correct drug ratios at sufficient concentrations to be effective at the target site. Carrier mediated delivery has been explored as a method to circumvent these challenges.[49]

Platinum (II) Delivery

Cisplatin (*cis*-dichlorodiamine platinum (II)) is a commonly used chemotherapeutic agent for the treatment of tumors such lung, ovarian, and testicular; however, nephrotoxicity, ototoxicity, and neurotoxicity still present significant challenges during treatment.[50,51] Efforts to design less toxic, but more soluble derivatives have been mostly unsuccessful. Only three platinum compounds have received FDA approval: cisplatin in 1978, carboplatin in 1989, and oxaliplatin in 2002 (Figure 1.5). Pt(II) drugs are administered as inactive prodrugs composed of platinum atoms bearing two amino ligands (generally *cis*, but recent studies have shown efficacy with transplatinum compounds)[52] to two leaving groups, most commonly dichloride or dicarboxylate.[53] *In vivo,* the leaving groups begin to dissociate from the Pt complex forming the active mono aquato species which can then bind to DNA-guanine bases. Loss of the second leaving group forms 1,2-GpG intrastrand DNA adducts, causing a kink in the DNA and ultimately cell death.[54]
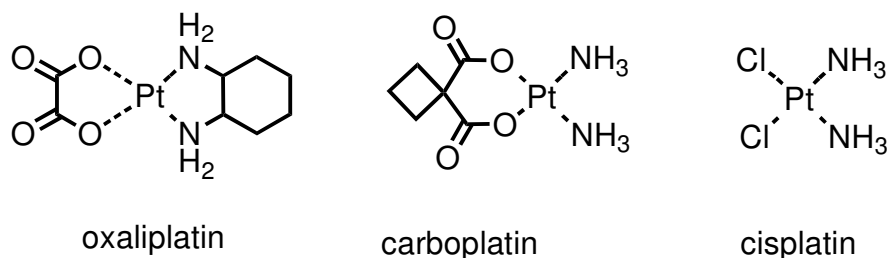

Figure 1.5. Platinum (II) drugs approved for use in patients.

Thus far, only three companies have polymer or liposomal Pt drugs in clinical trials (Table 1.2). Access Pharmaceuticals tested HPMA-oxaliplatin (AP5346) and HPMA-cisplatin (AP5280), with both systems giving improved circulation times and reduced nephrotoxicity in Phase I studies. AP5280 could be dosed at high Pt concentrations, but patients did not show any significant responses and further research was discontinued.[55] A PhaseI/II study of AP5346 gave responses comparable to oxaliplatin with partial patient responses, and neurotoxicity was the main side effect.[56] Nanocarrier is investigating Kataoka's poly-glutamic acid platinum micelles. The oxaliplatin micelles have just entered Phase I studies. The cisplatin micelles (NC-6004) gave stable responses and reduced toxicity.[57,58] Regulon has developed liposomal formulations of cisplatin and oxaliplatin. Lipoplatin has shown variable responses in clinical trials with the best responses observed in combination treatments with Gemcitabine or 5-FU.[59] Lipoxal gave partial responses in some patients but as with HPMA-oxaliplatin, neurotoxicity was still present.[60] SPI-077 was a liposomal cisplatin formulation removed from clinical trials after no activity was observed.[61,62] A maximum tolerated dose was never achieved as the platinum bioavailability was very poor. Aroplatin was a lipophilic oxaliplatin analogue formulated into liposomes.[63] Activity was comparable to oxaliplatin with reduced toxicity, but further studies were discontinued for economic reasons.[64]

Table 1.2. Platinum therapeutics in clinical trials.

Compound	Pt	Carrier	% wt loading	M_w	Circulation $t_{1/2}$	Maximum Dose
AP5346[56]	Oxaliplatin	HPMA	8.5	25 kDa	72 hr	640 mg/m^2
AP5280[55]	Cisplatin	HMPA	8.5	25 kDa	116 hr	3300 mg/m^2
NC-6004[57,58]	Cisplatin	Poly-L-Glutamate	39	~ 20 kDa	74 hr	90 mg/m^2
NC-4016[57,58]	Oxaliplatin	Poly-L-Glutamate	39	~ 20 kDa	NA	NA
Lipoplatin[59]	Cisplatin	Liposome	10	-	120 hr	Not reached
Lipoxal[60]	Oxaliplatin	Liposome	10	-	35 hr	300 mg/m^2
SPI-077[61,62]	Cisplatin	Liposome	6.7	-	60 hr	Not reached
Aroplatin[63,64]	Oxaliplatin	Liposome	6	-	36 hr	300 mg/m^2

Although moderate responses have been observed with the different treatments, reducing toxicity and controlling platinum release still remains a challenge. A series of polymer chelators were designed to further study the controlled release of platinum, as described in Chapter 3. In Chapter 4, the hydrazone linkage was appended to heterocyclic chelators to explore pH sensitive platinum release. Because platinum liposomes have shown comparable activity to polymer systems, leaky liposomes formulations were studied in Chapters 5 and 6 to increase platinum bioavailability.

Conclusions

Polymers and liposomes can be used to modulate drug properties to increase efficacy, reduce toxicity, and improve targeting. Care in designing drug delivery vehicles is important for maintaining half lives on the order of hours to promote tumor accumulation and for controlling drug release kinetics. This challenge is a common theme present in many of the camptothecin and Pt(II) drug clinical trials. Continued research is needed to bring new drug conjugates into clinics.

REFERENCES
(1)   Guengerich, F. P. *Annu. Rev. Pharmacol. Toxicol.* **1999**, *39*, 1–17.
(2)   Courjault, F.; Leroy, D.; Coquery, L.; Toutain, H. *Arch. Toxicol.* **1993**, *67*, 338–346.
(3)   Scott, D. O.; Bindra, D. S.; Sutton, S. C.; Stella, V. J. *Drug Metab Dispos* **1994**, *22*, 438–442.
(4)   Morgan, M. T.; Carnahan, M. A.; Immoos, C. E.; Ribeiro, A. A.; Finkelstein, S.; Lee, S. J.; Grinstaff, M. W. *J. Am. Chem. Soc.* **2003**, *125*, 15485–15489.

(5)   Müller, C. E. *Chem. Biodiversity* **2009**, *6*, 2071–2083.

(6)   Duncan, R. *Nat. Rev. Drug Discovery* **2003**, *2*, 347–360.

(7)   Torchilin, V. P. *Nat. Rev. Drug Discovery* **2005**, *4*, 145–160.

(8)   Peer, D.; Karp, J. M.; Hong, S.; Farokhzad, O. C.; Margalit, R.; Langer, R. *Nat. Nanotechnol.* **2007**, *2*, 751–760.

(9)   Yoo, J.-W.; Irvine, D. J.; Discher, D. E.; Mitragotri, S. *Nat. Rev. Drug Discovery* **2011**, *10*, 521–535.

(10)   Fox, M. E.; Szoka, F. C.; Fréchet, J. M. J. *Acc. Chem. Res.* **2009**, *42*, 1141–51.

(11)   Matsumura, Y.; Maeda, H. *Cancer Res.* **1986**, *46*, 6387–6392.

(12)   Gillies, E. R.; Fréchet, J. M. J. *J. Am. Chem. Soc.* **2002**, *124*, 14137–14146.

(13)   Kratz, F.; Mueller, I. A.; Ryppa, C.; Warnecke, A. *ChemMedChem* **2007**, *3*, 20–53.

(14)   Duncan, R. *Nat. Rev. Cancer* **2006**, *6*, 688–701.

(15)   Allen, T. M.; Hansen, C.; Martin, F.; Redemann, C.; Yau-Young, A. *Biochim. Biophys. Acta* **1991**, *1066*, 29–36.

(16)   Immordino, M. L.; Dosio, F.; Cattel, L. *Int. J. Nanomedicine* **2006**, *1*, 297–315.

(17)   Phillips, M. C.; Johnson, W. J.; Rothblat, G. H. *Biochim. Biophys. Acta* **1987**, *906*, 223–276.

(18)   Hamilton, J. A. *Curr. Opin. Lipidol.* **2003**, *14*, 263–271.

(19)   Kan, C. C.; Yan, J.; Bittman, R. *Biochemistry* **1992**, *31*, 1866–1874.

(20)   Haran, G.; Cohen, R.; Bar, L. K.; Barenholz, Y. *Biochim. Biophys. Acta* **1993**, *1151*, 201–215.

(21)   Barenholz, Y. (Chezy) *J. Control. Release* **2012**, *160*, 117–134.

(22)   Drummond, D. C.; Meyer, O.; Hong, K.; Kirpotin, D. B.; Papahadjopoulos, D. *Pharmacol. Rev.* **1999**, *51*, 691–744.

(23)   Wall, M. E.; Wani, M. C.; Cook, C. E.; Palmer, K. H.; McPhail, A. T.; Sim, G. A. *J. Am. Chem. Soc.* **1966**, *88*, 3888–3890.

(24)   Burke, T. G.; Mi, Z. *J. Med. Chem.* **1994**, *37*, 40–46.

(25)   Venditto, V. J.; Simanek, E. E. *Mol. Pharmaceutics* **2010**, *7*, 307–349.

(26)   Hecht, J. R. *Oncology* **1998**, *12*, 72–78.

(27)   Armstrong, D.; O'Reilly, S. *Oncologist* **1998**, *3*, 4–10.

(28)   Verma, R. P.; Hansch, C.; About, M.; Article, T. *Pharm. Res.* **2009**, *109*, 213–235.

(29)   Schoemaker, N. E.; Kesteren, C. van; Rosing, H.; Jansen, S.; Swart, M.; Lieverst, J.; Fraier, D.; Breda, M.; Pellizzoni, C.; Spinelli, R.; Porro, M. G.; Beijnen, J. H.; Schellens, J. H. M.; Huinink, W. W. ten B. *Br. J. Cancer* **2002**, *87*, 608–614.

(30)   Sarapa, N.; Britto, M. R.; Speed, W.; Jannuzzo, M.; Breda, M.; James, C. A.; Porro, M.; Rocchetti, M.; Wanders, A.; Mahteme, H.; Nygren, P. *Cancer Chemother. Pharmacol.* **2003**, *52*, 424–430.

(31)   Bissett, D.; Cassidy, J.; Bono, J. S. de; Muirhead, F.; Main, M.; Robson, L.; Fraier, D.; Magnè, M. L.; Pellizzoni, C.; Porro, M. G.; Spinelli, R.; Speed, W.; Twelves, C. *Br. J. Cancer* **2004**, *91*, 50–55.

(32)   Wachters, F. M.; Groen, H. J. M.; Maring, J. G.; Gietema, J. A.; Porro, M.; Dumez, H.; Vries, E. G. E. de; Oosterom, A. T. van *Br. J. Cancer* **2004**, *90*, 2261–2267.

(33)   Rowinsky, E. K.; Rizzo, J.; Ochoa, L.; Takimoto, C. H.; Forouzesh, B.; Schwartz, G.; Hammond, L. A.; Patnaik, A.; Kwiatek, J.; Goetz, A.; Denis, L.; McGuire, J.; Tolcher, A. W. *J. Clin. Oncol.* **2003**, *21*, 148–157.

(34) Homsi, J.; Simon, G. R.; Garrett, C. R.; Springett, G.; De Conti, R.; Chiappori, A. A.; Munster, P. N.; Burton, M. K.; Stromatt, S.; Allievi, C.; Angiuli, P.; Eisenfeld, A.; Sullivan, D. M.; Daud, A. I. *Clin. Cancer Res.* **2007**, *13*, 5855–5861.

(35) Bennet, N. *Lancet Oncology* **2012**, *13*, 18.

(36) Yurkovetskiy, A. V.; Fram, R. J. *Adv. Drug Delivery Rev.* **2009**, *61*, 1193–1202.

(37) Padilla De Jesús, O. L.; Ihre, H. R.; Gagne, L.; Fréchet, J. M. J.; Szoka, F. C. *Bioconjugate Chem.* **2002**, *13*, 453–461.

(38) Lee, C. C.; Gillies, E. R.; Fox, M. E.; Guillaudeu, S. J.; Fréchet, J. M. J.; Dy, E. E.; Szoka, F. C. *Proc. Natl. Acad. Sci. U.S.A.* **2006**, *103*, 16649–16654.

(39) Guillaudeu, S. J.; Fox, M. E.; Haidar, Y. M.; Dy, E. E.; Szoka, F. C.; Fréchet, J. M. J. *Bioconjugate Chem.* **2008**, *19*, 461–469.

(40) Fox, M.; Guillaudeu, S.; Fréchet, J.; Jerger, K.; Macaraeg, N.; Szoka, F. *Mol. Pharmaceutics* **2009**, *6*, 1562–1572.

(41) Floyd, W. C.; Datta, G. K.; Imamura, S.; Kieler-Ferguson, H. M.; Jerger, K.; Patterson, A. W.; Fox, M. E.; Szoka, F. C.; Fréchet, J. M. J.; Ellman, J. A. *ChemMedChem* **2011**, *6*, 49–53.

(42) Aletti, G. D.; Gallenberg, M. M.; Cliby, W. A.; Jatoi, A.; Hartmann, L. C. *Mayo Clin. Proc.* **2007**, *82*, 751–770.

(43) Molina, J. R.; Yang, P.; Cassivi, S. D.; Schild, S. E.; Adjei, A. A. *Mayo Clin. Proc.* **2008**, *83*, 584–594.

(44) Mayer, L. D.; Harasym, T. O.; Tardi, P. G.; Harasym, N. L.; Shew, C. R.; Johnstone, S. A.; Ramsay, E. C.; Bally, M. B.; Janoff, A. S. *Mol Cancer Ther* **2006**, *5*, 1854–1863.

(45) Buckner, J. C.; Brown, P. D.; O'Neill, B. P.; Meyer, F. B.; Wetmore, C. J.; Uhm, J. H. *Mayo Clin. Proc.* **2007**, *82*, 1271–1286.

(46) Gitler, M. S.; Monks, A.; Sausville, E. A. *Mol. Cancer Ther.* **2003**, *2*, 929–932.

(47) Chou, T.-C. *Pharmacol. Rev.* **2006**, *58*, 621–681.

(48) Dancey, J. E.; Chen, H. X. *Nat. Rev. Drug Discovery* **2006**, *5*, 649–659.

(49) Greco, F.; Vicent, M. J. *Adv. Drug Delivery Rev.* **2009**, *61*, 1203–1213.

(50) Boulikas, T.; Pantos, A.; Bellis, E.; Christofis, P. In *Anticancer Therapeutics*; Missailidis, S., Ed.; John Wiley & Sons, Ltd; pp. 55–78.

(51) Boulikas, T.; Vougiouka, M. *Oncol. Rep.* **2004**, *11*, 559–595.

(52) Kostova, I. *Recent Pat. Anti-Cancer Drug Discovery* **2006**, *1*, 1–22.

(53) Wang, X.; Guo, Z. *Dalton T.* **2008**, 1521–1532.

(54) Jung, Y.; Lippard, S. J. *Chem. Rev.* **2007**, *107*, 1387–1407.

(55) Rademaker-Lakhai, J. M.; Terret, C.; Howell, S. B.; Baud, C. M.; Boer, R. F. de; Pluim, D.; Beijnen, J. H.; Schellens, J. H. M.; Droz, J.-P. *Clin. Cancer Res.* **2004**, *10*, 3386–3395.

(56) Nowotnik, D. P.; Cvitkovic, E. *Adv. Drug Delivery Rev.* **2009**, *61*, 1214–9.

(57) Plummer, R.; Wilson, R. H.; Calvert, H.; Boddy, A. V.; Griffin, M.; Sludden, J.; Tilby, M. J.; Eatock, M.; Pearson, D. G.; Ottley, C. J.; Matsumura, Y.; Kataoka, K.; Nishiya, T. *Br. J. Cancer* **2011**, *104*, 593–598.

(58) Matsumura, Y. *Jpn. J. Clin. Oncol.* **2008**, *38*, 793–802.

(59) Wheate, N. J.; Walker, S.; Craig, G. E.; Oun, R. *Dalton T.* **2010**, *39*, 8113–8127.

(60) Stathopoulos, G. P.; Boulikas, T.; Kourvetaris, A.; Stathopoulos, J. *Anticancer Res.* **2006**, *26*, 1489–1493.

(61) Harrington, K. J.; Lewanski, C. R.; Northcote, A. D.; Whittaker, J.; Wellbank, H.; Vile, R. G.; Peters, A. M.; Stewart, J. S. *Ann. Oncol.* **2001**, *12*, 493–496.

(62) Meerum Terwogt, J. M.; Groenewegen, G.; Pluim, D.; Maliepaard, M.; Tibben, M. M.; Huisman, A.; ten Bokkel Huinink, W. W.; Schot, M.; Welbank, H.; Voest, E. E.; Beijnen, J. H.; Schellens, J. M. *Cancer Chemother. Pharmacol.* **2002**, *49*, 201–210.

(63) Perez-Soler, R.; Lopez-Berestein, G.; Lautersztain, J.; Al-Baker, S.; Francis, K.; Macias-Kiger, D.; Raber, M. N.; Khokhar, A. R. *Cancer Res.* **1990**, *50*, 4254–4259.

(64) Dragovich, T.; Mendelson, D.; Kurtin, S.; Richardson, K.; Von Hoff, D.; Hoos, A. *Cancer Chemother. Pharmacol.* **2006**, *58*, 759–764.

Chapter 2
Strategies to Deliver Camptothecin via Hydrazone Linkage and in Combination with Doxorubicin

ABSTRACT
A pH sensitive linker suitable for attachment of hydroxylated drugs has the potential to reduce unwanted drug hydrolysis in the blood and subsequent toxicity. A small library of aromatic carbonyl linkers were investigated in regards to their rates of hydrazone hydrolysis. The fastest and slowest were appended to camptothecin. The fastest linker exhibited similar cytoxicity and *in vivo* efficacy as compared to the more standard ester-linked camptothecin. Additionally, we explored the dual delivery of camptothecin and doxorubicin from one dendrimer. While more favorable synergistic activity was characterized *in vitro* for the dual drug system, the mixture of EA-CPT and EA-DOX gave significantly better tumor regression and survival than the dual-drug dendrimer.

INTRODUCTION
  20(S)-Camptothecin (CPT) is a potent alkaloid which suffers from poor solubility and bioavailability and thus cannot be used *in vivo*.[1] In particular, an equilibrium exists between the inactive-carboxylate form and the active- lactone form which is dependent upon a high affinity for serum albumin and the pH.[2] CPT is amenable to modifications which can improve solubility and stabilize the lactone ring. Extensive structure activity relationship studies have led to the synthesis of numerous derivatives, but only Irinotecan and Topotecan are used clinically.[3,4] The camptothecins inhibit Topoisomerase I, an enzyme which nicks and then re-ligates the DNA backbone to relieve strand tension.[5] Upon formation of the DNA-Topo I-CPT complex, re-ligation is inhibited and the cell undergoes apoptosis. To improve drug efficacy, delivery of the camptothecins with various carriers including polymers, liposomes, and micelles has also been explored.[4] Concurrent to this study, our lab investigated the polymeric delivery of CPT via a glycine ester linker.[6] Survival was significantly improved with a 24 mg/kg dose compared to a 10 mg/kg dose of CPT and 50 mg/kg x4 dose of Irinotecan. Further optimization with a 12 mg/kg x3 dose resulted in one tumor free survivor and a tumor growth delay of 155%; the free drugs had a tumor growth delay of < 20%. Likewise, the Szoka lab designed a folate targeted Irinotecan liposome which had a tumor growth delay of 100% and a 44% increase in survival time.[7]
  Previous work by our group has investigated drug polymer conjugates utilizing a pH responsive release mechanism.[8,9] Doxorubicin was attached via a pH sensitive acyl hydrazone linkage (Figure 2.1A) that allows for drug release in the acidic interstitial space of the tumor[10] or within the endosome[11] or lysosome[12] of the cell, rather than the blood. Conjugates have performed well in chemotherapy studies, with complete recovery of all mice treated.[8] We would like to expand this pH sensitive approach to include other chemotherapy agents that do not contain an aldehyde or ketone necessary for the formation of a hydrazone, specifically camptothecin.
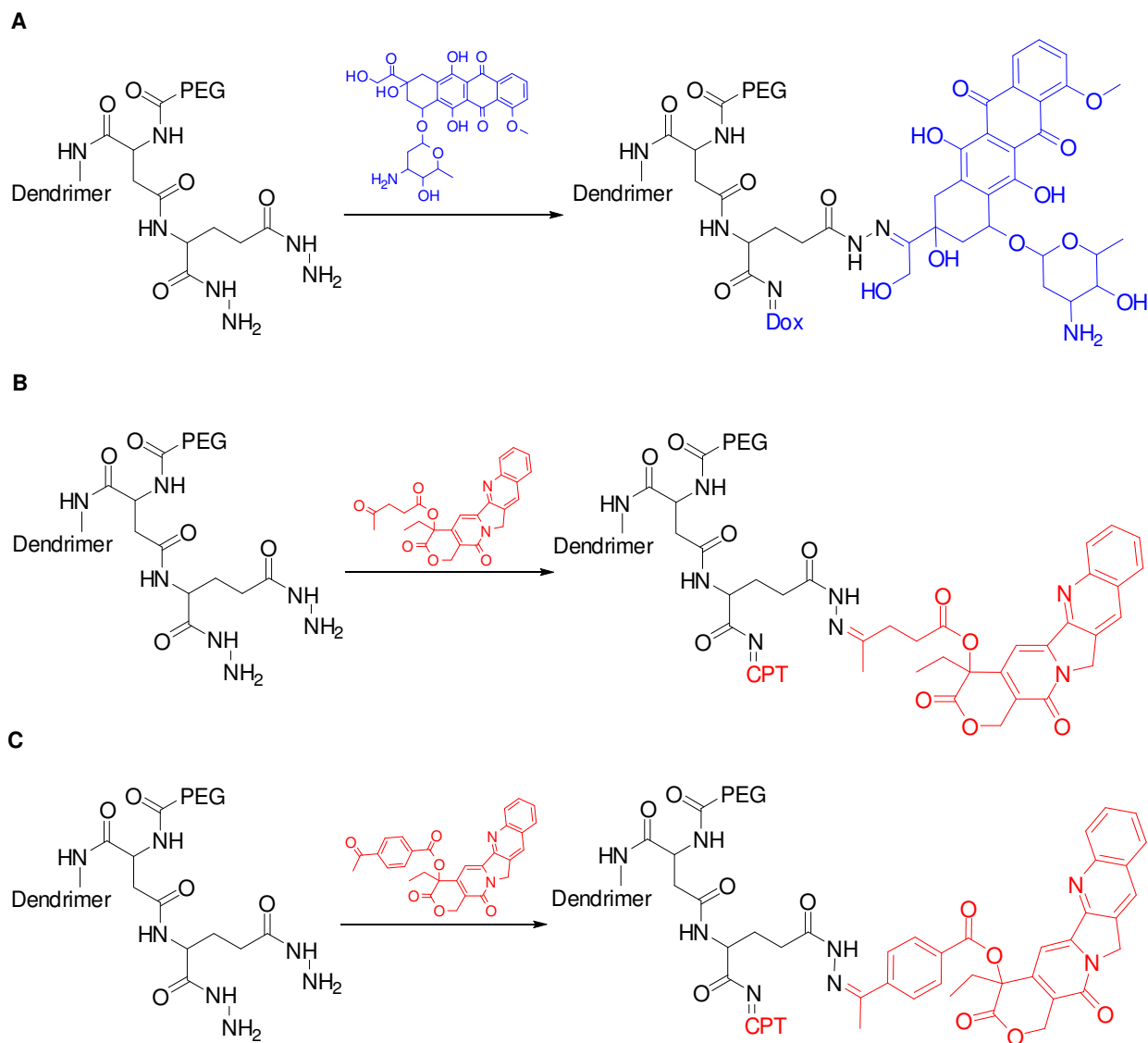
Figure 2.1 General conjugation scheme of several chemotherapeutics to dendrimers through the N-acyl hydrazone linkage. A) Attachment of doxorubicin. B) Attachment of camptothecin via a levulinic acid linker. C) Attachment of camptothecin via an aromatic linker.

The goal of this project is two-fold. The first is to synthesize a camptothecin prodrug to be conjugated to a dendrimer using a hydrazone linkage. Specifically, the tertiary alcohol of camptothecin will be used to append the appropriate carbonyl functionality for hydrazone formation. Preliminary studies focused on attachment of camptothecin to dendrimers via a levulinic acid linker (Fig 2.1B) to acquire the favorable release rates observed with the Dox hydrazone linkage (over 48 hrs, 100 % release, pH 5.0; 10% release, pH 7.4).[8] Unfortunately, the drug-polymer conjugate was not stable, presumably due to intramolecular lactam formation resulting in the release of camptothecin. In order to circumvent this problem, we were interested in designing aromatic spacers in an attempt to prevent cyclization and loss of the free drug (Figure 2.1C). Furthermore, synthesis of a small library of compounds would allow the release

kinetics to be modulated via structural change to the aromatic linker. Model hydrazones were prepared to evaluate hydrolysis rates and identify a suitable linker to derivatize camptothecin.

The second goal of this project is to pursue studies on the possible synergy arising from co-dosing camptothecin and doxorubicin. Drug combinations are used to control drug resistance, reduce drug dosage to limit toxicity while not compromising efficacy, and create multiple modes of cellular stress.[13] Once an appropriate combination has been designed, delivering the exact same drug concentration to every tumor cell is difficult. To circumvent this problem, we designed a polymer to accommodate the attachment of both camptothecin and doxorubicin in defined ratios, which will be maintained during circulation and cellular uptake. This technique has been successful across a variety of delivery platforms including polymers,[14–16] liposomes,[15,16] and nanoparticles.[17] Camptothecin and doxorubicin were selected because both target different classes of topoisomerase enzymes. DOX affects topoisomerase II,[18] which prevents re-ligation of DNA double strand breaks to induce apoptosis. When one topoisomerase enzyme is inhibited, studies have found that the corresponding enzyme is up-regulated to preserve cellular activity.[19,20] Targeting both topoisomerase enzymes in tandem could lead to improved therapeutic efficacy. Synergistic activity is dependent on the cell line, the CPT:DOX ratio, and the dosing schedule.[21] We have chosen to focus on only concurrent drug treatments as accurately replicating *in vitro* sequential schedules *in vivo* is beyond the scope of this project.

RESULTS AND DISCUSSION
Designing a Dendrimer-Camptothecin Prodrug
Synthesis of Hydrazone Models

In this study, we were interested in designing a series of model hydrazone containing compounds built around the commercially available hydrazide Girard reagent T as a simple way to explore camptothecin prodrugs. As illustrated in Figure 2.2, hydrazones **1-8** were prepared by condensation of the appropriate aldehyde or ketone with Girard reagent T. Aldehydes and ketones (**9-13**) were obtained commercially or prepared in one step from modified literature procedures. Girard reagent T was selected because of water solubility and structural similarity to the acyl hydrazide previously used. Structural studies have
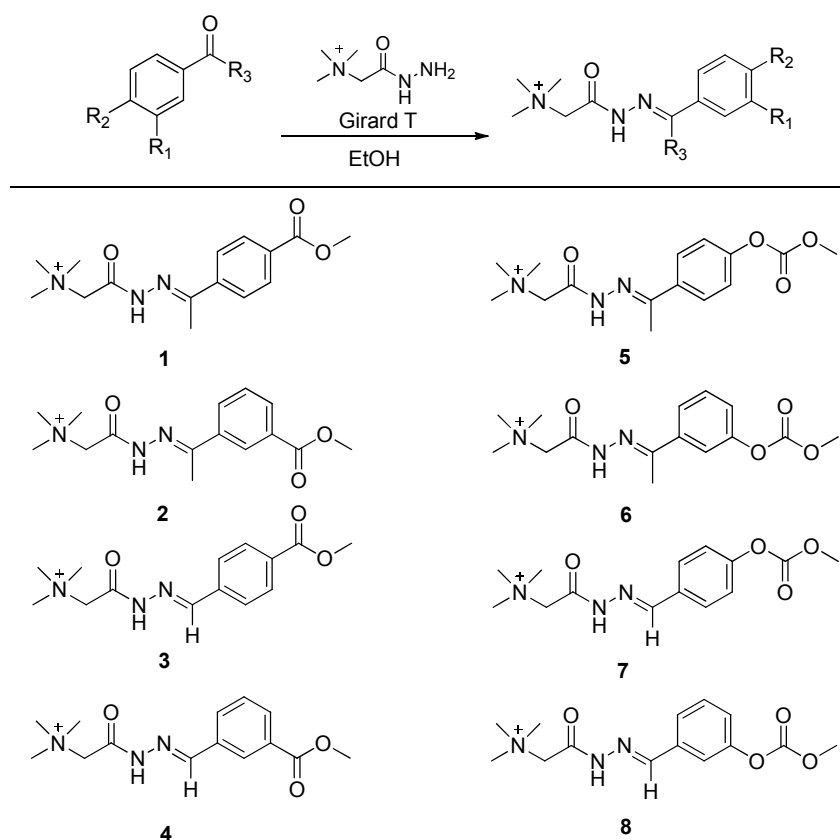

Figure 2.2. Model hydrazone compounds synthesized from Girard reagent T and carbonyl linkers.

shown that changes to the carbon α to the carbonyl do not affect the rates of hydrolysis.[22] The ester hydrazones **1-4** were crystallized from absolute ethanol. The carbonate hydrazones **5-8** were recrystallized in an ethanol/ether mix, which resulted in lower yields.

Kinetic Analysis of Hydrazone Hydrolysis

The rate of hydrolysis of hydrazone model compounds **1-8** was monitored by UV/Vis at 37 °C (Figure 2.3). Based upon previous hydrolysis studies with aromatic Girard T hydrazones, we expected pseudo first order kinetics, and the decomposition of the tetrahedral intermediate as the rate determining step, independent of pH changes.[23]
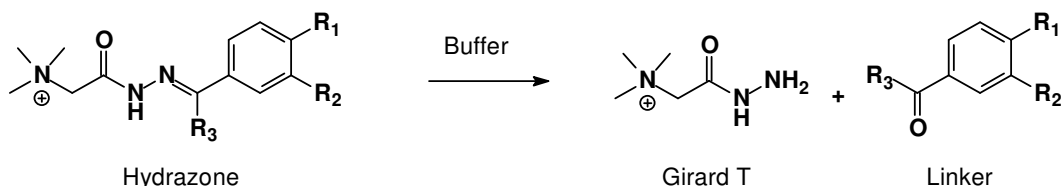

Figure 2.3. Hydrolysis of Hydrazone in Buffer.

To verify that the hydrazone was more sensitive to acidic conditions, the study was replicated in four different buffered solutions (pH 4.0, 5.0, 6.5, and 7.4). Minimal absolute EtOH was used to dissolve the hydrazone before dilution and to keep the linkers and Girard reagent T from precipitating during hydrolysis (0.1% EtOH present in the final solutions). The hydrolysis of hydrazones **1-8** was monitored at 273 nm; however, absorbance from the corresponding linkers and Girard reagent T was also present. To calculate the half-lives of hydrazones **1-8**, the absorbance from the hydrazones, linkers, and Girard T was calculated using Beer's Law (Equation 1), where x is the % hydrolysis of the hydrazone and c = initial $[hydrazone]_{t=0}$.

$$Abs = \varepsilon_{hydrazone}bc(1-x) + \varepsilon_{Girard\ T}\,bc(x) + \varepsilon_{linker}bc(x) \qquad (1)$$
$$Abs = Abs_{hydrazone} + Abs_{Girard\ T} + Abs_{linker}$$

The value of ε was calculated from the absorbance of solutions of hydrazones **1-8**, Girard T, and the linkers at various concentrations. Natural log plots of the hydrazone absorbance versus time were indicative of pseudo first order kinetics.

As desired, hydrolysis of hydrazones **1-8** was minimal at pH 6.5 and 7.4 (< 5% over 12 hours), but significant at pH 4.0 and 5.0. Hydrolysis rates over the pH range were important to assess, but pH 5.0 half-lives were significant because the pH in the lysozome and endosome aligns more closely with this value. The hydrolysis half-life of models **1-8** at pH 4.0 (0.1M Acetate buffer) and 5.0 (0.1M Acetate buffer) are shown in Table 2.1.

General trends of hydrolysis were revealed based upon structure through kinetic analysis. Previous work has established that hydrolysis of methyl ketone derived hydrazones proceeds at a higher rate than aldehyde derived hydrazones.[23] This can be attributed to the ability of the methyl group to stabilize the protonated carbonyl after the decomposition of the tetrahedral intermediate. Consistent with these results, hydrazones synthesized from ketone substrates (**1**, **2**, **5**, **6**) underwent hydrolysis at a rate higher than aldehyde derived substrates (**3**, **4**, **7**, **8**) at pH 4.0 and 5.0 (ranging from ~1.5 – 3x faster). The trends for carbonate and ester species are a bit less straightforward as they are coupled to the trends in electronics. It was expected that carbonate

**Table 2.1.** Half-life of hydrazone at pH 4.0 and 5.0

Hydrazone	$t_{1/2}$ (hr), pH 4.0	$t_{1/2}$ (hr), pH 5.0
5	1.2 ± 0.2	6.6 ± 0.3
2	1.6 ± 0.2	8.8 ± 0.5
6	1.8 ± 0.1	10.6 ± 1.4
1	2.0 ± 0.1	12.8 ± 1.0
7	4.3 ± 0.3	21.1 ± 0.6
4	5.6 ± 0.8	31.2 ± 3.4
8	5.1 ± 0.2	31.8 ± 4.2
3	7.4 ± 0.1	39.9 ± 0.8

substrates would hydrolyze at a rate higher than the ester substrates because the carbonate group is slightly electron donating, while the ester group is electron withdrawing. It was also anticipated that hydrazones containing substituents in the para position would have a greater effect on the rate than those in the meta position due to resonance effects. The trends observed were similar to the expected results. A comparison of the hydrazones containing para substituents revealed that carbonate compounds (**7**, **5**) hydrolyze at a rate higher than the ester (**3**, **1**) for both aldehydes and ketones. For the ketone series, the hydrolysis rates for the meta substituents (**2**, **6**) lie between the para carbonate hydrazone **5** and the para ester hydrazone **1**; this trend was also observed with the aldehyde series. Hydrazone **5** containing a ketone and carbonate linkage in the para position exhibited the highest hydrolysis rate, while hydrazone **3** containing an aldehyde and ester linkage in the para position possessed the lowest hydrolysis rate. These two extremes were chosen for further studies with camptothecin to evaluate the range of prodrug hydrolysis rates. The prodrug should exhibit significant hydrolysis under mildly acidic conditions, but limited hydrolysis at physiological pH. The potential success of a camptothecin prodrug over camptothecin will also depend upon enhanced pharmacokinetics and improved drug efficacy, specifically tumor suppression or increased mouse survival and limited general toxicity.
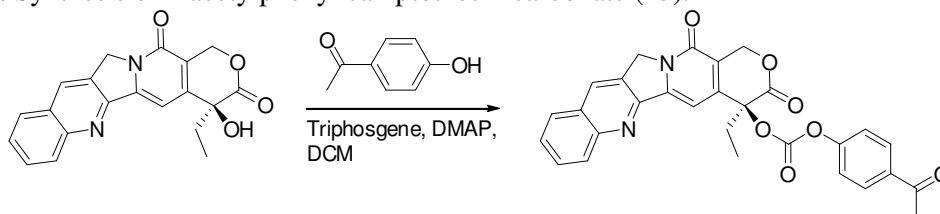
Synthesis of Dendrimer-Camptothecin Conjugates

Camptothecin was coupled with 4-hydroxyacetophenone and 4-formylbenzoic acid to give prodrugs with a carbonate and ester para to a ketone or aldehyde, respectively. The general strategy for synthesis of the two linkers was to use a carbodiimide coupling to form the ester bond (Scheme 2.1) and triphosgene to form the carbonate bond (Scheme 2.2). Given the limited solubility of camptothecin and the difficulty in separating free camptothecin from coupled camptothecin, reaction conditions producing 100% conversion were desired. Even with reagents in excess, conversion was incomplete and products were purified by silica gel flash column chromatography with 1% MeOH in chloroform or by loading the product onto a silica plug, washing with 1:1 HEX:EA, and eluting with 10:1 $CHCl_3$:MeOH.

**Scheme 2.1.** Synthesis of camptothecin 4-formyl benzoate (**14**).
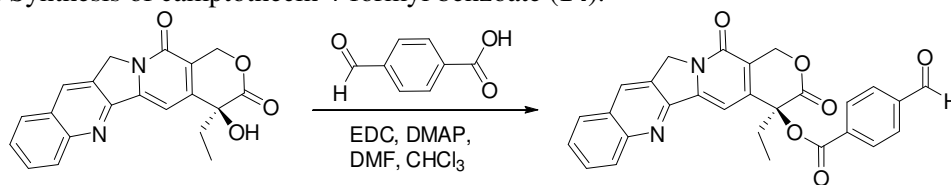
Treatment of 4-formylbenzoic acid with EDC, dimethylaminopyridine (DMAP), DMF and camptothecin afforded the camptothecin 4-benzoate linker (CPT-Ald) in 36% yield. Treatment of camptothecin with triphosgene, DMAP, and 4-hydroxy acetophenone yielded 65% of the 4-acetylphenyl camptothecin carbonate linker (CPT-Ket).

Scheme 2.2. Synthesis of 4-acetylphenyl camptothecin carbonate (**15**).

A PEGylated polylysine dendrimer was selected to be functionalized with camptothecin conjugates **14** and **15**. This polymer was being used concurrently by another member of the group to study camptothecin conjugated via a glycine-ester linkage. We were interested in comparing the *in vitro* and *in vivo* efficacy of both systems before selecting the most potent and synthetically accessible linkage for future combination studies. Lysine dendrimer[24] **16** was used as the starting material. Its peripheral amines were acylated with PNP-Asp(Bn)Boc to afford dendrimer **17** (Scheme 2.3), which required the PCP additive to prevent the formation of a 5-membered amino succinyl byproduct formed via amidolysis of the benzyl ester protected side chain. Deprotection of the amino groups of the aspartate termini and PEGylation with PEG-*p*-nitrophenyl carbonate afforded **18**. Glutamic acid was functionalized with t-butyl carbazate to install the hydrazide moiety and coupled to the dendrimer to give **19**. The glutamic acid spacer was required to prevent the nucleophilic hydrazides from cyclizing to cleave off PEG, but also doubled the number of drug attachment sites. Deprotection of the Boc groups followed by conjugation of either **14** or **15** in 5% Pyr/AcOH in MeOH at 60 °C afforded PLL-CPT-Ald **20b** and PLL-CPT-Ket **20a**, respectively. CPT loading was quantified by UV/Vis at 365 nm, giving weight loadings on average of 4-6% (theoretical loading of 6.5%).

Scheme 2.3. Synthesis of PEGylated PLL dendrimers with camptothecin prodrugs conjugated via hydrazone linkage.
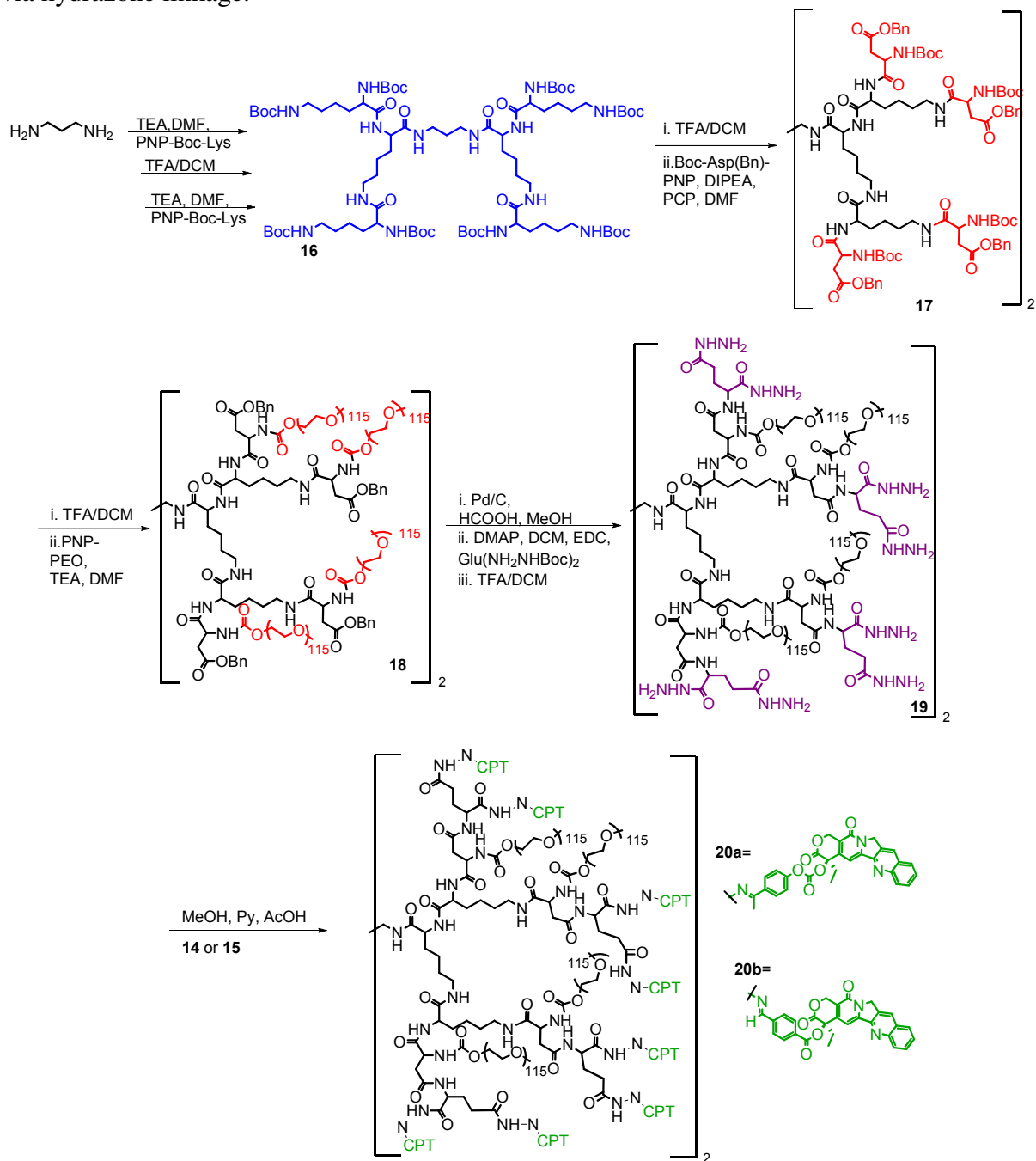
Camptothecin Conjugates Hydrolysis and Toxicity

Prodrugs **14** and **15** were screened against C26 murine colon carcinoma cells to evaluate the effect of the aromatic linker on toxicity and activity. Both CPT-Ket and CPT-Ald were less toxic than camptothecin due to the hydrolysis of the aromatic linker needed to release the active drug. Likewise, once linked to the dendrimer, we expected a further decrease in toxicity of CPT-Ket and CPT-Ald as the polymers undergo pinocytosis and the drugs are released (Table 2.2). Furthermore, the solubility of the prodrugs is greatly improved after attachment to the polymer

17

and DMSO is no longer needed to solubilize the drugs. PLL is completely water soluble even at high drug concentrations.

After verifying the activity of both the free and polymer bound drugs, the rate of hydrolysis was determined by HPLC. Because ester bonds are more readily hydrolyzed at neutral pH, the presence of CPT was monitored and found released in small amounts at pH 7.4. PLL-CPT-Ket, which was predicted to have a higher rate of hydrolysis by utilizing an aromatic carbonate and ketone, released significantly more camptothecin than PLL-CPT-Ald at pH 5.

Table 2.2. Hydrolysis and Cytotoxicity of Camptothecin Conjugates in C26 murine cells.

	Acetate buffer, pH 5.0	PBS, pH 7.4	Free Drug IC_{50} (nM)	Polymer-drug IC_{50} (nM)
CPT	-	-	32 ± 4	-
CPT-Ket	$t_{1/2} = 28$ h	< 1 % release in 24 h	403 ± 4	640 ± 6
CPT-Ald	3% release in 24 h	< 1 % release in 24 h	1152 ± 6	8370 ± 10
CPT-Gly[6]	< 2 % release in 24 h	$t_{1/2} = 21$ h	-	665 ± 50

We were pleased to see that the hydrolysis predictions from the model hydrazone study could be applied to our polymer camptothecin system. The carbonate linkage and aromatic ketone gave the best release profile while the aromatic aldehyde-ester combination was relatively inactive. This trend held true both *in vitro* and during hydrolysis. In contrast, PLL-Gly-CPT releases CPT at pH 7.4 rather than at pH 5, which could induce greater systemic toxicity *in vivo*. Despite these different release mechanisms, hydrolysis in serum versus cellular compartments, PLL-Gly-CPT and PLL-CPT-Ket had similar toxicities. Given this result, we were interested in comparing the toxicity and efficacy of these two systems *in vivo*.

In vivo Efficacy

Evaluating the toxicity of PLL-CPT-Ket in healthy mice is an important parameter for setting a therapeutic dose in future chemotherapy studies. Escalating doses of the polymer were injected *i.v.* via the tail vein from 18 mg CPT/kg to 64 mg CPT/kg. Mice were monitored for signs of toxicity including weight loss, lethargy, and ruffled fur. All doses caused some degree of toxicity with both 64 mg CPT and 48 mg CPT being lethal. One of the two mice dosed with 36 mg CPT also needed to be removed from the study, so a maximum tolerated dose was set at 24 mg CPT/kg. This result is comparable to the MTD of
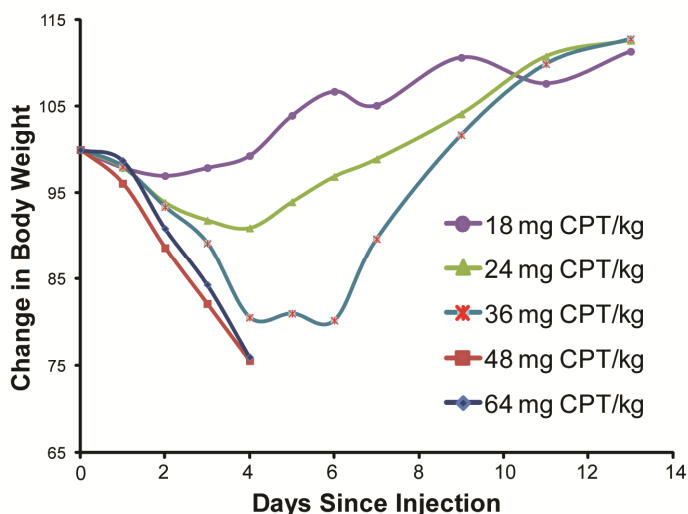

Figure 2.4. *in vivo* toxicity of PLL-CPT-Ket in healthy, female Balb/C mice.
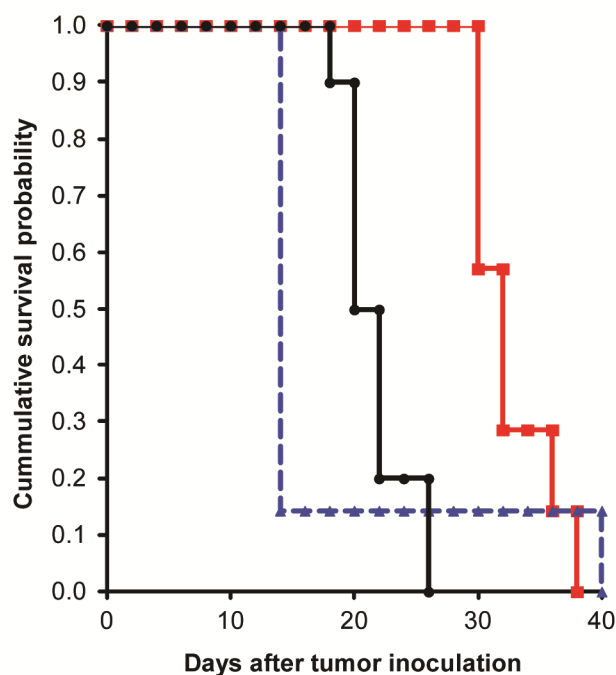
18

Figure 2.5. Kaplan Meier survival plot for PLL-Gly-CPT and PLL-CPT-Ket. Mice were treated with a single dose of ● PBS, ▲ PLL-Gly-CPT (24 mg CPT/kg), and ■ PLL-CPT-Ket (24 mg CPT/kg) on day 8.

PLL-Gly-CPT at 32 mg CPT/kg.[6]

After finding an appropriate PLL-CPT dose, subcutaneous C26 murine colon carcinomas were established in female Balb/C mice. At 8 days post tumor induction, mice were treated with either PLL-CPT-Ket or PLL-Gly-CPT at 24 mg CPT/kg. Tumor volume and mouse weight was monitored for the duration of the study. Despite re-purification of PLL-Gly-CPT, which had been previously synthesized for an earlier study, the sample proved to be unusually toxic. The mice lost a significant amount of weight only after the tumors had disappeared, which suggests some variability in the C26 cells used for tumoring, with this study getting a more sensitive batch of cells. With such rapid tumor regression, a lower PLL-Gly-CPT dose would likely have improved survival outcome. In a previous study, this treatment gave favorable survival outcomes with minimal toxicity.[6] PLL-CPT-Ket had significant tumor regression and survival compared to the PBS controls (p<0.0001) with less than 5% drop in weight after treatment.

Conclusions

Model hydrazones **1-8** were synthesized and their hydrolysis rates were evaluated. Hydrazone **5** with a carbonate moiety para to a methyl ketone exhibited the highest rate of hydrolysis (6.6 hrs at pH 5.0) and the features were translated into camptothecin prodrug **15**. Alternatively, the lowest rate of hydrolysis was observed from hydrazone **3** with an ester bond para to an aldehyde (40 hrs at pH 5.0) and this functionality was incorporated into camptothecin prodrug **14**. CPT-Ket and CPT-Ald were attached to a PLL dendrimer where toxicities and rates of hydrolysis spanned an order of magnitude. PLL-CPT-Ket was compared to a similar dendrimer CPT species, PLL-Gly-CPT, and found to have similar *in vitro* and *in vivo* activities.

Designing a Dual Drug CPT-DOX Polymer
Synthesis of CPT-DOX Polymer

While completing the PLL-CPT-Ket study, we set out to design a more efficient and synthetically accessible dendrimer. The ester amide dendrimer features a hydrolytically degradable ester core with a more chemically resistant amide periphery to give a biodegradable yet robust dendrimer, better suited for *in vivo* studies. As shown in Scheme 2.4, pentaerythritol is treated with PNP-lysine to install the ester core (**21**). The amine protecting groups were then removed and the core reacted with orthogonally protected PNP-glutamic acid to give **22**. Glutamic acid was selected over aspartic acid to circumvent the cyclization and degradation problems experienced with the PLL dendrimer as described earlier in this chapter. Quantitative removal of the Boc protecting groups and subsequent PEGylation with 5 kDa PNP-PEG afforded

19

dendrimer **23**. After removal of the benzyl ester protecting groups via hydrogenolysis, the dendrimer could be functionalized in a number of ways to accommodate the drug of choice. To conjugate doxorubicin via a hydrazone linkage, the carboxylic acids were treated with *t*-butyl carbazate and 1-ethyl-3-(3-dimethylaminopropyl)carbodiimide (EDC) to give **24**. Removal of the Boc groups and subsequent condensation with doxorubicin in 5% pyridine/acetic acid solution of methanol at 60 ^{o}C gave EA-DOX (**25**).

Scheme 2.4. Synthesis of hybrid ester amide dendrimer with 8 protected benzyl esters sites for future drug attachment.
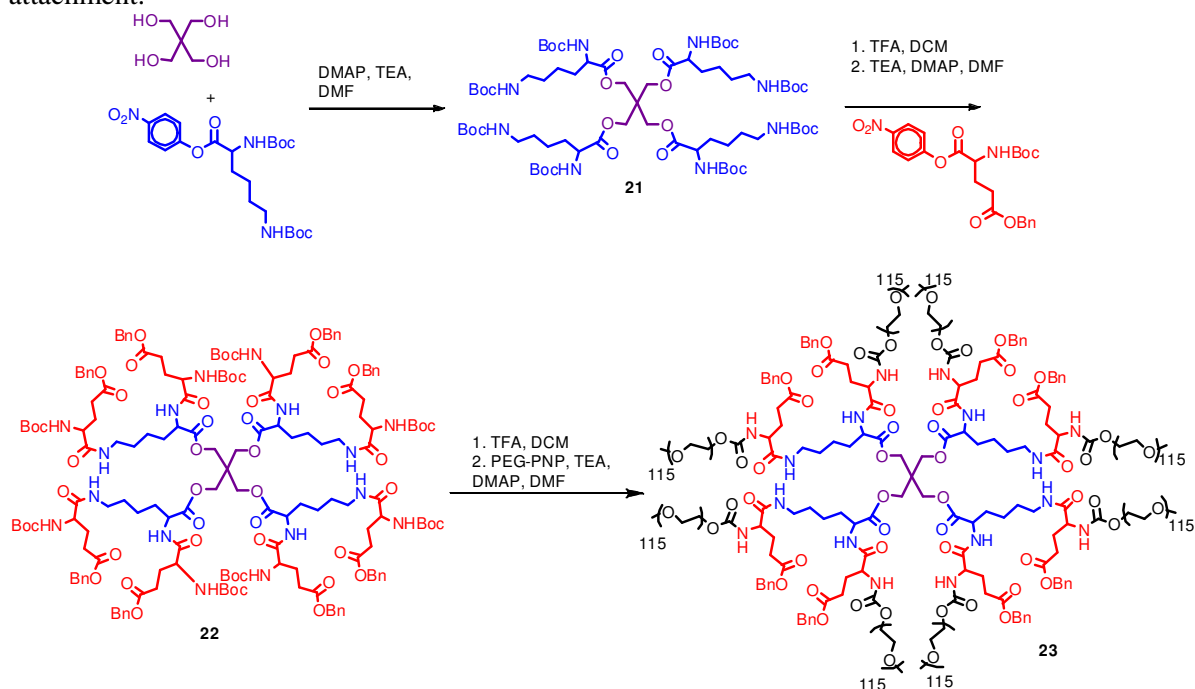
We elected to use Gly-CPT rather than the CPT-Ket in the combination studies as synthetically, attachment of a hydrazone-linked drug and an ester-linked drug gave us more control over the loading. To install camptothecin, the carboxylic acids were treated with Gly-CPT, HBTU, and PCP to give EA-CPT (**26**). Lastly, to put both drugs on the same dendrimer, a second generation of orthogonally protected glutamic acid was added to the carboxylic acids (**27**). Removal of the t-butyl ester protecting group and subsequent attachment of t-butyl carbazate installed the protected hydrazide (**28**). Hydrogenolysis removed the benzyl ester protecting groups and Gly-CPT was attached as before to give **29**. Quantitative removal of the Boc groups, followed by addition of doxorubicin as previously described gave EA-CPT-DOX (**30**). Camptothecin and doxorubicin loading was quantified by UV/Vis at 360 nm and 486 nm, respectively. It should be noted that by UV/Vis, no significant loss of camptothecin occurred during the conjugation of doxorubicin.

Scheme 2.5. Differentiation of ester amide dendrimer periphery to conjugate camptothecin (**26**), doxorubicin (**25**), or both drugs (**30**).
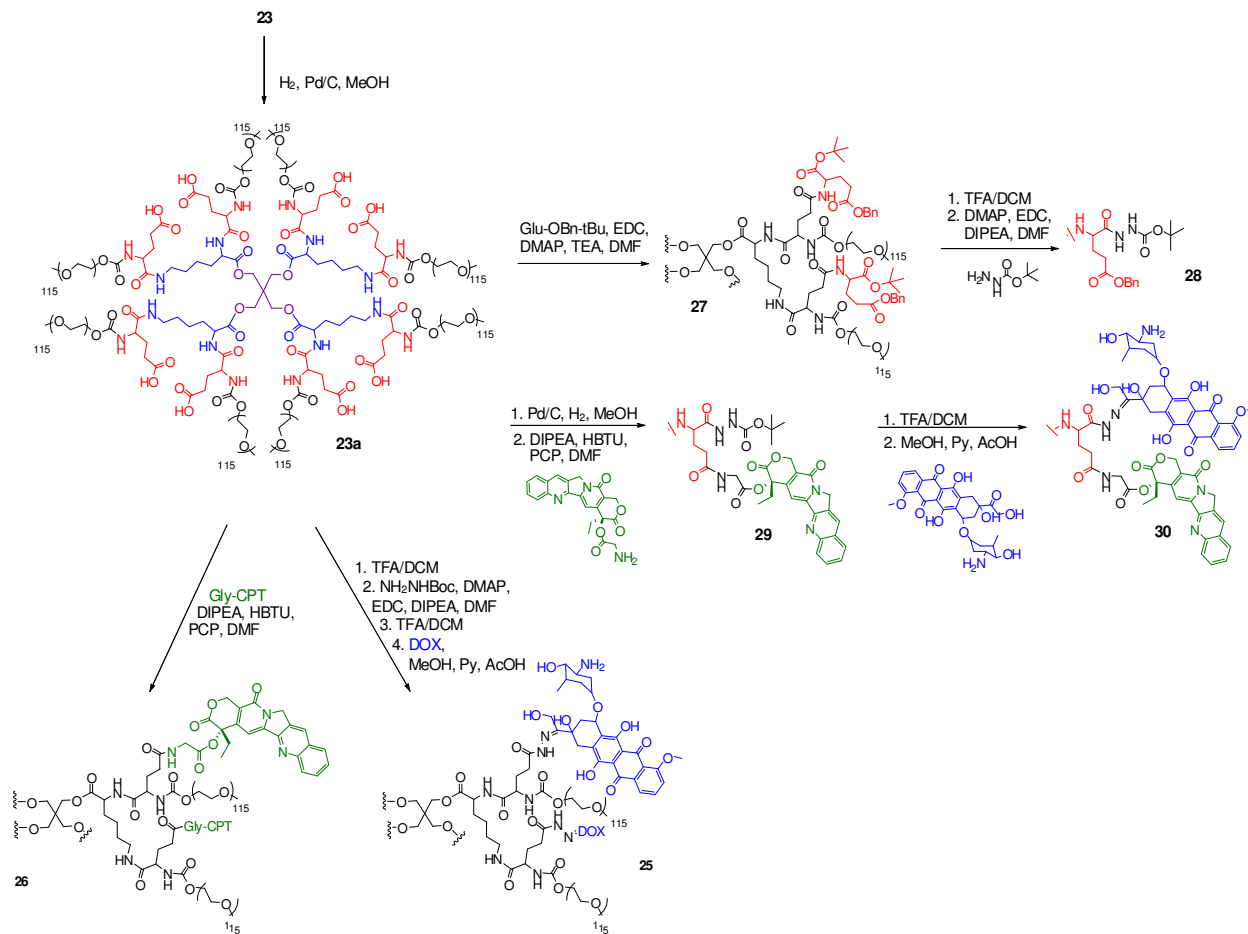
Efficacy of Camptothecin and Doxorubicin Dosed in Combination

Synergy between camptothecin and doxorubicin has been shown to be dependent upon dosing schedule, drug ratios, and cell type.[21,25–28] For ease, we limited our screen to the C26 murine colon carcinoma and HT-29 human colon carcinoma cell lines, and only concurrent treatments as sequential dosing is difficult to replicate *in vivo*. Preliminary studies[29] shown in Table 2.3 indicated that the synergistic free drug combinations did not correlate to polymer combinations, so these were not repeated. To explore the synergism between polymer CPT and DOX, a standard 3-day MTT assay was used. We were interested in making dendrimers with loadings ranging from 10:1 CPT:DOX to 1:10 CPT:DOX; however, controlling the drug ratios proved to be significantly more difficult than expected. Polymers with a 2:1 and 1:1 CPT:DOX ratio could be synthesized repeatedly, so these were screened in the combination studies.

Table 2.3: Summary of the synergism of free drug DOX and CPT combinations for fractions affected above 0.8.

Schedule/Ratio DOX:CPT	Synergy of combination Free Drug	Synergy of combination Polymer-bound Drug
10:1	additive/antagonistic	synergistic/additive
5:1	additive	synergistic/additive
1:1	additive/antagonistic	additive
1:5	synergistic/additive	additive
1:10	additive/antagonistic	additive

To evaluate whether a combination is synergistic, additive, or antagonistic, Chou and Talalay developed the median effect method.[30,31] This method is based upon the median effect equation (Equation 2), which is derived from the law of mass action.

$$\frac{f_a}{f_u} = \left(\frac{D}{D_{50}}\right)^m \qquad (2)$$

D is the dose, f_a and f_u represent the fraction of cells affected and unaffected, D_{50} is the dose required to produce a 50% response, and m specifies the shape of the dose-response curve. To simplify the synergy calculation, the combination index (CI) equation for a two drug system was derived (Equation 3).

$$CI_x = \frac{D_1}{(D_1)_x} + \frac{D_2}{(D_2)_x} + \frac{D_1 D_2}{(D_1)_x (D_2)_x} \qquad (3)$$

D_1 and D_2 represent the dose for the two drugs and D_x is the dose to kill x fraction (ie. x=50 is IC_{50}). In general, CI values < 0.9 are considered synergistic, while 0.9-1.1 is considered additive and values > 1.1 are antagonistic. The method becomes more inaccurate at the upper and lower limits, so analysis was restricted between $0.1 < f_a < 0.9$, with an emphasis on achieving synergy at higher kill fractions (x > 50) because *in vivo,* drugs are dosed at the max tolerated dose to maximize efficacy. The CalcuSyn (Biosoft) computer program creates the median effect plot (a log-log plot of dose (x-axis) and effect (y-axis)) from the supplied dose and f_a values and then derives CI values at any kill fraction.

The dendrimers were screened as both the dual-drug combination (EA-CPT-DOX) and as the drug mixture (EA-CPT/EA-DOX). The dual-drug combination gave better synergistic activity at higher fractions affected (kill doses) than the mixture did (Figure 2.6) at both ratios tested. Most importantly, synergistic activity was observed at higher f_a. Likewise, activity was maintained in the HT-29 human colon carcinoma cell line which has responded positively to CPT treatments in the past.[6] Given these promising results, we were interested in evaluating the dual drug system *in vivo*.

In vivo Analysis

The *in vivo* toxicity of both EA-CPT-DOX and the co-dosed EA-CPT/EA-DOX was evaluated in healthy female Balb/C mice (Figure 2.7). The drugs were dosed at a 2:1 molar ratio, which based upon the molecular weight gave 30 mg/kg of CPT and 27 mg/kg of DOX as the highest

concentration, with subsequent dilutions. Mice were monitored for 10 days and no significant toxicity was observed.
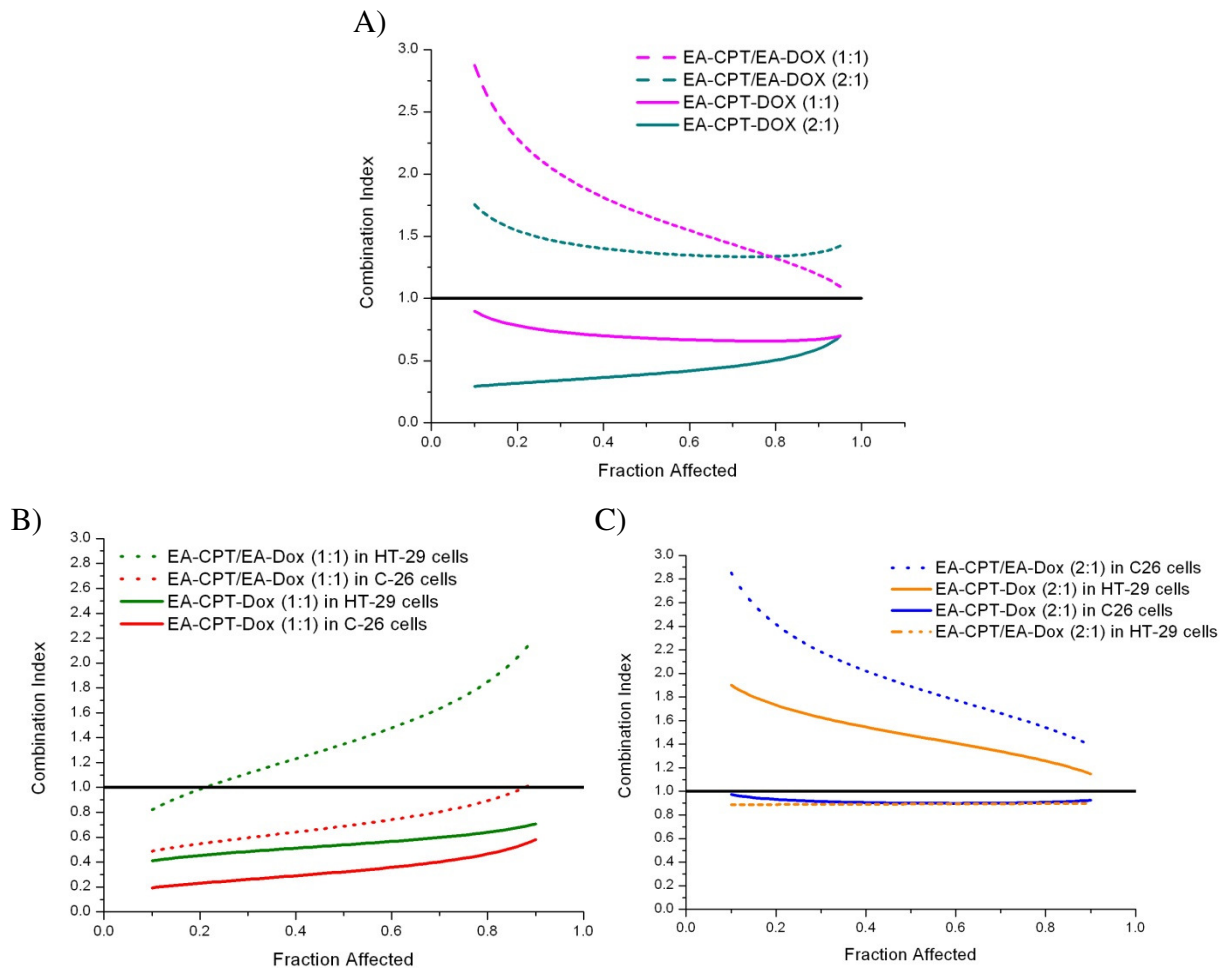

Figure 2.6. Combination index values for EA-CPT-DOX compared to co-dosing EA-CPT and EA-DOX. CI < 0.9 indicates synergy and CI > 1.1 indicates antagonism. A) Average CI in C26 cells for 2:1 and 1:1 CPT:DOX molar ratios B) Comparison of synergy at 1:1 CPT:DOX ratio in C26 and HT-29 cells C) comparison of synergy at 2:1 CPT:DOX ratio in C26 and HT-29 cells.

The C26 tumor model was used for the antitumor efficacy study. Mice were treated on day 8 and monitored for 60 days. The treatment groups were EA-CPT (24 mg/kg), EA-DOX (20 mg/kg), EA-CPT-DOX in combination (24 mg CPT/20 mg DOX, 18 mg CPT/15 mg DOX, 12 mg CPT/10 mg DOX/kg) or EA-CPT and EA-DOX mixed in the same ratios. All the treatment groups had statistically significant survival compared to the PBS control, but mixing the two dendrimers produced better efficacy compared to the dual carrier. Although we saw favorable *in vitro* results, the dual carrier didn't have better efficacy or synergy *in vivo*. Tumor tissue will have a different exposure profile compared to a monolayer of cells and the 3 day MTT assay may introduce too many new variables for accurate *in vitro* to *in vivo* translations. Modifications to the drug exposure time may aid in designing a synergistic combination.
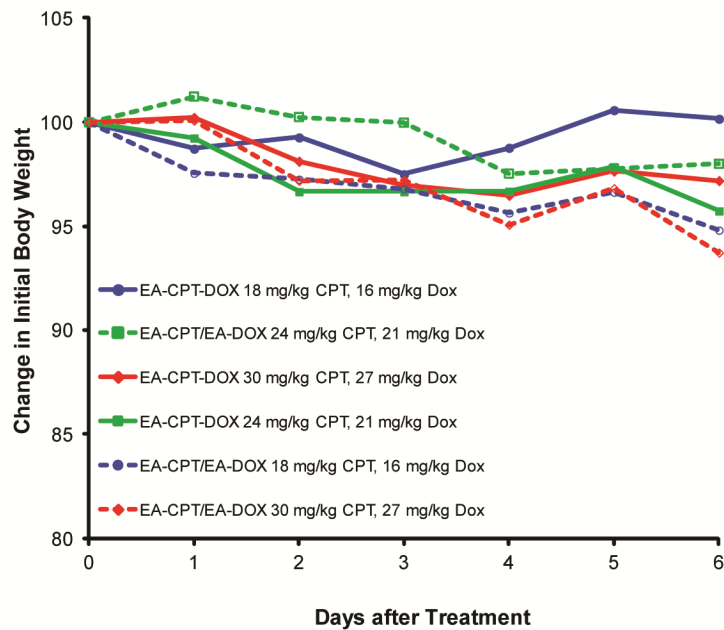
Figure 2.7. *In vivo* toxicity in healthy Balb/C mice with CPT and DOX dosed in a 2:1 molar ratio.
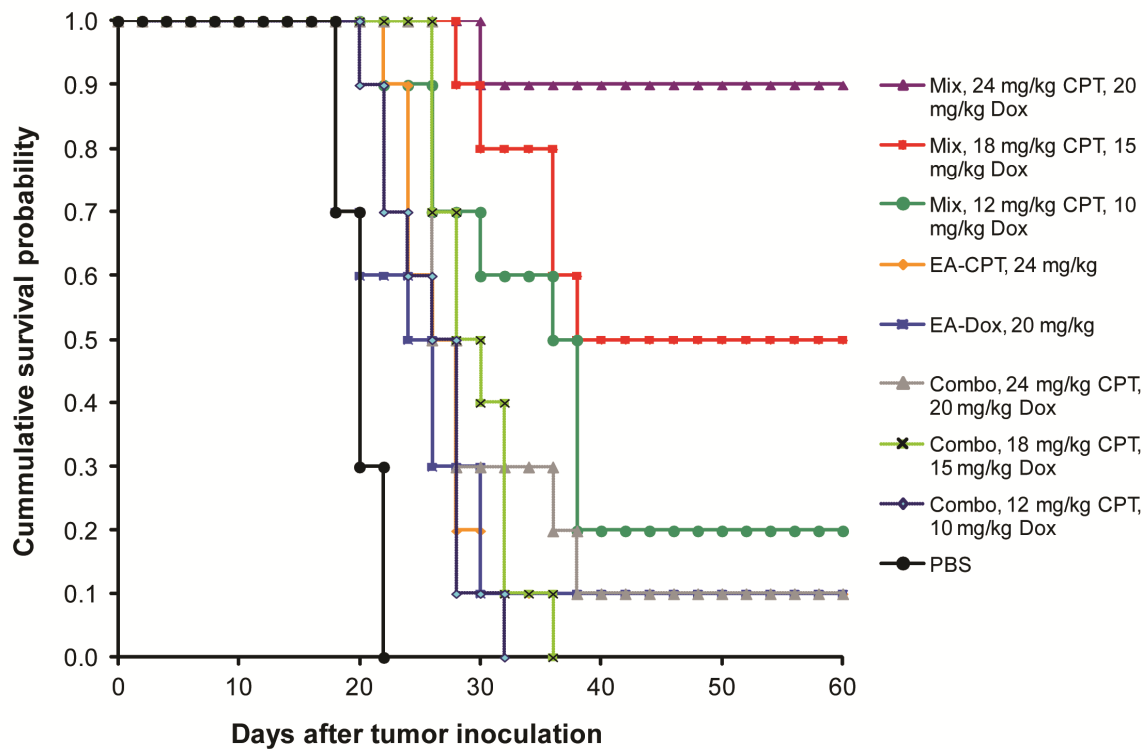

Figure 2.8. Kaplan Meier survival for female Balb/C mice with s.q. C26 colon carcinoma tumors. Mice treated with a single dose on day 8. EA-CPT-DOX represents the dual delivery and EA-CPT/EA-DOX represents the dendrimer mixture.

Conclusions

A dendrimer carrier was designed with an orthogonally protected linker to facilitate the attachment of an ester-linked camptothecin and a hydrazone-linked doxorubicin. While moderate drug loading could be achieved, controlling the drug ratios proved to be a challenge. EA-CPT-DOX was screened against EA-CPT and EA-DOX in both the C26 and HT-29 cell lines to find synergistic combinations amenable for *in vivo* studies. A 2:1 drug ratio was selected for further studies. The mixture of EA-DOX and EA-CPT gave better survival and tumor regression at all doses than EA-CPT-DOX. Overall, the experiments showed limited synergistic activity in the C26 mouse model. We observed that the *in vitro* screen did not correlate well with the *in vivo* efficacy study; this could be due to the cells responding differently in a media-based environment than in a tumor mass. We believe that any future combination studies should be carried out using drugs on individual polymer carriers, thereby allowing for easier formulation modifications and more extensive *in vitro* screens.

EXPERIMENTAL

Materials. All reagents were purchased from commercial sources and used without further purification unless specified otherwise. Poly(ethylene glycol) was purchased from Laysan Biosciences Inc. Amino acid derivatives were purchased from Bachem. Girard reagent T was recrystallized from absolute ethanol. Methylene chloride (DCM), pyridine, and *N,N*-dimethylformamide (DMF) were purchased from Fischer and vigorously purged with nitrogen for 1 h before passing through two columns of neutral alumina (for methylene chloride) or activated molecular sieves (for DMF). Unless otherwise specified, liquid reagents were added to the reaction flask via syringe. Organic extracts were dried over anhydrous $MgSO_4$ and filtered, and solvents were removed under reduced pressure using a rotary evaporator.

Characterization. NMR spectra were recorded on Bruker AVB 400, AVQ 400, or DRX 500 MHz instruments. Spectra were recorded in $CDCl_3$, MeOD, or D_2O solutions and were referenced to TMS or the solvent residual peak and taken at ambient temperature. Elemental analyses and mass spectroscopy were performed by the University of California at Berkeley Micro-Mass Facility. IR spectroscopy was performed on a Varian 3100 FT-IR spectrometer. All IR samples were prepared as thin film from $CHCl_3$ or MeOH on a NaCl plate. UV/Vis spectrometry was recorded with a Perkin Elmer Lamda 35 UV/Vis spectrometer (PerkinElmer, Wellesley, MA). Measurements were performed in sealed, standard 1-cm quartz cells in millipore water (Dox) or $CHCl_3$ (CPT) at room temperature. Size exclusion chromatography (SEC) was performed using one of two systems:

SEC System A: a Waters 515 pump, a Waters 717 autosampler, a Waters 996 Photodiode Array detector (210-600 nm), and a Waters 2414 differential refractive index (RI) detector. SEC was performed at 1.0 mL/min in a PLgel Mixed B (10 µm) and a PLgel Mixed C (5 µm) column (Polymer Laboratories, both 300 x 7.5 mm), in that order, using DMF with 0.2% LiBr as the mobile phase and linear PEO (4,200-478,000 MW) as the calibration standards. The columns were thermostated at 70 °C.

SEC System B: The same equipment as System A, but performed at 1.0 mL/min in two SDV Linear S (5 µm) columns (Polymer Standards Service, 300 x 8 mm) using DMF with 0.2% LiBr as the mobile phase.

Synthesis of 3-formylphenyl-methyl carbonate (9). The title compound was prepared according to a modified literature procedure.[32] In a dry 100 ml round bottom flask, 3-hydroxy

benzaldehyde (1.001 g, 7.35 mmol) was dissolved in dry pyridine (7.0 ml, 86.5 mmol) and cooled to 0 °C. Methyl chloroformate (1.3 ml, 16.9 mmol) was added dropwise over 30 min and the mixture was stirred overnight under an argon atmosphere. The mixture was transferred with ether, concentrated under reduced pressure, and re-dissolved in water (10 ml). The product was extracted with ether and washed with two 10 ml portions of 1.0 M HCl, two 10 ml potions of 5% cold NaOH, and two 10 ml portions of water. The organic layer was dried, filtered, and evaporated to give a white solid. Yield: 0.6351g (43 %). Spectroscopic data were consistent with the previous literature report.[33]

Synthesis of 4-formylphenyl-methyl carbonate (10). The title compound was prepared in a similar manner as **9**, using 4-hydroxy benzaldehyde (1.006 g, 7.35 mmol), dry pyridine (6.2 ml, 76.6 mmol), and methyl chloroformate (1.3 ml, 16.9 mmol). Compound **10** was obtained as a pale yellow solid. Yield: 0.3587g (24%). Spectroscopic data were consistent with the previous literature report.[34]

Synthesis of 3-acetylphenyl-methyl carbonate (11). The title compound was prepared in a similar manner as **9**, using 3-hydroxy acetophenone (1.001 g, 7.35 mmol), dry pyridine (6.7 ml, 80.4 mmol), and methyl chloroformate (1.3 ml, 16.9 mmol). Compound **11** was obtained as a white solid. Yield: 0.9857 g (69 %). ^{1}H NMR (400 MHz, CDCl$_3$) δ 2.57 (s, 3H), 3.89 (s, 3H), 7.36 (d, J=8.1 Hz, 2H), 7.47 (t, J=7.9 Hz, 1H), 7.73 (s, 1H), 7.82 (d, J=7.8 Hz, 1H). ^{13}C NMR (100 MHz, CDCl$_3$) δ 26.7, 55.6, 120.9, 125.8, 126.0, 129.8, 138.6, 151.3, 154.0, 196.8. IR 3072, 3006, 2961, 2928, 2853, 1762 cm^{-1}. Anal Calc for C$_{10}$H$_{10}$O$_4$: C, 61.85; H, 5.19. Found: C, 61.79; H, 5.14. Calcd: [M]$^+$ (C$_{10}$H$_{10}$O$_4$) m/z = 194.0579 Found EI-HRMS: [M]$^+$ m/z = 194.0579.

Synthesis of 4-acetylphenyl-methyl carbonate (12). The title compound was prepared in a similar manner as **9**, using 4-hydroxy acetophenone (1.001 g, 7.35 mmol), dry pyridine (6.7 ml, 84.1 mmol), and methyl chloroformate (1.3 ml, 16.9 mmol). Compound **12** was obtained as a white solid. Yield: 0.498 g (33 %). Spectroscopic data were consistent with the previous literature report.[35]

Synthesis of Methyl 3-acetylbenzoate (13). The title compound was prepared according to a modified literature procedure.[36] A mixture of 3-acetylbenzoic acid (0.400 g, 2.44 mmol), methanol (3.40 ml, 83.9 mmol), and H$_2$SO$_4$ (0.30 ml, 5.63 mmol) was heated at reflux and under nitrogen atmosphere for 4 h. The mixture was cooled to room temperature and concentrated under reduced pressure. The mixture was poured into a cold 5% sodium bicarbonate solution (15 ml) and extracted with three 10 ml portions of ethyl acetate. The combined organic layers were washed with water (10 ml), two 10 ml portions of brine, and two 10 ml portions of water. The organic layer was dried, filtered, and evaporated to give a pale yellow solid. Yield: 0.347g (80 %). Spectroscopic data were consistent with the previous literature report.[37]

Synthesis of Methyl 4-acetylbenzoate Hydrazone (1). The title compound was prepared according to a modified literature procedure.[38] Methyl 4-acetylbenzoate (0.1087 g, 0.61 mmol) and Girard's reagent T (0.1023 g, 0.61 mmol) were dissolved in EtOH (10 ml, 171.3 mmol) and the mixture was heated at reflux for 2.5 h. After cooling, the solid was filtered, washed with cold EtOH, and recrystallized from EtOH to give a white solid. Yield: 85.8 mg (43 %). mp 207-210 °C. ^{1}H NMR (400 MHz, MeOD-d_4) δ 2.32 (s, 2.43 H, E-isomer), 2.44 (s, 0.55 H, Z-isomer), 3.43 (s, 9H), 3.92 (s, 1H), 7.93-8.06 (m, 2H), 8.15 (d, J=8.7 Hz, 2H). ^{13}C NMR (100 MHz, MeOD-d_4) δ 12.4, 51.3, 53.2, 53.5, 126.2, 126.7, 129.1, 141.9, 149.6, 165.9, 166.6. IR 3029, 2965, 1718, 1275 cm^{-1}. Anal Calc for C$_{15}$H$_{22}$ClN$_3$O$_3$: C, 54.96; H, 6.76; N, 12.82. Found: C, 54.77; H, 6.74; N, 12.81. Calcd: [M]$^+$ (C$_{15}$H$_{22}$ClN$_3$O$_3$) m/z = 292.1656 Found ESI-HRMS: [M]$^+$ m/z = 292.1662.

Synthesis of Methyl 3-acetylbenzoate Hydrazone (2). Compound **13** (0.0964 g, 0.541 mmol) and Girard's reagent T (0.0860 g, 0.513 mmol) were dissolved in EtOH (3 ml, 51.4 mmol) and the mixture was heated at reflux for 2 h. Compound **2** was obtained as a white solid. Yield: 134.0 mg (80 %). mp 214-216 °C. ^{1}H NMR (400 MHz, MeOD-d_4) δ 2.33 (s, 2.38 H, *E*-isomer), 2.44 (s, 0.62 H, *Z*-isomer), 3.43 (s, 9H), 3.93 (s, 3H), 4.47 (s, 0.38 H, *Z*-isomer), 4.84 (s, 1.6 H, *E*-isomer), 7.55 (t, *J*=7.8 Hz, 1H), 8.05-8.14 (m, 2H), 8.40 (s, 0.78 H, *E*-isomer), 8.48 (s, 0.21 H, *Z*-isomer). ^{13}C NMR (100 MHz, MeOD-d_4) δ 12.5, 51.3, 53.2, 53.5, 126.9, 128.4, 130.0, 130.2, 130.4, 130.7, 131.1, 138.8, 149.8, 165.8, 166.7. IR 3019, 2956, 1708, 1260 cm^{-1}. Anal Calc for $C_{15}H_{22}ClN_3O_3$: C, 54.96; H, 6.76; N, 12.82. Found: C, 51.78; H, 6.95; N, 11.92 (monohydrate). Calcd: [M][+] ($C_{15}H_{22}ClN_3O_3$) *m/z* = 292.1656 Found FAB-HRMS: [M][+] *m/z* = 292.1668.

Synthesis of Methyl 4-formylbenzoate Hydrazone (3). The title compound was prepared in a similar manner as **2**, using methyl 4-formylbenzoate (0.1035 g, 0.630 mmol), Girard's reagent T (0.1045 g, 0.620 mmol), and EtOH (8 ml, 137 mmol). Compound **3** was obtained a white solid. Yield: 172.4 mg (89 %). mp 230-233 °C. ^{1}H NMR (100 MHz, MeOD-d_4) δ 3.41 (s, 9H), 3.93 (s, 3H), 7.85 (d, *J*=8.4 Hz, 1.38 H, *E*-isomer), 7.91 (d, *J*=8.4 Hz, 0.38 H, *Z*-isomer), 8.07 (d, *J*=8.0 Hz, 2H), 8.04 (s, 0.87 H, *E*-isomer), 8.30 (s, 0.19 H, *Z*-isomer). ^{13}C NMR (400 MHz, MeOD-d_4) δ 51.4, 53.2, 53.5, 126.9, 129.5, 131.7, 137.9, 165.1, 166.4. IR 3015, 2954, 1700, 1293 cm^{-1}. Anal Calc for $C_{14}H_{20}ClN_3O_3$: C, 53.59; H, 6.42; N, 13.39. Found: too hydroscopic. Calcd: [M][+] ($C_{14}H_{20}ClN_3O_3$) *m/z* = 278.1500 Found ESI-HRMS: [M][+] *m/z* = 278.1595.

Synthesis of Methyl 3-formylbenzoate Hydrazone (4). The title compound was prepared in a similar manner as **2**, using methyl 3-formylbenzoate (0.1115 g, 0.704 mmol), Girard's reagent T (0.1063 g, 0.634 mmol), and EtOH (8 ml, 137.0 mmol). After cooling, the solid was filtered and washed with cold EtOH to give a white solid. Yield: 126.1 mg (63 %). mp 241-242 °C. ^{1}H NMR (400 MHz, MeOD-d_4) δ 3.44 (s, 9H), 3.94 (s, 3H), 4.33 (s, 0.37H, *Z*-isomer), 4.84 (s, 1.63 H, *E*-isomer), 7.57 (t, *J*=7.8 Hz, 1H), 8.00-8.31 (m, 3H), 8.33 (s, 0.79 H, *E*-isomer), 8.43 (s, 0.18 H, *Z*-isomer). ^{13}C NMR (100 MHz, MeOD-d_4) δ 51.4, 53.3, 53.6, 127.8, 128.8, 130.8, 131.2, 134.2, 145.0, 149.4, 165.0, 166.4. IR 3033, 2953, 1701, 1212 cm^{-1}. Anal Calc for $C_{14}H_{20}ClN_3O_3$: C, 53.39; H, 6.42; N, 13.39. Found: C, 53.32; H, 6.43; N, 13.11. Calcd: [M][+] ($C_{14}H_{20}ClN_3O_3$) *m/z* = 278.1500 Found ESI-HRMS: [M][+] *m/z* = 278.1503.

Synthesis of 4-acetylphenyl methyl carbonate Hydrazone (5). The title compound was prepared in a similar manner as **2**, using compound **12** (0.1143 g, 0.589 mmol), Girard's reagent T (0.0974 g, 0.581 mmol), and EtOH (3 ml, 51.4 mmol). Compound **5** was recrystallized from EtOH and ether and obtained as a white solid. Yield: 107.8 mg (31 %). mp 152-152 °C. ^{1}H NMR (400 MHz, MeOD-d_4) δ 2.30 (s, 0.63 H, *Z*-isomer), 2.42 (s, 2.38 H, *E*-isomer), 3.42 (9H), 3.89 (s, 3H), 4.48 (s, 0.41 H, *Z*-isomer), 4.83 (s, 1.67 H, *Z*-isomer), 7.24 (d, *J*=8.3 Hz, 2H), 7.88/7.93 (d, *J*=8.3 Hz, 2H). ^{13}C NMR (100 MHz, MeOD-d_4) δ 53.3, 53.6, 54.7, 120.8, 127.5, 128.0, 135.5, 150.1, 152.3, 154.1, 165.8. IR 3015, 2963, 1770, 1700, 1268, 1218 cm^{-1}. Anal Calc for $C_{15}H_{22}ClN_3O_4$: C, 52.40; H, 6.45; N, 12.22. Found: C, 47.60; H, 6.73; N, 10.99 (dihydrate). Calcd: [M][+] ($C_{15}H_{22}ClN_3O_4$) *m/z* = 308.1605 Found ESI-HRMS: [M][+] *m/z* = 308.1612.

Synthesis of 3-acetylphenyl methyl carbonate Hydrazone (6). The title compound was prepared in a similar manner as **2**, using compound **11** (0.1153 g, 0.594 mmol), Girard's reagent T (0.0971 g, 0.579 mmol), and EtOH (3 ml, 51.4 mmol). Compound **6** was purified by vapor diffusion with ether and obtained as a white solid. Yield: 22.7 mg (11 %). Mp 145-147 °C. ^{1}H NMR (400 MHz, MeOD-d_4) δ 2.31 (s, 2.44 H, *E*-isomer), 2.43 (s, 0.58 H, *Z*-isomer), 3.44 (s, 9H), 3.91 (s, 3H), 4.49/4.84 (s, 2H), 7.26 (d, *J*=8.0, 1H), 7.48 (t, *J*=8.0, 1H), 7.68-7.78 (m, 2H). [13]C (100 MHz, MeOD-d_4) δ 12.6, 53.2, 53.6, 54.6, 118.8, 122.1, 123.9, 129.2, 139.3, 151.4,

154.3, 165.8. IR 3021, 2962, 1763, 1699, 1264, 1206 cm^{-1}. Calcd: [M]$^+$ (C$_{15}$H$_{22}$ClN$_3$O$_4$) m/z = 308.1605 Found ESI-HRMS: [M]$^+$ m/z = 308.1607.

Synthesis of 4-formylphenyl methyl carbonate Hydrazone (7). The title compound was prepared in a similar manner as **2**, using compound **10** (0.1054 g, 0.585 mmol), Girard's reagent T (0.0949 g, 0.566 mmol), and EtOH (2 ml, 34.3 mmol). Compound **7** was obtained as a white solid. Yield: 86.8 mg (49 %). mp 190-191 °C. ^{1}H NMR (400 MHz, MeOD-d_4) δ 3.41 (9H), 3.89 (s, 3H), 4.31 (s, 0.38 H, Z-isomer), 4.81 (s, 1.82 H, E-isomer), 7.27 (d, J=8.5 Hz, 2H), 7.79 (d, J=8.6 Hz, 1.6 H, E-isomer), 7.86 (d, J=8.6 Hz, 0.45 H, Z-isomer), 7.99 (s, 0.81 H, E-isomer), 8.26 (s, 0.21 H, Z-isomer). ^{13}C NMR (100 MHz, MeOD-d_4) δ 53.4, 53.6, 54.7, 121.3, 128.3, 131.6, 145.0, 152.9, 154.0, 165.0. IR 3028, 2959, 1763, 1696, 1271, 1231 cm^{-1}. Anal Calc for C$_{14}$H$_{22}$ClN$_3$O$_4$: C, 50.99; H, 6.11; N, 12.74. Found: C, 48.03; H, 6.22; N, 11.83 (monohydrate). Calcd: [M]$^+$ (C$_{14}$H$_{20}$ClN$_3$O$_4$) m/z = 294.1449 Found ESI-HRMS: [M]$^+$ m/z = 294.1456.

Synthesis of 3-formylphenyl methyl carbonate Hydrazone (8). The title compound was prepared in a similar manner as **2**, using compound **9** (0.1105 g, 0.613 mmol), Girard's reagent T (0.0994 g, 0.593 mmol), and EtOH (2 ml, 34.3 mmol). Compound **8** was obtained as a white solid. Yield: 58.0 mg (31 %). mp 152-156 °C. ^{1}H NMR (400 MHz, MeOD-d_4) δ 3.41 (s, 9H), 3.89 (s, 3H), 4.34 (s, 0.39 H, Z-isomer), 4.81 (s, 1.64 H, E-isomer), 7.27 (d, J=7.8 Hz, 1H), 7.48 (t, J=8.0 Hz, 1H), 7.59-7.87, (m, 2H), 8.00 (s, 0.79 H, E-isomer), 8.27 (s, 0.21 H, Z-isomer). ^{13}C NMR (100 MHz, MeOD-d_4) δ 53.3, 53.6, 54.7, 118.9, 123.3, 125.2, 129.7, 135.3, 144.8, 149.3, 151.7, 154.2, 165.0. IR 3026, 2961, 1763, 1699, 1267, 1241 cm^{-1}. Anal Calc for C$_{14}$H$_{22}$ClN$_3$O$_4$: C, 50.99; H, 6.11; N, 12.74. Found: C, 50.68; H, 6.33; N, 12.39. Calcd: [M]$^+$ (C$_{14}$H$_{20}$ClN$_3$O$_4$) m/z = 294.1449 Found ESI-HRMS: [M]$^+$ m/z = 294.1453.

Synthesis of camptothecin 4-formylbenzoate (14). In a 100 ml round bottom flask, 4-formylbenzoic acid (0.2642 g, 1.76 mmol) was dissolved in DMF (20 drops) and chloroform (15 ml) and cooled to 0 °C. EDC (0.1775 g, 0.926 mmol) and DMAP (0.0732 g, 0.600 mmol) were added, followed by camptothecin (0.1028 g, 0.295 mmol). The solution was allowed to warm to room temperature under a nitrogen atmosphere and stirred for 2 days. The mixture was washed with three 15 ml portions of water and 20 ml followed by 30 ml of saturated bicarbonate solution, and the organic layer was dried, filtered, and evaporated. The product was purified by silica gel chromatography with 1% MeOH in chloroform as the eluent. The product was further purified by recrystallization in acetonitrile to give yellow crystals. Yield: 51.0 mg (36 %). mp 261-262 °C. ^{1}H NMR (500 MHz, CDCl$_3$) δ 1.12 (t, J=7.5 Hz, 3H), 2.32 (dt, J_{AV}=7.2 Hz, 1H), 2.45 (dt, J_{AV}=7.4 Hz, 1H), 5.30 (d, J=4.4 Hz, 2H), 5.46 (d, J=18.9 Hz, 1H), 5.77 (d, J=18.9 Hz, 1H), 7.313 (s, 1H), 7.6 (t, J=7.5 Hz, 1H), 7.80 (t, J=7.7 Hz, 1H), 7.93 (d, J=8.1 Hz, 1H), 8.00 (d, J=8.2 Hz, 2H), 8.14 (d, J=8.6 Hz, 1H), 8.2 (d, J=8.1 Hz, 2H), 8.43 (s, 1H), 10.13 (s, 1H). ^{13}C NMR (125 MHz, CDCl$_3$) δ 7.7, 32.0, 49.9, 67.2, 76.8, 95.9, 120.4, 128.11, 128.12, 128.2, 128.4, 129.3, 129.6, 130.7, 130.8, 131.3, 133.5, 139.7, 145.5, 146.3, 148.6, 152.1, 157.3, 164.3, 167.1, 194.5. IR 3057, 2980, 1757, 1617, 1271 cm^{-1}. Calcd: [M + H]$^+$ (C$_{28}$H$_{21}$N$_2$O$_6$) m/z = 481.1321 Found FAB-HRMS: [M + H]$^+$ m/z = 481.1405.

Synthesis of 4-acetylphenyl camptothecin carbonate (15) was prepared following a modified literature procedure.[39] Camptothecin (0.1024 g, 0.294 mmol) was suspended in methylene chloride (15 ml). Upon addition of triphosgene (0.0342 g, 0.115 mmol) and DMAP (0.1139 g, 0.932 mmol), the yellow solution turned purple and the camptothecin dissolved. After 10 min of stirring, additional triphosgene (5.7 mg, 0.0192 mmol) and DMAP (8.5 mg, 0.0696 mmol) were added to maintain homogeneity. After an additional 10 min of stirring, 4-hydroxy acetophenone (0.2600 g, 1.91 mmol) was added to the solution. The covered solution was stirred under

nitrogen for 18 h. The mixture was washed with 1.0 M NaHSO$_4$ (25 ml), water (25 ml), and brine (25 ml) and the organic layer dried, filtered and evaporated. The product and reactants were purified by silica gel chromatography with 1% MeOH in chloroform as the eluent, but one impurity remained. The product was washed with two 10 ml portions of 5% NaOH, water (10 ml) and brine (10 ml), dried with K$_2$CO$_3$, filtered, and evaporated. The product was purified by silica gel chromatography with 1% MeOH in chloroform as the eluent and obtained as a yellow powder. Yield: 97.3 mg (65 %). mp 269-270 °C. ^{1}H NMR (400 MHz, CDCl$_3$) δ 1.04 (t, J=7.5 Hz, 3H), 2.4 (dt, J=7.2 Hz, 1H), 2.22 (dt, J_{AV}=7.2 Hz, 1H), 2.53 (s, 3H), 5.29 (d, J_{AV}=4.1 Hz, 2H), 5.40 (d, J=17.3 Hz, 1H), 5.68 (d, J=17.3 Hz, 1H), 7.32 (d, J=8.8 Hz, 2H), 7.48 (s, 1H), 7.69 (t, J=7.1 Hz, 1H), 7.86 (t, J=7.8 Hz, 1H), 7.91 (d, J=8.9 Hz, 2H), 7.95 (d, J=8.2 Hz, 1H), 8.27 (d, J=8.5 Hz, 1H), 8.43 (s, 1H). ^{13}C NMR (125 MHz, CDCl$_3$) δ 7.6, 26.6, 31.9, 50.0, 67.4, 78.9, 96.4, 120.7, 121.1, 128.20, 128.23, 128.4, 128.5, 129.1, 129.2, 129.9, 131.2, 131.3, 135.0, 145.0, 151.7, 151.8, 154.1, 157.1, 166.9, 196.6. IR 3062, 2922, 1757, 1685, 1273 cm^{-1}. Calcd: $[M + H]^+$ (C$_{29}$H$_{23}$N$_2$O$_7$) m/z = 511.1427 Found FAB-HRMS: $[M]^+$ m/z = 511.1505.

Procedure for kinetic studies. Hydrazone samples (*ca.* 3-5 x 10^{-5} M) were prepared in four buffers (1X PBS buffer- pH 7.4, pH 6.5; Acetate buffer (0.1 M)- pH 4.0, pH 5.0) with 0.1 % ethanol. Triplicate UV/Vis measurements were recorded at 273.0 nm in quartz cuvettes (1 cm) at 37 °C. Rate constants were determined by calculating the absorbance for the hydrazone, Girard T, and aromatic linker, and plotting the log(Absorbance$_{hydrazone}$) against time.

PLL dendrimer (18)- Synthesized as previously reported.[6]

PLL-G$_2$-(Asp(Glu(NNBoc)$_2$)PEO)$_8$ (19). Compound **18** (958 mg, 202 µmol COOH) and Glu(NNBoc)$_2$ (760 mg, 2.0 mmol) were added to a 20 mL reaction vial. Under a nitrogen atmosphere, DMF (4 mL) was added, followed by DIPEA (700 µL, 5 mmol); upon dissolution, HBTU (767 mg, 2.0 mmol) was added and the reaction stirred at room temperature overnight. The reaction was dialyzed against MeOH in 3500 Da MWCO dialysis with 3 solvent changes over 24 h. Concentration of the bag contents *in vacuo* gave **19** (922 mg) as a white solid. ^{1}H NMR (400 MHz, D$_2$O) δ 1.25 (s, 24H), 1.45 (br s, 110 H), 2.7-3.0 (br m, 66 H), 3.38 (s, 24 H), 3.5-3.9 (br m, 4070 H), 4.1-4.5 (br m, 50H).

PLL-G$_2$-(Asp(Glu(NNCPT-Ket)$_2$)PEO)$_8$ (20a). Compound **19** (134 mg, 142 µmol NNBoc) was dissolved in 1:1 TFA:DCM for 1 h. The solvent was removed by rotary evaporation. The solid was re-dissolved in DCM and evaporated twice to remove residual TFA. The solid was dissolved in DMF (2.5 mL), pyridine (100 µL), and acetic acid (100 µL), and **15** (76 mg, 150 µmol) was added. The reaction was purged with nitrogen and stirred at 60 °C in the dark for 16 h. The reaction was dialyzed against MeOH in 3500 Da MWCO regenerated cellulose with 3 solvent changes over 24 hrs. The sample was dried and the solid material was further purified using a Biorad PD-10 column with water as the eluent. After lyophilization, 100 mg of yellow powder remained. The CPT loading was quantified using the absorbance at 360 nm (ε = 21,856)[40] to be 4.8% (theoretical 6%).

PLL-G$_2$-(Asp(Glu(NNCPT-Ald)$_2$)PEO)$_8$ (20b). Prepared using the same procedure as **20a** execpt using compound **14**. CPT loading was 6.0% (6% theoretical).

EA-G$_1$-Lys(Boc)$_8$ (21). Pentaerythritol (353mg, 2.6 mmol), BocLys(Boc)-ONp (5.500 g, 11.8 mmol) and DMAP (125 mg, 1.0 mmol) were added to a 20 ml reaction vial. Under a nitrogen atmosphere, DMF (5.5 mL) and triethylamine (1.6 mL, 11.5 mmol) were added and the reaction stirred for 48 h. MALDI-ToF analysis confirmed the reaction had gone to completion. *N,N*-dimethylethylene diamine (300 µL, 4.1 mmol) was added to quench excess PNP esters. After 10 min, the mixture was diluted with ether (200 mL) and washed with three 100 mL portions of 1M

NaOH, three 100 mL portions of 1M NaHSO$_4$, 100 mL DI water, and 100 mL of brine. The organic layer was dried over Na$_2$SO$_4$ and evaporated to dryness to give **21** (3.455 g, 93% yield) as a white foam. ^{1}H NMR (400 MHz, CDCl$_3$): δ 1.26-1.49 (m, 88H), 1.58-1.83 (m, 8H), 3.09-3.11 (m, 8H), 4.08-4.18 (m, 12H), 4.80 (s, 4H), 5.3-5.6 (br d, 4H). ^{13}C NMR (100 MHz, CDCl$_3$): δ 22.5, 28.3, 28.4, 29.6, 31.5, 39.9, 53.4, 62.2, 79.0, 79.8, 155.7, 156.1. Calc [M]$^+$ (C$_{69}$H$_{124}$N$_8$O$_{24}$) m/z = 1448.87. Found MALDI-ToF [M+Na]$^+$ m/z = 1470.0.

EA-G$_1$-Lys(NH$_3$TFA)$_8$ (21a). Compound **21** (209 mg, 144 µmol) was dissolved in 1:1 TFA:DCM for 1 h. Quantitative deprotection was confirmed by MALDI-ToF analysis. The solvents were removed under reduced pressure to give **21a** as a gummy solid in quantitative yield. ^{1}H NMR (400 MHz, MeOD): δ 1.40-1.60 (m, 8H), 1.67-1.75 (m, 8H), 1.87-2.10 (m, 8H), 2.99 (t, J = 8 Hz, 8H), 4.21 (t, J = 6 Hz, 4H), 4.40 (s, 8H). ^{13}C NMR (100 MHz, MeOD): δ 21.8, 26.5, 29.5, 38.7, 42.5, 52.3, 62.9, 161.4, 161.7, 168.6. Calc [M]$^+$ (C$_{29}$H$_{60}$N$_8$O$_8$) m/z = 648.45. Found MALDI-ToF [M+H]$^+$ m/z = 649.6.

EA-G$_1$-Lys(Glu(Bn)Boc)$_8$ (22). Compound **21a** (89 mg, 63 µmol) and BocGlu(OBz)-ONp (290 mg, 632 µmol) were added to a 20 ml reaction vial. Under a nitrogen atmosphere, DMF (1 mL) and triethylamine (140 µL, 1.0 mmol) were added and the reaction was allowed to stir for 4 h. MALDI-ToF analysis showed a single peak corresponding to the fully functionalized dendrimer. *N,N*-dimethylethylene diamine (50 µl, 690 µmol) was added to quench excess PNP esters. The reaction was diluted with ethyl acetate (100 mL) and washed with three 50 mL portions of 1M NaHSO$_4$, three 50 mL portions of saturated K$_2$CO$_3$, 50 mL of DI water, and 50 mL brine. The organic layer was dried over Na$_2$SO$_4$ and evaporated to dryness to give **22** (171 mg, 87% yield) as a white foam. ^{1}H NMR (400 MHz, MeOD): δ 1.41-1.56 (bm, 96H), 1.60-1.75 (m, 4H), 1.70-2.13 (m, 16H), 2.25-2.40 (m, 4H), 2.44-2.51 (m, 12H), 2.58-2.61 (m, 4H), 3.10-3.20 (m, 8H), 4.09-4.25 (m, 12H), 4.35-4.40 (m, 4H) 5.08-5.09 (2s, 16H), 7.28-7.38 (m, 40H). ^{13}C NMR (100 MHz, MeOD): δ 23.8, 28.6, 31.5, 40.8, 44.6, 49.0, 54.4, 64.9, 163.4, 163.8, 170.7. Calc [M]$^+$ (C$_{165}$H$_{228}$N$_{16}$O$_{48}$) m/z = 3201.59. Found MALDI-ToF [M+Na]$^+$ m/z = 3223.3.

EA-G$_1$-Lys(Glu(Bn)NH$_3$TFA)$_8$ (22a). Compound **22** (100 mg, 31 µmol) was dissolved in 1:1 TFA:DCM for 1 h. Quantitative deprotection was confirmed by MALDI-ToF analysis. The solvents were removed under reduced pressure to give **22a** as a gummy solid in quantitative yield. ^{1}H NMR (400 MHz, MeOD): δ 1.19-1.35 (m, 16H), 1.45-1.65 (m, 8H), 2.04-2.20 (m, 16H), 2.38-2.46 (m, 8H), 2.51-2.63 (m, 8H), 2.89-2.93 (m, 4H), 3.09-3.12 (m, 4H), 3.89-3.96 (m, 12H), 4.11 (t, J = 4.4 Hz, 4H), 4.30-4.33 (m, 4H), 4.80-5.00 (m, 16H), 7.17-7.26 (m, 40H). ^{13}C NMR (100 MHz, MeOD): δ = 24.1, 27.7, 29.7, 30.3, 30.5, 31.6, 40.2, 53.5, 53.9, 54.1, 63.9, 67.8, 116.7, 119.6, 129.2, 129.3, 129.6, 137.3, 162.8, 163.2, 169.8, 170.3, 172.7, 173.6, 173.8. Calc [M]$^+$ (C$_{125}$H$_{164}$N$_{16}$O$_{32}$) m/z = 2402.73. Found MALDI-ToF [M+Na]$^+$ m/z = 2424.8.

EA-G$_1$-Lys(Glu(Bn)PEO)$_8$ (23). PNP-PEG carbonate (986 mg, 192 µmol) and **22a** (81 mg, 25 µmol NH$_3$) were added to a 20 ml reaction vial. Under a nitrogen atmosphere, DMF (3 mL) was added. After using a warm water bath to dissolve the starting material, triethylamine (120 µL, 0.863 mmol) was added. After stirring for 48 h (reaction monitored by SEC anlaysis), no further increase in the molecular weight was observed and the reaction was considered complete. Piperidine (50 µL, 0.506 mmol) was added to quench remaining PNP carbonate. After 1 h, acetic anhydride (400 µL, 4.24 mmol) was added to acylate any remaining primary amines on the dendrimer that had not reacted with the PNP-PEG carbonate. After stirring an additional hour, the reaction mixture was precipitated into ether (300 mL) and **23** (999 mg) was collected by filtration as a fluffy white solid. In some cases residual 5kDa PEG was observed after the PEGylation was considered complete. This could be removed by dialysis using 100,000 MWCO

tubing against water for 24 hours. ^{1}H NMR (500 MHz, D$_2$O): δ 1.20-1.80 (br m, 24H), 1.80-2.10 (br d, 16H), 2.35-2.55 (br s, 16H), 3.05-3.20 (br s, 8H), 3.38 (s, 24H), 3.40-3.90 (br m, ~3,900H), 4.00-4.40 (br m, 36H), 5.09-5.15 (br s, 16H), 7.25-7.40 (br m, 40H). DMF SEC: Mn: 32,000 Da, Mw: 35,000 Da, PDI: 1.09.

EA-G$_1$-Lys(GluPEO)$_8$ (23a). Compound **23** (402 mg, 10.1 µmol) was added to a 20 ml reaction vial and dissolved in MeOH (9 mL). Activated Pd/C (10 wt%, 50 mg) was added and the reaction put under hydrogen atmosphere. The reaction was stirred overnight, then filtered and solvent removed via rotary evaporation to give **23a** (387 mg) as a white solid. ^{1}H NMR (500 MHz, D$_2$O): δ 1.20-1.80 (br m, 24H), 1.80-2.1 (br d, 16H), 2.40-2.51 (m, 16H), 3.15-3.25 (br s, 8H), 3.38 (s, 24H), 3.40-3.90 (br m, ~3,900H), 4.00-4.40 (br m, ~36H).

EA-G$_1$-Lys(Glu(NNBoc)PEO)$_8$ (24). Compound **23a** (710 mg, 142 µmol COOH), *t*-butyl carbazate (94 mg, 711 µmol), and DMAP (10 mg, 81 µmol) was added to a 20 ml reaction vial. Under a nitrogen atmosphere, DCM (8 mL) was added dropwise. The solution was cooled to 0 ^{o}C followed by the addition of EDC (136 mg, 709 µmol). The reaction was allowed to warm to room temperature and stirred overnight. The reaction was dialyzed against MeOH in 12kDa-14kDa MWCO dialysis with 3 solvent changes over 18 h. Concentration of the bag contents *in vacuo* gave **26** (660 mg) as a white solid. ^{1}H NMR (500 MHz, D$_2$O): δ 1.30-1.60 (br m, 100H), 1.65-2.20 (br m, 20H), 2.30-2.45 (br s, 16H), 3.15-3.25 (br s, 8H), 3.38 (s, 24H), 3.50-3.90 (br m, ~3,900H), 4.00-4.45 (br m, 40H).

EA-G$_1$-Lys(Glu(NNH$_3$TFA)PEO)$_8$ (24a). Compound **24** (102 mg) was dissolved in 1:1 TFA:DCM for 1 h. The solvents were removed under reduced pressure to give **24a** as a gummy solid. Quantitative deprotection was confirmed by ^{1}H NMR.

EA-G$_1$-Lys(Glu(NNDox)PEO)$_8$ (25). Compound **24a** (200 mg, 40 µmol NNBoc) and doxorubicin (70 mg, 120 µmol) were added to a 20 ml reaction vial and were dissolved in MeOH (4 mL), pyridine (130 µL), and acetic acid (130 µL). The reaction was purged with nitrogen and stirred at 60 ^{o}C in the dark for 18 h. The reaction mixture was loaded directly onto a Sephadex LH-20 column and eluted with methanol. The first dark red band was collected and the solvent removed by rotary evaporation. The solid material was further purified using a Biorad PD-10 column with water as the eluent. After lyophilization 175.1 mg of red powder remained. The Dox loading was quantified using the absorbance at 486 nm (ε = 11,500)[40] to be 5.9% (9% theoretical).

EA-G$_1$-Lys(Glu(Gly-CPT)PEO)$_8$ (26). Compound **23a** (520 mg, 104 µmol COOH), camptothecin glycinate trifluoroacetate (97 mg, 239 µmol), HBTU (90.7 mg, 239 µmol), and pentachlorophenol (63.6 mg, 239 µmol) were added to a 20 mL reaction vial and dissolved in DMF (3 mL). After stirring for 5 min, DIPEA (126 µL, 728 µmol) was added. The reaction was purged with nitrogen and stirred in the dark overnight. The reaction mixture was precipitated into rapidly stirring isopropanol (400 mL), filtered, rinsed, and dried overnight under vacuum. The polymer was further purified using a Biorad PD-10 column with water as the eluent. Lyophilization gave compound **26** as a yellow powder (484.4 mg). The CPT loading was quantified using the absorbance at 360 nm (ε = 21,856)[40] to be 3.6% (6% theoretical).

EA-G$_1$-Lys(Glu(Glu-OBn-OtBu))PEO)$_8$ (27). Compound **23a** (350 mg, 70 µmol COOH), Glu(OBn)-OtBu (115 mg, 350 µmol), and 4-dimethylaminopyridine (DMAP) (4.5 mg, 35 µmol) were added to a 20 mL reaction vial, dissolved in DCM (3 mL), and purged with nitrogen. The solution was cooled to 0 ^{o}C followed by the dropwise addition of EDC(67 mg, 350 µmol) and DCM (2 mL) slurry. The reaction was allowed to warm to room temperature and stirred overnight. The reaction was diluted with MeOH (1 mL) and dialyzed against MeOH (700 mL) in

3,500 MWCO regenerated cellulose with 3 solvent changes over 24 hr. The contents of the bag were removed via rotary evaporation to give **27** (330 mg, 94%) as a white solid. . ^{1}H NMR (400 MHz, D$_2$O): δ 1.27-1.69 (br m, 93H), 2.04-2.21 (br d, 39H), 2.30-2.58 (m, 33H), 2.89 (s, 12H), 3.15-3.25 (br s, 23H), 3.34 (s, 26H), 3.40-3.90 (br m, ~3,900H), 4.00-4.40 (br m, ~60H), 5.1 (s, 21H), 7.30-7.43 (m, 40H).

EA-G$_1$-Lys(Glu(Glu-OBn-NNBoc))PEO)$_8$ (28). Compound **27** (460 mg, 92 µmol COOH) was dissolved in 1:1 TFA:DCM for 30 min. Solvents were removed under reduced pressure. The crude material, DMAP (5.6 mg, 46 µmol), and *t*-butyl carbazate (60.8 mg, 460 µmol) were dissolved in DCM (3 mL) and purged with nitrogen. The solution was cooled to 0 ^{o}C followed by the dropwise addition of an EDC (88.2 mg, 460 µmol) and DCM (2 mL) slurry. The reaction was allowed to warm to room temperature and stirred overnight. The reaction was diluted with MeOH (1 mL) and dialyzed against MeOH (500 mL) in 3,500 MWCO regenerated cellulose with 2 solvent changes over 19 hr. The contents of the bag were removed via rotary evaporation to give **28** (410 mg, 89%) as a white solid. ^{1}H NMR (400 MHz, D$_2$O): δ 1.13-1.51 (br m, 103H), 1.72-2.16 (br d, 34H), 2.16-2.50 (m, 31H), 2.93-3.19 (br s, 12H), 3.34 (s, 26H), 3.40-3.90 (br m, ~3,900H), 4.00-4.40 (br m, ~50H), 4.89-5.12 (br s, 18H), 7.13-7.40 (m, 40H).

EA-G$_1$-Lys(Glu(Glu-OH-NNBoc))PEO)$_8$ (28a). Compound **28** (410 mg) was dissolved in MeOH (10 mL) and purged with nitrogen. Activated Pd/C (41 mg) was added and the reaction put under a hydrogen atmosphere. The reaction was stirred overnight, filtered, and dried via rotary evaporation to give **28a** (410 mg) as a white solid. ^{1}H NMR (400 MHz, D$_2$O): δ 1.01-1.70 (br m, 100H), 1.70-2.15 (br d, 34H), 2.18-2.51 (m, 32H), 2.75-3.10 (br s, 12H), 3.28 (s, 26H), 3.40-3.90 (br m, ~3,900H), 4.00-4.40 (br m, ~50H), 4.95-5.10 (br s, 15H).

EA-G$_1$-Lys(Glu(Glu-Gly CPT-NNBoc))PEO)$_8$ (29). Compound **28a** (400 mg, 80 µmol COOH) and camptothecin glycinate trifluoroacetate (74 mg, 184 µmol) were added to a 20 mL reaction vial and dissolved in DMF (3 mL) with mild heating. After cooling to RT, HBTU (70 mg, 184 µmol) and pentachlorophenol (49 mg, 184 µmol) were added. After stirring 5 min, DIPEA (100 µL, 550 µmol) was added and the reaction stirred overnight in the dark. The reaction mixture was precipitated into rapidly stirring isopropanol (400 mL), filtered, rinsed with isopropanol (10 mL) and ether (10 mL), and dried overnight under vacuum to give **29** as a yellow powder (400 mg). The CPT loading was quantified using the absorbance at 360 nm (ε = 21,856)[40] to be 2.6% (6% theoretical).

EA-G$_1$-Lys(Glu(Glu-Gly CPT-NNDox))PEO)$_8$ (30). Compound **29** (525 mg, 105 µmol) was dissolved in 1:1 TFA:DCM for 30 min. Solvents were removed under reduced pressure and deprotection confirmed by ^{1}H NMR. The crude material was dissolved in MeOH (10 mL), pyridine (333 µL), and acetic acid (300 µL) and doxorubicin added (183 mg, 315 µmol). The reaction was purged with nitrogen and stirred at 60 ^{o}C in the dark for 24 hr. The reaction mixture was loaded directly onto a Sephadex LH-20 column and eluted with methanol. The first dark red band was collected and the solvent removed by rotary evaporation. The solid material was further purified using a Biorad PD-10 column with water as the eluent. After lyophilization 520 mg of red powder remained. The Dox loading was quantified using the absorbance at 486 nm (ε = 11,500)[41] to be 1.5% (9% theoretical).

Combination Studies in Cells. The cytotoxicities of EA-Dox, EA-CPT, and EA-CPT-Dox were determined by using the MTT assay with C26 cells. Cells were seeded onto a 96-well plate at a density of 5 x10^3 cells per well in 100 µL of medium and incubated overnight (37 °C, 5% CO$_2$, and 80% humidity). An additional 100 µL of new medium (C26: RPMI medium 1640, 10% FBS, 1% penicillin-streptomycin, 1% Glutamax; HT-29: DMEM, 10% FBS, 1% penicillin-

streptomycin) containing varying concentrations of each dendrimer was added to each well. After incubation for 72 h, 40 μL of media containing thiazolyl blue tetrazolium bromide (5 mg/mL) was added. The cells were incubated for 2 h, after which time the medium was carefully removed. To the resulting purple crystals was added 200 μL of DMSO and 25 μL of pH 10.5 glycine buffer (0.1 M glycine/0.1 M NaCl). Optical densities were measured at 570 nm by a SpectraMAX 190 microplate reader (Molecular Devices, Sunnyvale, CA). Optical densities measured for wells containing cells that received neither dendrimer nor drug were considered to represent 100% viability. Combination Index (CI) values were calculated using CalcuSyn Version 2.0 software (Biosoft, Cambridge, Great Britain).

Animal and Tumor Models. All animal experiments were performed in compliance with National Institutes of Health guidelines for animal research under a protocol approved by the Committee on Animal Research at the University of California (San Francisco, CA) (UCSF). C26 colon carcinoma cells obtained from the UCSF cell culture facility were cultured in RPMI medium 1640 containing 10% FBS. Female BALB/c mice were obtained from Simonsen Laboratories, Inc. (Gilroy, CA).

Toxicity in Healthy Mice. Female Balb/C mice were injected via tail vein injection with either Dend-CPT-DOX or Dend-CPT and Dend-Dox at a 2:1 molar ratio (30 mg CPT/27 mg Dox, 24 mg CPT/21 mg DOX, or 18 mg CPT/16 mg DOX). Mice weight and general health were monitored over 7 days. When gross toxicity was observed, loss of greater than 15% of initial body weight, lethargy and ruffled fur, mice were removed from the study.

Chemotherapy in Balb/C Mice. While under anesthesia, female Balb/C mice were shaved, and C26 cells (3×10^5 cells in 50 μL) were injected subcutaneously in the right hind flank. At eight days post-tumor implantation, mice were randomly distributed into treatment groups of 10 animals. Mice were injected by means of the tail vein with EA-CPT (24 mg/kg), EA-DOX (20 mg/kg), EA-CPT-DOX (24 mg CPT/20 mg DOX, 18 mg CPT/15 mg DOX, 12 mg CPT/10 mg DOX/kg) or EA-CPT and EA-DOX in the same ratios in approximately 200 μL of solution. Mice were weighed and tumors measured every other day. The tumor volume was estimated by measuring the tumor volume in three dimensions with calipers and calculated using the formula tumor volume = length x width x height. Mice were removed from the study when (i) a mouse lost 15% of its initial weight, (ii) any tumor dimension was > 20 mm, or (iii) the mouse was found dead. The mice were followed until the final mouse was removed from the study at day 34. Statistical analysis was performed as previously described[6] using MedCalc 8.2.1.0 for Windows (MedCalc Software, Mariakerke, Belgium). The tumor growth delay was calculated based upon a designated tumor volume of 400 mm^3.

REFERENCES

(1)   Wall, M. E.; Wani, M. C.; Cook, C. E.; Palmer, K. H.; McPhail, A. T.; Sim, G. A. *J. Am. Chem. Soc.* **1966**, *88*, 3888–3890.

(2)   Gabr, A.; Kuin, A.; Aalders, M.; El-Gawly, H.; Smets, L. A. *Cancer Res.* **1997**, *57*, 4811–4816.

(3)   Verma, R. P.; Hansch, C.; About, M.; Article, T. *Pharm. Res.* **2009**, *109*, 213–235.

(4)   Venditto, V. J.; Simanek, E. E. *Mol. Pharmaceutics* **2010**, *7*, 307–349.

(5)   Armstrong, D.; O'Reilly, S. *Oncologist* **1998**, *3*, 4–10.

(6)   Fox, M.; Guillaudeu, S.; Fréchet, J.; Jerger, K.; Macaraeg, N.; Szoka, F. *Mol. Pharmaceutics* **2009**, *6*, 1562–1572.

(7)   Riviere, K. Investigation of the Enhancement of Drug Synergy by Co-delivery in Targeted Liposomes. Ph.D. Thesis, University of California-San Francisco: San Francisco, 2009.

(8)   Lee, C. C.; Gillies, E. R.; Fox, M. E.; Guillaudeu, S. J.; Fréchet, J. M. J.; Dy, E. E.; Szoka, F. C. *Proc. Natl. Acad. Sci. U.S.A.* **2006**, *103*, 16649-16654.

(9)   Guillaudeu, S.; Fox, M.; Haidar, Y.; Dy, E.; Szoka, F.; Fréchet, J. *Bioconjugate Chem.* **2008**, *19*, 461-469.

(10)   Gerweck, L. E.; Seetharaman, K. *Cancer Res.* **1996**, *56*, 1194–1198.

(11)   Kaneko, T.; Willner, D.; Monkovic, I.; Knipe, J. O.; Braslawsky, G. R.; Greenfield, R. S.; Vyas, D. M. *Bioconjugate Chem.* **1991**, *2*, 133–141.

(12)   Ulbrich, K.; Šubr, V. *Adv. Drug Delivery Rev.* **2004**, *56*, 1023–1050.

(13)   Dancey, J. E.; Chen, H. X. *Nat. Rev. Drug Discovery* **2006**, *5*, 649–659.

(14)   Vicent, M. J.; Greco, F.; Nicholson, R. I.; Paul, A.; Griffiths, P. C.; Duncan, R. *Angew. Chem. Int. Ed.* **2005**, *44*, 4061–4066.

(15)   Greco, F.; Vicent, M. J. *Adv. Drug Delivery Rev.* **2009**, *61*, 1203–1213.

(16)   Han, Y.; He, Z.; Schulz, A.; Bronich, T. K.; Jordan, R.; Luxenhofer, R.; Kabanov, A. V. *Mol. Pharmaceutics* **2012** Article ASAP.

(17)   Aryal, S.; Hu, C.-M. J.; Zhang, L. *Mol. Pharmaceutics* **2011**, *8*, 1401–1407.

(18)   Hande, K. R. *Eur. J. Cancer* **1998**, *34*, 1514–1521.

(19)   Lefevre, D.; Riou, J. F.; Ahomadegbe, J. C.; Zhou, D. Y.; Benard, J.; Riou, G. *Biochem. Pharmacol.* **1991**, *41*, 1967–1979.

(20)   Eng, W. K.; McCabe, F. L.; Tan, K. B.; Mattern, M. R.; Hofmann, G. A.; Woessner, R. D.; Hertzberg, R. P.; Johnson, R. K. *Mol. Pharmaceutics* **1990**, *38*, 471–480.

(21)   Pavillard, V.; Kherfellah, D.; Richard, S.; Robert, J.; Montaudon, D. *Br. J. Cancer* **2001**, *85*, 1077–1083.

(22)   Kruger, M.; Beyer, U.; Schumacher, P.; Unger, C.; Zahn, H.; Kartz, F. *Chem. Pharm. Bull.* **1997**, *45*, 399–401.

(23)   Masui, M.; Ohmori, H. *J. Chem. Soc. B* **1967**, 762–771.

(24)   Denkewalter, R. G.; Kolc, J.; Lukasavage, W. J. *US Patent 4,360,646* **1982**.

(25)   Kaufmann, S. H. *Cancer Res.* **1991**, *51*, 1129–1136.

(26)   Kim, R.; Hirabayashi, N.; Nishiyama, M.; Jinushi, K.; Toge, T.; Okada, K. *Int. J. Cancer* **1992**, *50*, 760–766.

(27)   Bertrand, R.; O'Connor, P. M.; Kerrigan, D.; Pommier, Y. *Eur. J. Cancer* **1992**, *28A*, 743–748.

(28)   Hammond, L. A.; Eckardt, J. R.; Ganapathi, R.; Burris, H. A.; Rodriguez, G. A.; Eckhardt, S. G.; Rothenberg, M. L.; Weiss, G. R.; Kuhn, J. G.; Hodges, S.; Von Hoff, D. D.; Rowinsky, E. K. *Clin. Cancer Res.* **1998**, *4*, 1459–1467.

(29)   Fox, M. E. Dendritic polymers for the delivery of chemotherapeutic agents. Ph.D. Thesis, University of California-Berkeley: Berkeley, 2009.

(30)   Chou, T. C.; Talalay, P. *Adv. Enzyme Regul.* **1984**, *22*, 27–55.

(31)   Chou, T.-C. *Pharmacol. Rev.* **2006**, *58*, 621–681.

(32)   Skiles, J. W.; Cava, M. P. *J. Org. Chem.* **1979**, *44*, 409–412.

(33)   Katritzky, A. R.; Wang, Z.; Hall, C. D.; Ji, Y.; Akhmedov, N. G. *Tetrahedron Lett.* **2002**, *43*, 3449–3451.

(34) Neubert, M. E.; Citano, C. M.; Ezenyilimba, M. C.; Jirousek, M. R.; Sabol-keast, S.; Sharma, R. B. *Molecular Crystals and Liquid Crystals* **1991**, *206*, 103–116.

(35) Barcelo, G.; Grenouillat, D.; Senet, J.-P.; Sennyey, G. *Tetrahedron* **1990**, *46*, 1839–1848.

(36) Salem, O. I. A.; Frotscher, M.; Scherer, C.; Neugebauer, A.; Biemel, K.; Streiber, M.; Maas, R.; Hartmann, R. W. *J. Med. Chem.* **2005**, *49*, 748–759.

(37) Chou, S. S. P.; Tsai, C. Y. *J. Org. Chem.* **1988**, *53*, 5305–5308.

(38) Chen, Q.; Deady, L. W.; Baguley, B. C.; Denny, W. A. *J. Med. Chem.* **1994**, *37*, 593–597.

(39) Greenwald, R. B.; Pendri, A.; Conover, C. D.; Lee, C.; Choe, Y. H.; Gilbert, C.; Martinez, A.; Xia, J.; Wu, D.; Hsue, M. *Bioorg. Med. Chem.* **1998**, *6*, 551–562.

(40) Dey, J.; Warner, I. M. *J. Lumin.* **1997**, *71*, 105–114.

(41) Gabbay, E. J.; Grier, D.; Fingerle, R. E.; Reimer, R.; Levy, R.; Pearce, S. W.; Wilson, W. D. *Biochemistry* **1976**, *15*, 2062–2070.

Chapter 3
Exploring Polymeric Chelators for Controlled Release of Oxaliplatin

ABSTRACT

A series of platinum (II) chelators were designed with a range of platinum release rates to investigate the influence of drug release on *in vitro* toxicity and *in vivo* antitumor efficacy. Amino acid inspired chelators containing oxygen, nitrogen, and sulfur ligands were loaded with diaminocyclohexane platinate (DACHPt). We observed a direct correlation between drug release rate and drug toxicity both *in vitro* and *in vivo*. The lower Pt release rate was also correlated with a better tolerability in mice. In the C26 colon carcinoma model, moderately improved survival and reduced tumor growth was achieved with a cysteine chelator which had a lower release rate compared to the other polymers tested and the more traditional dicarboxylate chelator. However, to obtain a therapeutic effect a 22-fold greater amount of the cysteine dendrimer compared to the other treatment groups had to be administered to the animals. Additional biodistribution studies are required to determine if the modest improvement in survival is correlated with a higher accumulation in tumor tissue and increased Pt-DNA adducts.

INTRODUCTION

Platinum (II) drugs are among the more effective and widely used cytotoxic cancer therapies.[1] Platinum complexes have demonstrated both broad antitumor activity and high efficacy, and demonstrated synergistic activity when used in combination with other chemotherapeutic agents.[2] Despite these advantages, clinical use of platinates is often limited by severe side effects. Cisplatin and other Pt(II) analogues are usually administered as inactive prodrugs composed of platinum atoms bearing two amino ligands *cis* to two leaving groups, most commonly dichloride or dicarboxylate.[3] Upon injection and cellular uptake, the leaving groups begin to dissociate from the Pt complex forming the active mono or diaquo species followed by cross-linking of DNA, and ultimately apoptosis or necrosis.[4] Premature ligand disassociation leads to increased toxicity, and Pt can interact with sulfur containing molecules and other circulating biomolecules, leading to drug deactivation or unwanted trafficking.[5–7] Furthermore, Pt drugs are rapidly excreted from the body due to their low molecular weight.[5]

Macromolecular approaches for delivery of platinum prodrugs have shown improvements in drug efficacy, due in large part to the extended circulation half-life of the polymer drug conjugate and the isolation of the polymer bound payload from deactivating agents.[8] The large size and extended circulation time of the macromolecule allows for the conjugated drug to preferentially accumulate at the site of the tumor because of the enhanced permeation and retention (EPR) effect.[9] Polymeric carriers such as linear polymers,[10–12] micellar assemblies,[13–15] dendrimers,[16,17] hyperbranched polymers,[18] and polymeric[19–21] and gold[22] nanoparticles are among the nanoscopic architectures that have been explored for platinum delivery. Direct attachment of Pt(II) drugs to a polymeric architecture is most commonly achieved by noncovalent binding of a pendent carboxylate[8,23] or hydroxyl[24,25] containing chelators.

While the dicarboxylate leaving group is effective for platinum drugs with a short plasma residence, its rapid release is not optimized, and many of the reported platinum delivery systems do not significantly reduce the systemic toxicity of the platinum compared to small molecule platinum drugs.[8] Access Pharmaceuticals has carried out extensive [195]Pt experiments with their

AP5346 polymer to investigate the chelation mode of platinum to an aspartic acid moiety. They observed that platinum chelation exists in a pH dependent equilibrium between the (O,O) and (N,O) forms, proposing the (N,O) form present during circulation converts to the (O,O) form after endocytosis;[10] however, the exact nature of this equilibrium *in vivo* is still uncertain.[10,12,26,27] It is known that the chelation mode can impact release rates of platinum containing polymeric nanoparticles.[21] These studies suggest that the dicarboxylate chelator may not be the best chelator and a more strongly coordinating chelator may improve efficacy.

Inspired by Met residues in the Cu transporter *hCtr1* needed for active Pt transport into cells,[28–30] we designed a series of polymeric Pt(II) chelators designed to modulate *in vivo* toxicity, drug release rates, and tumor Pt accumulation. To the best of our knowledge, this is the first systematic comparison of platinum attached to a single carrier through a variety of coordination modes. A keystone of this work is the development of strong chelators that when paired with a biologically relevant PEGylated dendrimer,[31–33] do not release the active drug until extravasation into tumors has occurred.

RESULTS AND DISCUSSION
Synthesis of PEG-Pt Chelators

We initially synthesized the chelators as part of a small library of polyethylene glycol (PEG) conjugated platinum complexes based on FDA approved Oxaliplatin, and evaluated these molecules with respect to their release rates and *in vitro* toxicity. Differences in ligand strength and ring size were examined in order to correlate toxicity with molecular structure, and ultimately determine complexes capable of effective *in vivo* platinum delivery. Linear polyethylene glycol (PEG) was chosen as a model polymeric carrier due to the ease of functionalization. This allowed for rapid access to a library of characterized PEGylated Pt(II)
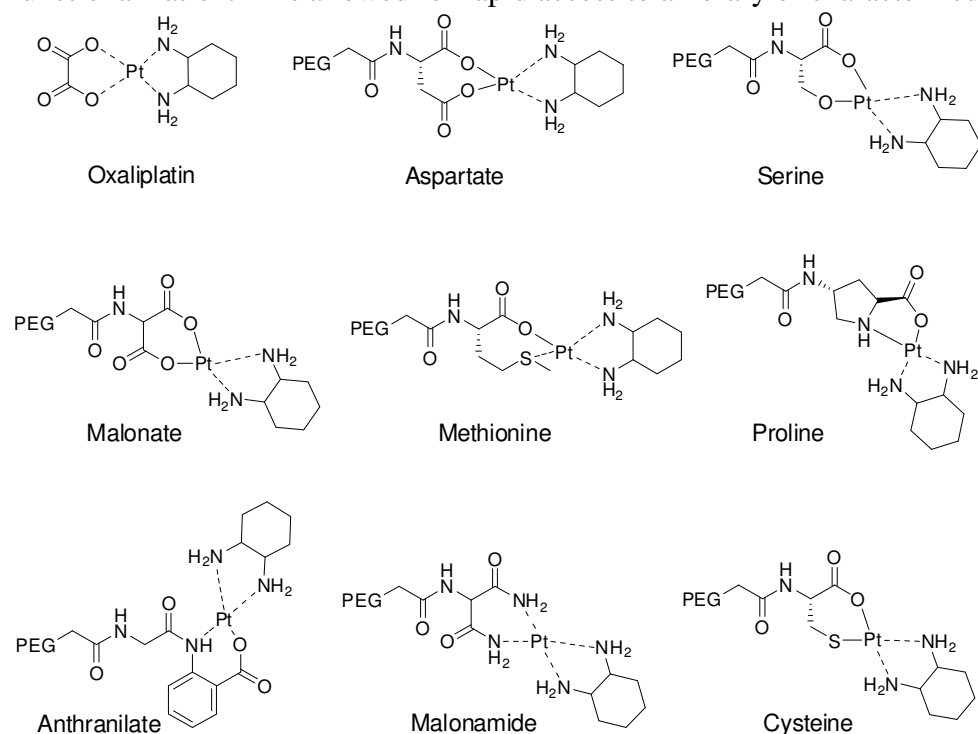

**Figure 3.1.** Structural representation of Oxaliplatin and PEG-Pt complexes.

complexes (Figure 3.1). Amino acids or amino acid-inspired molecules were chosen as chelating moieties because they provide a variety of chelation modes, are readily available, and are easily functionalized. Scheme 3.1 outlines the synthetic approach to a small library of protected chelating derivatives, utilizing one free amine for attachment onto a PEG carrier.

**Scheme 3.1.** Synthesis of PEG-chelators.
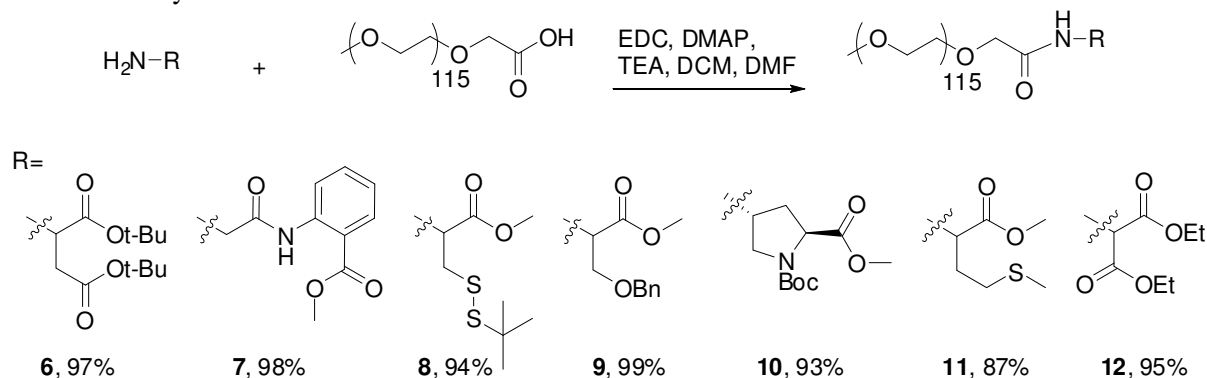
Using standard carbodiimide-mediated amidation chemistry, the ligand precursors were coupled to PEG. The chelator molecules were all either commercially available or prepared from commercial materials (Scheme 3.2). In each case, the product was isolated by precipitation into a rapidly stirring 1:1 mixture of diethylether and isopropanol. The PEG-chelator conjugates were subsequently deprotected and loaded with the dinitrato salt of diaminocyclohexyl palatinate as

Scheme 3.2. Synthesis of chelator precursors.
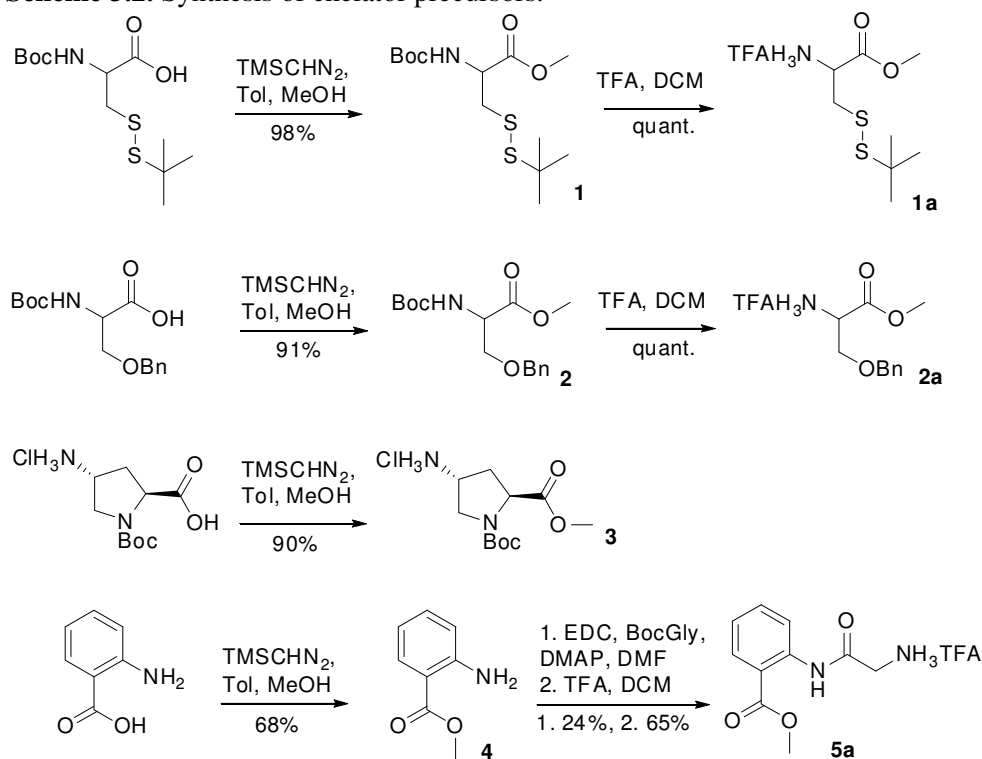
Scheme 3.3. PEG-chelator deprotection and platinum loading.
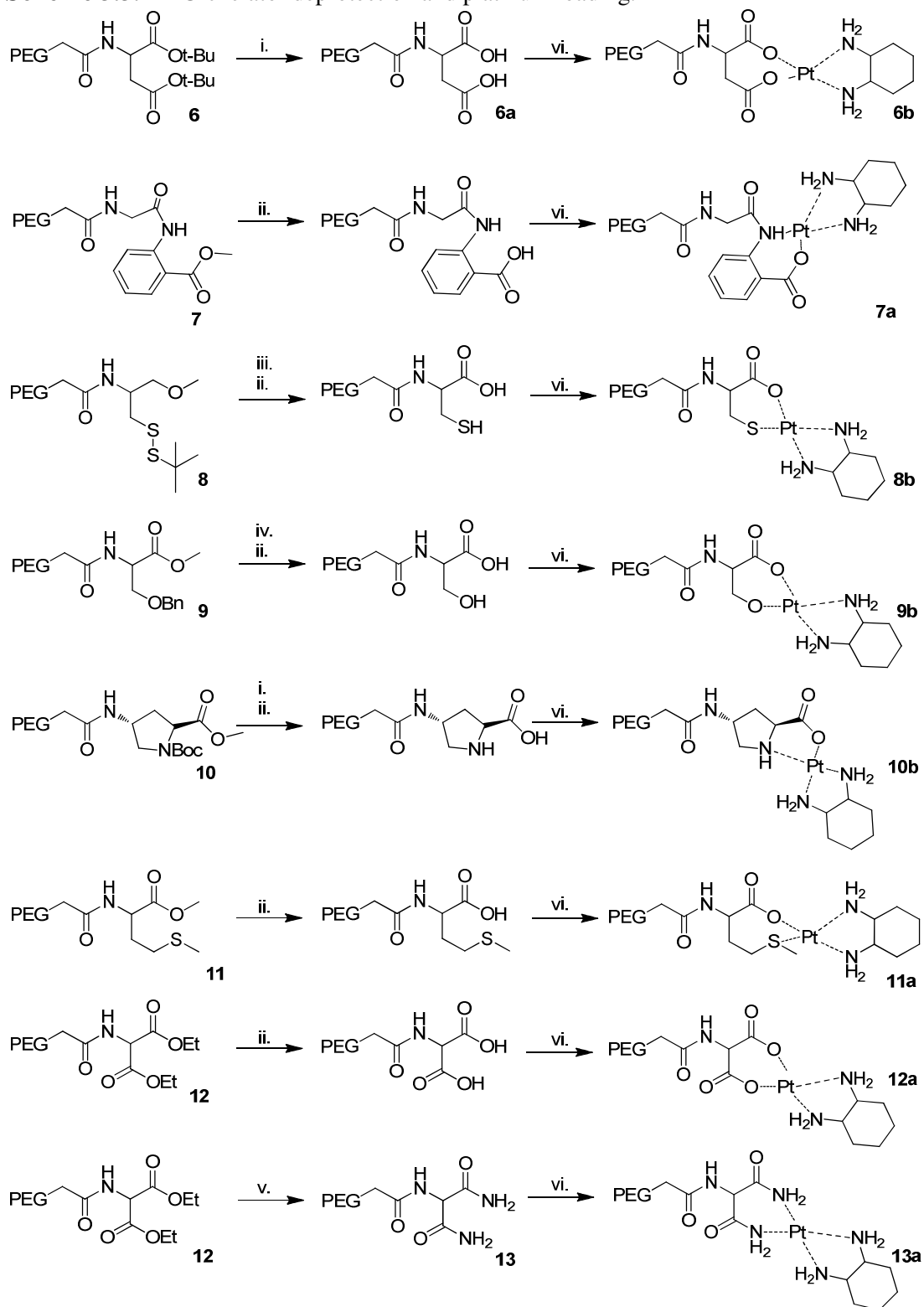
i. TFA, DCM; ii. 2M NaOH; iii. TCEP, H₂O; iv. TFA, Thioanisol, DCM; v. 7N NH₄OH;
vi. DACHPt(NO₃)₂, ~pH 5

shown in Scheme 3.3. It is important to note that under physiological conditions, the PEGylated complexes in Figure 3.1 can convert to additional binding modes in which the proximal amide group acts as a ligand.[10] Due to poor signal-to-noise ratios, we were not able to quantify the presence of multiple binding modes by ^{195}Pt or ^{1}H NMR.

Toxicity and Pt Release

The cytotoxicity of each PEG-Pt complex was measured against C26 colon carcinoma cells and compared to the cytotoxicity of oxaliplatin and cisplatin. Table 3.1 presents IC$_{50}$ and weight percent loading for each derivative. The library was designed to span a range of toxicities as a direct consequence of variation in both ligand strength and ring size, such that softer sulfur and nitrogen ligands should bind more tightly to the Pt(II) center than harder oxygen ligands. As expected carboxylate and hydroxyl chelators showed the highest toxicity in our library and the ligands bearing sulfur atoms showed the greatest decrease in toxicity.

Despite concerns of stable sulfur platinum adducts, each derivative maintained activity, with the IC$_{50}$ values spanning two orders of magnitude in platinum concentration. While sulfur nucleophiles inactivate Pt drugs, a current hypothesis suggests Pt can also be scavenged as the kinetically stable Pt-S adduct, which then converts to the thermodynamically stable DNA-Pt product.[34–36] We hypothesize that incorporating sulfur or nitrogen bearing chelators for platinum delivery could improve the state of the art in platinum delivery systems by preventing premature release and ultimately lead to improved efficacy with greater platinum accumulation in tumor tissue and lowering systemic toxicity.

Table 3.1. Platinum loading and toxicity data in C26 cells for the evaluated polymers.

Compound	Pt Content (wt %)	IC$_{50}$ (μM)
Cisplatin	-	0.4 ± 0.1
Oxaliplatin	-	0.6 ± 0.1
PEG-Aspartate (**6b**)	3.6	6.7 ± 1.4
PEG-Anthranilate (**7a**)	0.7	7.4 ± 6.1
PEG-Serine (**9b**)	0.9	8.4 ± 0.1
PEG-Malonate (**12a**)	2.8	11.2 ± 0.9
PEG-Malonamide (**13a**)	1.3	26.5 ± 1.4
PEG-Proline (**10b**)	0.9	29.3 ± 5.0
PEG-Methionine (**11a**)	3.6	33.3 ± 2.6
PEG-Cysteine (**8b**)	4.8	126.4 ± 2.4
Cisplatin	-	0.6 ± 0.2
Oxaliplatin	-	1.0 ± 2.2
Dend-Aspartate (**17**)	4.0	3.7 ± 7
Dend-Methionine (**18**)	3.4	42.1 ± 14
Dend-Cysteine (**19**)	4.4	62.2 ± 11

The rate of platinum release from the polymer is an important parameter in predicting *in vivo* performance. We expected the cellular toxicity to be directly related to the rate of platinum release because the drug cannot bind to DNA until it has come off the polymer and exposed two open coordination sites. The design criteria for the chelators in our library include, not only the tunability of release rate, but also that the chemistry used to synthesize the molecules be amenable to a variety of more sophisticated and biodegradable delivery systems. For example,

the deprotection conditions should be mild and the platinum loading efficiency should be high. For further study, we chose to determine the release profiles of the aspartate (**6b**), malonate (**12a**), methionine (**11a**) and cysteine (**8b**) conjugates, as they span a range of toxicities and meet these design requirements.

We measured the platinum release using a dialysis procedure that is similar to techniques previously reported.[16,18,21,37–39] Figure 3.2 shows the platinum release for polymers containing each type of linkage. At pH 7.4, our lib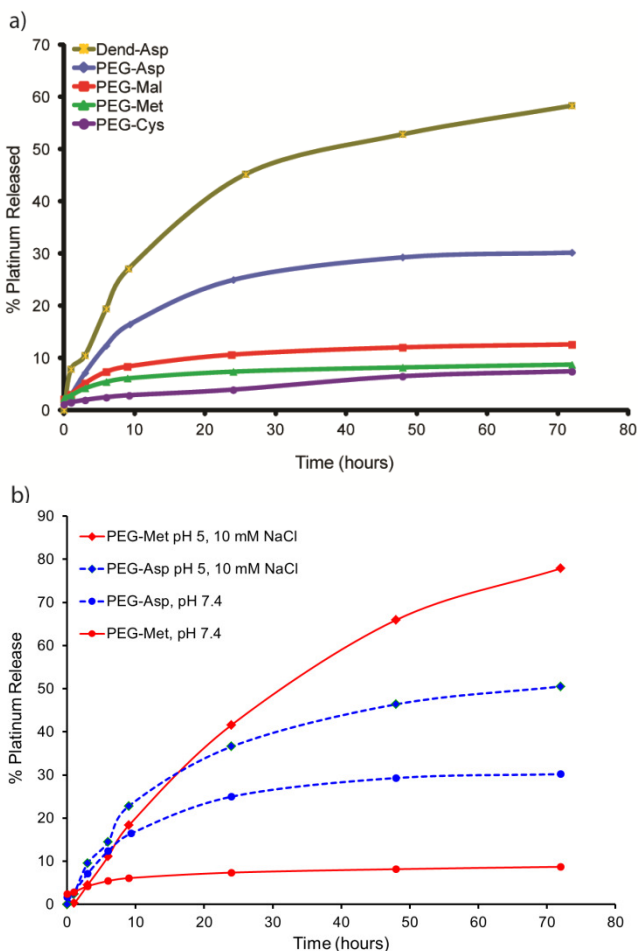rary shows a range of hydrolysis rates, and as expected, the extent of platinum release correlated well with the *in vitro* cytotoxicity. In agreement with previous reports on HPMA carriers, we have found that the aspartate chelator releases small molecule Pt species considerably faster than the malonate chelator due to the decreased chelate stability from the 7-membered ring formed by the aspartate dicarboxylate compared to the 6-membered ring formed by the malonate.[40] The methionine and cysteine linkers both show decreased release rates because of the more favorable Pt-S interactions. Under acidic conditions (pH 5) like those found in the lysosome, PEG-Asp and PEG-Met had similar release profiles, which suggests that a variety of chelators could be active *in vivo*.

Figure 3.2. Hydrolysis of platinum from selected polymers at 37°C. Platinum content analyzed by ICP-AES. a) PBS, pH 7.4 b) Conditions representing *in vivo* conditions encountered by circulating polymers including physiological pH and salt concentrations (pH 7.4/150 mM NaCl), and acidic pH with intracellular salt concentrations (pH 5/10 mM NaCl).

Dendrimer Attachment

After characterizing the platinum chelators with respect to toxicity, rates of hydrolysis, and chemistry, a polymer more suited for *in vivo* applications was selected to replace linear PEG. The PEGylated dendrimer (**14**) chosen is biodegradable and nontoxic, easily functionalized with drug payloads at its core, and has favorable circulation time and uptake by tumor tissue.[30] A series of the platinum drugs were attached to the dendrimer and their *in vivo* activity evaluated as a function of the drug release

rate and *in vitro* toxicity. Specifically, the aspartate, methionine, and cysteine chelators were attached to the dendrimer and loaded with the Pt(II) drug as shown in Scheme 3.4. The aspartate and methionine precursors were commercially available, while the cysteine derivative **16** was prepared by forming the *t*-butyl ester of BocCys(Trityl)-OH. Selective deprotection of the Boc group was achieved by treating **15** with anhydrous hydrochloric acid in dioxane. The 8

Scheme 3.4. Conjugation and platination of aspartate, methionine, and cysteine chelators to PEGylated dendrimer.
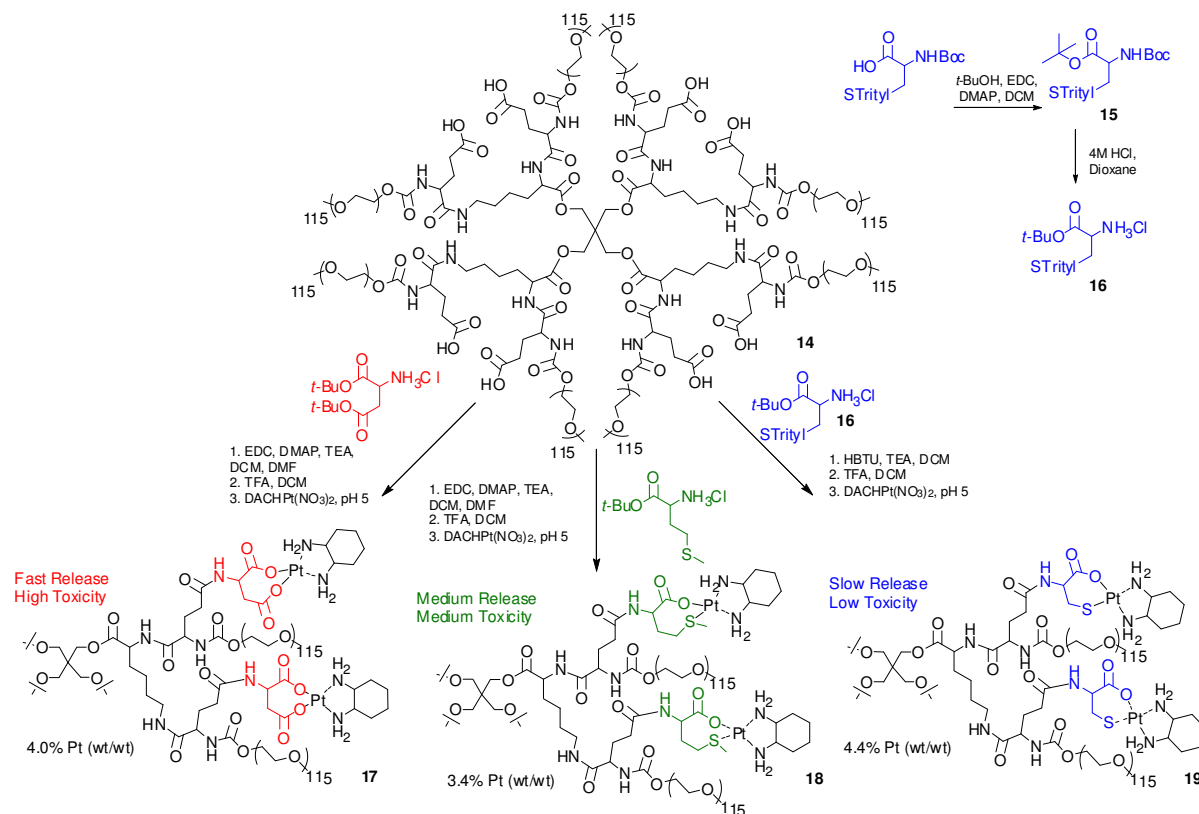
dendrimer carboxylic acids were functionalized with the aspartic acid, methionine and cysteine chelator precursor molecules via amidation reactions. In the case of the cysteine functionlized dendrimer, the more reactive HBTU coupling reagent was used instead of EDC because it provided higher loadings of the bulky, trityl protected ligand onto the dendrimer scaffold. Global cleavage of the protecting groups with trifluoroacetic acid followed by platination gave Dend-Asp (**17**), Dend-Met (**18**), and Dend-Cys (**19**). The excess platinum was removed by aqueous dialysis, the platinum loading determined by ICP, and the cytotoxicity of the three dendrimers
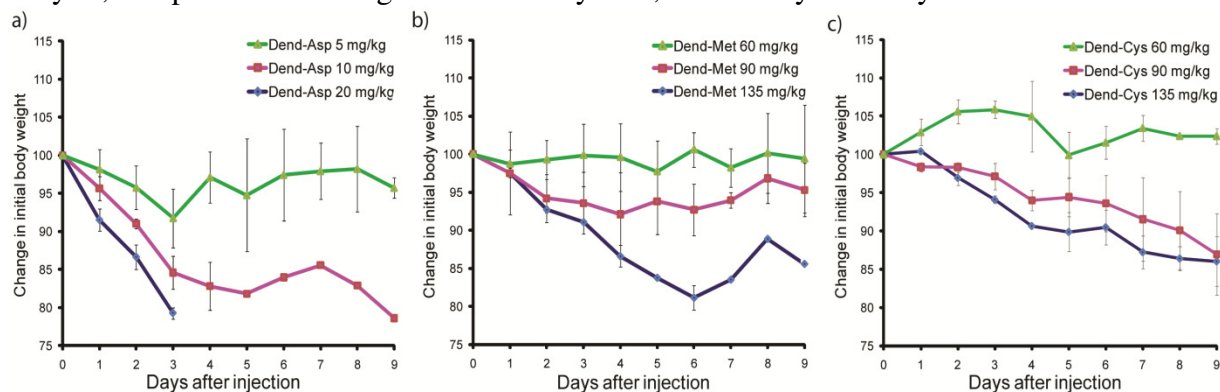

Figure 3.3. Weight loss observed in healthy Balb/C mice injected with (a) Dend-Asp **17**, (b) Dend-Met **18**, (c) Dend-Cys **19**.
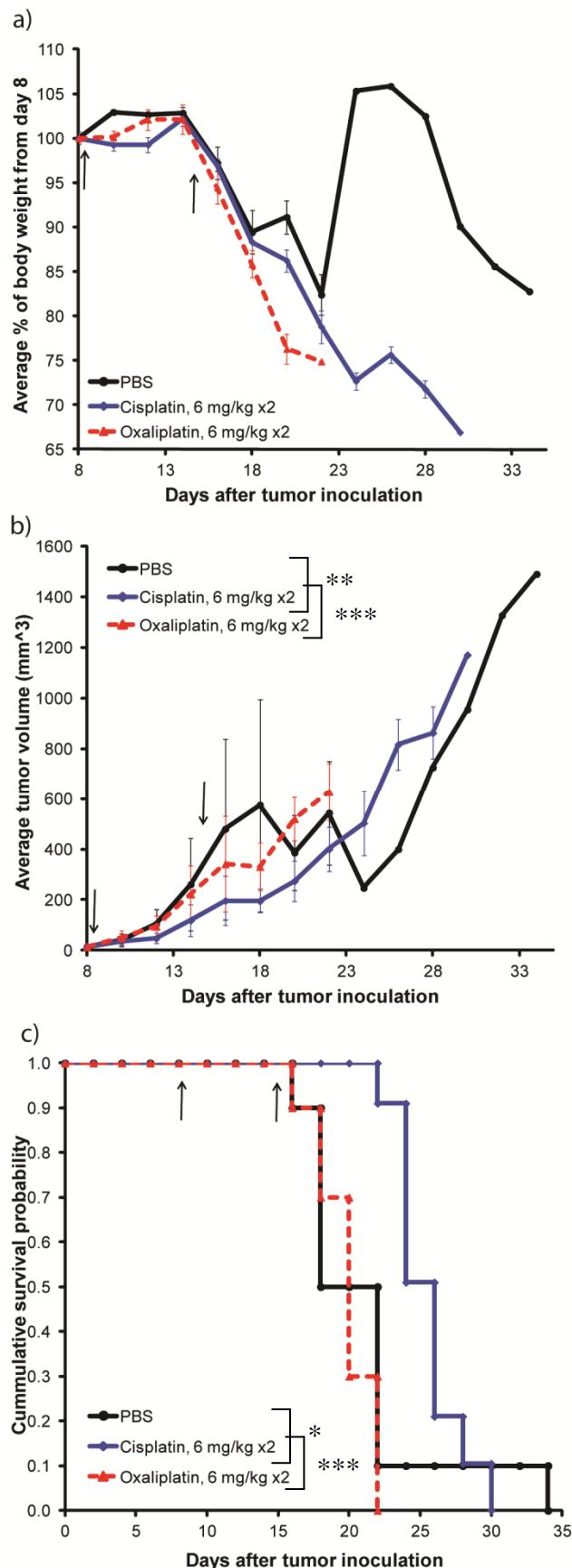
a)

b)

c)

Figure 3.4. Chemotherapy in Balb/C mice tumored with s.c. C26 colon carcinoma. (a) Weight change calculated from day 8. (b) Growth inhibition; tumor growth inhibition calculated from time of growth to 400 mm^3. (c) Kaplan-Meier survival plot. Arrows indicate treatment days. * p < 0.1, ** p < 0.005, *** p < 0.0001.

was measured against C26 cells (Table 3.1). Platinum was released to a greater extent from the dendrimer than from the PEG model system, suggesting the dendritic polymers were good candidates for *in vivo* assessment (Figure 3.2).

In vivo activity

The *in vivo* toxicity of **17**, **18**, and **19** was evaluated in female Balb/C mice. The maximum tolerated dose (MTD) was determined by administering the drug conjugate via tail vein injection at increasing doses, until mice lost >15% of their initial body mass. The *in vivo* toxicity trend followed the *in vitro* toxicity and platinum release trends (Figure 3.3). Dend-Asp had the highest toxicity with a MTD somewhere between 5-10 mg/kg, similar to the free drug. Dend-Met had a maximum tolerated dose of approximately 90 mg/kg and Dend-Cys did not cause a 15% body weight loss even at the highest dose tested, 135 mg/kg.

The antitumor efficacy of the three dendrimers was also evaluated in female Balb/C mice bearing C26 murine colon carcinoma. In a previous study, Oxaliplatin did not significantly extend survival or suppress tumor growth (Figure 3.4); therefore we selected the more robust cisplatin as the positive control. Although the mice lost > 15% of their initial body weight after treatments, blood urea nitrogen levels on day 22 were elevated for mice dosed with Oxaliplatin but lower for cisplatin. Mice were treated with cisplatin (6 mg/kg) and Dend-Asp **17** (6 mg/kg), once a week for 3 weeks, which is the same dosing schedule previously reported for

cisplatin in this model.[41] Dend-Met **18** (90 mg/kg), and Dend-Cys **19** (135 mg/kg) were treated one time at their MTD because of the high platinum dose. We decided that if this high dose did not provide a strong antitumor effect, these polymer platinates would not be candidates for further development. As expected due to Dend-Asp having an equivalent MTD to cisplatin, the two treatments exhibited comparable survival efficacy (Figure 3.5 and Table 3.2). One treatment related death occurred in the cisplatin group, but none of the other mice exhibited toxicity manifested in severe weight loss. Both cisplatin and Dend-Asp groups had one tumor free survivor at the end of the study; however the extended circulation time of the dendrimer[30] reduces toxic deaths, delays tumor growth, and increases average survival time of Dend-Asp. Dend-Cys, despite the very slow release of Pt under physiological conditons, had the best efficacy of all the treatments with better long term survival and tumor growth delay. Gratifyingly, activity was maintained and similar treatment efficacy observed even with a difference in Pt release rates between Dend-Asp and Dend-Cys, suggesting that when properly selected a variety of chelation modes could be effective for platinum delivery.

Table 3.2. In vivo efficacy of dendrimer-Pt and controls against Balb/C mice with C26 colon carcinoma.

Treatment Group	No. mice	Dose (mg/kg)	No. of injections	Treatment days	Mean TGD (%)	Median survival time (days)	LTS
PBS	10	-	1	8	-	20	0
Cisplatin	10	6	3	8,15,22[a]	59[b]	26[c]	1
Dend-Asp (**17**)	10	6	3	8,15,22	88[b]	30[c]	1
Dend-Met (**18**)	10	90	1	8	24	24[b]	0
Dend-Cys (**19**)	10	135	1	8	97[b]	32[c]	2

TGD, tumor growth delay, calculate from time of growth to 400 mm^3; LTS, long term survivors; [a] One treatment related death. [b] Compared to PBS, $p \leq 0.05$. [c] Compared to PBS, $p < 0.005$.
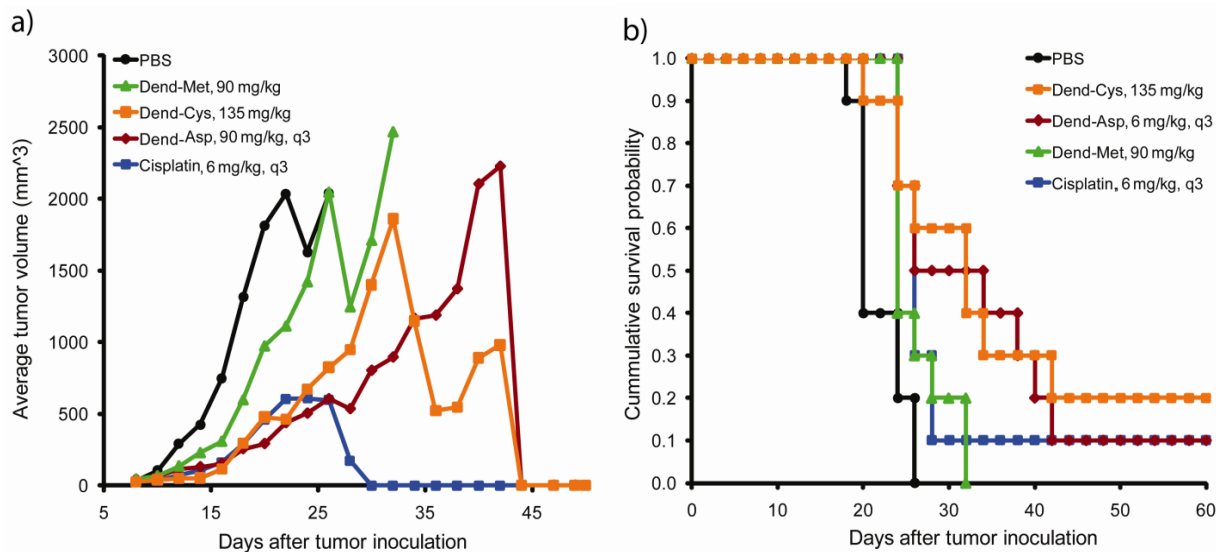
Figure 3.5. Balb/C mice bearing s.c. C26 colon carcinoma treated on day 8 with Dend-Met **18**, Dend-Cys **19**, and PBS or day 8, 15, 22 with Cisplatin and Dend-Asp **17**. (a) Growth inhibition, (b) Kaplan-Meier plot of survival data.

CONCLUSIONS

A family of Pt(II) chelators have been explored for their potential as platinum delivery agents in a wide range of nanomaterials. A range of *in vitro* toxicities as well as drug release rates was observed. This study is the first extensive examination of how various attachment modes of a known drug will alter the drug conjugate toxicity, drug release rates, and *in vivo* activity. We believe that the prolonged stability of sulfur containing chelator complexes, evidenced by slower Pt release at pH 7.4 in the methionine and cysteine chelators, may prevent premature Pt release and reduce uptake by competing endogenous ligands and offers new directions for protecting groups of platinum containing drugs.

EXPERIMENTAL

Materials. Materials were used as obtained from commercial sources unless otherwise noted. The platinum ICP standard was purchased from VHG Labs, Manchester, NH. Dimethylformamide (DMF) and CH_2Cl_2 (DCM) for syntheses were purged 1 h with nitrogen and further dried by passing them through commercially available push stills (Glass Contour). Monomethoxypolyethyleneglycol carboxymethyl (mPEG-CM) was purchased from Laysan Bio, Inc. Solvents were removed under reduced pressure using a rotary evaporator or by vacuum pump evacuation.

Characterization. NMR spectra were recorded on Bruker AV 300, AVB 400, AVQ 400, or DRX 500 MHz instruments. Size exclusion chromatography (SEC) system A consisted of a Waters 515 pump, a Waters 717 autosampler, a Waters 996 Photodiode Array detector (210-600 nm), and a Waters 2414 differential refractive index (RI) detector. SEC was performed at 1.0 mL/min in a PLgel Mixed B (10 μm) and a PLgel Mixed C (5 μm) column (Polymer Laboratories, both 300 x 7.5 mm), in that order, using DMF with 0.2% LiBr as the mobile phase and linear PEO (4,200-478,000 MW) as the calibration standards. The columns were kept at 70 °C. SEC system C consisted of a B Waters Alliance separation module 2695 and a Waters 410

differential RI detector. SEC was performed in a Shodex SB-804 HQ column at ambient temperature using phosphate buffered saline (pH 7.4) as the mobile phase. Inductively coupled plasma-atomic emission spectroscopy (ICP-AES) was carried out on a Perkin Elmer Optima 7000 DV Optical Emission Spectrometer.

General procedure for esterification of chelator precursors.

BocCys(S*t*-Bu)OMe (1). BocCys(S*t*-Bu)OH (210 mg, 0.68 mmol) was dissolved in 4 mL of a 3:2 toluene methanol mixture. Trimethylsilyldiazomethane (TMSCHN$_2$) as a 2M solution in diethyl ether was added dropwise (~850 µl) until a faint yellow color persisted and no gas evolution was observed. After 30 min of stirring at room temperature the solvents were removed to give 213 mg of pure product in 97% yield. ^{1}H NMR (400 MHz, CDCl$_3$): δ 1.31 (s, 9H), 1.44 (s, 9H), 3.14 (d, *J*=4.4 Hz, 2H), 4.58 (d, *J*=7.6 Hz, 1H), 5.38 (d, *J* =7.6, 1H). ^{13}C NMR (100 MHz, CDCl$_3$): δ 28.3, 29.7, 42.6, 48.1, 52.5, 53.1, 80.1, 155.0, 171.2. Calcd [M+Na]$^+$ (C$_{13}$H$_{25}$NO$_4$S$_2$) *m/z*= 346.1123. Found FAB [M+Na] $^+$ *m/z*= 346.1109.

BocSer(OBz)OMe (2). BocSer(OBz)OH (305 mg, 1.03 mmol) was treated as described in the general procedure. 91% yield. ^{1}H NMR (400 MHz, CDCl$_3$) δ 1.45 (s, 9H), 3.73 (s, 3H), 3.76 (dm, *J*=2.8, 2H), 4.43-4.55 (m, 3H), 5.44 (d, *J*=8.4, 1H), 7.25-7.35 (m, 5H). ^{13}C NMR (100 MHz, CDCl$_3$): δ 28.3, 52.4, 53.9, 69.9, 71.8, 73.2, 79.9, 127.6, 127.8, 128.4, 137.5, 155.5, 171.1. Calcd [M]$^+$ (C$_{16}$H$_{23}$NO$_5$) *m/z*= 332.1474. Found FAB [M+Na] $^+$ *m/z*= 332.1468.

2-Amino proline methylester (3). (2S, 4R)-1-Boc-4-Amino-pyrrolidine-2-carboxylic acid•HCl (300 mg, 1.12 mmol) was dissolved in a 3:2 toluene/methanol mixture (2 mL). TMSCHN$_2$ (2M) (450 µl, 0.89 mmol) was added dropwise to the solution. After 45 min, the solvent was evaporated. The residual oil was then flashed through a silica plug using 10% methanol in DCM (90% yield). Note: If an excess of TMSCHN$_2$ is used under extended reaction times, a small amount (< 3%) of N-methylation is observed. ^{1}H NMR (400 MHz, D$_2$O rotamers present): δ 1.39, 1.45 (2s, 9H), 2.17-2.20 (m, 2H), 3.23-3.30 (m, 1H), 3.60-3.67 (m, 2H), 3.79 (s, 3H), 4.41-4.5 (m, 1H). ^{13}C NMR (100 MHz, CDCl$_3$ rotamers present): δ 28.3, 28.4, 39.0, 39.6, 49.6, 50.4, 52.0, 52.2, 54.5, 54.8, 57.9, 58.2, 80.1, 153.8, 154.4, 173.3, 173.6. Calcd [M+H]$^+$ (C$_{11}$H$_{20}$N$_2$O$_4$) *m/z*= 245.1501. Found FAB [M+H] $^+$ *m/z*= 245.1497.

Synthesis of Methyl Anthranoate (4). Anthranilic acid (1 g, 7.3 mmol) was dissolved in a 3:2 toluene/methanol mixture (80 mL). Trimethylsilyldiazomethane (2M) (4 mL, 8 mmol) was added dropwise to the solution until the yellow color in the solution persisted. After 2 h, the solvent was evaporated. A silica gel column was run in 5% ethyl acetate and 95% hexanes to give 754 mg of a yellow oil in 68% yield. ^{1}H NMR (400 MHz, CDCl$_3$): δ 3.85 (s, 3H), 5.66 (bs, 2H), 6.63 (t, *J*=7.6 Hz, 2H), 7.25 (t, *J*=7.2 Hz, 1H), 7.85 (d, *J*=7.2 Hz, 1H). ^{13}C NMR (100 MHz, CDCl$_3$): δ 49.5, 108.7, 114.3, 114.7, 129.2, 132.1, 148.5, 166.6. Calcd [M+H]$^+$ (C$_8$H$_9$NO$_2$) *m/z*= 152.0633. Found EI [M+H] $^+$ *m/z*= 152.0712.

Synthesis of Glycine Boc protected methyl anthranoate (5). Methyl anthranoate (**4**) (356 mg, 2.355 mmol), BocGlyOH (2.475 g, 14.131 mmol), and 4-dimethylaminopyridine (DMAP) (14.4 mg, 0.118 mmol) were dissolved in dry DMF (2 mL). 1-ethyl-3-[3-dimethylaminopropyl]carbodiimide hydrochloride (EDC) (2.708 g, 14.131 mmol) was added. After 16 h, the solution was diluted with ethyl acetate (100 mL) and washed with 1 M NaHSO$_4$ (3 x 100 mL), 1 M NaOH (3 x 100 mL), and water (2 x 100 mL). The organic layer was dried with Na$_2$SO$_4$, filtered, and the solvent was evaporated to yield a yellow oil which was recrystallized with ether/hexanes to give 172 mg of a white crystalline solid in 24% yield. ^{1}H NMR (400 MHz, CDCl$_3$) δ 1.50 (s, 9H), 3.91 (s, 3H), 4.01 (d, *J*=5.6 Hz, 2H), 5.27 (bs, 1H), 7.10

(t, J=7.6 Hz, 1H), 7.54 (t, J=8 Hz, 1H), 7.85 (d, J=8 Hz, 1H), 8.71 (d, J=8.8 Hz, 1H), 11.55 (bs, 1H). ^{13}C NMR (100 MHz, CDCl$_3$): δ 28.4, 45.4, 52.3, 80.3, 115.3, 120.4, 122.9, 130.8, 134.7, 140.9, 155.9, 168.5, 168.6. Calcd [M]$^+$ (C$_{15}$H$_{20}$N$_2$O$_5$) *m/z*= 308.1372. Found EI [M] $^+$ *m/z*= 308.1377.

General procedure for Boc deprotections.

TFA•NH$_3$Cys(S*t*-Bu)OMe (1a). BocCys(S*t*-Bu)OMe (**1**) (105 mg, 0.32 mmol) was placed in a reaction vial equipped with a Teflon septum. The vial was evacuated and backfilled with nitrogen gas. A solution of 1:1 TFA:DCM (3 mL) was added and the reaction was allowed to stir at room temperature for 1 h. The solvents were removed under reduced pressure to give 104 mg of product as a viscous oil in quantitative yield. ^{1}H NMR (400 MHz, MeOD) δ 1.33 (s, 9H), 3.18-3.31 (m, 2H), 3.85 (s, 3H), 4.38 (t, J=4.8 Hz, 1H). ^{13}C NMR (100 MHz, MeOD): δ 28.7, 39.0, 51.6, 52.5, 114.5, 117.4, 159.9, 168.2. Calcd [M+H]$^+$ (C$_8$H$_{17}$NO$_2$S$_2$) *m/z*= 224.0779. Found FAB [M+H] $^+$ *m/z*= 224.0774.

TFA•NH$_3$BocSer(OBz)OMe (2a). Treated as described in the general procedure. ^{1}H NMR (400 MHz, MeOD) δ 3.80-3.98 (m, 2H), 3.70 (s, 3H), 4.19 (t, J=2.4 Hz, 1H), 4.63 (q, J=9.6 Hz, 2H), 7.3-7.36 (m, 5H). ^{13}C NMR (100 MHz, MeOD): δ 52.3, 53.0, 66.4, 73.0, 114.4, 117.2, 127.7, 128.1, 136.9, 159.7, 160.1, 167.6. Calcd [M+H]$^+$ (C$_{11}$H$_{16}$NO$_3$S) *m/z*= 210.1130. Found FAB [M+H] $^+$ *m/z*= 210.1125.

Glycine methyl anthranoate TFA salt (5a). The Boc-protected glycine methyl anthranoate (**5**) (150 mg, 0.487 mmol) was dissolved in a solution of 1:1 TFA:DCM. After 30 min, the solvent was evaporated. The product was recrystallized in methanol/ether to yield a white solid (102 mg, quant). ^{1}H NMR (400 MHz, CDCl$_3$): δ 3.83 (s, 3H), 3.89 (s, 2H), 7.10 (t, J=7.6 Hz, 1H), 7.49 (t, J=8.4 Hz, 1H), 7.93 (d, J=8 Hz, 1H), 8.31 (d, J=8.4 Hz, 1H). ^{13}C NMR (100 MHz, CDCl$_3$): δ 43.8, 54.1, 80.3, 119.6, 123.6, 126.2, 133.1, 136.4, 141.6, 166.9, 170.6. Calcd [M+H]$^+$ (C$_{10}$H$_{12}$N$_2$O$_3$) *m/z*= 209.0926. Found EI [M+H]$^+$ *m/z*= 209.0931.

General procedure for coupling chelators to mPEG-COOH. The general procedure for coupling protected chelators onto linear PEG chains was inspired by a procedure reported by Zhao et al.[42]

Synthesis of PEG-Asp(Ot-Bu)-OtBu (6). mPEG-CM (300 mg, 0.06 mmol), H-Asp(OtBu)-OtBu•HCl (84 mg, 2.99 mmol) and DMAP (5 mg, 0.04 mmol) were added to a reaction vial equipped with a septum. The vial was evacuated and backfilled with N$_2$ three times. Via syringes, 100 µl of triethyl amine, 200 µl of DMF, and 1.5 mL of DCM were added. The solution was cooled to 0ºC and EDC (92 mg, 0.48 mmol) was added. The reaction was allowed to warm to room temperature and stirred overnight before being precipitated into 300 mL of 1:1 isopropanol:ether mixture. The product was isolated (290 mg) as a fluffy solid in 97% yield. ^{1}H NMR (500 MHz, CDCl$_3$): δ 1.37-1.39 (2s, 14H), 2.66-2.79 (dd, 1.5 H) 3.31 (s, 3H), 3.42-3.72 (br m, ~500H), 3.97 (d, J=8 Hz, 1.65 H), 4.66 (m, 0.75H).

Synthesis of PEG-Glycine methyl anthranoate (7). Compound **5a** (82 mg, 0.255 mmol), 5 kDa PEG (254.5 mg, 0.051 mmol), and DMAP (6.2 mg, 0.051 mmol) were added to a 20 mL reaction vial equipped with a septum. The vial was evacuated under vacuum and backfilled with N$_2$ three times. Via a syringe, diisopropylethylamine (DIPEA) (0.044 mL, 0.253 mmol), DMF (0.4 mL) and DCM (3 mL) were added. The solution was then cooled to 0ºC and EDC (78.1 mg, 0.407 mmol) was added. After 16 h, the solution was precipitated into a 1:1 ether/isopropyl alcohol mixture and filtered to yield 248 mg of fluffy white solid in 98% yield. ^{1}H NMR (500

MHz, CDCl$_3$): δ 3.30 (s, 3H), 3.42-3.83 (br m, ~500H), 4.09-4.12 (m, 4H), 7.02 (t, *J*=7.5 Hz, 0.6), 7.46 (t, *J*=7.5 Hz, 0.65), 7.88 (s, 0.86H), 7.94 (d, *J*= 8 Hz, 1H), 8.65 (d, *J*=8 Hz, 1H).

Synthesis of PEG-Cys(St-Bu)-OMe (8). Prepared as according to the general procedure. ^{1}H NMR (500 MHz, D$_2$O): δ 1.34 (s, 9H), 3.1-3.25 (m, 1.8H), 3.36 (s, 3H), 3.54-3.83 (br m, ~500H), 4.14 (d, *J*=5 Hz, 2H), 4.88 (m, 1H).

Synthesis of PEG-Ser(OBn)-OMe (9). Prepared as according to the general procedure. ^{1}H NMR (500 MHz, CDCl$_3$): δ 3.31 (s, 3H), 3.42-3.72 (br m, ~500H), 3.97 (d, *J*=3.5 Hz, 1.65 H), 4.54 (m, 2H, 1.60), 4.75 (m, 1H), 7.28-7.34 (m, 5H).

Synthesis of PEG-Boc-Pro-OMe (10). Prepared as according to the general procedure. ^{1}H NMR (500 MHz, D$_2$O rotamers present): δ 1.39 (s, 6H), 1.44 (s, 3H), 2.35 (m, 2H), 3.37 (s, 3H), 3.54-3.83 (br m, ~500H), 4.07 (s, 1.7H), 4.40-4.50 (m, 1H).

Synthesis of PEG-Met-OMe (11). Prepared as according to the general procedure. ^{1}H NMR (500 MHz, D$_2$O): δ 1.84-1.90 (m, 0.7 H), 1.93 (s, 3H), 2.01-2.04 (m, 0.7H), 2.51-2.68 (m, 1.5H), 3.37 (s, 3H), 3.55-3.83 (br m, ~500H), 4.13 (s, 1.4H), 4.65 (m, 0.6H).

Synthesis of PEG-diethyl Malonate (12). Prepared as according to the general procedure. ^{1}H NMR (500 MHz, CDCl$_3$): δ 1.27 (t, *J*=7 Hz, 6H), 3.36 (s, 3H), 3.54-3.83 (br m, ~500H), 4.18 (s, 2H), 4.29 (m, 4H).

PEG-Asp(OH)-OH Deprotection (6a). PEG-Asp(Ot-Bu)-OtBu (**6**) (250 mg) was dissolved in 1.5 mL of 1:1 DCM: TFA for 3 h at room temperature. The solvents were evaporated and the resulting solid was redissolved in 1 mL of DCM and precipitated into rapidly stirring ether to yield 248 mg of white solid. Complete removal of O*t*-Bu groups confirmed by ^{1}H NMR.

PEG-Cys(SH)-OMe (8a). PEG-Cys(St-Bu)-OMe (**8**) (200 mg) was dissolved in 0.5 mL of Millipore water. Two equivalents of tris-carboxyethyl phosphine (23 mg, 0.08 mmol) were added and the solution was allowed to stir overnight. The resulting solution was dialyzed in methanol using 1000 MWCO regenerated cellulose tubing with three solvent changes over 24 h, and dried to yield 170 mg of white solid. Complete removal of the S*t*-Bu protecting groups was confirmed by ^{1}H NMR.

PEG-Ser(OH)-OMe (9a). PEG-Ser(OBn)-OMe (**9**) (203 mg) was dissolved in 2 mL of 1:1 DCM:TFA and 0.2 mL of thioanisole. The solution was allowed to stir for 24 h before being precipitated into rapidly stirring ether, yielding 180 mg of white solid. Complete removal of the OBn protecting groups was confirmed by ^{1}H NMR.

PEG-Pro-OMe (10a). PEG-Boc-Pro-OMe (**10**) (200 mg) was dissolved in 2 mL of 1:1 DCM:TFA and stirred at room temperature for 3 h. The resulting solution was precipitated into rapidly stirring ether, yielding 185 mg of white solid. Complete removal of the Boc protecting groups was confirmed by ^{1}H NMR.

PEG-Malonamide (13).[43] PEG-diethyl malonate (**12**) (90 mg) was dissolved in 7 N NH$_4$OH and stirred at RT overnight. The resulting solution was precipitated into rapidly stirring ether, yielding 70 mg of white solid. ^{1}H NMR (500 MHz, CDCl$_3$): δ 3.33 (s, 3H), 3.45-3.74 (br m, ~500H), 4.07 (s, 2H), 5.07 (d, *J*=7.5 Hz, 1H), 6.16 (s, 2H), 7.09 (s, 2H), 8.01 (d, *J*=6.5 Hz, 1H).

Dendrimer-Pt synthesis. The synthesis of dendrimer **14** was described in Chapter 2.

BocCys(STrityl)Ot-Bu (15). BocCys(STrityl)OH (5 g, 10.8 mmol) and DMAP (658 mg, 5.4 mmol) were added to a 100 mL round bottom flask. The flask was evacuated and backfilled with nitrogen three times before the addition of 25 mL DCM and *t*-butanol (1.199 g, 18.2 mmol). The solution was cooled to 0 °C and then the EDC was added (2.678 g, 14.0 mmol). The solution slowly warmed to room temperature and stirred overnight. The DCM was evaporated and the

crude material was redissolved in ethyl acetate before being washed with three 100 mL portions of 1M NaHSO$_4$, three 100 mL portions of saturated K$_2$CO$_3$, and one 100 mL portion of brine. The organic layer was dried over sodium sulfated and the solvent removed by rotary evaporation. The residual material was further purified by flash chromatography using 66% hexanes, 33% ethyl acetate as an eluent to give 4.81 grams of white foam in 86% yield. ^{1}H NMR (400 MHz, Acetone d-6) δ 1.37 (s, 9H), 1.42 (s, 9H), 2.56 (ddd, J = 16.84, 12.09, 6.44 Hz, 2H) 3.99 (dt, J = 8.11, 5.03 Hz, 1H), 6.10 (d, J = 8.10 Hz, 1H), 7.26 (t, J = 7.21 Hz, 3H), 7.34 (t, J = 7.59 Hz, 6H), 7.42 (d, J = 7.65 Hz, 6H). ^{13}C NMR (100 MHz, CDCl$_3$): δ 29.04, 29.52, 35.61, 55.62, 68.30, 80.35, 82.89, 128.60, 129.77, 131.29, 131.29, 146.53, 156.91, 171.50. Calcd [M+Na]$^+$ (C$_{31}$H$_{37}$NO$_4$S) m/z= 542.2341. Found FAB [M+Na] $^+$ m/z= 542.2336.

Cl•NH$_3$Cys(STrityl)Ot-Bu (16). Compound **16** was prepared as previously reported.[44] Briefly, **15** (1.005 g, 1.9 mmol) was added to a 100 mL round bottom flask evacuated and backfilled with nitrogen. Via syringe, 1.5 mL of 4M HCl in dioxane was added. The solution was stirred at room temperature for 3 h before the solvent was removed by rotary evaporation. The residual material was purified by column chromatography using 15:5:1 mixture of DCM:ethyl acetate:MeOH as an eluent to give 481 mg of a glassy solid in 55% yield. ^{1}H NMR (400 MHz, MeOD d-4□□□ ppm 1.41 (s, 9H), 2.48 (dq, J = 12.23, 6.25 Hz, 1H), 3.04 (t, J = 6.19 Hz, 1H), 7.19 (t, J = 7.22 Hz, 1H), 7.26 (t, J = 7.50 Hz, 1H), 7.41 (d, J = 7.66 Hz, 1H). ^{13}C NMR (100 MHz, MeOD d-4): δ 28.41, 37.81, 67.95, 82.76, 128.02, 129.14, 130.82, 146.02, 173.87.

General Procedure for chelator attachment to 40,000 Da dendrimer scaffold.

Dendrimer Aspartate protected. Dendrimer **14** (518 mg), Cl•NH$_3$Asp(Ot-Bu)Ot-Bu (292 mg, 1.04 mmol), and DMAP (10 mg, 0.08 mmol) were added to a 20 mL reaction vial equipped with a septum. The vial was evacuated and backfilled with nitrogen before the addition of 4 mL of DCM, 0.6 mL of DMF, and 400 μL TEA. Once all the solids dissolved, the solution was cooled to 0 ^{o}C and EDC (198 mg, 1.04 mmol) was added. The reaction mixture stirred at room temperature overnight before being transferred to a 12,000-14,000 MWCO dialysis bag in methanol. The dialysis solvent was changed four times of 18 hours. The content of the bag was concentrated to give 469 mg of white solid. Product confirmed by ^{1}H NMR.

Dendrimer Methionine protected. Dendrimer **14** (526 mg), Cl•NH$_3$MetOt-Bu (254 mg, 1.04 mmol), and DMAP (10 mg, 0.08 mmol). Recovered 488 mg of white solid. Product confirmed by ^{1}H NMR.

Dendrimer Cysteine protected. Dendrimer **14** (400 mg), **16** (365 mg, 0.8 mmol), HBTU (303 mg, 0.8 mmol). Recovered 423 mg of white solid. Product confirmed by ^{1}H NMR.

General Procedure for Deprotection of Chelator Precursors. In a typical deprotection, dendrimer Asp (233 mg) was added to a 20 mL reaction vial equipped with a septum. The vial was evacuated and backfilled with nitrogen prior to the syringe addition of a premixed solution of 1.5 mL DCM, 1.5 mL of TFA, and 100 μL of triethyl silane. The reaction was allowed to stir at room temperature for approximately 3 h before being precipitated into rapidly stirring ether. The product (183 mg) was collected by filtration as a white solid and confirmed by ^{1}H NMR.

General Procedure for Platinum Loading. Platinum loading was carried out by first preparing a stock solution of the dinitrato salt of DACHPt(OH$_2$)$_2$$^{2+}$. This was done by treating DACHPtCl$_2$ with two equivalents of AgNO$_3$ and a few drops of nitric acid in water at 70°C, a procedure reported by Sood et al.[10] The solution was stirred in the dark for 17 h. The AgCl salts were filtered off through a 0.22 μm Teflon filter. The aspartate (**6a**) and malonamide (**13**)

polymers were dissolved in 1 mL Millipore water followed by the addition of two equivalents of the platinum solution. The solutions were maintained at pH 3-5 by the addition of 1M NaOH and 5% HNO_3 and stirred in the dark at room temperature overnight. The anthranilate (**7**), cysteine (**8a**), serine (**9a**), proline (**10a**), methionine (**11**), and malonate (**12**) polymer conjugates were dissolved in 0.5 mL of 2M NaOH for one hour to saponify the methyl ester protecting groups. To the same reaction vials, portions of the platinum solution were added. The solutions were maintained at pH 3-5 by the addition of 5% HNO_3 and 1M NaOH and stirred in the dark at room temperature overnight. In the case of the PEGylated dendrimers, the deprotected dendrimer-chelators were dissolved in Millipore water at concentration of ~200 mg/mL. The $DACHPt(OH_2)_2^{2+}$ solution (1.5 equivalents per chelator) was added and the pH was raised to 5.5-6.0 by the careful addition of 0.1M NaOH solution. To remove excess small molecule species, the reaction solutions were dialyzed in Millipore water using 3500 MWCO regenerated cellulose with three solvent changes over 24 hours. The residual white fluffy solids were passed through PD-10 size exclusion columns to give PEG-Asp (**6b**), PEG-Ant (**7a**), PEG-Cys (**8b**), PEG-Ser (**9b**), PEG-Pro (**10b**), PEG-Met (**11a**), PEG-Mal (**12a**), PEG-Malonamide (**13a**), Dend-Asp (**17**), Dend-Met (**18**), and Dend-Cys (**19**), followed by Pt loading, cytotoxicity and platinum release measurements.

Measurement of Pt content. The platinum content of each polymer was determined using inductively coupled plasma atomic emission spectroscopy (ICP-AES). First, known quantities of polymer are dissolved in a known volume of water and the platinum concentration is measured. This value is used to back calculated the original weight percentage of platinum on the polymer. Platinum content was measured by weighing out ~5 mg polymer samples on a microbalance and dissolving in 1 mL of Millipore water. The resulting solutions were allowed to sit at room temperature for one hour. From each sample, 400 µl was removed and diluted to 10 mL in a 20% HCl solution. Calibration standards were prepared by successive dilutions 10 mg/L, 5 mg/L, 1 mg/L, 0.1 mg/L and blank in 20% HCl matrix. The resulting calibration curve had a correction coefficient of 0.999993. Samples were measured in triplicate for their emission at 214.423 nm. Free platinum was measured by taking an additional 400 µl of the Pt-PEG solutions and transferred to prewashed Microcon YM-3 ultracentrifugation devices with a nominal molecular weight cut-off of 3 kDa. The devices were centrifuged at 10,000 rpm for 90 min. 275 µl of the filtrate was drawn up and diluted to 10 mL in 20% HCl matrix. The resulting samples were measured for emission at 214.423 nm. In each case, the amount of small molecule platinum species present was less than 0.1%

Platinum Release Measurements. Of the various techniques for platinum release measurements reported, we chose a method inspired by a procedure reported by Cabral et al.[31] A known quantity of PEG-platinum was dissolved in 1X PBS (150 mM NaCl, pH 7.4) and placed inside a dialysis bag. The bag was then placed into 500 ml PBS preheated to 37°C and aliquots are taken out at set time points over a period of 72 hours and measured for platinum content by ICP. As a negative control, an identical experiment was carried out where small molecule oxaliplatin was placed inside the dialysis bag. This was to ensure that the release measurements under diffusion control and sink conditions. The method was changed slightly for the dendrimer samples to avoid the dialysis method. At specific time points, dendrimer-pt aliquots were passed through a PD-10 column to remove free Pt and the resulting polymer measured for platinum by ICP. This method avoided any platinum interaction with the dialysis tubing and the necessity to analyze dilute platinum samples.

Toxicity of PEG-Pt complexes, Dend-Pt complexes, Cisplatin, and Oxaliplatin in C26 cells. Cells were seeded onto a 96-well plate at a density of 5.0 x 10^3 cells per well in 100 μl of medium and incubated overnight (37 °C, 5% CO_2, and 80% humidity). An additional 100 μl of new medium (RPMI medium 1640/10% FBS/1% penicillin-streptomycin) containing either PEG-Pt (**6b, 7a, 8b, 9b, 10b, 11a, 12a, 13a**), Dend-Pt (**17, 18, 19**), or Oxaliplatin with concentrations ranging from 4 nM to 5 mM Pt equivalents, was added to the cells. The tests were conducted in replicates of three for each concentration. After incubation for 72 h, 40 μl of media containing thiazolyl blue tetrazolium bromide solution (5 mg/mL) was added. The cells were incubated for 3 h, after which time the medium was carefully removed. To the resulting purple crystals was added 200 μl of DMSO, followed by 25 μl of pH 10.5 glycine buffer (0.1 M glycine/0.1 M NaCl). The optical densities at 570 nm were measured by using a SpectraMAX 190 microplate reader (Molecular Devices, Sunnyvale, CA). Optical densities measured for wells containing cells that received neither polymer nor drug were considered to represent 100% viability. IC_{50} values were obtained from sigmoidal fits of semilogarithmic plots of the percentage of viability versus platinum concentration by using Origin 7 SR4 8.0552 software (OriginLab, Northhampton, MA).

Animal and Tumor Models. All animal experiments were performed in compliance with National Institutes of Health guidelines for animal research under a protocol approved by the Committee on Animal Research at the University of California (San Francisco, CA) (UCSF). C26 colon carcinoma cells obtained from the UCSF cell culture facility were cultured in RPMI medium 1640 containing 10% FBS. Female BALB/c mice were obtained from Simonsen Laboratories, Inc. (Gilroy, CA).

Maximum Tolerated Dose in Healthy Mice. Female Balb/C mice were injected with via tail vein injection with Dend-Asp **17** (5, 10, and 20 mg/kg), Dend-Met **18** (60, 90, 135 mg/kg), Dend-Cyst **19** (60, 90, and 135 mg/kg). Mice weight and general health was monitored over 9 days. When gross toxicity was observed, loss of greater than 15% of initial body weight, lethargy and ruffled fur, mice were removed from the study.

Platinum Drug Chemotherapy Screen in Balb/C Mice. While under anesthesia, female Balb/C mice were shaved, and C26 cells (3 x 10^5 cells in 50 μL) were injected subcutaneously in the right hind flank. At eight days post-tumor implantation, mice were randomly distributed into treatment groups of 10 animals. Mice were injected by means of the tail vein with cisplatin (6 mg/kg once a week for 2 weeks) or oxaliplatin (6 mg/kg once a week for 2 weeks) in approximately 200 μL of solution. Mice were weighed and tumors measured every other day. Blood urea nitrogen levels were quantified with Quantichrome Urea Assay Kit (BioAssay Systems, Hayward, CA). The tumor volume was estimated by measuring the tumor volume in three dimension with calipers and calculated using the formula tumor volume = length x width x height. Mice were removed from the study when (i) a mouse lost 15% of its initial weight, (ii) any tumor dimension was > 20 mm, or (iii) the mouse was found dead. The mice were followed until the final mouse was removed from the study at day 34. Statistical analysis was performed as previously described[45] using MedCalc 8.2.1.0 for Windows (MedCalc Software, Mariakerke, Belgium). The tumor growth delay was calculated based upon a designated tumor volume of 400 mm^3.

Chemotherapy Experiment in Tumored Mice. While under anesthesia, female Balb/C mice were shaved, and C26 cells (3 x 10^5 cells in 50 μL) were injected subcutaneously in the right hand flank. At eight days post-tumor implantation, mice were randomly distributed into treatment groups of 10 animals. Mice were injected by means of the tail vein with cisplatin (6

mg/kg once a week for 3 weeks), Dend-Asp **17** (6 mg/kg once a week for 3 weeks), Dend-Met **18** (90 mg/kg), or Dend-Cys **19** (135 mg/kg) in approximately 200 µL of solution. Mice were weighed and tumors measured every other day. Mice were treated as described above.

REFERENCES

(1)   Weiss, R. B.; Christian, M. C. *Drugs* **1993**, *46*, 360–377.

(2)   Kelland, L. *Nat. Rev. Cancer* **2007**, *7*, 573–84.

(3)   Wang, X.; Guo, Z. *Dalton T.* **2008**, 1521–1532.

(4)   Jung, Y.; Lippard, S. J. *Chem. Rev.* **2007**, *107*, 1387–1407.

(5)   Siddik, Z. H.; Newell, D. R.; Boxall, F. E.; Harrap, K. R. *Biochem. Pharmacol.* **1987**, *36*, 1925–1932.

(6)   Reedijk, J. *Chem. Rev.* **1999**, *99*, 2499–2510.

(7)   Hegmans, A.; Kasparkova, J.; Vrana, O.; Kelland, L. R.; Brabec, V.; Farrell, N. P. *J. Med. Chem.* **2008**, *51*, 2254–2260.

(8)   Haxton, K. J.; Burt, H. M. *J. Pharm. Sci.* **2009**, *98*, 2299–2316.

(9)   Matsumura, Y.; Maeda, H. *Cancer Res.* **1986**, *46*, 6387–6392.

(10)   Sood, P.; Thurmond, K. B.; Jacob, J. E.; Waller, L. K.; Silva, G. O.; Stewart, D. R.; Nowotnik, D. P. *Bioconjugate Chem.* **2006**, *17*, 1270–1279.

(11)   Ye, H.; Jin, L.; Hu, R.; Yi, Z.; Li, J.; Wu, Y.; Xi, X.; Wu, Z. *Biomaterials* **2006**, *27*, 5958–5965.

(12)   Song, R.; Joo Jun, Y.; Ik Kim, J.; Jin, C.; Sohn, Y. S. *J. Control. Release* **2005**, *105*, 142–150.

(13)   Cabral, H.; Nishiyama, N.; Kataoka, K. *J. Control. Release* **2007**, *121*, 146–155.

(14)   Huynh, V. T.; Chen, G.; de Souza, P.; Stenzel, M. H. *Biomacromolecules* **2011**, *12*, 1738–1751.

(15)   Kaida, S.; Cabral, H.; Kumagai, M.; Kishimura, A.; Terada, Y.; Sekino, M.; Aoki, I.; Nishiyama, N.; Tani, T.; Kataoka, K. *Cancer Res.* **2010**, *70*, 7031–7041.

(16)   Malik, N.; Evagorou, E. G.; Duncan, R. *Anticancer Drugs* **1999**, *10*, 767–776.

(17)   Kapp, T.; Dullin, A.; Gust, R. *Bioconjugate Chem.* **2010**, *21*, 328–337.

(18)   Haxton, K. J.; Burt, H. M. *Dalton T.* **2008**, 5872–5875.

(19)   Dhar, S.; Gu, F. X.; Langer, R.; Farokhzad, O. C.; Lippard, S. J. *Proc. Natl. Acad. Sci. U.S.A.* **2008**, *105*, 17356–17361.

(20)   Aryal, S.; Hu, C.-M. J.; Zhang, L. *ACS Nano* **2009**, *4*, 251–258.

(21)   Paraskar, A. S.; Soni, S.; Chin, K. T.; Chaudhuri, P.; Muto, K. W.; Berkowitz, J.; Handlogten, M. W.; Alves, N. J.; Bilgicer, B.; Dinulescu, D. M.; Mashelkar, R. A.; Sengupta, S. *Proc. Natl. Acad. Sci. U.S.A.* **2010**, *107*, 12435–12440.

(22)   Dhar, S.; Daniel, W. L.; Giljohann, D. A.; Mirkin, C. A.; Lippard, S. J. *J. Am. Chem. Soc.* **2009**, *131*, 14652–14653.

(23)   Wang, Y.; Kang, G.; Zhao, M.; Wu, J.; Zhang, X.; Yang, Y.; Liu, J.; Peng, S. *Mol. BioSyst.* **2011**, *7*, 3245-3254.

(24)   Johnson, M. T.; Komane, L. L.; N′da, D. D.; Neuse, E. W. *J. Appl. Polym. Sci.* **2005**, *96*, 10–19.

(25)   Neuse, E. W.; Mphephu, N.; Netshifhefhe, H. M.; Johnson, M. T. *Polym. Adv. Technol.* **2002**, *13*, 884–894.

(26)   Furin, A.; Guiotto, A.; Baccichetti, F.; Pasut, G.; Deuschel, C.; Bertani, R.; Veronese, F. M. *Eur. J. Med. Chem.* **2003**, *38*, 739–749.

(27) Kim, Y.-S.; Song, R.; Chung, H. C.; Jun, M. J.; Sohn, Y. S. *J. Inorg. Biochem.* **2004**, *98*, 98–104.

(28) Ishida, S.; Lee, J.; Thiele, D. J.; Herskowitz, I. *Proc. Natl. Acad. Sci. U.S.A.* **2002**, *99*, 14298–14302.

(29) Arnesano, F.; Scintilla, S.; Natile, G. *Angew. Chem., Int. Ed.* **2007**, *46*, 9062–9064.

(30) Arnesano, F.; Banci, L.; Bertini, I.; Felli, I. C.; Losacco, M.; Natile, G. *J. Am. Chem. Soc.* **2011**, *133*, 18361–18369.

(31) van Der Poll, D. G.; Kieler-Ferguson, H. M.; Floyd, W. C.; Guillaudeu, S. J.; Jerger, K.; Szoka, F. C.; Fréchet, J. M. *Bioconjugate Chem.* **2010**, *21*, 764–73.

(32) Lee, C. C.; Gillies, E. R.; Fox, M. E.; Guillaudeu, S. J.; Fréchet, J. M. J.; Dy, E. E.; Szoka, F. C. *Proc. Natl. Acad. Sci. U.S.A.* **2006**, *103*, 16649–16654.

(33) Guillaudeu, S. J.; Fox, M. E.; Haidar, Y. M.; Dy, E. E.; Szoka, F. C.; Fréchet, J. M. J. *Bioconjugate Chem.* **2008**, *19*, 461–469.

(34) van Boom, S. S. G. E.; Reedijk, J. *J. Chem. Soc., Chem. Commun.* **1993**, 1397-1398.

(35) Barnham, K. J.; Djuran, M. I.; del Socorro Murdoch, P.; Sadler, P. J. *J. Chem. Soc., Chem. Commun.* **1994**, 721–722.

(36) Reedijk, J. *Chem. Comm.* **1996**, 801–806.

(37) Rieter, W. J.; Pott, K. M.; Taylor, K. M. L.; Lin, W. *J. Am. Chem. Soc.* **2008**, *130*, 11584–11585.

(38) Cabral, H.; Nishiyama, N.; Okazaki, S.; Koyama, H.; Kataoka, K. *J. Control. Release* **2005**, *101*, 223–232.

(39) Ohya, Y.; Shirakawa, S.; Matsumoto, M.; Ouchi, T. *Polym. Adv. Technol.* **2000**, *11*, 635–641.

(40) Gianasi, E.; Buckley, R. G.; Latigo, J.; Wasil, M.; Duncan, R. *J. Drug Targeting* **2002**, *10*, 549–556.

(41) Newman, M. S.; Colbern, G. T.; Working, P. K.; Engbers, C.; Amantea, M. a *Cancer Chemother. Pharmacol.* **1999**, *43*, 1–7.

(42) Zhao, H.; Rubio, B.; Sapra, P.; Wu, D.; Reddy, P.; Sai, P.; Martinez, A.; Gao, Y.; Lozanguiez, Y.; Longley, C.; Greenberger, L. M.; Horak, I. D. *Bioconjugate Chem.* **2008**, *19*, 849–859.

(43) Laxer, A.; Major, D. T.; Gottlieb, H. E.; Fischer, B. *J. Org. Chem.* **2001**, *66*, 5463–5481.

(44) West, K. R.; Bake, K. D.; Otto, S. *Org. Lett.* **2005**, *7*, 2615–2618.

(45) Fox, M.; Guillaudeu, S.; Fréchet, J.; Jerger, K.; Macaraeg, N.; Szoka, F. *Mol. Pharmaceutics* **2009**, *6*, 1562–1572.

Chapter 4
Redesigning Platinum (II) Drugs for pH Sensitive Polymeric Delivery

ABSTRACT

A challenge for polymeric delivery of platinum (II) is to devise a way to attach the organometallic complex to the polymer in an efficient manner so it can be released from the polymer in the tumor. Most platinum delivery platforms rely upon coordination through carboxylic acid based chelators which can release platinum before tumor extravasation has occurred. Here we report an approach toward pH sensitive release of platinum (II) drugs via a hydrazone linkage to improve tumor uptake and reduce toxicity. A small library of new platinum (II) drugs containing a ketone were prepared and evaluated with respect to *in vitro* and *in vivo* toxicity as well as antitumor activity. Complexes forming a 6-membered platinum chelate with appended aromatic ligands, had toxicities comparable to Oxaliplatin.

INTRODUCTION

Platinum (II) polymeric delivery has focused on a sustained release mechanism whereby platinum is attached to the polymer through the leaving group portion of the drug (Figure 4.1a). Installing a triggered release mechanism for the cytotoxic payload holds great potential to further decrease systemic toxicity, improve tumor uptake, reduce acquired resistance, and counteract platinum inactivation. Recent efforts to improve platinum anticancer drugs have focused on the development of small molecule Pt(IV) prodrugs that are activated to Pt(II) drugs after an intracellular reduction event.[1,2] The Lippard group has collaborated with a number of drug delivery groups to attach the Pt(IV) prodrugs to a polymer support such as peptides,[3] carbon nanotubes,[4] PEG-PLGA nanoparticles[5] and gold nanoparticles.[6] There is also a recent report of incorporating Pt(IV) prodrugs into a nanoparticle via a hydrazone linkage to create a carrier that is redox and pH responsive.[7] Our group has had success using our PEGylated dendrimer scaffold with doxorubicin attached through a hydrazone;[8–10] therefore, we hypothesized that a platinum (II) drug could be attached to a polymer through a hydrazone with a
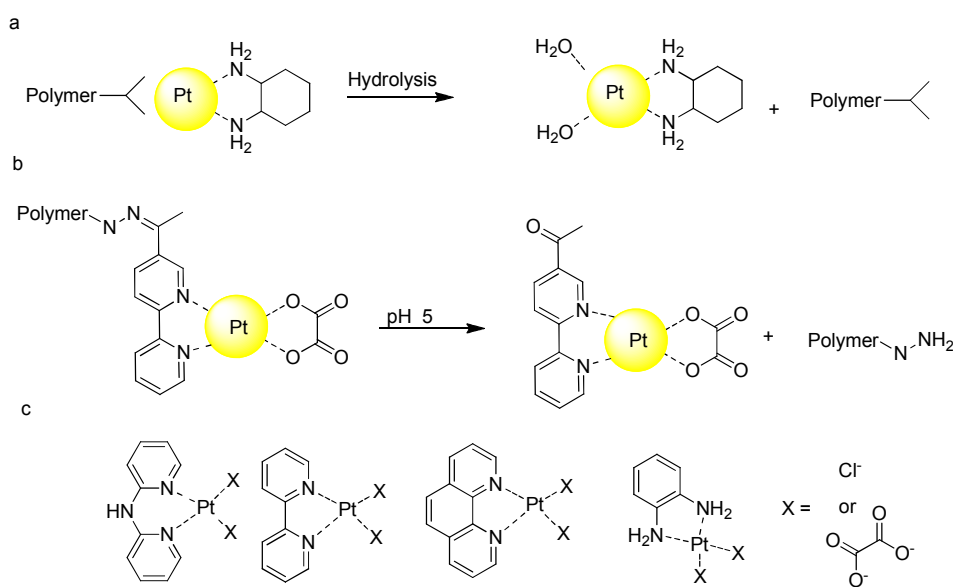

Figure 4.1. Platinum strategies. (a) sustained platinum release. (b) pH triggered platinum release. (c) representative aromatic ligands for platinum drugs.

54

diamine ligand containing a ketone. Figure 4.1b outlines an approach in which the diamine portion of the drug is appended with a ketone moiety that can then be attached to a hydrazide containing polymer. The drugs will be stably bound while circulating in the blood, but undergo selective release in the acidic compartments of the tumor tissue.

Potential drug scaffolds include heterocyclic bidentate ligands, such as those shown in Figure 4.1c, which have gained interest in the literature for exhibiting high potency *in vitro,* reduced platinum deactivation by sulfur nucleophiles, and increased activity against cisplatin resistant cancer cell lines.[11–23] The size and shape of these ligands can not only affect the potency and stability of the drug, but also an ability to limit cellular resistance.[24] Thus far, poor solubility and bioavailability have limited their continued application and success *in vivo.* We believe these ligands are amenable to use with our polymer delivery system to improve solubility, bioavailability, and tumor targeting.

RESULTS AND DISCUSSION
Design and synthesis of ketone containing Pt (II) ligands

To rapidly assemble a diverse library of bidentate Pt(II) derivatives, a modular synthesis relying on standard cross-coupling chemistry was designed. We selected 2-bromo-5-acetopyridine (**1**) as the primary component because it gave us the versatility to explore a variety of heterocyclic building blocks. It should be noted that 2-pyridine boronic acid could not be coupled to **2** under any of standard Suzuki conditions, a documented challenge;[25] however, stannyl pyridine (**1**) coupled to **2** in good yield. The 8-quinoline boronic acid could be coupled to

Scheme 4.1. Synthesis of platinum (II) complexes containing a ketone.
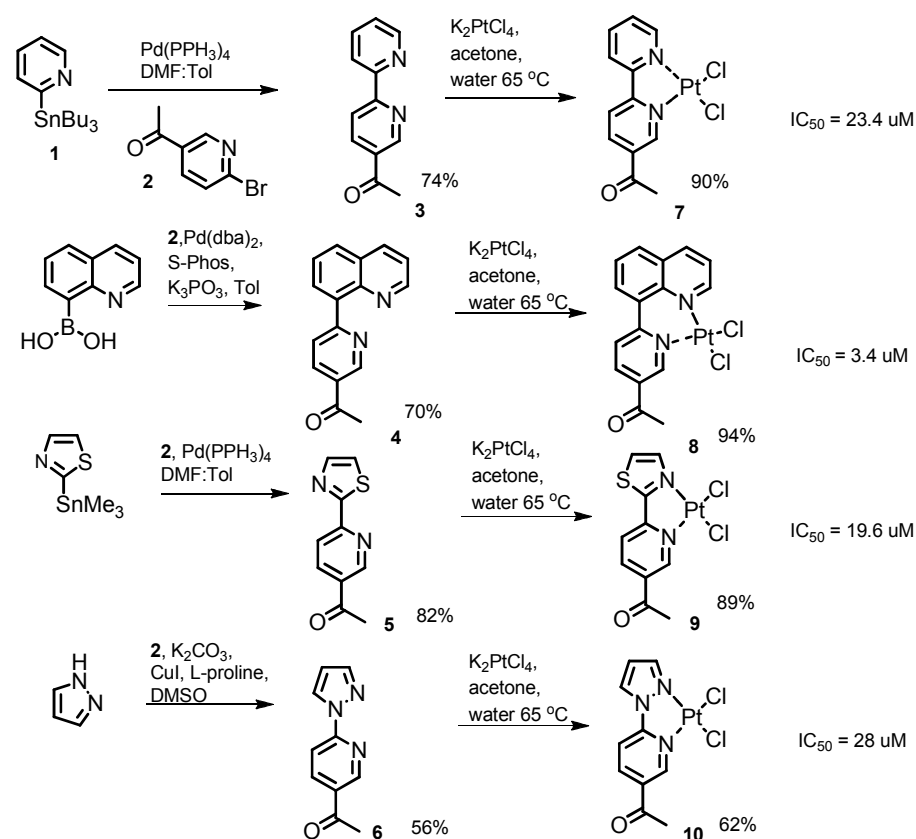
2 by a Suzuki coupling to give **4**. The pyridine-thiazole ligand (**5**) was prepared by a Stille coupling between **2** and 2-trimethystannyl thiazol. Finally, the pyrazole-pyridine ligand (**6**) was prepared by a copper catalyzed Ullman-like C-N bond formation between **2** and pyrazole. The ligands were dissolved in acetone and added drop wise to a stirring solution of K_2PtCl_4 at 65˚C to form the platinum complexes shown in Scheme 4.1. The toxicity of the four complexes was measured against Oxaliplatin (IC_{50} =1.2 uM) in the C26 cell line,

with only Quinoline (**8**), which formed a 6-membered complex, having comparable toxicity. Despite only minor changes to ligand structure, Bipy (**7**), Thiazole (**9**), and Pyrazole (**10**), which all formed a 5-membered complex, were over an order of magnitude less toxic than Oxaliplatin. It should be noted that the lack of water solubility required the complexes to be dissolved in DMSO before dilution (1:10) with media. Unfortunately, DMSO can inactivate palatinates via insertion,[26] so the compounds were briefly heated for < 5 min to increase solubility. If heated for up to 1h, the complexes lost all activity. To examine if the platinum interfered with pH dependent hydrazone hydrolysis, drug release from the polymer was measured. In this study, the only complex with measurable release was the Pyrazole. The reduction in release for the other complexes is not understood.

After quantifying both the toxicity and hydrazone release activity of the four complexes, we designed a SAR study to better understand the factors contributing to ligand potency, including steric bulk, ketone electronics, and chelator geometry. Because drug release from the polymer is essential for favorable activity, the pyrazole complex **10** was selected as the parent drug from which all modifications would be made. We envisioned that the pyrazole could be modified in the 4 position using bromination and subsequent cross-coupling chemistry to append bulky ligands such as a *t*-butylphenyl group and increase activity. As previously mentioned, this method is a modular way to access a number of different complexes from a common starting material. Likewise, because the ketone is in conjugation with the ligand, resonance and inductive effects may play a significant role in the hydrolysis of the complex. Therefore, changing the position of the ketone on the complex may offer additional control over the rate of hydrolysis. Lastly, we were interested in exploring whether the 6-membered Pt chelate formed by the quinoline complex had any effect on potency and could be applied to other complexes.

We began the SAR study with synthesis of several bulky chelators (Scheme 4.2). Selective bromination of the pyrazole complex could be achieved using *N*-bromo succinimide to give compound **11**. Next, two different arylboronic acids were Suzuki coupled onto the bromopyrazole to give ligands **12** and **13**. Additionally, 3-trimethylstannyl pyridine was attached using a Stille coupling to give **14**. The final pyrazole-pyridine ligand, **15**, was made with the same Ullman type coupling between 2-bromo-5-aceto-pyridine and 3,5-dimethylpyrazole. The platinum was loaded as previously described. Each ligand was dissolved in acetone and added dropwise to a solution of K_2PtCl_4 in water at 65˚C. The cytoxicity of each derivative is listed underneath the final structure. As a control, the toxicity of **11**-**15** and K_2PtCl_4 salt were measured and found to be negligible. Interestingly, steric bulk did improve chelator potency, but only for phenyl based ligands- tbutyl phenyl (**18**) and mesitylene (**17**). The addition of pyridine (**19**), bromide (**16**), or pyrazole methylation (**20**) had a negative effect on cytotoxicity causing a decrease in potency as compared to the original four complexes.

Scheme 4.2. Second generation of platinum complexes with enhanced steric bulk.

IC$_{50}$ = 37.4 µM   9.9 µM   4.1 µM   34.8 µM   49.0 µM
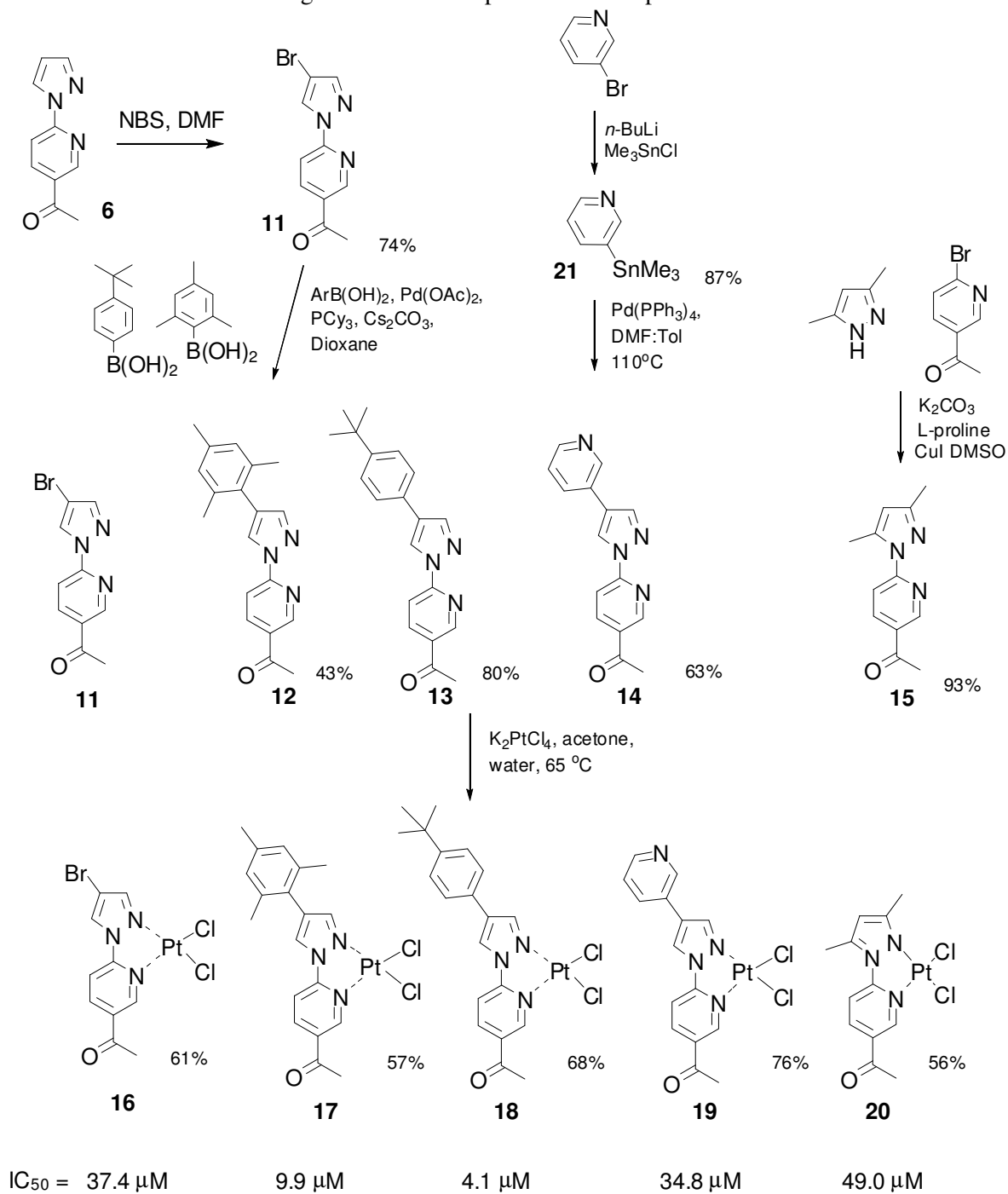
After the importance of ligand bulk was probed, the final series of complexes (Scheme 4.3) were synthesized, in which the location of the ketone and the chelator geometry is altered. First, compound **23** was prepared as a building block for ligands **29** and **30**. These ligands are of interest because they are structurally similar to the ligands used to make complexes **17**-**19**, however as illustrated in Figure 4.2, the ketone in **29** is more electron rich than the ketone in **30**.

We hypothesized that the *meta* and aliphatic ketones would exhibit more rapid hydrazone release profiles. Secondly, a pyrazole-quinoline starting material (**25**) was constructed such that 6-membered chelates could be combined with the varied ketone positions. Ligands **31**-**33** were

Scheme 4.3. Synthesis of platinum complexes with different ketone positions and chelator geometry.
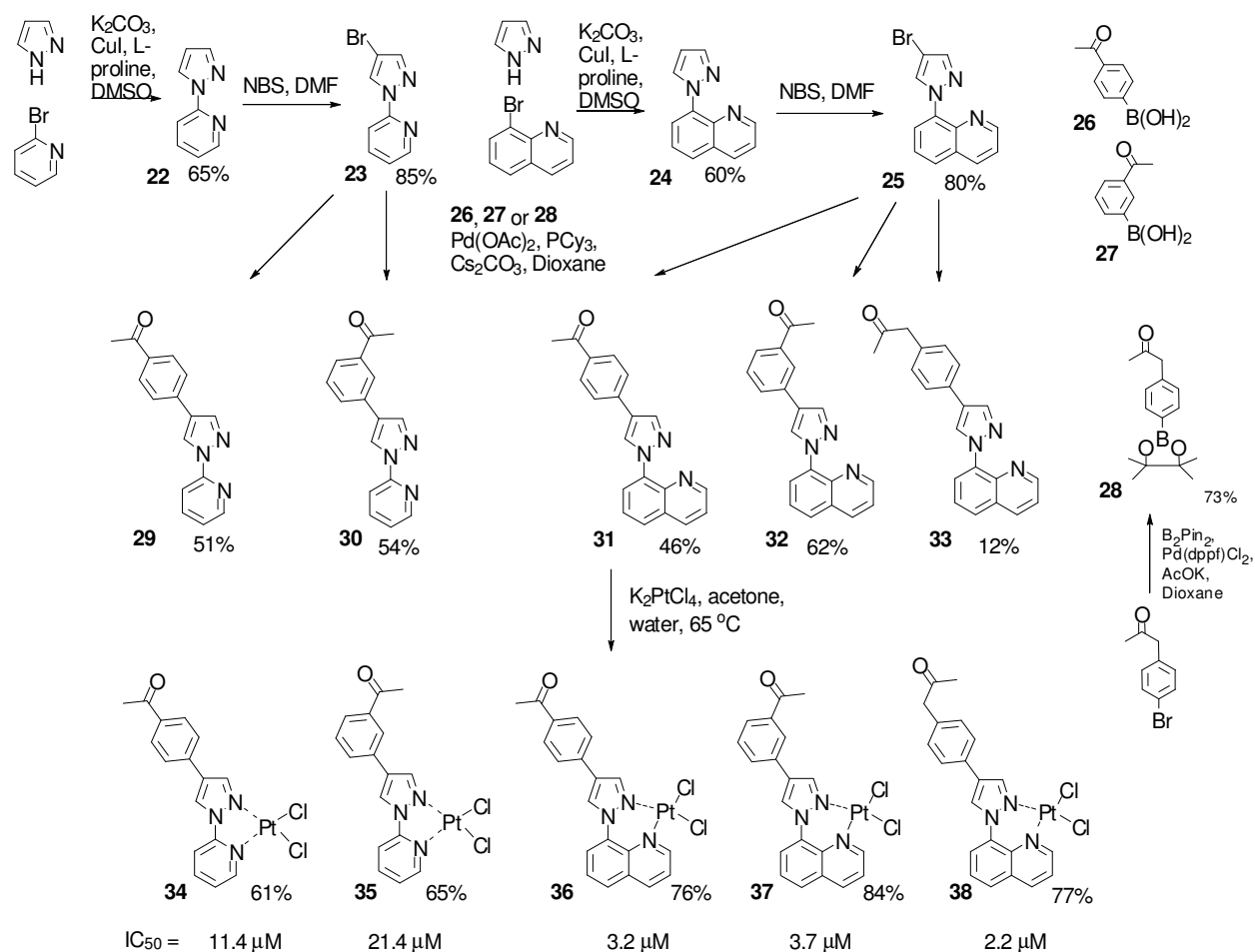
prepared with the same chemistry as **29** and **30** but can form the more potent 6-membered chelate. The ligand **33** also differs in that there is a methylene spacer between the ketone and the aromatic system. The result is a hydrazone that should be much less affected by electronic resonance and induction. While the ketone location doesn't affect the toxicity of the small molecule, the addition of the 6-membered chelate dramatically increased the toxicity of complexes **36-38** (Para, Meta, and Aliphatic respectively) compared to that of the original quinoline complex.
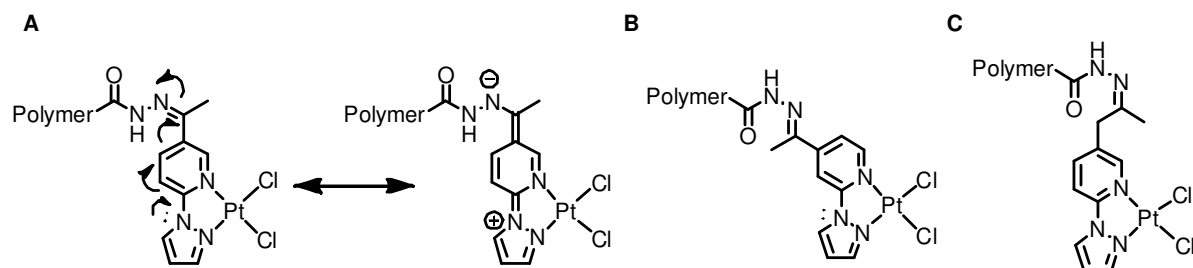
Figure 4.2. Electronic considerations for hydrazone hydrolysis with A) *para*-aromatic ketone. B) *meta*-aromatic ketone. C) aliphatic ketone.

To explore this change in toxicity, computational models of the complexes were generated by the Gaussian 09 program and the optimized structures for Quin and Bipy are shown in Figure 4.3. When observing the molecules from the flat face, few differences are observed. However, when the complex is viewed down the plane of the square planar geometry, the 6-membered quinoline is puckered, exposing the platinum atom while the bipy ligand maintains a completely planar complex. This could allow Quin to bind DNA more efficiently, alter the Pt-DNA adduct to inhibit DNA repair resulting in higher potency, or protect the platinum from deactivation. Cisplatin and other square planar species tend to undergo an associative mechanism of substitution where sulfur nucleophiles attack platinum and a leaving group is subsequently removed. Access to the platinum center is more limited with sterically hindered molecules and a dissociative mechanism is believed to be preferred, where a ligand must leave before glutathione can coordinate.[27] This is an unfavorable mechanism so sulfur coordination and subsequent degradation is limited.
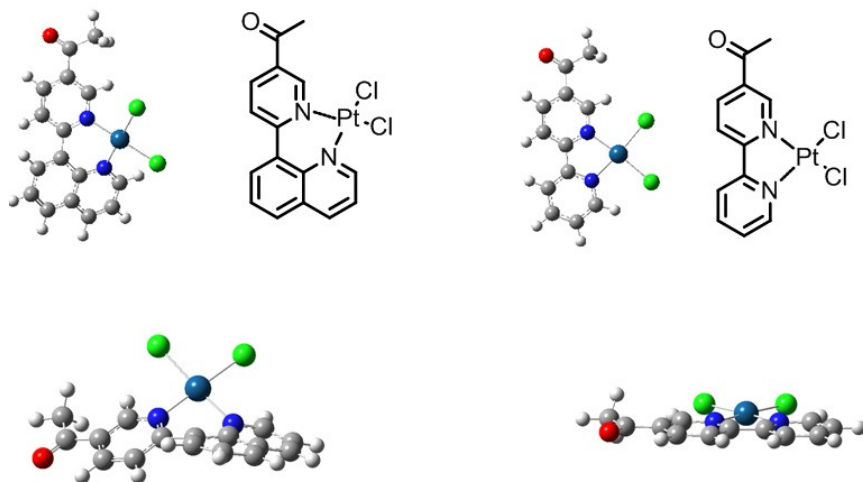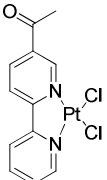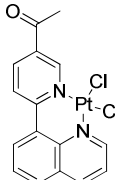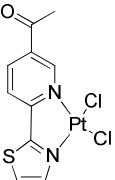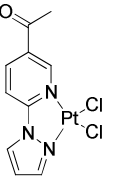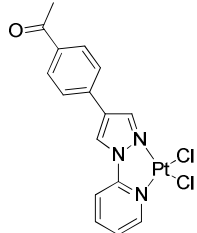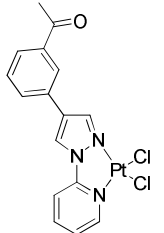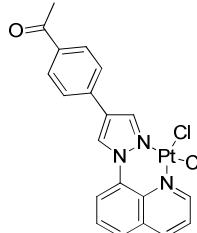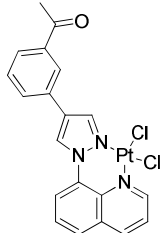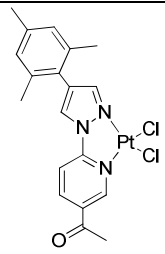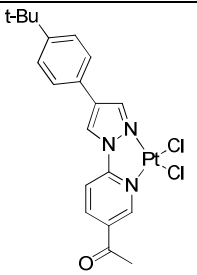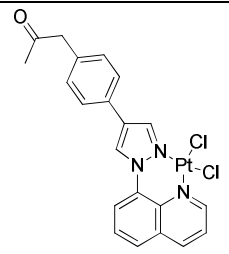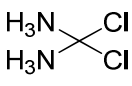

Figure 4.3. Comparison of complex geometries based on gas phase calculations.

Additionally, the entire library was screened against a variety of human cancer cell lines. Because platinum activity varies widely between cancers, it was important confirm that activity was not specific to just mouse models or colon cancers. As seen in Table 4.1, while all the platinates were less cytotoxic in the human cancers, the general trends in toxicity were preserved.

Furthermore, chelates containing 6-membered rings were consistently more toxic than those containing 5-membered rings (Figure 4.3).

Table 4.1. Comparative toxicities of Pt compounds with C26 (murine colon), HeLa (human cerivcal), SK-BR-3 (human breast), A549 (human lung), and CAOV-3 (human ovarian) cells.

Bipy IC$_{50}$ (uM) C26 23.5 HeLa 40.0 SK-BR-3 27.0 A549 68.1 CAOV-3 62.4	**Quinoline** IC$_{50}$ (uM) C26 3.8 HeLa 16.3 SK-BR-3 11.7 A549 50.9 CAOV-3 12.5	**Thiazole** IC$_{50}$ (uM) C26 22.1 HeLa 22.3 SK-BR-3 18.0 A549 50.5 CAOV-3 26.6	**Pyrazole** IC$_{50}$ (uM) C26 31.0 HeLa 74.1 SK-BR-3 36.9 A549 118.4 CAOV-3 73.2
p-Phenyl IC$_{50}$ (uM) C26 11.4 HeLa 20.0 SK-BR-3 19.5 A549 124.5 CAOV-3 20.7	**m-Phenyl** IC$_{50}$ (uM) C26 21.0 HeLa 25.9 SK-BR-3 25.7 A549 121.5 CAOV-3 27.2	**Para** IC$_{50}$ (uM) C26 3.2 HeLa 13.6 SK-BR-3 15.6 A549 74.6 CAOV-3 18.7	**Meta** IC$_{50}$ (uM) C26 3.7 HeLa 14.2 SK-BR-3 7.8 A549 117.2 CAOV-3 22.0
Mesitylene IC$_{50}$ (uM) C26 9.9 HeLa 29.9 SK-BR-3 30.3 A549 159.1 CAOV-3 39.1	**t-Butyl** IC$_{50}$ (uM) C26 4.1 HeLa 10.0 SK-BR-3 12.3 A549 82.5 CAOV-3 10.5	**Aliphatic** IC$_{50}$ (uM) C26 2.2 HeLa 36.7 SK-BR-3 32.4 A549 63.2 CAOV-3 29.2	**Cisplatin** IC$_{50}$ (uM) C26 1.2 HeLa 9.4 SK-BR-3 10.0 A549 5.8 CAOV-3 5.7

60
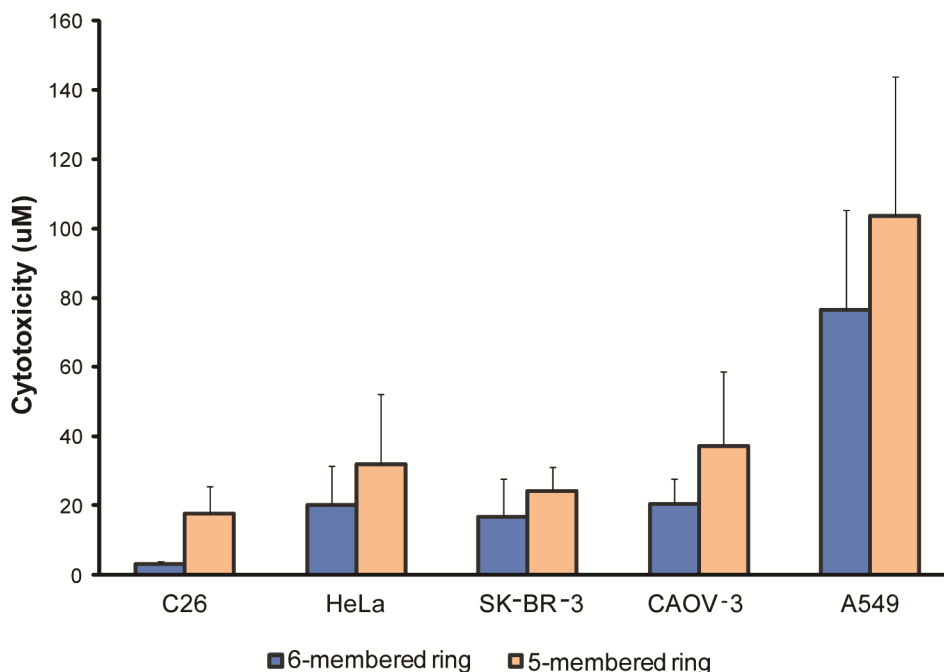
Figure 4.3. Comparative average toxicities of Pt complexes in different tumor cell lines based upon chelate size.

Lastly, complex **37** could be recrystallized by a vapor diffusion crystallization of methanol into dimethylsulfoxide. The crystal structure in Figure 4.4 shows that the solid state conformation of the quinoline-pyrazole chelate is in agreement with the gas phase calculations of the optimized geometry. As predicted, the platinum center remains in a non-planer conformation with the rest of the molecule. The dihedral angle about the C-N biaryl bond connecting the pyrazole and quinoline rings was found to be -30.38° in the crystal structure and -34.0 in the gas phase calculation. The increased planarity in the crystal structure is believed to be caused by stabilization from the crystal packing.
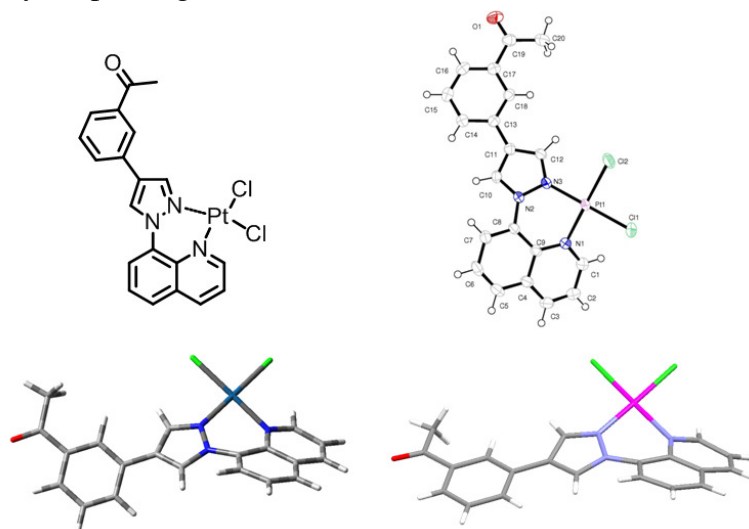
Figure 4.4. Comparison of gas phase calculations and crystal structure for complex **37**.

Polymer Attachment

After preparing the small library of complexes, six compounds representative of the structural changes made were chosen for further study on a polymer scaffold to look at toxicity and rates of hydrazone hydrolysis. The original toxic complex Quin (**8**) was selected, as well as the less toxic and slow releasing Bipy (**7**) and the bulky t-butyl (**18**). To explore the different drug release rates due to the differences in ketone position, Meta (**37**), Para (**36**), and Ali (**38**) were chosen. The complexes were attached to both a linear 5 kDa PEG chain with an acylhydrazide chain end and the 40 kDa PEGylated ester-amide dendrimer used in Chapter 2. The conjugates were prepared by stirring the dendrimer or PEG with an excess of the complex at 60°C in dimethylformamide (DMF) overnight (Scheme 4.4). The resulting polymer was precipitated into ether to remove the DMF. The polymer was re-dissolved in methanol and filtered through a 20 μm filter to remove most of the insoluble small molecule platinum. The polymer was then purified by size exclusion chromatography through an LH-20 resin with methanol as the eluent to remove any trace free drug. Finally, the polymer samples were re-dissolved in water and passed through PD-10 desalting columns and lyophilized. Removal of the small molecule platinum species was confirmed by size exclusion chromatography (SEC) and platinum loading quantified by ICP-AES. The resulting solids were soluble in water at concentrations greater than 250 mg polymer/mL. The Dend-Pt species had platinum loadings (%wt/wt) between 2-3% (3.3% theoretical), while the PEG-Pt loading was between 0.8-3% (3.7% theoretical), as shown in Table 4.2.

Scheme 4.4. Complex loading onto linear PEG and PEGylated dendrimer carriers.
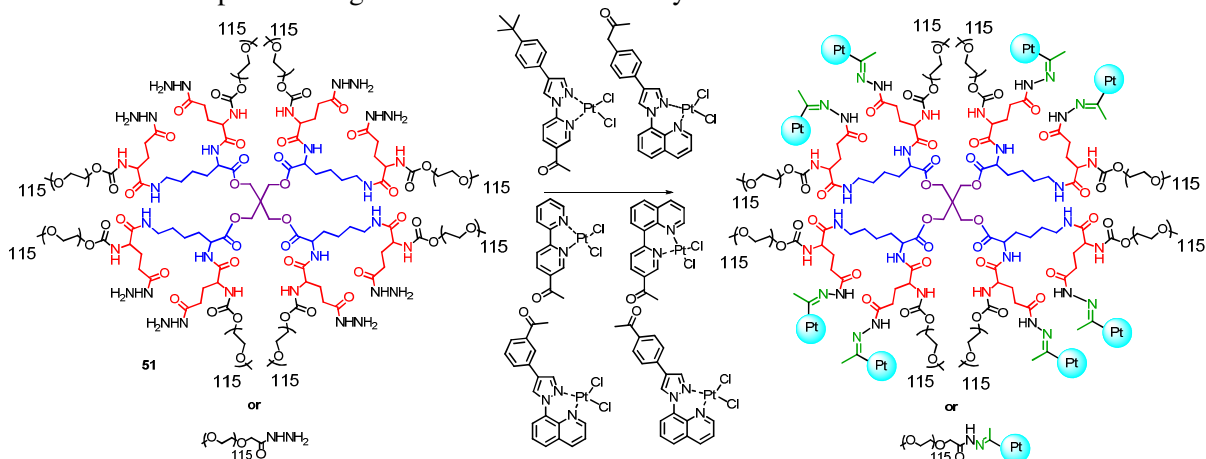
Polymer-Pt Toxicity and Hydrolysis

We measured the cytotoxicity of the Dend-Pt drugs against the C26 cell line. As described in Chapter 2, we generally observe about a 10-fold decrease in toxicity when the drug is attached to the polymer. The change in toxicity is affected by the rate at which the polymer is taken up into the cell via pinocytosis, as well the rate of drug release from the polymer. Based upon the modifications generated in the small molecule drugs, the Dend-Pt compounds had a range of toxicities (Table 4.2). As predicted by the earlier release study, pyrazole containing complexes had better polymer activity than the slower releasing ligands.

Table 4.2. Toxicity and drug loading data for polymer platinum conjugates.

	Bipy (**7**)	Quin (**8**)	*t*-butyl (**18**)	Meta (**37**)	Para (**36**)	Ali (**38**)
IC_{50} Free Drug (μM)	21.4	3.4	4.1	3.7	3.2	2.2
IC_{50} Dendrimer (μM)	800	70	27.8	10.1	61	12.1
Dend-Pt Loading (wt/wt %)	2.8% (**39**)	2.9% (**40**)	2.0% (**41**)	2.6% (**42**)	2.2% (**43**)	3.0% (**44**)
PEG Pt Loading (wt/wt %)	0.8% (**45**)	2.5% (**46**)	1.5% (**47**)	2.2% (**48**)	2.9% (**49**)	0.9% (**50**)

To confirm this hypothesis, the differing rates of hydrazone hydrolysis were explored. Unfortunately, the small molecule complexes are very insoluble in water and the release experiments proved to be a challenge. For ease, we decided to measure the release from the linear PEG conjugates. While the solubility of the released Pt-complexes could be improved by supplementing the dialysis buffer with 20% DMSO, this solvent mixture is not suitable to analysis by ICP; therefore, we could not use the standard dialysis technique. Instead, an aqueous size exclusion column with 30% acetonitrile in water was used to measure the drug released from the polymer. As expected, no platinum was released from any of the polymer samples at pH 7.4. Conversely, there was significant release for most of the polymer samples at pH 5, as shown in Figure 4.6. There was no release at pH 5 from the PEG-*t*-butyl and PEG-Bipy polymers, but the poor solubility may have caused Bipy (**7**) and t-butyl (**18**) to precipitate on the column upon hydrolysis, leading to no observed signal in the SEC trace. The Meta, Para, and Ali complexes showed differing release rates at pH 5, which agreed with our hypothesis that varying the ketone position will alter the electronic environment of the hydrazone and affect the rate of hydrolysis.

Figure 4.6. Hydrolysis of platinum complexes from PEG hydrazones in pH 5 buffer.

In vivo efficacy

Determining a maximum tolerated dose is an important parameter for evaluating *in vivo* toxicity and establishing an appropriate therapeutic dose. The drug loaded dendrimers were injected at doses of 15, 45 and 90 mg/kg of platinum equivalents. At 90 mg/kg, an *i.p.* injection was necessary as the polymer solutions were too viscous for the standard *i.v.* injection. Mice were monitored for signs of toxicity including weight loss exceeding 15% of the starting weight, lethargy, and ruffled fur. As seen in Figure 4.7, mild to moderate toxicity was observed for all doses. Three toxic deaths occurred at the 90 mg/kg dose, with one mouse being from the Dend-Quin (**40**), Dend-Bipy (**39**), and Dend-t-butyl (**41**) groups. None of the other mice experienced excessive weight loss, providing an upper boundary for a permissible dose during a chemotherapy experiment.
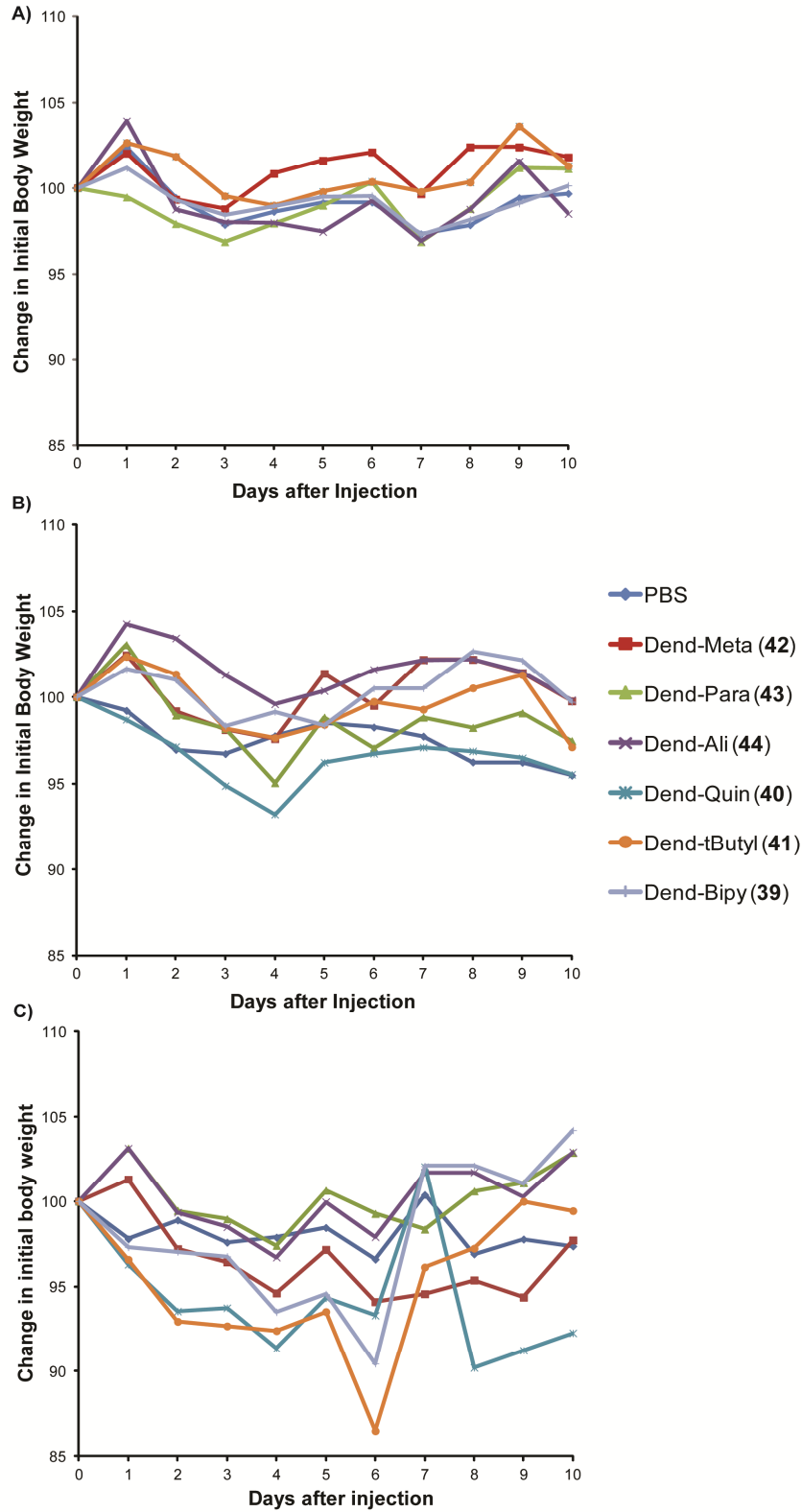
Figure 4.7. In vivo toxicity of platinum-dendrimer conjugates. A) Mice injected *i.v.* with 15 mg Pt/kg. B) Mice injected *i.v.* with 45 mg Pt/kg. C) Mice injected *i.p.* with 90 mg Pt/kg.

Next, a biodistribution study was carried out to confirm that the platinum conjugates have favorable tumor accumulation properties similar to those seen in previous dendrimer-drug conjugates made in our group.[9,28–30] Ten days after the C26 tumors were established, mice were injected with Dend-Ali (**44**), Dend-t butyl (**41**), PEG-Ali (**50**), the small molecule drug Aliplatin (**38**), or cisplatin at 6 mg Pt/kg. Platinum in the tissue and blood was quantified with ICP after extensive digestion in 70% nitric acid. The polymer samples achieved favorable circulation in the blood as well as high accumulation in the tumor after 48 hours (Figure 4.8). As expected, the Dend-Pt samples had better distribution profiles than PEG-Ali due to the higher MW, longer circulation, and better passive targeting. Meanwhile, aliplatin and cisplatin were virtually undetectable due to the rapid clearance.
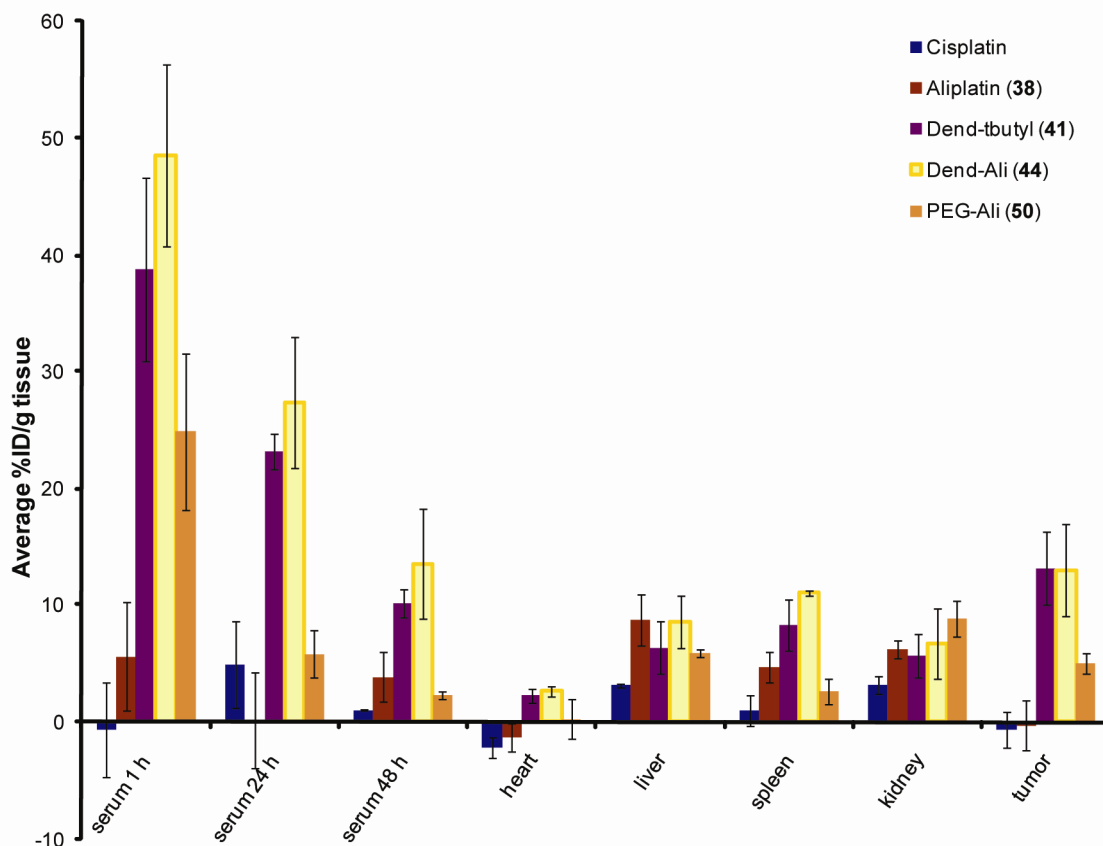
Figure 4.8. Biodistribution of platinum in tumored mice.

With favorable *in vitro* and *in vivo* responses, the antitumor activity of the platinum conjugates was tested against the C26 colon carcinoma model. Female Balb/C mice were tumored in the right flank and treated on day 8. The treatment groups (6 mice per group) were PBS, Cisplatin (6 mg/kg), Aliplatin (**38**, 10 mg Pt/kg)**,** and Dend-Meta (**42**), Dend-Para (**43**), Dend-Ali (**44**), Dend-Bipy (**39**), and Dend-tbutyl (**41**) all at 36 mg Pt/kg. Dend-Quin (**40**) was omitted from the experiment because after injection, the mouse died. Further analysis did not reveal any anomalies with the dendrimer, Pt loading, or sample preparation. Aliplatin (**38**) had one tumor free survivor at the end of the study; unfortunately, none of the treatment groups had median survival (Figure 4.9A) or tumor growth delay (Figure 4.9B) that was significantly different than cisplatin or PBS.
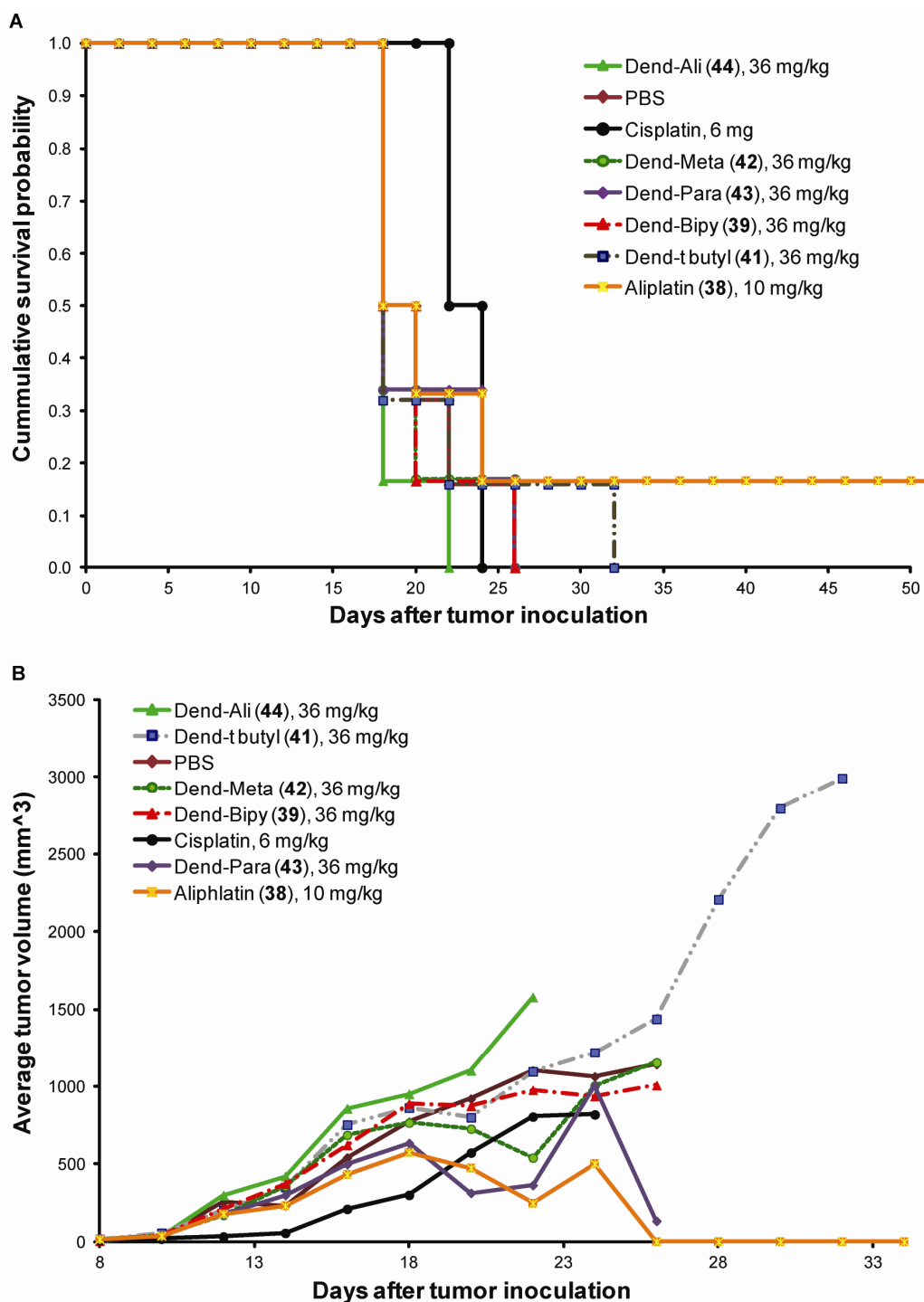
Figure 4.9. A) Kaplan-Meier survival probability plot. B) Average tumor volume versus time for platinum conjugates injected in mice inoculated with C26 colon carcinoma.

We have identified a number of potential challenges which could be causing poor *in vivo* efficacy. The difficulty in quantifying Pt release from the polymers suggests that perhaps the Pt drugs are diffusing from the dendrimer too slowly and becoming inactivated before interacting with DNA. The PEG-Pt compounds were screened in a small follow up chemotherapy study;

however, no improvement in efficacy was observed. Likewise, any attempts to encapsulate the complexes within liposomes resulted in large vesicles that could not be extruded and did not release Pt. A simplified, hydrazide containing polymer with a less hydrophobic core, such as the 3-arm PEG stars designed by our group,[31] could facilitate drug release and subsequent DNA interactions. It may be that the potency of the platinum drugs developed was still not enough to achieve antitumor activity, despite selective delivery of large payloads. The complexes had activity in multiple cell lines, therefore a different tumor model more responsive to Pt(II) drugs could exhibit better efficacy. Similarly, exploring a variety of dosing regimens could identify a better treatment schedule. Furthermore, improving drug solubility would improve efficacy. A new synthetic scheme would need to be designed to install additional solubilizing functionality to the chelator backbone. The bidentate design could be augmented as a monodentate ligand paired with the standard amine, but this idea would be better approached as a separate project rather than an extension of this work.

CONCLUSIONS

The design and synthesis of a small library of heterocyclic diamine ligands containing a ketone functional group has been carried out. These ligands have been used to create Pt (II) drugs specially tailored for polymeric delivery via a pH-sensitive hydrazone bond. The *in vitro* toxicity of these complexes has been evaluated and select complexes were attached to polymeric carriers for further evaluation. The drugs did in fact have pH-sensitive release profile, and the polymer bound payload had promising cytotoxic activity *in vitro*. We were encouraged to measure a high level of platinum accumulation in the tumor for the three polymer-Pt species. However, this high tumor level did not translate into significant antitumor activity for these conjugates as we have seen for hydrazone-linked drugs in the past. This proof of concept study validated the pH release strategy and points towards making the released chelates more water soluble. These design changes could lead to better *in vivo* activity in future investigations.

EXPERIMENTAL

Materials. Materials were used as obtained from commercial sources unless otherwise noted. The platinum ICP standard was purchased from VHG Labs, Manchester, NH. Dimethylformamide (DMF) and CH_2Cl_2 (DCM) for syntheses were purged 1 h with nitrogen and further dried by passing them through commercially available push stills (Glass Contour). Monomethoxypolyethyleneglyco-hydrazide (mPEG-HZ) was purchased from Laysan Bio, Inc. Solvents were removed under reduced pressure using a rotary evaporator or by vacuum pump evacuation.

Characterization. NMR spectra were recorded on Bruker AV 300, AVB 400, AVQ 400, or DRX 500 MHz instruments. Elemental analyses were performed at the UC Berkeley Mass Spectrometry Facility. Size exclusion chromatography (SEC) system A consisted of a Waters 515 pump, a Waters 717 autosampler, a Waters 996 Photodiode Array detector (210-600 nm), and a Waters 2414 differential refractive index (RI) detector. SEC was performed at 1.0 mL/min in a PLgel Mixed B (10 μm) and a PLgel Mixed C (5 μm) column (Polymer Laboratories, both 300 x 7.5 mm), in that order, using DMF with 0.2% LiBr as the mobile phase and linear PEO (4,200-478,000 MW) as the calibration standards. The columns were kept at 70 °C. SEC system C consisted of a B Waters Alliance separation module 2695 and a Waters 410 differential RI detector. Inductively coupled plasma-atomic emission spectroscopy (ICP-AES) was carried out on a Perkin Elmer Optima 7000 DV Optical Emission Spectrometer.

Synthesis of 3. Compound **2** (500 mg, 2.5 mmol), 2-(trimethylstannyl) pyridine (725 mg, 3.0 mmol) and tetrakis(triphenylphosphine)palladium (145 mg, 0.13 mmol) were weighed into a 250 mL 3-neck flask equipped with a condenser. The flask was evacuated and backfilled with nitrogen 3 times. Freshly degassed DMF (10 mL) and freshly degassed toluene (40 mL) were added to the flask via syringe. The reaction stirred at 110 ˚C overnight. The reaction was diluted with dichloromethane and washed three times with water. The organic layer was dried over sodium sulfate and concentrated by rotary evaporation. The residue was purified by silica gel chromatography using 60% ethyl acetate 40% Hexanes as an eluent. 367 mg of a white solid were collected in 74% yield. ^{1}H NMR (500 MHz, CDCl$_3$) δ 2.68 (s, 3H), 7.35-7.38 (m, 1H), 7.84-7.87 (m, 1H), 8.34 (d, J =10.5 Hz, 1H), 8.48 (d, J = 8Hz, 1H), 8.53 (d, J = 8 Hz, 1H), 8.72 (d, J = 5 Hz, 1 H), 9.21 (s, 1H). ^{13}C NMR (125 MHz, CDCl$_3$) δ 27.06, 121.00, 122.14, 124.76, 132.05, 136.76, 137.29, 149.64, 149.79, 155.16, 159.68, 196.84. MS (EI) Calc [M]$^+$ (C$_{12}$H$_{10}$N$_2$O) m/z = 198.08. Found [M]$^+$ m/z = 198.0.

Synthesis of 4. Compound **2** (241 mg, 1.2 mMol), quinoline-8-boronic acid (250 mg, 1.45 mmol), Tris(dibenzylideneacetone)dipalladium (7 mg, 0.01 mmol), 2-Dicyclohexylphosphino-2',6'-dimethoxybiphenyl (10 mg, 0.02 mmol) and tribasic potassium phosphate (1.277 g, 6.02 mmol) where weighed into a 100 mL 3-neck flask equipped with a reflux condenser. The flask was evacuated and backfilled with nitrogen 3 times. Freshly degassed toluene (12 mL) was added via syringe and the reaction was left to stir at 100 ˚C for 36 hours. The reaction mixture was then diluted with 100 mL of ether and the solids were filtered off. The filtrate was concentrated by rotary evaporation and loaded onto a silica gel column. A gradient column was run from 0 to 50% ethyl acetate in hexane to give 209 mg of white solid in 70% yield. ^{1}H NMR (400 MHz, CDCl$_3$) δ 2.70 (s, 3H), 7.52-7.44 (m, 1H), 7.76-7.66 (m, 1H), 7.98-7.92 (m, 1H), 8.23-8.19 (m, 1H), 8.31-8.23 (m, 2H), 8.40-8.33 (m, 1H), 8.97 (m , 1H), 9.35-9.31 (m, 1H). ^{13}C NMR (100 MHz, CDCl$_3$) δ 26.81, 121.27, 126.45, 126.82, 128.63, 129.70, 130.46, 131.51, 134.98, 136.55, 137.71, 145.68, 149.76, 150.55, 160.95, 196.84. MS (EI) Calc [M]$^+$ (C$_{16}$H$_{12}$N$_2$O) m/z = 248.09. Found [M]$^+$ m/z = 248.0.

Synthesis of 5. Compound **2** (100 mg, 0.5 mmol), 2-tributylstannyl thiazole (224 mg, 0.6 mmol), and tetrakis(triphenylphosphine)palladium (29 mg, 0.03 mmol) were weighed into a 100 mL 3-neck flask equipped with a condenser. The flask was evacuated and backfilled with nitrogen 3 times. Freshly degassed DMF (2 mL) and freshly degassed toluene (8 mL) were added to the flask via syringe. The reaction stirred at 110 ˚C overnight. The reaction was diluted with dichloromethane and washed three times with water. The organic layer was dried over sodium sulfate and concentrated by rotary evaporation. The residue was purified through a gradient silica gel column from 0% to 30% ethyl acetate in hexanes to give 90 mg of white solid in 82% yield. ^{1}H NMR (400 MHz, CDCl$_3$) δ 2.62 (s, 3H), 7.50 (d, J = 3.09 Hz, 1H), 7.94 (d, J = 3.07 Hz, 1H), 8.26 (dd, J = 18.44, 8.24 Hz, 2H), 9.10 (s, 1H). ^{13}C NMR (100 MHz, CDCl$_3$) δ 26.72, 119.26, 122.82, 132.22, 136.67, 144.57, 149.78, 154.21, 167.78, 195.89. MS (EI) Calc [M]$^+$ (C$_{10}$H$_8$N$_2$OS) m/z = 204.04. Found [M]$^+$ m/z = 204.0.

Synthesis of 6. Compound **2** (1.756 g, 8.8 mmol), pyrazole (896 mg, 13.2 mmol), copper (I) iodide (334 mg, 1.76 mmol), l-proline (405 mg, 3.51 mmol), and potassium carbonate (6.066 g, 43.9 mmol) were added to a 250 mL round bottom flask. The flask was evacuated and backfilled with nitrogen three times. Anhydrous DMSO was added via syringe and the reaction stirred at 100 degrees C overnight. The reaction was diluted with ethyl acetate and washed three times with water. The organic layer was dried over sodium sulfate and concentrated by rotary

evaporation. The residue was purified through a silica gel column with 40% ethyl acetate in hexane as the eluent to give 890 mg of white solid in 53% yield. ^{1}H NMR (400 MHz, CDCl$_3$) δ 2.60 (s, 3H), 6.47 (t, J = 1.6 Hz, 1H), 7.74 (s, 1H), 8.05 (d, J = 8.65 Hz, 1H), 8.34 (dd, J = 8.64, 2.29 Hz, 1H), 8.60 (d, J = 2.58 Hz, 1H), 8.95 (d, J = 1.86 Hz, 1H). ^{13}C NMR (100 MHz, CDCl$_3$) δ 26.82, 108.91, 112.18, 127.96, 130.38, 138.75, 143.39, 149.56, 153.99, 195.71. MS (EI) Calc [M]$^+$ (C$_{10}$H$_9$N$_3$O) m/z = 187.07. Found [M]$^+$ m/z = 187.0.

Synthesis of 11. Compound **6** (870 mg, 4.65 mmol) and *N*-bromosuccinimide (1.241 g, 6.97 mmol) were added to a 20 mL reaction vial. The solids were dissolved in DMF and stirred in the dark at room temperature for 24 hours. The reaction mixture was diluted with 50 mL of ethyl acetate and washed with 10% NaOH in 3 50 mL portions. The organic layer was dried over sodium sulfate and concentrated by rotary evaporation to give 920 mg of white solid in 74% yield. ^{1}H NMR (400 MHz, CDCl$_3$) δ 2.64 (s, 3H), 7.71 (s, 1H), 8.02 (d, J = 8.63 Hz, 1H), 8.36 (dd, J = 8.62, 1.99 Hz, 1H), 8.63 (s, 1H), 8.95 (s, 1H). ^{13}C NMR (100 MHz, CDCl$_3$) δ 26.91, 97.73, 111.77, 128.09, 130.82, 138.96, 143.79, 149.56, 153.20, 195.63. . MS (EI) Calc [M]$^+$ (C$_{10}$H$_8$N$_3$O) m/z = 264.99. Found [M]$^+$ m/z = 265.0.

Synthesis of 12. Compound **11** (61 mg, 0.23 mmol), 2-mesityleneboronic acid (41 mg, 0.25 mmol) and bis(tri-*tert*-butylphosphone) palladium(0) (6 mg,0.01mmol) were added to a 20 mL microwave reaction vial under nitrogen atmosphere. Degassed tetrahydrofuran (5 mL) and degassed 2M Na$_2$CO$_3$ (1.5 mL) were added and the reaction was irradiated in a microwave reactor at 160˚ C for 45 min. The contents of the vial was diluted with 50 mL of ethyl acetate and washed with three 50 mL portions of water. The organic layer was concentrated and loaded onto a silica column with 40% ethyl acetate in hexanes as an eluent to give 30 mg of white solid in 43% yield. ^{1}H NMR (400 MHz, CDCl$_3$) δ 2.18 (s, 6H), 2.33 (s, 3H), 2.65 (s, 3H), 6.97 (s, 2H), 7.669 (s, 1H), 8.11-1.13 (m, 1H), 8.38-8.40 (m, 1H), 8.50 (s, 1H), 8.99 (s, 1H). ^{13}C NMR (100 MHz, CDCl$_3$) δ 21.20, 21.31, 111.95, 123.05, 126.75, 128.29, 128.52, 130.27, 137.51, 138.73, 144.35, 149.64, 154.01, 195.70. MS (EI) Calc [M]$^+$ (C$_{19}$H$_{19}$N$_3$O) m/z = 305.15. Found [M]$^+$ m/z = 305.1.

Synthesis of 13. Compound **11** (57 mg, 0.21 mmol), 4-*tert*-butylphenylboronic acid (41 mg, 0.23 mmol) and bis(tri-*tert*-butylphosphine) palladium(0) (6 mg, 0.01 mmol) were added to a 20 mL microwave reaction vial under nitrogen atmosphere. Degassed tetrahydrofuran (5 mL) and degassed 2M Na$_2$CO$_3$ (1.5 mL) were added and the reaction was irradiated in a microwave reactor at 160˚ C for 45 min. The contents of the vial was diluted with 50 mL of ethyl acetate and washed with three 50 mL portions of water. The organic layer was concentrated and loaded onto a silica column with 40% ethyl acetate in hexanes as an eluent to give 53 mg of white solid in 80% yield. ^{1}H NMR (400 MHz, CDCl$_3$) δ 1.36 (s, 9H), 2.65 (s, 3H), 7.43-7.56 (m, 4H), 8.05-8.10 (m, 2H), 8.34-8.38 (m, 1H), 8.83 (s, 1H), 9.00 (s, 1H). ^{13}C NMR (100 MHz, CDCl$_3$) δ 26.65, 31.29, 34.59, 111.86, 123.58, 125.58, 125.64, 125.91, 128.51, 130.09, 138.51, 141.18, 149.40, 150.41, 153.65, 195.49. MS (EI) Calc [M]$^+$ (C$_{20}$H$_{21}$N$_3$O) m/z = 319.17. Found [M]$^+$ m/z = 319.1.

Synthesis of 14. Compound **11** (48.5 mg, 0.18 mmol), compound **21** (45 mg, 0.2 mmol), tetrakis(triphenylphosphine)palladium(0) (10.5 mg, 0.01 mmol) were dissolved in degassed dimethylformamide (0.6 mL) and degassed toluene (2.5 mL). The solution was heated to 110˚ C for 24 h and then diluted with ethyl acetate (50 mL) and washed with three 50 mL portions of water. The organic layer was concentrated and loaded on to a silica gel column with 66% ethyl acetate in hexanes as the eluent to give 30 mg of a tan solid in 63% yield. *Note: this sample was contaminated with a small amount of triphenylphosphine* ^{1}H NMR (400 MHz, CDCl$_3$) δ 2.65 (s,

3H), 7.32-7.35 (m, 1H), 7.84-7.84 (m, 1H), 8.35-8.36 (m, 2H), 8.55 (s, 1H), 8.81-9.01 (m, 3H). ^{13}C NMR (100 MHz, CDCl$_3$) δ 26.67, 111.97, 122.24, 123.76, 124.25, 127.50, 128.40, 128.52, 130.45, 132.00, 132.10, 132.92, 138.67, 140.70, 147.14, 148.41, 149.35, 153.32, 195.42. MS (EI) Calc [M]$^+$ (C$_{15}$H$_{12}$N$_4$O) m/z = 264.10. Found [M]$^+$ m/z = 265.0.

Synthesis of 15. Compound **2** (300 mg, 1.5 mmol), 3,5-dimethylpyrazole (288 mg, 3.0 mmol), copper (I) iodide (57 mg, 0.3 mmol), l-proline (69 mg, 0.6 mmol), and potassium carbonate (828 mg, 6 mmol) were added to a 250 mL round bottom flask. The flask was evacuated and backfilled with nitrogen three times. Anhydrous DMSO was added via syringe and the reaction stirred at 130 degrees C for three days. The reaction was diluted with ethyl acetate and washed three times with water. The organic layer was dried over sodium sulfate and concentrated by rotary evaporation. The residue was purified through a silica gel column with 40% ethyl acetate in hexane as the eluent to give 890 mg of white solid in 53% yield. ^{1}H NMR (400 MHz, CDCl$_3$) δ 2.60 (s, 3H), 6.47 (t, J = 1.6 Hz, 1H), 7.74 (s, 1H), 8.05 (d, J = 8.65 Hz, 1H), 8.34 (dd, J = 8.64, 2.29 Hz, 1H), 8.60 (d, J = 2.58 Hz, 1H), 8.95 (d, J = 1.86 Hz, 1H). ^{13}C NMR (100 MHz, CDCl$_3$) δ 26.82, 108.91, 112.18, 127.96, 130.38, 138.75, 143.39, 149.56, 153.99, 195.71. MS (EI) Calc [M]$^+$ (C$_{12}$H$_{13}$N$_3$O) m/z = 215.11. Found [M]$^+$ m/z = 215.1.

Synthesis of 21. 3-Bromopyridine (1.78 g, 11.3 mmol) was added to a flame dried, 500 mL one neck flask. 100 mL of dry ether was added via syringe and the solution was cooled to -78˚C. n-Butyl lithium (5.41 mL, 13.5 mmol) was added via syringe as 2.5M solution in hexane. The mixture stirred at -78˚C for one hour and then trimethyltin chloride (2.694 g, 13.5 mmol) was added. The reaction was allowed to stir for 4 hours and gradually warm to room temperature and then washed with three 50 mL portions of 10% NaOH. The organic layer was dried over sodium sulfate and concentrated by rotary evaporation to give 2.38 g of clear oil in 87% yield. ^{1}H NMR (400 MHz, CDCl$_3$) δ 0.3 (s, 9H), 7.19-7.24 (m, 1H), 7.68-7.82 (m, 1H), 8.48-8.53 (m, 1H), 8.56-8.65 (m, 1H). ^{13}C NMR (100 MHz, CDCl$_3$) δ -9.45, 124.01, 137.26, 143.58, 149.51, 155.69.

Synthesis of 1. Prepared using the identical procedure described above with 2-bromopyridine as a starting material. ^{1}H NMR (400 MHz, CDCl$_3$) δ 0.33 (s, 9H), 7.09-7.13 (m, 1H), 7.40-7.52 (m, 2H), 8.72-8.73 (m, 1H).

Synthesis of 22. Pyrazole (776 mg, 11.4 mmol), 2-bromopyridine (1.5 g, 9.5 mmol), copper (I) iodide (362 mg, 1.9 mmol), l-proline (437 mg, 3.8 mmol) and potassium carbonate (6.56 g, 47.5 mmol) were added to a 100 mL round bottom flask. The flask was evacuated and backfilled with nitrogen followed by the addition of 30 mL of anhydrous DMSO via syringe. The reaction mixture stirred at 90˚C overnight and was then diluted with 200 mL of ethyl acetate and washed with three 100 mL portions of water. The organic layer was dried over sodium sulfate and concentrated by rotary evaporation. The residue was purified through a silica gel column with 25% ethyl acetate in hexane as the eluent to give 702 mg of white solid in 51% yield. ^{1}H NMR (400 MHz, CDCl$_3$) δ 6.45 (s, 1H), 7.10-7.25 (m, 1H), 7.14-7.77 (m, 2H), 7.94-7.96 (m, 1H), 8.73 (s, 1H), 8.55 (s, 1H). ^{13}C NMR (100 MHz, CDCl$_3$) δ 107.88, 112.48, 121.46, 127.09, 138.78, 142.12, 148.09, 151.64. MS (EI) Calc [M]$^+$ (C$_8$H$_7$N$_3$) m/z = 145.06. Found [M]$^+$ m/z = 145.1.

Synthesis of 23. Compound **22** (607 mg, 4.18 mmol) and *N*-bromosuccinimide (1.116 g, 6.29 mmol)) were added to a 250 mL reaction vial. The solids were dissolved in DMF (50 mL) and stirred in the dark at room temperature for 24 hours. The reaction mixture was diluted with 300 mL of ethyl acetate and washed with 10% NaOH in three 50 mL portions. The organic layer was dried over sodium sulfate and concentrated by rotary evaporation to give 800 mg of white solid in 85% yield. ^{1}H NMR (400 MHz, CDCl$_3$) δ 7.19-7.22 (m, 1H), 7.67 (s, 1H), 7.79-7.84 (m, 1H), 7.93 (d, J = 8 Hz, 1H), 8.38-8.40 (m, 1H), 8.58 (s, 1H). ^{13}C NMR (100 MHz, CDCl$_3$) δ 96.33.

111.85, 121.83, 127.22, 138.76, 142.34, 148.03, 150.79. MS (EI) Calc [M]$^+$ (C$_8$H$_6$BrN$_3$) m/z = 222.97. Found [M]$^+$ m/z = 223.0.

Synthesis of 24. Pyrazole (663 mg, 9.7 mmol) 8-bromoquinoline (1.008 grams, 4.87 mmol), copper (I) iodide (185 mg, 0.97 mmol), l-proline (224 mg, 1.94 mmol), and potassium carbonate (3.365 g, 24.3 mmol) were added to a 250 mL round bottom flask. The flask was evacuated and backfilled with nitrogen three times. Anhydrous DMSO (20 mL) was added via syringe and the reaction stirred at 110 degrees C overnight. The reaction was diluted with ethyl acetate and washed three times with water. The organic layer was dried over sodium sulfate and concentrated by rotary evaporation. The residue was purified through a silica gel column with 33% ethyl acetate in hexane as the eluent to give 570 mg of clear oil in 60% yield. ^{1}H NMR (400 MHz, CDCl$_3$) δ 6.55 (t, J = 7.1 Hz, 1H), 7.44 (dd, J = 8.32, 4.16 Hz, 1H), 7.62 (t, J = 7.87 Hz, 1H), 7.76 (d, J = 8.18, 1.24 Hz, 1H), 7.82 (d, J = 1.54 Hz, 1H), 8.19 (m, 2H), 8.74 (d, J = 2.35 Hz, 1H), 8.95 (dd, J = 4.12, 1.66 Hz, 1H). ^{13}C NMR (100 MHz, CDCl$_3$) δ 106.76, 121.62, 124.02, 126.59, 126.86, 129.29, 129.59, 133.71, 136.52, 137.23, 140.81, 150.44. MS (EI) Calc [M]$^+$ (C$_{12}$H$_9$N$_3$) m/z = 195.08. Found [M]$^+$ m/z = 195.1.

Synthesis of 25. Compound **24** (2.62 g, 13.4 mmol) and *N*-bromosuccinimide (3.56 g, 20.0 mmol) were added to a 250 mL reaction vial. The solids were dissolved in DMF (50 mL) and stirred in the dark at room temperature for 24 hours. The reaction mixture was diluted with 300 mL of ethyl acetate and washed with 10% NaOH in 3 50 mL portions. The organic layer was dried over sodium sulfate and concentrated by rotary evaporation to give 2.84 g of white solid in 78% yield. ^{1}H NMR (400 MHz, CDCl$_3$) δ 7.46-7.49 (m, 1H), 7.61-7.64 (m, 1H), 7.75 (s, 1H), 7.78-7.80 (m, 1H), 8.17-8.23 (m, 2H), 8.88 (s, 1H), 8.96 (m, 1H). ^{13}C NMR (100 MHz, CDCl$_3$) δ 94.60, 121.72, 123.30, 126.47, 127.20, 129.15, 133.75, 136.38, 136.53, 140.26, 141.12, 150.42. MS (EI) Calc [M]$^+$ (C$_{12}$H$_8$N$_3$Br) m/z = 272.99. Found [M]$^+$ m/z = 273.0.

Synthesis of 28. 4-bromophenylacetone (1.234 g, 5.79 mmol), bis(pinacolato)diboron (1.550 g, 6.08 mmol), dichloro 1,1'-bis(diphenylphosphino)ferrocene palladium(II) (94 mg, 0.12 mmol), and potassium acetate (1.563 g, 15.93 mmol) were suspended in 30 mL of degassed dioxane and heated at 110°C overnight. The reaction mixture was then diluted with 100 mL of ethyl acetate and washed with water in three 100 mL portions. The organic layer was dried over sodium sulfate and concentrated by rotary evaporation. The residue was purified through a silica gel column with 25% ethyl acetate in hexane as the eluent to give 1.104 g of yellow oil in 73% yield. ^{1}H NMR (400 MHz, CDCl$_3$) δ 1.33 (s, 12H), 2.12 (s, 3H), 3.69 (s, 2H), 7.20 (d, J = 7.86 Hz, 2H), 7.78 (d, J = 7.85 Hz, 2H). ^{13}C NMR (100 MHz, CDCl$_3$) δ 24.96, 29.37, 51.35, 71.94, 83.89, 128.90, 135.34, 137.50, 206.18. MS (EI) Calc [M]$^+$ (C$_{15}$H$_{21}$BO$_3$) m/z = 260.16. Found [M]$^+$ m/z = 260.1.

Synthesis of 29. Compound **23** (200 mg, 0.90 mmol), 4-acetylphenylboronic acid **26** (210 mg, 1.28 mmol) and cesium carbonate (771 mg, 2.37 mmol) were added to a 3-neck round bottom flask equipped with a reflux condenser under nitrogen atmosphere. Degassed dioxane (15 mL) was added via syringe followed by the addition of palladium acetate (10 mg, 0.04 mmol) and tricyclohexylphosphine (25mg, 0.08 mmol). The solution was heated to reflux for 24 h and the reaction mixture was then cooled to room temperature, diluted with ethyl acetate (100 mL) and washed with three 50 mL portions of water. The organic layer was concentrated and loaded onto a silica column with 40% ethyl acetate in hexanes as an eluent to give 90 mg of white solid in 38% yield. ^{1}H NMR (400 MHz, CDCl$_3$) δ 2.61 (s, 3H), 7.20-7.23 (m, 1H), 7.65-7.71 (m, 2H), 7.81-7.85 (s, 1H), 7.97-8.06 (m, 4H), 8.43-8.44 (m, 1H), 8.90 (s, 1H). MS (EI) Calc [M]$^+$ (C$_{16}$H$_{13}$N$_3$O) m/z = 263.1. Found [M]$^+$ m/z = 263.1.

Synthesis of 30. Compound **23** (213 mg, 0.95 mmol), 3-acetylphenylboronic acid **27** (210 mg, 1.28 mmol) and cesium carbonate (771 mg, 2.37 mmol) were added to a 3-neck round bottom flask equipped with a reflux condenser under nitrogen atmosphere. Degassed dioxane (15 mL) was added via syringe followed by the addition of palladium acetate (11 mg, 0.05 mmol) and tricyclohexylphosphine (26.5 mg, 0.1 mmol). The solution was heated to reflux for 24 h and the reaction mixture was then cooled to room temperature, diluted with ethyl acetate (100 mL) and washed with three 50 mL portions of water. The organic layer was concentrated and loaded onto a silica column with 40% ethyl acetate in hexanes as an eluent to give 136 mg of white solid in 54% yield. ^{1}H NMR (400 MHz, CDCl$_3$) δ 2.64 (s, 3H), 7.18-7.22 (m, 1H), 7.46-7.50 (m, 1H), 7.74-7.77 (m, 3H), 7.80-7.84 (m, 1H), 8.06 (s, 1H), 8.15 (s, 1H), 8.42-8.44 (m, 1H), 8.88 (s, 1H). ^{13}C NMR (100 MHz, CDCl$_3$) δ 26.86, 112.46, 121.81, 123.83, 123.97, 125.35, 126.97, 129.31, 130.28, 132.57, 137.73, 138.93, 139.75, 148.16, 151.25, 198.31. MS (EI) Calc [M]$^+$ (C$_{16}$H$_{13}$N$_3$O) m/z = 263.1. Found [M]$^+$ m/z = 263.1.

Synthesis of 31. Compound **25** (403 mg, 1.47 mmol), 4-acetylphenylboronic acid **26** (361 mg, 2.2 mmol) and cesium carbonate (1.433 g, 4.4 mmol) were added to a 3-neck round bottom flask equipped with a reflux condenser under nitrogen atmosphere. Degassed dioxane (20 mL) was added via syringe followed by the addition of palladium acetate (16 mg, 0.07 mmol) and tricyclohexylphosphine (41.1 mg, 0.14 mmol). The solution was heated to reflux for 24 h and the reaction mixture was then cooled to room temperature, diluted with ethyl acetate (100 mL) and washed with three 50 mL portions of water. The organic layer was concentrated and loaded onto a silica column with 40% ethyl acetate in hexanes as an eluent to give 220 mg of white solid in 47% yield. ^{1}H NMR (400 MHz, CDCl$_3$) δ 2.55 (s, 3H), 7.39-7.42 (m, 1H), 7.55-7.63 (m, 3H), 7.71-7.73 (m, 1H), 7.91 (d, J= 6.8 Hz), 8.08 (s, 1H), 8.17 (q, J= 7.8 Hz, 2H), 8.93 (s, 1H), 9.12 (s, 1H). ^{13}C NMR (100 MHz, CDCl$_3$) δ 26.53, 121.63, 122.73, 123.55, 125.37, 126.44, 127.08, 129.09, 129.16, 131.12, 134.93, 136.49, 136.52, 137.45, 138.47, 140.36, 150.38, 197.46. MS (ESI) Calc [M]$^+$ (20$_{20}$H15N$_3$O) m/z = 313.1. Found [M+H]$^+$ m/z = 314.1.

Synthesis of 32. Compound **25** (120 mg, 0.44 mmol), 3-acetylphenylboronic acid **27** (97 mg, 0.59 mmol) and cesium carbonate (284 mg, 0.87 mmol) were added to a 3-neck round bottom flask equipped with a reflux condenser under nitrogen atmosphere. Degassed dioxane (10 mL) was added via syringe followed by the addition of palladium acetate (7 mg, 0.03 mmol) and tricyclohexylphosphine (17 mg, 0.06 mmol). The solution was heated to reflux for 24 h and the reaction mixture was then cooled to room temperature, diluted with ethyl acetate (100 mL) and washed with three 50 mL portions of water. The organic layer was concentrated and loaded onto a silica column with 40% ethyl acetate in hexanes as an eluent to give 85 mg of white solid in 62% yield. ^{1}H NMR (400 MHz, CDCl$_3$) δ 2.60 (s, 3H), 7.41-7.42 (m, 2H), 7.65-7.66 (m, 1H) 7.80-7.82 (m, 3H), 8.12-8.24 (m, 4H), 9.00 (s, 1H), 9.12 (s, 1H). ^{13}C NMR (100 MHz, CDCl$_3$) δ 26.63, 121.43, 122.75, 123.04, 124.95, 126.26, 126.33, 126.80, 128.87, 128.98, 130.09, 130.52, 133.01, 136.31, 136.46, 137.39, 138.15, 140.24, 150.21, 198.06. MS (ESI) Calc [M]$^+$ (20$_{20}$H15N$_3$O) m/z = 313.12. Found [M+H]$^+$ m/z = 314.1288.

Synthesis of 33. Compound **25** (503 mg, 1.82 mmol), **28** (569 mg, 2.19 mmol) and cesium carbonate (1.786 g, 5.48 mmol) were added to a 3-neck round bottom flask equipped with a reflux condenser under nitrogen atmosphere. Degassed dioxane (20 mL) was added via syringe followed by the addition of palladium acetate (21 mg, 0.09 mmol) and tricyclohexylphosphine (51 mg, 0.18 mmol). The solution was heated to reflux for 24 h and the reaction mixture was then cooled to room temperature, diluted with ethyl acetate (100 mL) and washed with three 50 mL portions of water. The organic layer was concentrated and loaded onto a silica column with

40% ethyl acetate in hexanes as an eluent to give 318 mg of white solid in 53% yield. ^{1}H NMR (400 MHz, CDCl$_3$) δ 2.19 (s, 3H), 3.73 (s, 2H), 7.24-7.26 (m, 2H), 7.48-7.51 (m, 1H), 7.48-7.68 (m, 3H), 7.80-7.82 (m, 1H), 8.09 (s, 1H), 8.25 (d, $J = 7.6$ Hz, 2H), 9.01 (s, 1H), 9.07 (s, 1H). ^{13}C NMR (100 MHz, CDCl$_3$) δ 25.02, 29.48, 50.91, 71.99, 121.76, 123.68, 123.78, 126.34, 126.71, 127.02, 129.40, 130.06, 130.53, 131.69, 132.54, 136.75, 136.97, 138.61, 140.65, 150.51, 206.74. Calc [M+Na]$^+$ (C$_{21}$H$_{17}$N$_3$O) m/z = 350.1275. Found Hi Res ESI [M+Na] = 350.1264.

General Procedure for preparing platinum complexes. Complexes were prepared according to a procedure reported by Newkome et al.[32] Briefly, potassium tetrachloroplatinate (II) is dissolved in water at 65 °C and then an equimolar amount of the ligand is added dropwise in a solution of acetone. The solution is maintained at 65 °C for 6h and then cooled to room temperature and filtered. The precipitate is washed excessively with water and acetone. The solids were screened for their in vitro toxicity. Only the complexes that were taken forward to polymer attachment and *in vivo* evaluation were fully analyzed.

Synthesis of 7. ^{1}H NMR (500 MHz, DMSO-d_6) δ 2.69 (s, 3H), 7.89 (s, 1H), 8.43 (s, 1H), 8.63-8.67 (m, 2H), 8.21-8.24 (m, 1H), 9.56 (s, 1H), 10.00 (s, 1H). Anal. Calcd for C$_{12}$H$_{10}$Cl$_2$N$_2$OPt: C, 31.05; H, 2.17; N, 6.03. Found: C, 31.27; H, 1.98; N, 5.88.

Synthesis of 8. ^{1}H NMR (500 MHz, DMSO-d_6) δ 2.70 (s, 3H), 7.74-7.76 (m, H), 8.02 (t, $J = 7.5$ Hz, 1H), 8.25 (d, $J = 8.5$ Hz, 1H), 8.48 (d, $J = 8$ Hz, 1H), 8.68 (d, $J = 8.5$ Hz, 1H), 8.87-8.92 (m, 2H), 9.46 (d, $J = 5$ Hz, 1H), 9.98 (s, 1H). Anal. Calcd for C$_{16}$H$_{12}$Cl$_2$N$_2$OPt: C, 37.37; H, 2.15; N, 5.45. Found: C, 36.79; H, 2.09; N, 5.15.

Synthesis of 18. ^{1}H NMR (500 MHz, DMSO-d_6) δ 1.32 (s, 9H), 2.67 (s, 3H), 7.51-7.79 (m, 4H), 8.37 (d, $J = 8.5$ Hz, 1H), 8.70 (s, 1H), 8.99 (d, $J = 7$ Hz, 1H), 9.56 (s, 1H), 9.86 (s, 1H). Anal. Calcd for C$_{16}$H$_{12}$Cl$_2$N$_2$OPt: C, 41.03; H, 3.62; N, 7.18. Found: C, 40.15; H 3.07; N, 7.76.

Synthesis of 36. ^{1}H NMR (500 MHz, DMSO-d_6) δ 2.60 (s, 3H), 7.69-7.71 (m, 1H), 7.78 (t, $J = 7.5$ Hz, 1H), 7.88-8.01 (m, 4H), 8.08 (d, $J = 5$ Hz), 8.17 (d, $J = 6$ Hz, 1H), 8.41 (s, 1H), 8.55-8.57 (m, 1H), 9.05-9.06 (m, 1H), 9.26 (s, 1H). Anal. Calcd for C$_{20}$H$_{15}$Cl$_2$N$_3$OPt: C, 41.46; H, 2.44; N, 7.25. Found: C, 41.84; H, 2.55; N, 6.92.

Synthesis of 37. ^{1}H NMR (500 MHz, DMSO-d_6) δ 2.66 (s, 3H), 7.58 (t, $J = 8$ Hz, 1H), 7.69-7.71 (m, 1H), 7.78 (t, $J = 8$ Hz, 1H), 7.99-8.01 (m, 1H), 8.16-8..18 (m, 1H), 8.26 (s, 1H), 8.55-8.57 (m, 1H), 9.06-9.07 (m, 1H), 9.25 (s, 1H). Anal. Calcd for C$_{20}$H$_{15}$Cl$_2$N$_3$OPt: C, 41.46; H, 2.44; N, 7.25. Found: C, 41.52; H, 2.55; N, 7.29.

Synthesis of 38. ^{1}H NMR (500 MHz, DMSO-d_6) δ 2.15 (s, 3H), 3.78 (s, 2H), 7.23-7.25 (m, 2H), 7.66-7.71 (m, 3H), 7.77 (t, $J = 7$ Hz, 1H), 8.06 (d, $J = 8$ Hz, 1H), 8.17 (d, $J = 7.5$ Hz, 1H), 8.27 (s, 1H), 8.55 (d, $J = 8.5$ Hz, 1H), 9.04-9.05 (m, 1H), 9.15 (s, 1H). Anal. Calcd for C$_{21}$H$_{17}$Cl$_2$N$_3$OPt: C, 42.51; H, 2.89; N, 7.08. Found: C, 40.99; H, 2.11; N, 7.25.

General Procedure for Platinum Attachment to Polymer. Dendrimer **51** was prepared by the same procedure outlined in Chapter 2. The polymer and three equivalents of complex per hydrazide were weighed into a 20 mL reaction vial that is under nitrogen atmosphere. The solids are dissolved in dry DMF at a concentration of ~100 mg/mL with respect to the polymer. The solution was stirred at 60° C for 18h and then precipitated into ether. The polymer was re-dissolved in methanol and filtered through a 20 μm filter to remove excess small molecule platinum, which is not soluble in methanol. The polymer is then purified by size exclusion chromatography through an LH-20 size exclusion resin with methanol as the eluent to remove

any trace free drug. Finally, the polymer samples are re-dissolved in water and passed through PD-10 desalting columns and lyophilized. The drug loading of the final conjugates was determined by inductively coupled plasma atomic emission spectroscopy (ICP-AES).

Toxicity of Platinum Complexes in Murine and Human Cells. C26 murine cells were seeded onto a 96-well plate at a density of 5.0×10^3 cells per well in 100 μl of medium and incubated overnight (37 °C, 5% CO_2, and 80% humidity). Human HeLa, CAOV-3, SK-BR-3, and A549 cells were seeded at a density of 1.0×10^4 cells per well. An additional 100 μl of new medium (RPMI medium 1640/10% FBS/1% Glutamax/1% penicillin-streptomycin for C26 and DMEM medium/10% FBS/1% P-S for human cells) containing the platinum complexes, or oxaliplatin and cisplatin controls, was added to the cells. Small molecule drugs were tested at concentrations ranging from 450 μM to 0.2 μM Pt equivalents, PEG-Pt from 900 μM to 0.4 μM, and dendrimer-Pt from 1.1 mM to 0.3 μM. The tests were conducted in triplicate for each concentration. After incubation for 72 h, 40 μl of media containing thiazolyl blue tetrazolium bromide solution (2.5 mg/mL) was added. The cells were incubated for 2 h, after which time the medium was carefully removed. To the resulting purple crystals was added 200 μl of DMSO, followed by 25 μl of pH 10.5 glycine buffer (0.1 M glycine/0.1 M NaCl). The optical densities at 570 nm were measured by using a SpectraMAX 190 microplate reader (Molecular Devices, Sunnyvale, CA). Optical densities measured for wells containing cells that received neither polymer nor drug were considered to represent 100% viability. IC_{50} values were obtained from sigmoidal fits of semilogarithmic plots of the percentage of viability versus platinum concentration by using Origin 7 SR4 8.0552 software (OriginLab, Northhampton, MA).

Drug Release Experiments. Hydrolysis of the platinum drug was monitored by HPLC with SEC system C and a Shodex SB-804 HQ column maintained at 37 °C. An isocratic flow rate of 0.7 mL/min was used with a 70%/30%/0.05% water/acetonitrile/TFA mobile phase. Each sample was dissolved in 37 °C acetate buffer (pH 5, 100 mM) at a concentration of ~ 2 mg/ml and filtered. Samples were kept at 37 °C for the duration of the study with 25 μL aliquots injected over 48 h.

Animal and Tumor Models. All animal experiments were performed in compliance with National Institutes of Health guidelines for animal research under a protocol approved by the Committee on Animal Research at the University of California (San Francisco, CA) (UCSF). C26 colon carcinoma cells obtained from the UCSF cell culture facility were cultured in RPMI medium 1640 containing 10% FBS. Female BALB/c mice were obtained from Simonsen Laboratories, Inc. (Gilroy, CA).

Toxicity in Healthy Mice. Female Balb/C mice were injected with polymers **39**-**44** via tail vein injection (15 mg Pt/kg and 45 mg Pt/kg) or via intraperitoneal (90 mg Pt/kg) injection. Mice weight and general health was monitored over 10 days. When gross toxicity was observed- loss of greater than 15% of initial body weight, lethargy and ruffled fur, mice were removed from the study.

Biodistribution Study in Tumored Mice. Six- to eight week-old female Balb/C mice were injected in the right hind flank with 3×10^5 C26 cells. Ten days after tumor inoculation, mice were randomized into five groups of two mice each. Mice were injected by means of the tail vein either with Cisplatin (6 mg/kg), **38** (6 mg/kg), **50** (6 mg Pt/kg), **41** (6 mg Pt/kg) or **44** (6 mg Pt/kg) in ~200 μL of PBS. Blood was collected by submandibular bleeds 60 min and 24 h after dosing; mice were sacrificed 48 h postinjection. The blood (collected by heart puncture), heart, liver, spleen, kidney, and tumor were collected for analysis. Blood was collected in vials coated with 10 μL heparin (50 mg/mL) to prevent clotting and centrifuged for 10 min at 5,000 rpm to

allow for serum removal. Each organ was weighed and 200-300 mg of the collected organs were homogenized with zirconium beads and 250 µL deionized water. The tissue and 48 h serum samples were diluted with 583 μL concentrated HNO_3 and the remaining serum samples were diluted with 200 µL dI water and 466 µL HNO_3 (~70% acid solution). Samples were gently heated at 40 °C overnight. Supernatant (500 µL) was added to 3.5 mL 20% HCl and briefly centrifuged to remove any insoluble particulates. Platinum content in each sample was analyzed by ICP at 265 nm.

Chemotherapy Experiment in C26 Tumored Mice. While under anesthesia, female Balb/C mice were shaved, and C26 cells (3 x 10^5 cells in 50 µL) were injected subcutaneously in the right hind flank. At eight days post-tumor implantation, mice were randomly distributed into treatment groups of 6 animals. Mice were injected by means of the tail vein with Cisplatin (6 mg/kg), **38** (10 mg/kg), and polymers **39**-**44** (36 mg Pt/kg) in approximately 200 µL of solution. Doxil (20 mg Dox/kg) was used as an internal standard to verify consistent tumor responses between studies. Five out of six mice treated were tumor free at the end of the study, which is comparable to previous experiments. Mice were weighed and tumors measured every other day. The tumor volume was estimated by measuring the tumor volume in three dimension with calipers and calculated using the formula tumor volume = length x width x height. Mice were removed from the study when (i) a mouse lost 15% of its initial weight, (ii) any tumor dimension was > 20 mm, or (iii) the mouse was found dead. The mice were followed until day 60 post-tumor inoculation.

Computational Modeling. Computational studies were conducted at the Molecular Graphics and Computation Facility, College of Chemistry, University of California, Berkeley. Molecular geometries were optimized to an energy minimum using Gaussian 09 program at the DFT B3LYP level with lanl2dz basis set on Pt and 6-31G(d,p) on all other atoms.[33] Optimized geometries were confirmed as energy minima through a vibration calculation at the same level which yielded no negative frequencies. Bond distances and angles were taken from these optimized geometries.

Crystallography. Crystallographic data collection was conducted by the College of Chemistry X-Ray Crystallography Facility, University of California, Berkeley on a Bruker APEX II Quazar. A yellow rod 0.25 x 0.10 x 0.10 mm in size was mounted on a Cryoloop with Paratone oil. Data were collected in a nitrogen gas stream at 153(2) K using phi and omega scans. Crystal-to-detector distance was 60 mm and exposure time was 10 seconds per frame using a scan width of 0.3°. Data collection was 100.0% complete to 25.00° in θ. A total of 19953 reflections were collected covering the indices, $-9<=h<=9$, $-16<=k<=16$, $-20<=l<=20$. 3412 reflections were found to be symmetry independent, with an R_{int} of 0.0224. Indexing and unit cell refinement indicated a primitive, monoclinic lattice. The space group was found to be P2(1)/c (No. 14). The data were integrated using the Bruker SAINT software program and scaled using the SADABS software program. Solution by direct methods (SIR-2008) produced a complete heavy-atom phasing model consistent with the proposed structure. All non-hydrogen atoms were refined anisotropically by full-matrix least-squares (SHELXL-97). All hydrogen atoms were placed using a riding model. Their positions were constrained relative to their parent atom using the appropriate HFIX command in SHELXL-97.

Table 4.3. Crystal data and structure refinement for **37**.

X-ray ID	**37**
Sample/notebook ID	DV-5-76
Empirical formula	C20 H15 Cl2 N3 O Pt
Formula weight	579.34
Temperature	153(2) K
Wavelength	0.71073 Å
Crystal system	Monoclinic
Space group	P2(1)/c
Unit cell dimensions	a = 7.9363(13) Å $\alpha= 90°$.
	b = 13.778(2) Å $\beta= 101.499(2)°$.
	c = 17.356(3) Å $\gamma = 90°$.
Volume	1859.8(5) $Å^3$
Z	4
Density (calculated)	2.069 Mg/m^3
Absorption coefficient	7.848 mm^{-1}
F(000)	1104
Crystal size	0.25 x 0.10 x 0.10 mm^3
Crystal color/habit	yellow rod
Theta range for data collection	1.90 to 25.35°.
Index ranges	-9<=h<=9, -16<=k<=16, -20<=l<=20
Reflections collected	19953
Independent reflections	3412 [R(int) = 0.0224]
Completeness to theta = 25.00°	100.0 %
Absorption correction	Semi-empirical from equivalents
Max. and min. transmission	0.5075 and 0.2444
Refinement method	Full-matrix least-squares on F^2
Data / restraints / parameters	3412 / 0 / 245
Goodness-of-fit on F^2	1.033
Final R indices [I>2sigma(I)]	R1 = 0.0184, wR2 = 0.0439
R indices (all data)	R1 = 0.0193, wR2 = 0.0445
Largest diff. peak and hole	1.503 and -0.842 $e.Å^{-3}$
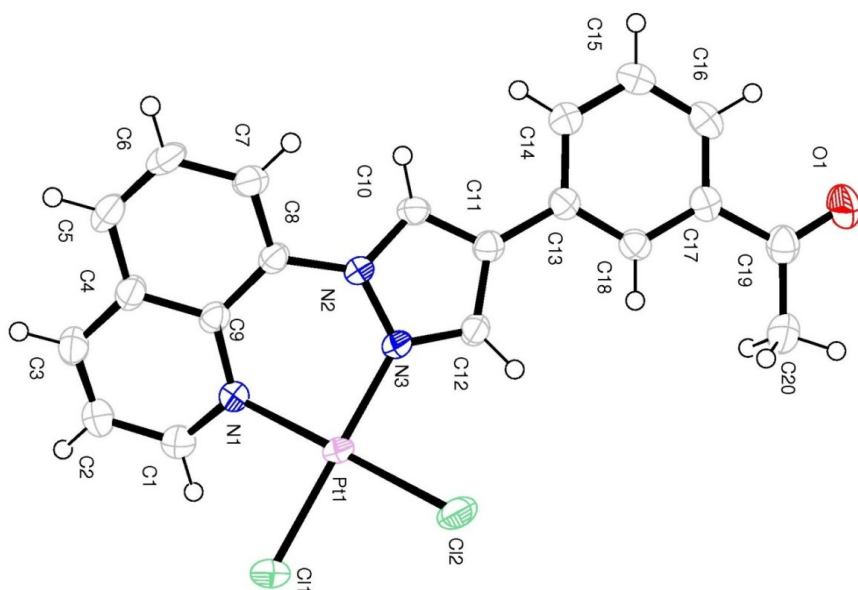
Table 4.4. Atomic coordinates (x 10^4) and equivalent isotropic displacement parameters (Å^2x 10^3) for **37**. U(eq) is defined as one third of the trace of the orthogonalized U^{ij} tensor.

	x	y	z	U(eq)
C(1)	12850(5)	980(3)	1803(2)	40(1)
C(2)	13950(5)	325(3)	1530(2)	48(1)
C(3)	13598(5)	66(3)	763(2)	42(1)
C(4)	12275(4)	534(2)	240(2)	33(1)
C(5)	11906(5)	316(3)	-578(2)	37(1)
C(6)	10700(5)	822(3)	-1080(2)	38(1)
C(7)	9835(5)	1594(3)	-800(2)	34(1)
C(8)	10148(4)	1829(2)	-16(2)	27(1)
C(9)	11305(4)	1270(2)	535(2)	28(1)
C(10)	8896(4)	3464(2)	-294(2)	29(1)
C(11)	8194(4)	4161(2)	115(2)	28(1)
C(12)	8346(4)	3780(2)	872(2)	28(1)
C(13)	7434(4)	5091(2)	-208(2)	28(1)
C(14)	7305(4)	5303(3)	-1003(2)	36(1)
C(15)	6568(5)	6164(3)	-1316(2)	42(1)
C(16)	5937(5)	6820(3)	-848(2)	37(1)
C(17)	6063(4)	6627(2)	-54(2)	31(1)
C(18)	6816(4)	5762(2)	264(2)	29(1)
C(19)	5328(5)	7359(3)	422(2)	38(1)
C(20)	5592(6)	7227(3)	1293(3)	52(1)
N(1)	11526(3)	1402(2)	1337(2)	29(1)
N(2)	9413(3)	2710(2)	196(2)	26(1)
N(3)	9072(3)	2905(2)	921(2)	26(1)
O(1)	4531(4)	8049(2)	104(2)	51(1)
Cl(1)	10142(1)	884(1)	2836(1)	42(1)
Cl(2)	7426(1)	2592(1)	2356(1)	44(1)
Pt(1)	9611(1)	1979(1)	1817(1)	27(1)

Table 4.5. Bond lengths [Å] and angles [°] for **37**.

C(1)-N(1)	1.326(4)	C(12)-N(3)	1.332(4)
C(1)-C(2)	1.403(5)	C(12)-H(12)	0.9500
C(1)-H(1)	0.9500	C(13)-C(18)	1.387(5)
C(2)-C(3)	1.353(5)	C(13)-C(14)	1.395(5)
C(2)-H(2)	0.9500	C(14)-C(15)	1.385(5)
C(3)-C(4)	1.401(5)	C(14)-H(14)	0.9500
C(3)-H(3)	0.9500	C(15)-C(16)	1.376(5)
C(4)-C(5)	1.422(5)	C(15)-H(15)	0.9500
C(4)-C(9)	1.429(4)	C(16)-C(17)	1.387(5)
C(5)-C(6)	1.351(5)	C(16)-H(16)	0.9500
C(5)-H(5)	0.9500	C(17)-C(18)	1.397(5)
C(6)-C(7)	1.405(5)	C(17)-C(19)	1.495(5)
C(6)-H(6)	0.9500	C(18)-H(18)	0.9500
C(7)-C(8)	1.373(5)	C(19)-O(1)	1.213(4)
C(7)-H(7)	0.9500	C(19)-C(20)	1.495(6)
C(8)-C(9)	1.414(5)	C(20)-H(20A)	0.9800
C(8)-N(2)	1.426(4)	C(20)-H(20B)	0.9800
C(9)-N(1)	1.379(4)	C(20)-H(20C)	0.9800
C(10)-N(2)	1.354(4)	N(1)-Pt(1)	2.035(3)
C(10)-C(11)	1.376(4)	N(2)-N(3)	1.364(4)
C(10)-H(10)	0.9500	N(3)-Pt(1)	1.991(3)
C(11)-C(12)	1.399(4)	Cl(1)-Pt(1)	2.2983(9)
C(11)-C(13)	1.478(4)	Cl(2)-Pt(1)	2.2903(9)
N(1)-C(1)-C(2)	123.2(3)	C(11)-C(10)-H(10)	125.8
N(1)-C(1)-H(1)	118.4	C(10)-C(11)-C(12)	104.8(3)
C(2)-C(1)-H(1)	118.4	C(10)-C(11)-C(13)	125.9(3)
C(3)-C(2)-C(1)	118.8(4)	C(12)-C(11)-C(13)	129.3(3)
C(3)-C(2)-H(2)	120.6	N(3)-C(12)-C(11)	110.7(3)
C(1)-C(2)-H(2)	120.6	N(3)-C(12)-H(12)	124.6
C(2)-C(3)-C(4)	119.8(3)	C(11)-C(12)-H(12)	124.6
C(2)-C(3)-H(3)	120.1	C(18)-C(13)-C(14)	118.7(3)
C(4)-C(3)-H(3)	120.1	C(18)-C(13)-C(11)	121.3(3)
C(3)-C(4)-C(5)	121.9(3)	C(14)-C(13)-C(11)	120.0(3)
C(3)-C(4)-C(9)	118.8(3)	C(15)-C(14)-C(13)	120.6(3)
C(5)-C(4)-C(9)	119.3(3)	C(15)-C(14)-H(14)	119.7
C(6)-C(5)-C(4)	120.9(3)	C(13)-C(14)-H(14)	119.7
C(6)-C(5)-H(5)	119.6	C(16)-C(15)-C(14)	120.5(3)
C(4)-C(5)-H(5)	119.6	C(16)-C(15)-H(15)	119.8
C(5)-C(6)-C(7)	120.0(3)	C(14)-C(15)-H(15)	119.8
C(5)-C(6)-H(6)	120.0	C(15)-C(16)-C(17)	119.8(3)
C(7)-C(6)-H(6)	120.0	C(15)-C(16)-H(16)	120.1
C(8)-C(7)-C(6)	121.1(3)	C(17)-C(16)-H(16)	120.1
C(8)-C(7)-H(7)	119.4	C(16)-C(17)-C(18)	119.8(3)
C(6)-C(7)-H(7)	119.4	C(16)-C(17)-C(19)	117.5(3)
C(7)-C(8)-C(9)	120.5(3)	C(18)-C(17)-C(19)	122.7(3)
C(7)-C(8)-N(2)	117.0(3)	C(13)-C(18)-C(17)	120.6(3)
C(9)-C(8)-N(2)	122.2(3)	C(13)-C(18)-H(18)	119.7
N(1)-C(9)-C(8)	123.0(3)	C(17)-C(18)-H(18)	119.7
N(1)-C(9)-C(4)	119.1(3)	O(1)-C(19)-C(20)	120.7(4)
C(8)-C(9)-C(4)	117.9(3)	O(1)-C(19)-C(17)	120.2(4)
N(2)-C(10)-C(11)	108.3(3)	C(20)-C(19)-C(17)	119.1(3)
N(2)-C(10)-H(10)	125.8	C(19)-C(20)-H(20A)	109.5

C(19)-C(20)-H(20B)	109.5
H(20A)-C(20)-H(20B)	109.5
C(19)-C(20)-H(20C)	109.5
H(20A)-C(20)-H(20C)	109.5
H(20B)-C(20)-H(20C)	109.5
C(1)-N(1)-C(9)	118.9(3)
C(1)-N(1)-Pt(1)	119.2(2)
C(9)-N(1)-Pt(1)	120.6(2)
C(10)-N(2)-N(3)	109.7(3)
C(10)-N(2)-C(8)	125.4(3)
N(3)-N(2)-C(8)	124.8(3)
C(12)-N(3)-N(2)	106.5(3)
C(12)-N(3)-Pt(1)	130.7(2)
N(2)-N(3)-Pt(1)	122.87(19)
N(3)-Pt(1)-N(1)	89.54(11)
N(3)-Pt(1)-Cl(2)	91.19(8)
N(1)-Pt(1)-Cl(2)	178.67(8)
N(3)-Pt(1)-Cl(1)	178.01(8)
N(1)-Pt(1)-Cl(1)	91.23(8)
Cl(2)-Pt(1)-Cl(1)	88.02(3)

Table 4.6. Anisotropic displacement parameters ($\text{Å}^2 \times 10^3$) for **37**. The anisotropic displacement factor exponent takes the form: $-2\pi^2[\ h^2 a^{*2} U^{11} + ... + 2\ h\ k\ a^*\ b^*\ U^{12}\ ]$

	U^{11}	U^{22}	U^{33}	U^{23}	U^{13}	U^{12}
C(1)	44(2)	44(2)	31(2)	2(2)	7(2)	10(2)
C(2)	51(2)	48(2)	45(2)	8(2)	13(2)	23(2)
C(3)	47(2)	35(2)	47(2)	4(2)	19(2)	13(2)
C(4)	40(2)	26(2)	37(2)	-1(1)	17(2)	1(1)
C(5)	46(2)	31(2)	41(2)	-8(2)	23(2)	-3(2)
C(6)	53(2)	37(2)	27(2)	-10(2)	17(2)	-7(2)
C(7)	43(2)	34(2)	27(2)	0(1)	10(2)	1(2)
C(8)	30(2)	28(2)	27(2)	-2(1)	11(1)	0(1)
C(9)	32(2)	25(2)	29(2)	0(1)	13(1)	-1(1)
C(10)	32(2)	32(2)	23(2)	3(1)	7(1)	0(1)
C(11)	24(2)	33(2)	29(2)	0(1)	7(1)	-1(1)
C(12)	28(2)	30(2)	27(2)	-4(1)	6(1)	3(1)
C(13)	22(2)	30(2)	32(2)	3(1)	6(1)	-1(1)
C(14)	40(2)	37(2)	33(2)	2(2)	11(2)	5(2)
C(15)	49(2)	45(2)	31(2)	8(2)	6(2)	6(2)
C(16)	36(2)	30(2)	41(2)	8(2)	3(2)	1(1)
C(17)	26(2)	29(2)	39(2)	2(1)	7(1)	-2(1)
C(18)	27(2)	30(2)	30(2)	3(1)	6(1)	-1(1)
C(19)	37(2)	30(2)	47(2)	2(2)	12(2)	1(2)
C(20)	64(3)	44(2)	52(2)	3(2)	24(2)	20(2)
N(1)	33(1)	30(2)	27(1)	2(1)	9(1)	6(1)
N(2)	29(1)	28(1)	22(1)	0(1)	8(1)	4(1)
N(3)	29(1)	29(1)	20(1)	-2(1)	6(1)	3(1)
O(1)	61(2)	33(2)	58(2)	2(1)	10(2)	16(1)
Cl(1)	58(1)	45(1)	26(1)	8(1)	14(1)	7(1)
Cl(2)	38(1)	69(1)	25(1)	-1(1)	11(1)	12(1)
Pt(1)	32(1)	32(1)	19(1)	-1(1)	7(1)	4(1)

Table 4.7. Hydrogen coordinates (x 10^4) and isotropic displacement parameters (Å^{2}x 10^3) for **37**.

	x	y	z	U(eq)
H(1)	13065	1130	2348	48
H(2)	14925	67	1878	57
H(3)	14246	-432	579	50
H(5)	12514	-191	-773	44
H(6)	10439	655	-1621	45
H(7)	9018	1960	-1159	41
H(10)	9001	3505	-829	34
H(12)	7980	4101	1295	34
H(14)	7727	4852	-1334	43
H(15)	6498	6302	-1858	50
H(16)	5416	7405	-1068	44
H(18)	6906	5632	808	35
H(20A)	5031	7759	1521	78
H(20B)	6826	7230	1520	78
H(20C)	5092	6607	1410	78

REFERENCES

(1)   Giandomenico, C. M.; Abrams, M. J.; Murrer, B. A.; Vollano, J. F.; Rheinheimer, M. I.; Wyer, S. B.; Bossard, G. E.; Higgins, J. D. *Inorg. Chem.* **1995**, *34*, 1015–1021.

(2)   Dhar, S.; Lippard, S. J. *Proc. Natl. Acad. Sci. U.S.A.* **2009**, *106*, 22199–22204.

(3)   Mukhopadhyay, S.; Barnés, C. M.; Haskel, A.; Short, S. M.; Barnes, K. R.; Lippard, S. J. *Bioconjugate Chem.* **2008**, *19*, 39–49.

(4)   Dhar, S.; Liu, Z.; Thomale, J.; Dai, H.; Lippard, S. J. *J. Am. Chem. Soc.* **2008**, *130*, 11467–11476.

(5)   Dhar, S.; Gu, F. X.; Langer, R.; Farokhzad, O. C.; Lippard, S. J. *Proc. Natl. Acad. Sci. U.S.A.* **2008**, *105*, 17356–17361.

(6)   Dhar, S.; Daniel, W. L.; Giljohann, D. A.; Mirkin, C. A.; Lippard, S. J. *J. Am. Chem. Soc.* **2009**, *131*, 14652–14653.

(7)   Aryal, S.; Hu, C.-M. J.; Zhang, L. *ACS Nano* **2009**, *4*, 251–258.

(8)   Lee, C. C.; Gillies, E. R.; Fox, M. E.; Guillaudeu, S. J.; Fréchet, J. M. J.; Dy, E. E.; Szoka, F. C. *Proc. Natl. Acad. Sci. U.S.A.* **2006**, *103*, 16649–16654.

(9)   van Der Poll, D. G.; Kieler-Ferguson, H. M.; Floyd, W. C.; Guillaudeu, S. J.; Jerger, K.; Szoka, F. C.; Fréchet, J. M. *Bioconjugate Chem.* **2010**, *21*, 764–773.

(10)   Floyd, W. C.; Datta, G. K.; Imamura, S.; Kieler-Ferguson, H. M.; Jerger, K.; Patterson, A. W.; Fox, M. E.; Szoka, F. C.; Fréchet, J. M. J.; Ellman, J. A. *ChemMedChem* **2011**, *6*, 49–53.

(11)   Gangopadhyay, S. B.; Roendigs, A.; Kangarloo, S. B.; Krebs, B.; Wolff, J. E. *Anticancer Res.* **2001**, *21*, 2039–2043.

(12)   Wilson, J. J.; Fedoce Lopes, J.; Lippard, S. J. *Inorg. Chem.* **2010**, *49*, 5303–5315.

(13)   Puscasu, I.; Mock, C.; Rauterkus, M.; Röndigs, A.; Tallen, G.; Gangopadhyay, S.; Wolff, J. E. A.; Krebs, B. *A Anorg AllG Chem* **2001**, *627*, 1292–1298.

(14)   Mansouri-Torshizi, H.; I-Moghaddam, M.; Divsalar, A.; Saboury, A.-A. *Bioorg. Med. Chem.* **2008**, *16*, 9616–9625.

(15) Mansuri-Torshizi, H.; Ghadimy, S.; Akbarzadeh, N. *Chem. Pharm. Bull.* **2001**, *49*, 1517–1520.

(16) Jin, V. X.; Ranford, J. D. *Inorg. Chim. Acta* **2000**, *304*, 38–44.

(17) Keter, F. K.; Kanyanda, S.; Lyantagaye, S. S. L.; Darkwa, J.; Rees, D. J. G.; Meyer, M. *Cancer Chemother. Pharmacol.* **2008**, *63*, 127–138.

(18) Elwell, K. E.; Hall, C.; Tharkar, S.; Giraud, Y.; Bennett, B.; Bae, C.; Carper, S. W. *Bioorg. Med. Chem.* **2006**, *14*, 8692–8700.

(19) Vo, V.; Kabuloglu-Karayusuf, Z. G.; Carper, S. W.; Bennett, B. L.; Evilia, C. *Bioorg. Med. Chem.* **2010**, *18*, 1163–1170.

(20) Marverti, G.; Cusumano, M.; Ligabue, A.; Di Pietro, M. L.; Vainiglia, P. A.; Ferrari, A.; Bergomi, M.; Moruzzi, M. S.; Frassineti, C. *J. Inorg. Biochem.* **2008**, *102*, 699–712.

(21) Lovejoy, K. S.; Todd, R. C.; Zhang, S.; McCormick, M. S.; D'Aquino, J. A.; Reardon, J. T.; Sancar, A.; Giacomini, K. M.; Lippard, S. J. *Proc. Natl. Acad. Sci. U.S.A.* **2008**, *105*, 8902–8907.

(22) Kostova, I. *Recent Pat. Anti-Cancer Drug Discovery* **2006**, *1*, 1–22.

(23) Park, G. Y.; Wilson, J. J.; Song, Y.; Lippard, S. J. *Proc. Natl. Acad. Sci. U.S.A.* **2012**.

(24) Kelland, L. *Nat. Rev. Cancer* **2007**, *7*, 573–584.

(25) Deng, J. Z.; Paone, D. V.; Ginnetti, A. T.; Kurihara, H.; Dreher, S. D.; Weissman, S. A.; Stauffer, S. R.; Burgey, C. S. *Org. Lett.* **2009**, *11*, 345–347.

(26) Sundquist, W. I.; Ahmed, K. J.; Hollis, L. S.; Lippard, S. J. *Inorg. Chem.* **1987**, *26*, 1524–1528.

(27) Holford, J.; Sharp, S. Y.; Murrer, B. A.; Abrams, M.; Kelland, L. R. *Br. J. Cancer* **1998**, *77*, 366–373.

(28) Guillaudeu, S. J.; Fox, M. E.; Haidar, Y. M.; Dy, E. E.; Szoka, F. C.; Fréchet, J. M. J. *Bioconjugate Chem.* **2008**, *19*, 461–469.

(29) Gillies, E. R.; Fréchet, J. M. J. *J. Am. Chem. Soc.* **2002**, *124*, 14137–14146.

(30) Fox, M.; Guillaudeu, S.; Fréchet, J.; Jerger, K.; Macaraeg, N.; Szoka, F. *Mol. Pharmaceutics* **2009**, *6*, 1562–1572.

(31) Padilla De Jesús, O. L.; Ihre, H. R.; Gagne, L.; Fréchet, J. M. J.; Szoka, F. C. *Bioconjugate Chem.* **2002**, *13*, 453–461.

(32) Newkome, G. R.; Theriot, K. J.; Fronczek, F. R.; Villar, B. *Organometallics* **1989**, *8*, 2513–2523.

(30) Gaussian 09, Revision **A.1**, Frisch, M. J.; Trucks, G. W.; Schlegel, H. B.; Scuseria, G. E.; Robb, M. A.; Cheeseman, J. R.; Scalmani, G.; Barone, V.; Mennucci, B.; Petersson, G. A.; Nakatsuji, H.; Caricato, M.; Li, X.; Hratchian, H. P.; Izmaylov, A. F.; Bloino, J.; Zheng, G.; Sonnenberg, J. L.; Hada, M.; Ehara, M.; Toyota, K.; Fukuda, R.; Hasegawa, J.; Ishida, M.; Nakajima, T.; Honda, Y.; Kitao, O.; Nakai, H.; Vreven, T.; Montgomery, Jr., J. A.; Peralta, J. E.; Ogliaro, F.; Bearpark, M.; Heyd, J. J.; Brothers, E.; Kudin, K. N.; Staroverov, V. N.; Kobayashi, R.; Normand, J.; Raghavachari, K.; Rendell, A.; Burant, J. C.; Iyengar, S. S.; Tomasi, J.; Cossi, M.; Rega, N.; Millam, N. J.; Klene, M.; Knox, J. E.; Cross, J. B.; Bakken, V.; Adamo, C.; Jaramillo, J.; Gomperts, R.; Stratmann, R. E.; Yazyev, O.; Austin, A. J.; Cammi, R.; Pomelli, C.; Ochterski, J. W.; Martin, R. L.; Morokuma, K.; Zakrzewski, V. G.; Voth, G. A.; Salvador, P.; Dannenberg, J. J.; Dapprich, S.; Daniels, A. D.; Farkas, Ö.; Foresman, J. B.; Ortiz, J. V.; Cioslowski, J.; Fox, D. J. Gaussian, Inc., Wallingford CT, 2009.

Chapter 5
Characterization of Sterol Modified Lipids

ABSTRACT
Bilayer stability is an important parameter in the design of effective liposomes. Sterol modified phospholipids have cholesterol covalently bound to the glycerol backbone which subsequently prevents cholesterol exchange with other membranes and increases stability. We measured the bilayer rigidity properties and correlated rigidity with content release using the fluorescent water-soluble carboxyfluorescein. Bilayer fluidity did not differ significantly between formulations, but leakage varied significantly, with leakage being more rapid as the SML acyl chain length decreased in length. A pharmacokinetic study confirmed that upon injection into mice, PEGylated SML liposomes with short acyl chain lengths (C8 or C12) released their contents much more rapidly than the longer acyl chain lengths (C16), although all three formulations had similar circulation times. This suggests that the SMLs could be useful for designing new drug formulations and studying liposomes *in vivo*.

INTRODUCTION
Liposomes are versatile drug carriers, which allow for the potential encapsulation of any drug, small molecule to protein, provided the correct formulation and encapsulation conditions are designed. Membrane stability is crucial to liposomal drug delivery, as unanticipated content release may have deleterious effects on both its safety and efficacy profiles. Liposome stability improves significantly with PEGylation and the incorporation of cholesterol into the lipid formulation. As with polymers, PEG provides a protective coating to limit interactions with other bilayers, limit opsonization, and increase circulation half-lives.[1] Likewise, cholesterol helps to maintain the integrity of the bilayer in the presence of external pressure such as serum proteins or osmotic gradients. Membranes under osmotic pressure will swell and burst causing rapid content release. In addition to osmotic stress, transfer of cholesterol from liposomal membranes to serum proteins and other membranes can induce content release.[2–4] Likewise, drug release rates can be controlled by the percentage of cholesterol in the bilayer.[5,6] Previously, the Szoka group has demonstrated that the covalent attachment of cholesterol to the PC lipid head group eliminates this cholesterol transfer.[7]

The sterol modified lipids[7,8] or SMLs were designed to improve the properties of the bilayer and subsequently improve drug efficacy. The bilayer properties have been studied extensively, verifying that SML liposomes have very similar properties to liposomes with unbound cholesterol. As expected, the lack of phase transitions upon the addition of cholesterol is also absent with SMLs. Further biophysical properties were explored by Langmuir isotherms, neutron reflectivity, and small angle neutron scattering.[9] Overall, the C16Chem SML had very similar bilayer properties compared to a DPPC/Chol liposome, with minor variations in head group hydration and lipid spacing. In contrast, content release varies considerably between formulations. To explore these differences further, fluorescence anisotropy measurements were conducted. Anisotropy requires the insertion of a fluorophore into the membrane, which can then be excited by plane polarized light. Rigid membranes will limit the motion of the fluorophore so the detected fluorescence intensity will not be diminished. Likewise, in fluid membranes the

fluorophore will have shifted completely out of the plane of detection, giving a significantly reduced signal.

Furthermore, we would like to explore the ability to track liposomes *in vivo* and more accurately determine the stability of the liposome. Carboxyfluorescein (CF) is a commonly used tracer dye to measure content release from liposomes, as the CF signal is quenched while concentrated in the aqueous compartment but easily quantifiable once leaked from the liposome.[10] While advantageous for serum samples, processing of tissues for fluorescence measurements often involves organic solvent extractions that may disrupt the liposomal membrane and affect content release. This step may confound measurement of entrapped and free contents. The fluorescent properties of the prodrug 4-methylumbelliferyl phosphate (MU-P) make it a useful alternative to CF as a tool for measuring liposome contents release. MU-P and its dephosphorylated form, methylumbelliferone (MU), an antiplasmodic agent[11], have distinct fluorescent spectra that allow for independent quantification. *In vivo*, MU-P released from the liposome may be quickly dephosphorylated by serum and tissue phosphatases to yield MU. We hypothesize that measuring both MU-P and MU in serum and tissue samples will yield insight into membrane stability *in vivo* that cannot be obtained by simply encapsulating CF. MU-P and MU signal may be representative of encapsulated and released contents, respectively.

In this study, we comprehensively assess a panel of SML liposome formulations for membrane fluidity and content release alongside liposomes composed of traditional PC lipids and cholesterol.

RESULTS AND DISCUSSION
SML Bilayer Fluorescence Anisotropy

Fluorescence anisotropy is a useful tool for analyzing the fluidity of membranes under a variety of conditions. A fluorophore capable of inserting into the lipid bilayer (we used 1,6-dephenyl-1,3,5-hexatriene (DPH)), is excited with vertical plane polarized light. In a process called photoselection, only the DPH molecules with absorption dipoles aligned with light become excited.[12] DPH emission is then measured vertically and horizontally. Membranes which are very rigid will restrict the motion of DPH and the vertical measurement will be preserved, whereas fluid membranes will have a significantly reduced vertical intensity. Anisotropy <r> is calculated as shown in Equation 1,

$$< r > = \frac{I_{VV} - G I_{VH}}{I_{VV} + 2 G I_{VH}} \qquad (1)$$

where *I* represents the intensity, the first subscript indicates that the excitation polarizer was aligned vertically, the second subscript is the emission polarizer, and *G* is a correction factor. Anisotropy values range from 0-0.4 with a membrane becoming more rigid with increasing <r>.
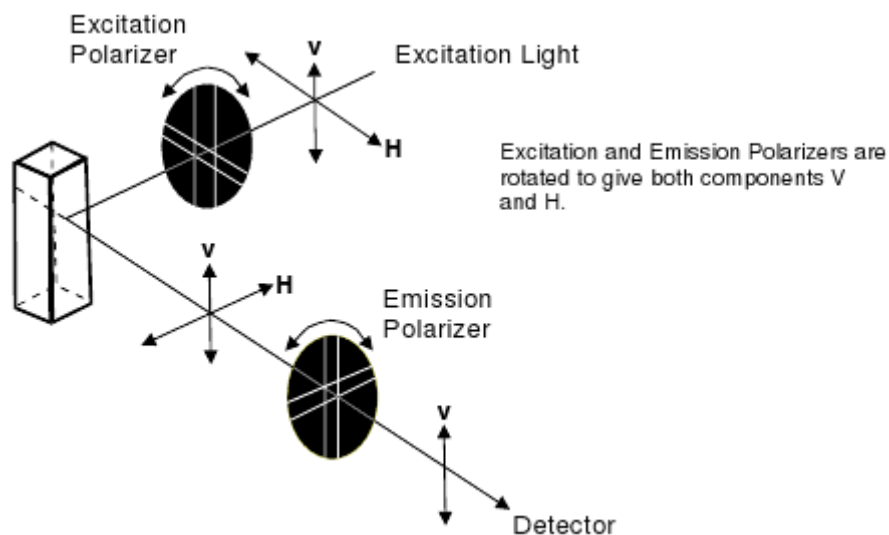
Figure 5.1. Polarization design to detect fluorescent intensities. Adapted from reference 12.

Liposomes from the six different categories shown in Figure 5.2 were formulated with DPH and the fluorescence intensity measured. We focused our efforts on the RChemsPC lipids (Figure 5.2F) as the one-step synthesis makes these amenable for large-scale use.
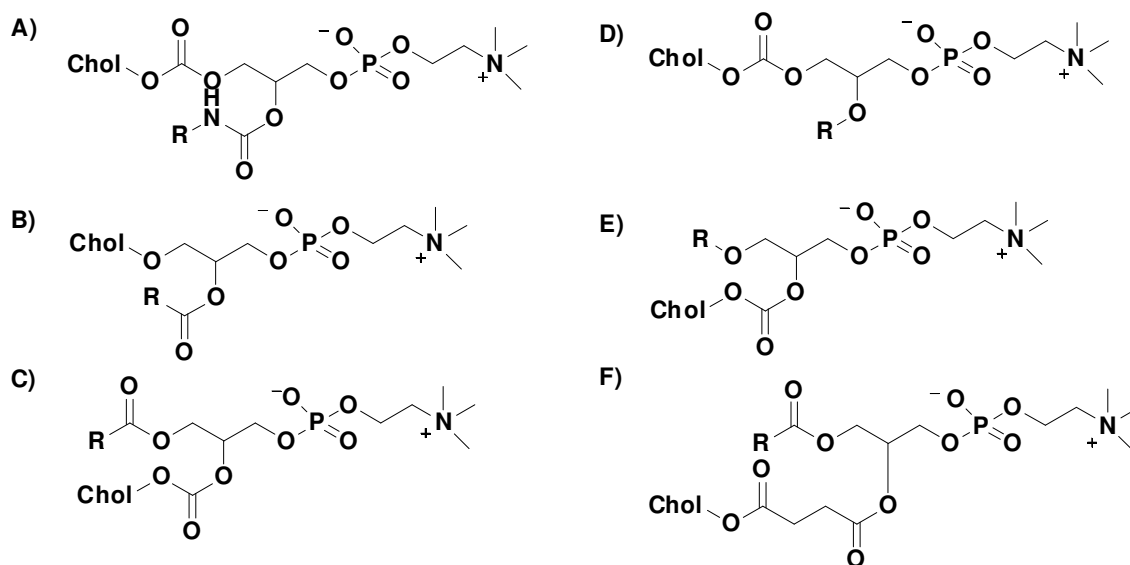

Figure 5.2. Sterol modified lipid categories with names based upon the linkage used for cholesterol and alkyl chain attachment. Abbreviations are as follows: Ch = cholesterol, c = carbonate linkage, a = amide linkage, e = ether linkage, R = alkyl chain where M is C14 and P is C16. The lack of a label indicates an ester linkage. A)ChcRaPC, B) ChcRePC, C) CheRPC, D) ReChcPC, E)RChcPC, F)RChemsPC.

Anisotropy for a typical PC lipid will follow a sigmoidal curve pattern: high <r> values at low temperatures are indicative of the rigid, crystalline state of the lipids, followed by a rapid change in anisotropy during the phase transition to the fluid, liquid crystal state. Addition of cholesterol into a membrane eliminates the lipid's natural T_m and keeps the bilayer in a gel-like state where

it is neither completely fluid nor rigid, an important element in the health and stability of biomembranes. Likewise, the anisotropy values will reflect this state. As seen in Figure 5.3, the reference DPPC:Chol mixture has an anisotropy value between 0.1-0.18, which doesn't fluctuate significantly with temperature changes. As was seen with the bilayer thickness study, the SML fluidity of the PChemsPC liposomes is 0.15 and is not significantly different than the PC:Cholesterol (5:4) prep. We see some variation based upon the type of cholesterol linkage and acyl chain length; however, these differences are not functionally significant. Taken together with previous studies, conjugation of cholesterol to the lipid backbone does not significantly modify the bilayer structure but does affect content release rates.
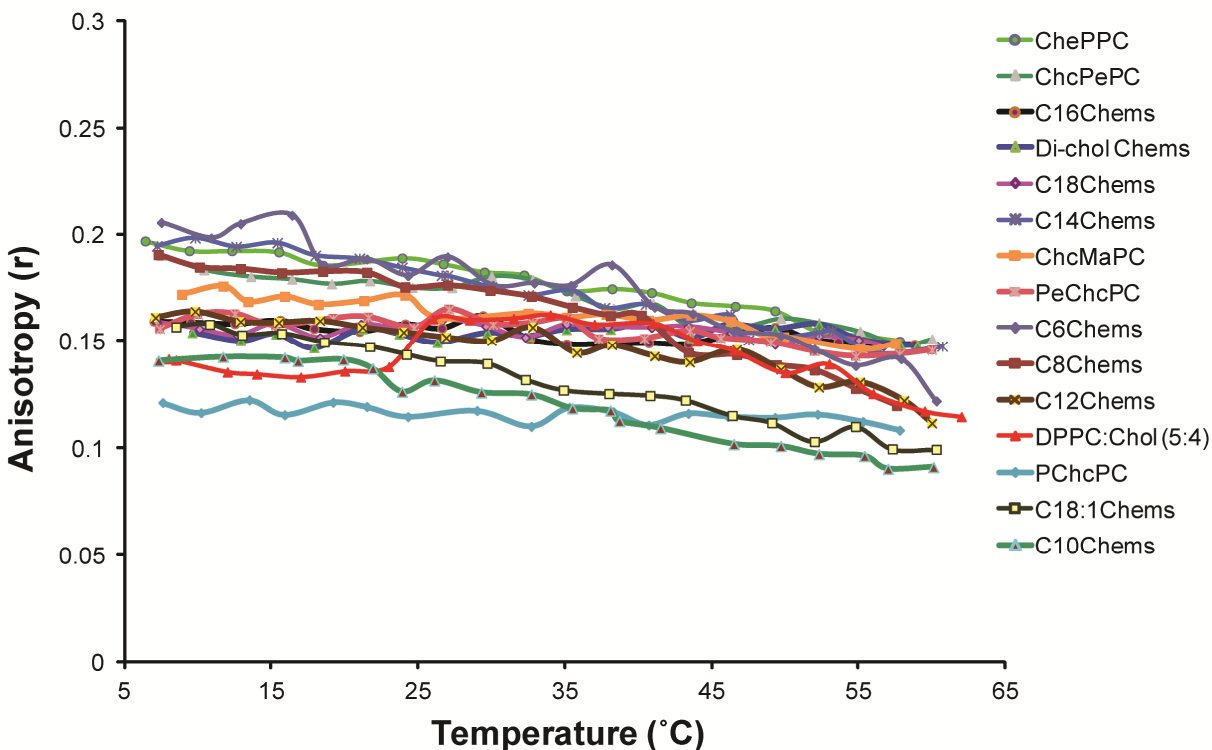

Figure 5.3. Anisotropy measurements of the six types of sterol modified lipids with an emphasis on the C6Chems to C18Chems liposomes.

Contents Retention of SML based Liposomes

Two anions, carboxyfluorescein (CF) and 4-methylumbelliferyl phosphate (MU-P) (Figure 5.4), were passively encapsulated into liposomes and their release with and without serum was monitored by fluorescence. The following liposomal formulations were assayed for content release: 1) Diacyl PC:Cholesterol:DSPE-PEG (55:40:5); 2) Diacyl PC:DiChems:DSPE-PEG (75:25:5); 3) SML:DSPE-PEG (95:5) and 4) Diacyl PC:SML:DSPE-PEG (55:40:5). For reference, representative lipid structures are shown in Figure 5.5.
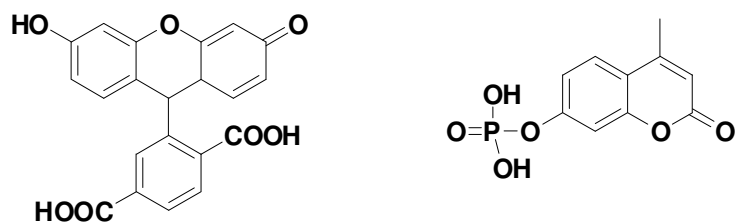
Figure 5.4. Structure of carboxyfluorescein (left) and 4-methylumbelliferyl phosphate (right)

Figure 5.5. Structure of lipids used in content release study. SML = C16Chems, Diacyl PC = DPPC

SML formulations encapsulating CF are most stable (Figure 5.6A/B) at intermediate chain length (16-18). In contrast, Diacyl:Cholesterol formulations are unstable at low chain length but extremely stable above chain lengths of 16. SML liposomes are more stable at low chain lengths (12,14) but still exhibit significant content leakage of more than 60%. Formulations incorporating DiChems as a substitute for cholesterol follow a similar pattern to Diacyl:Cholesterol formulations: they are unstable at low chain lengths but stable at high chain lengths. This binary switch in membrane stability is likely due to tighter membrane packing at high chain lengths.

Liposomes encapsulating MU-P demonstrate dramatically different leakage profiles to those containing CF which may be due to the dual negative charge on the phosphate interferes with MU-P crossing the hydrophobic membrane. At low chain lengths, the Diacyl:DiChems and Diacyl:SML formulations did not effectively retain contents. In contrast, these formulations demonstrated minimal leakage at longer chain lengths. This binary behavior may be due to a

88

difference in packing parameters at the different chain lengths. For example, at low chain lengths, the sterol modified lipids may not uniformly distribute in the membrane, inducing pore formation that facilitates content release. In contrast, the Diacyl:Cholesterol and SML liposomes demonstrate effective contents retention at all chain lengths. However, SML formulations decrease in stability at chain lengths above 20. As expected, the presence of serum increases the leakage of all formulations. The Diacyl:Cholesterol formulation seems to be the most stable in the presence of serum.
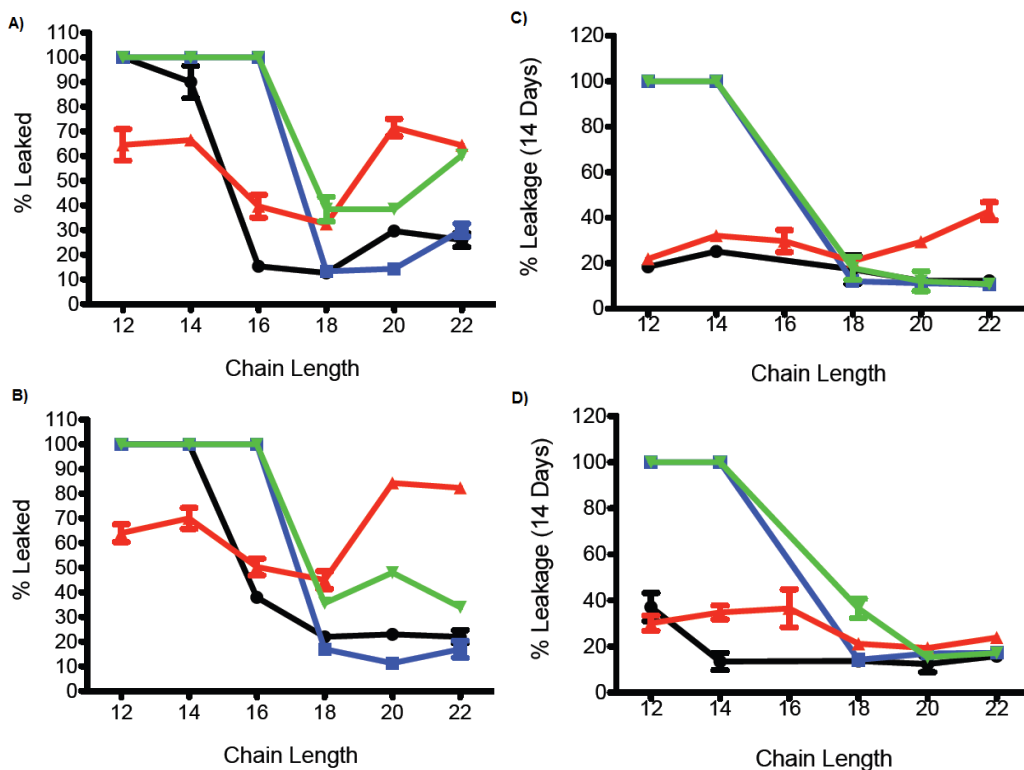

Figure 5.6. Content release of liposome formulations. ● Diacyl:Chol, ■ Diacyl:DiChems, ▲ SML, ▼ Diacyl:SML. A) CF in pH 7.4 HEPES buffer, B) CF in 30% serum/HEPES buffer, C) MU-P in pH 7.4 HEPES buffer, D) MU-P in 30% serum/HEPES buffer.

Overall, the SML lipids show similar contents retention of MU-P to Diacyl:Cholesterol formulations. At low chain lengths, SML formulations show improved retention of CF as compared to Diacy:Cholesterol formulations. At high chain lengths, formulations containing DiChems as the sterol show minimal leakage similar to Diacyl:Cholesterol formulations.

To further explore content release in a biological setting, the circulation of CF encapsulated liposomes was measured. Three lipids with different release profiles were selected for further study: C8Chems, C12Chems, and C16Chems. To accurately follow the liposomes, a membrane dye DiD was added to the formulation. Mice were injected with the different liposomes and blood samples were taken to quantify the concentration of CF compared to the DiD-tagged liposomes. All three formulations had favorable circulation profiles with > 20% of the dose remaining in the blood after 24 hours (Figure 5.7). As expected, the CF concentration was significantly reduced in the leakier C12Chems and C8Chems formulations while retained better

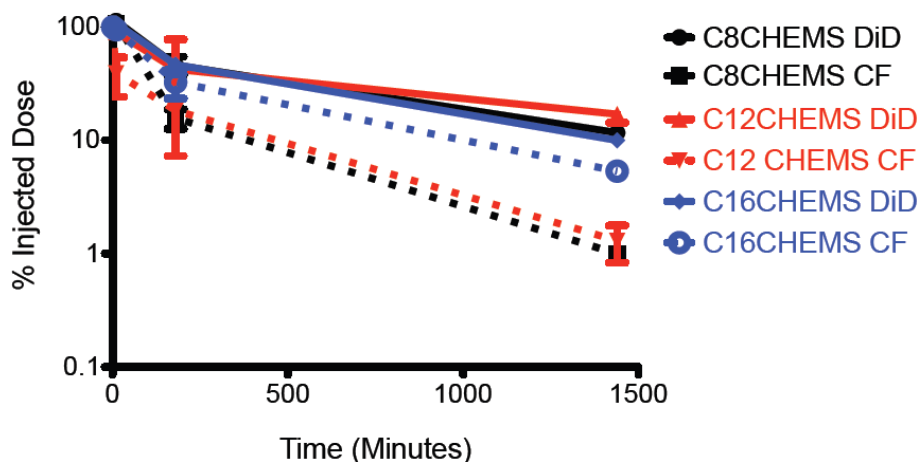in C16Chems. Encouraged by this result, the SMLs will be amenable for studying the biodistribution of MU-P/MU.

Figure 5.7. Circulation of carboxyfluorescein encapsulated liposomes in mice where liposomes are tracked with membrane dye DiD.

CONCLUSIONS AND FUTURE OUTLOOKS

A series of sterol modified liposomes were explored for their adjustable release of contents and bilayer structure. We found that the membrane fluidity did not differ from the traditional PC:Cholesterol formulation, but CF and MU-P release varied significantly based upon the formulation. All formulations were the most stable with acyl chain lengths of 18. MU-P was retained better at low chain lengths in the SMLs but at higher chain lengths for the DiChems:Diacyl liposomes. Overall, CF leaked to a greater extent than MU-P in the different formulations. All the lipid mixtures had some degree of leakage at the lower chain lengths and the SML mixtures had leakage at the higher chain lengths as well. These results are confirmed after different SML liposomes encapsulating CF were tracked *in vivo*. In general, MU-P gives better release profiles than CF and is amenable for use in biodistribution and PK studies.

Future work on this project will focus on the biodistribution of MU-P liposomes as an indicator of intact versus disrupted liposomes. Tracking the fate of liposomes and their contents in blood and tissue will help to better understand the behavior of the SMLs and explore other novel liposome formulations.

EXPERIMENTAL

Materials and Characterization. Materials were used as obtained from commercial sources unless otherwise noted. Lipids were purchased from Avanti Polar Lipids, kindly donated by Dr. Zhaohua Huang, or synthesized as previously described.[7,8] Solvents were removed under reduced pressure using a rotary evaporator. Average liposome diameter was determined by dynamic light scattering measurements (Malvern Instruments Zetasizer Nano ZS). Fluorescence spectroscopy was measured on a FluoroLog-3 spectrofluorometer (Horiba Jobin Yvon, Edison, NJ) equipped with a temperature controlled stage (LFI-3751) and a magnetic stirrer. A 450-W xenon light source was used for all recordings. Data acquisition was done through FluorEssence software (Horiba Scientific, Kyoto, Japan).

Fluorescent Anisotropy. Lipids were dissolved in chloroform, dried to form a thin film, and placed under high vacuum overnight. The films were hydrated with PBS at 65°C and vortexed to obtain a lipid concentration of 5 mM. The liposomes were sonicated at 65°C until opalescent and then extruded through 200 nm and 100 nm polycarbonate membranes at 65°C. Liposomes were diluted 8-fold with PBS and to a 3 ml sample was added 6 µl of 1,6-dephenyl-1,3,5-hexatriene (DPH) in THF (0.15 mg/ml). To allow the DPH to integrate into the bilayer, the mixture was incubated at 65°C for 1 hr. Anisotropy measurements were obtained as previously described[13] on a Horiba Fluorometer. Briefly, DPH was excited at 350 nm and the fluorescence detected at 430 nm. With mixing, the liposomes were heated or cooled in 5°C increments from 5-62°C, with a 5-10 min equilibration between transitions.

Liposomes for Content Leakage. Lipids were dissolved in chloroform, dried to form a thin film, and placed under high vacuum overnight. Lipid mixtures included Diacyl:Chol:PEG (55:40:5), Diacyl:SML:PEG (55:40:5), SML:PEG (95:5), and DiChems:Diacyl:PEG (20:75:5) with acyl chain lengths of C12-C22. The films were re-hydrated with 1 ml CF (50 mM) or 1 ml MU-P (300 mM) at 60°C and vortexed to obtain a lipid concentration of 5 mM. The liposomes were sonicated at 60°C until opalescent (~10 min) and extruded through 200 nm and 100 nm polycarbonate membranes at 60°C. Liposomes were purified on a Sephadex G-25 size exclusion column. Loading was quantified by disrupting the membrane with C12E10 surfactant and measuring the fluorescence of CF (ex 492 nm, em 517 nm) and MU-P (ex 319 nm, em 384 nm). Sodium azide (0.05%) was added to limit bacterial growth. The liposome samples were incubated at 37°C in the presence or absence of 30% fetal bovine serum (FBS) for 30 days. To calculate the leakage, a liposome aliquot was diluted with buffer, the fluorescence measured, and the membrane then disrupted with C12E10 to quantify the total loading. To measure retained MU-P in the liposomes, calf alkaline intestinal phosphatase (CIP) was added to catalyze the dephosphorylation of MU-P to MU (ex 360 nm, em 445 nm) and the total drug loading was quantified.

CF Pharmacokinetics. CF liposomes were prepared as described above. Lipid mixtures included: C16Chems:DiD:PEG (95:0.1:5), C12Chems:DiD:PEG (95:0.1:5), C18Chems:DiD:PEG (95:0.1:5), where DiD is a membrane dye used to track liposomes. Mice were injected with ~200 µl of liposome and blood was collected at 10 min, 60 min, and 24 h post- injection. PBS (1.5 ml) was added to 50 ul of blood and centrifuged for 10 min at 14,000 rpm. Serum (1 µl) was removed and diluted with 1 ml PBS and 20 µl C12E10. A standard curve was made by adding DiD liposomes to the serum from an untreated mouse. Encapsulated CF and DiD were quantified at 492 nm (ex)/ 517 nm (em) and 644 nm (ex)/ 664 nm (em), respectively.

REFERENCES

(1)   Moghimi, S. M.; Szebeni, J. *Prog. Lipid Res.* **2003**, *42*, 463–478.

(2)   Phillips, M. C.; Johnson, W. J.; Rothblat, G. H. *Biochim. Biophys. Acta* **1987**, *906*, 223–276.

(3)   Kan, C. C.; Yan, J.; Bittman, R. *Biochemistry* **1992**, *31*, 1866–1874.

(4)   Hamilton, J. A. *Curr. Opin. Lipidol.* **2003**, *14*, 263–271.

(5)   Drummond, D. C.; Meyer, O.; Hong, K.; Kirpotin, D. B.; Papahadjopoulos, D. *Pharmacol. Rev.* **1999**, *51*, 691–744.

(6)   Dos Santos, N.; Mayer, L. D.; Abraham, S. A.; Gallagher, R. C.; Cox, K. A. K.; Tardi, P. G.; Bally, M. B. *Biochim. Biophys. Acta, Biomembr.* **2002**, *1561*, 188–201.

(7)   Huang, Z.; Szoka, F. C. *J. Am. Chem. Soc.* **2008**, *130*, 15702–12.

(8)   Huang, Z.; Jaafari, M. R.; Szoka, F. C. *Angew. Chem., Int. Ed.* **2009**, *121*, 4210–4213.

(9)   Foglia, F.; Barlow, D. J.; Szoka, F. C.; Huang, Z.; Rogers, S. E.; Lawrences, M. J. *Langmuir* **2011**, *27*, 8275–8281.

(10)   Chen, R. F.; Knutson, J. R. *Anal. Biochem.* **1988**, *172*, 61–77.

(11)   Takeda, S.; Aburada, M. *J. Pharmacobio-Dyn.* **1981**, *4*, 724–734.

(12)   HORIBA Jobin Yvon Inc Polarizers for Spex Spectrofluorometers and FluorEssence Software Operation Manual.

(13)   Vest, R.; Wallis, R.; Jensen, L. B.; Haws, A. C.; Callister, J.; Brimhall, B.; Judd, A. M.; Bell, J. D. *J. Membr. Biol.* **2006**, *211*, 15–25.

Chapter 6
Designing Cisplatin Liposomes using Sterol Modified Lipids

ABSTRACT

Poor bioavailability has been a driving factor in the limited success of cisplatin containing liposomes. A new class of sterol modified lipids (SML) enables the production of liposomes with a wide range of content release rates which are a function of the acyl chain length and have a better correlation between *in vitro* and *in vivo* release of the encapsulated drug. Furthermore, a number of different formulation conditions such as the use of chaotropic agents were screened to increase cisplatin loading. SML-liposomes with shorter acyl chain lengths provided better cisplatin release, higher in vitro toxicities, and easier formulation conditions compared to traditional formulation compositions. We identified several promising SML candidate liposomes for *in vivo* studies. Favorable pharmacokinetic and biodistribution profiles were achieved, however, these formulations did not significantly improve antitumor activity in the murine colon carcinoma model as compared to the traditional cisplatin liposome formulation.

INTRODUCTION

The rationale behind polymer platinum delivery has been the design of chelators which release platinum slowly enough to reduce toxicity, but quickly enough to maintain activity. In contrast, liposomal delivery has focused on formulation conditions, which includes methods of encapsulation as well as lipid formulations that would provide appropriate platinum release *in vivo*. The instability of platinates make drug delivery more challenging. Cisplatin activity is increased by limiting light exposure, high salt solutions to prevent the loss of chloride and limit isomerization, and a lack of deactivating sulfur nucleophiles.[1,2] To this end, a variety of different lipid formulations have been explored for cisplatin[3–8], oxaliplatin[9–11] and other platinates.[12,13] Currently there are no FDA-approved platinum liposomes and only two formulations in clinical trials: Lipoplatin (cisplatin) and Lipoxal (oxaliplatin), developed by Regulon.[14,15]

SPI-077 (SEQUUS) is a well-known cisplatin formulation removed from clinical trials due to lack of activity. SPI-077 is composed of hydrogenated soy phosphatidylcholine (HSPC), cholesterol, and m-PEG-DSPE at a 51:44:5 molar ratio; this formulation exhibited superior results in animal models compared to both cisplatin and other cisplatin liposome formulations.[5] Despite having appreciable Pt uptake in tumor tissue and improved survival outcomes in mice, there was minimal activity in Phase I/II clinical trials.[16–19] Zamboni *et al*. used microdialysis in mice to track the bioavailability of cisplatin and found that only a small percentage of the drug was freely diffusible, despite the improved tumor accumulation.[20] These results were confirmed in a similar efficacy study by Bandak and coworkers, where less than 10% of cisplatin was released from liposomes and no improvement in efficacy was observed in lung, lymphoma and melanoma models.[21]

This data suggested to us that a new liposome formulation which increases the bioavailability of cisplatin is needed. Thus, we were interested in exploring the potential of the sterol modified lipids to deliver cisplatin, as the studies in Chapter 5 showed variable content release based upon chain length and lipid composition.

RESULTS AND DISCUSSION
Formulation Strategies

Our approach to designing a successful cisplatin liposome relied upon three important parameters: loading conditions, cisplatin solubility and stability. As we will show, focusing on one parameter can often lead to improvements while a different facet of the formulation suffers (Table 6.1). The initial focus was to improve cisplatin solubility and thus simplify encapsulation and increase Pt loading. The ethanol injection method used by SEQUUS[5] provides stable liposomes with moderate encapsulation efficiencies. Alternatively, solubilizing cisplatin in DMSO (~ 20 mg/ml) and lipids in EtOH prior to injection into a buffer solution[22] allows for easier handling of cisplatin; however, DMSO is known to rapidly form DMSO-cisplatin adducts.[23,24] As an alternative to DMSO, we tuned to chaotropic agents. For instance, Riviere, *et al* successfully increased the encapsulation efficiency of 5-fluoroorotic acid by solublizing the drug in 7M urea.[25]

Table 6.1. Formulation conditions explored to increase Cisplatin (CDDP) concentration in liposomes

	Loading (mg CPPD/ml)	Avg. Diameter (nm)	Benefit	Disadvantage
Cisplatin Solubility				
Urea	2-4	100-150	Increased CDDP solubility	CDDP degradation
Guanidinium HCl	0.2	140	Increased CDDP solubility	CDDP degradation
DMSO/EtOH	0.02	100	Increased CDDP solubility	CDDP degradation; difficult formulation
EtOH injection	1-1.7	110-140	CDDP stable	Lower CDDP loading
Cisplatin Stability				
Morpholide	-	-	Dual delivery, reduce CDDP degradation	Doesn't remain encapsulated
Poor Loading				
Dinitrato Pt Salt	< 1	110-130	Remote load CDDP	Poor stability upon heating; AgCl encapsulated

Cisplatin Solubility

To explore the use of chaotropic agents further, the solubility of cisplatin in various molar solutions of urea and guanidinum HCl (Guan HCl) was evaluated. Cisplatin was briefly heated in the respective solutions and diluted below 1 mg/ml to prevent precipitation upon cooling, and the concentration was analyzed by ICP. The remaining solution was allowed to cool to room temperature and the concentration quantified. Urea significantly improved the solubility of cisplatin in both temperature regimes, while Guan HCl was beneficial at higher temperatures only (Figure 6.1).
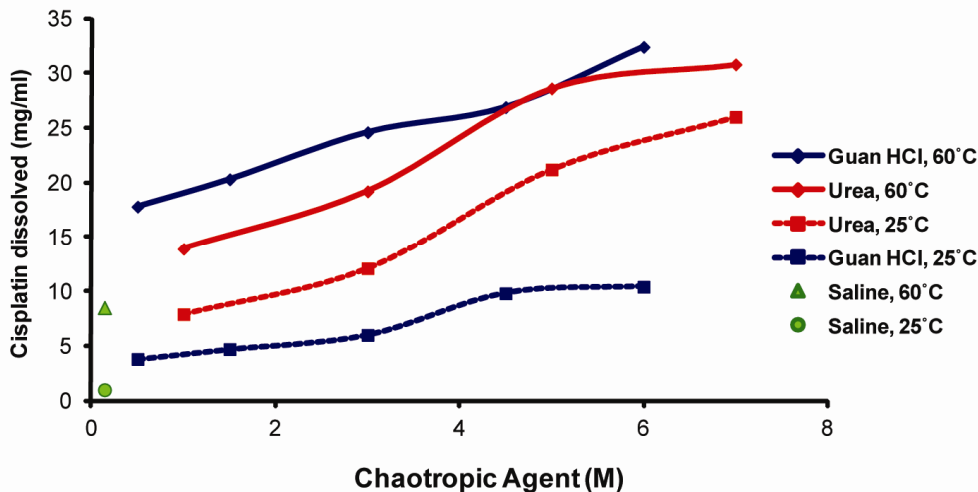
Figure 6.1. Solubility of cisplatin in saline (140 mM NaCl), urea, and guanidinium HCl as a function of temperature and solvent molarity. Cisplatin has a solubility of ~ 1 mg/ml at 25°C.

Liposome formulation was greatly improved when using 7M urea, as cisplatin did not precipitate during extrusion. Likewise, Pt loadings of up to 4 mg cisplatin/ml could be achieved. The change in Pt solubility after heating with urea was a concern given how easily Pt degrades in DMSO. To quickly screen for loss of activity, cisplatin was heated in 7M Urea, 140 mM NaCl or 6M Urea, 1M NaCl where a higher salt concentration may prevent chloride exchange. Samples were screened against C26 cells in a standard MTT assay and we observed a rapid loss of activity (Figure 6.2). Although liposomal cisplatin didn't show significant differences in toxicity as compared to other encapsulation methods, suggesting a slower rate of degradation, this method was abandoned.
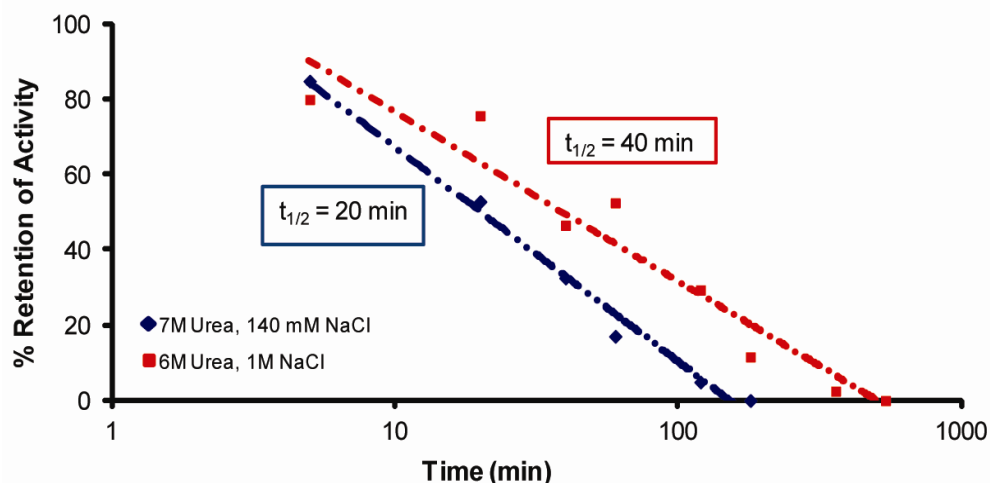

Figure 6.2. Degradation of cisplatin in urea characterized by toxicity in C26 cells.

Addressing Cisplatin Stability

Likewise, a challenge for platinum delivery in animals is limiting premature degradation by glutathione and other nucleophiles. The concern with liposomal delivery is that the lack of a burst release keeps the platinum concentration low enough to facilitate inactivation by tissue

95

associated nucleophiles. Diamides such as azodicarboxylic dimorpholide (ACM) can be used as thiol oxidizing reagents to reduce glutathione concentrations *in vitro*.[26,27] We hypothesized that co-encapsulation of ACM and cisplatin would locally knockdown glutathione and other sulfur-containing molecules and allow a higher concentration of active Pt to reach the nucleus. Unfortunately, ACM passes through membranes and cannot be retained in liposomes. A number of loading conditions were explored including the use of ammonium sulfate and dextran sulfate to trap ACM inside of the liposome, but these compounds did not readily complex with ACM. Additionally, diamides are susceptible to degradation in aqueous solutions. A visible color change occurs when ACM is left in water or PBS overnight. Heating accelerates the degradation in neutral-basic pH but sample integrity can be preserved in acidic solutions (Figure 6.3.) Even after 3 days in 250 mM Ammonium Sulfate, there was no change in the HPLC trace. While this method has the potential to reduce platinum deactivation, diamides more amenable for encapsulation would need to be synthesized.
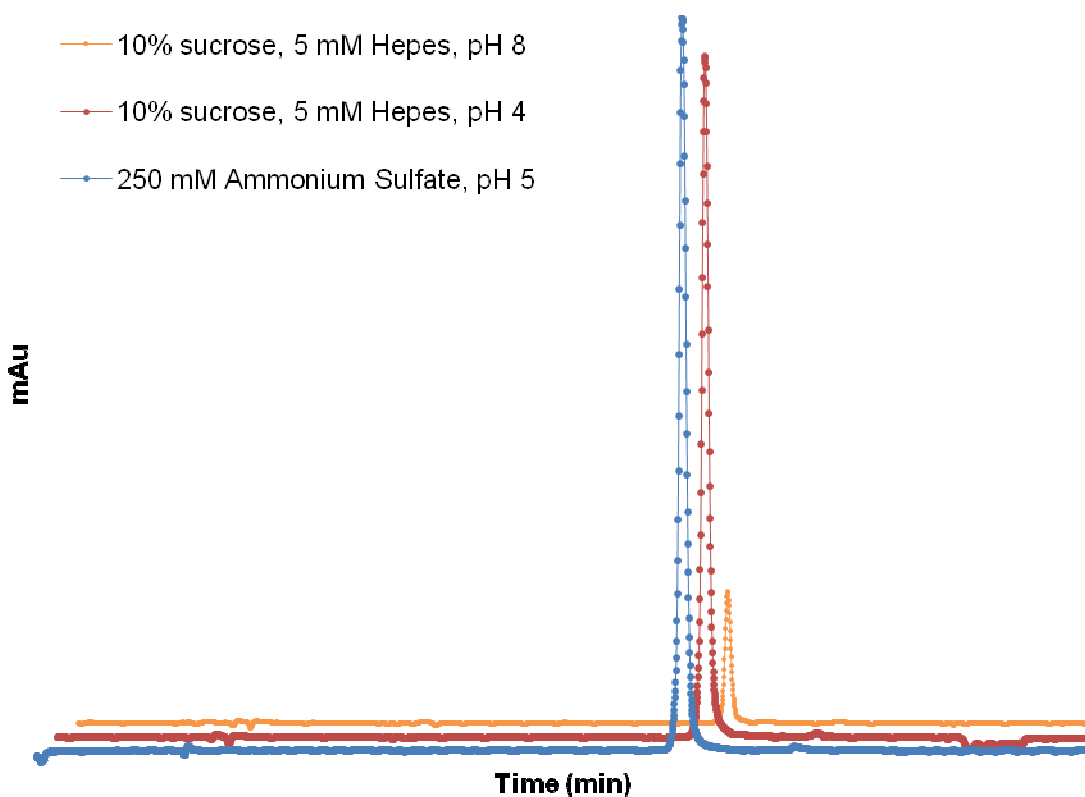

Figure 6.3. Degradation of azodicarboxylic dimorpholide after heating for 1.5 h at 65°C. HPLC trace monitored at 300 nm.

Active Loading Method

Finally, the previous loading methods relied upon passive encapsulation rather than remote loading, which results in lower encapsulation efficiencies. This method relies upon creating a transmembrane potential across the liposome through the encapsulation of various salts. When a drug such as doxorubicin passes through the bilayer, it becomes protonated, forms a salt complex, and becomes trapped inside the liposome. Unlike other drugs such as doxorubicin[28]

and irinotecan,[25] cisplatin cannot be actively loaded into a liposome. We hypothesized that the conversion of cisplatin to the aquato species would allow the drug to be trapped inside of the liposome through chelation or by conversion back to cisplatin (Figure 6.4). The dinitrato species is formed by heating cisplatin with $AgNO_3$ at pH 2 and then filtering to remove the precipitated AgCl. At this stage, the more soluble $(NH_3)_2Pt(OH_2)_2^{2+}$ will readily reform cisplatin if NaCl is introduced. The Pt solution was added to liposomes with encapsulated NaCl or Malonic Acid and heated at 65°C for up to 24 hours. Liposomes were dialyzed against HEPES and then HEPES/NaCl to remove unencapsulated Pt. Platinum loading and the presence of silver was quantified by ICP. The Malonic Acid liposomes had very low Pt loading while the NaCl liposomes had loadings up to 1 mg cisplatin/ml. Unfortunately, while extended heating improved the uptake of platinum, the liposomes turned grey as some of the cisplatin degraded to Pt(0). Shorter heating gave poor encapsulation and higher silver concentrations. Although there are alternate methods to synthesize the aquato Pt species, the lack of superior loading and degradation potential did not warrant further study of this loading method.
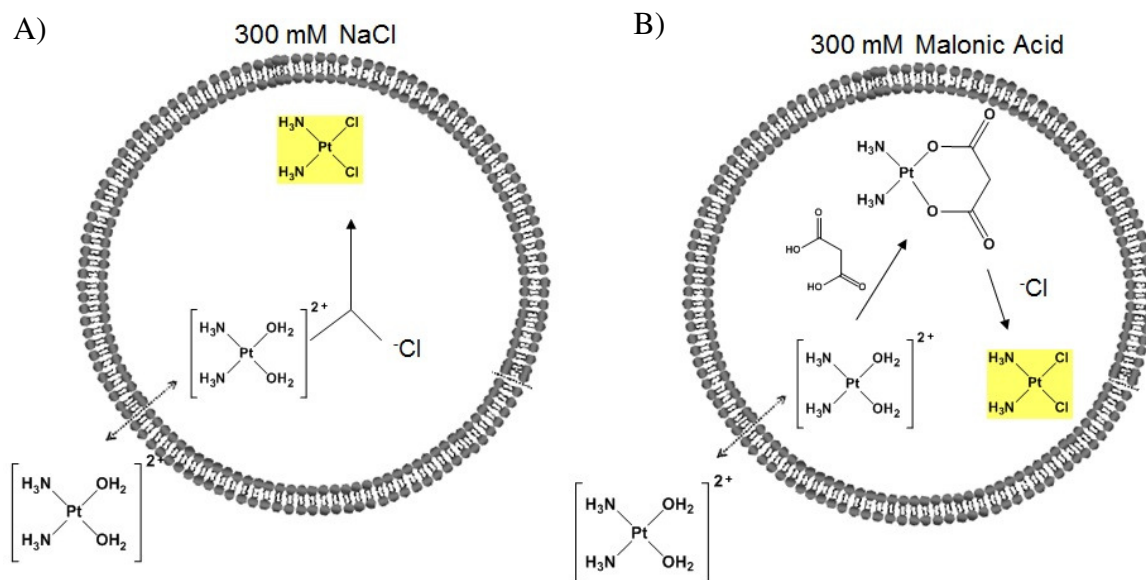

Figure 6.4. Proposed mechanism for cisplatin encapsulation. A) Dinitrato Pt salt passes through lipid membrane and interacts with the encapsulated NaCl to form the less soluble cisplatin. B) Dinatrato Pt salt chelates with the encapsulated malonic acid and upon the addition of NaCl, converts to cisplatin.

Although a variety of formulation methods were explored to encapsulate cisplatin, the EtOH injection method remained the best method. PEGylated liposomes were made from a number of different lipids including C8Chems, C10Chems, C16Chems, C18:1Chems, DChems, DChems/DPPC, HSPC, and POPC (molar ratios given in Table 6.2). Average liposome diameter and Zeta potential were measured and found to be on average ~100-140 nm and -2.0 mV, respectively. Cisplatin loading was quantified by ICP and ranged from 1-1.7 mg cisplatin/ml.

Liposomal Cisplatin Leakage and Toxicity

After exploring a variety of loading conditions, the potential to leak cisplatin was studied. To best replicate *in vivo* conditions, liposomes were heated at 37°C in 30% FBS. At various time points, liposomes were purified and the cisplatin concentration analyzed by ICP. Cisplatin can interact with serum proteins; therefore we elected to separate cisplatin liposomes from Pt-

proteins and free cisplatin via a SEC Sepharose GL-6B column rather than the dialysis method used in Chapter 2. Also, by quantifying liposomal cisplatin, the early time points were never below the Pt detection limit. As expected, the shorter chain SMLs had a greater degree of Pt release than the longer chain lipids. Likewise, the more fluid oleoyl (POPC) formulations had better release profiles than the saturated liposomes.

  Encouraged by the tunablity of the various formulations, the cytotoxicity of the liposome preps was screened against the C26 cell line. The IC_{50} values are shown in Table 6.2. As seen with the polymer systems in Chapter 2 and 3, a reduction in toxicity is to be expected when a delivery platform is used. If liposomes were sonicated prior to cellular addition, thus releasing cisplatin, toxicity was comparable to the free drug control. We were pleased to see that the leakier liposomes were also the most toxic, while the stable formulations were relatively non-toxic.

Table 6.2. Cisplatin Release in the Presence of Serum and Toxicity

Name	Formulation	% Release after 72 h	IC_{50} (µM)
C8Chems	Chems:PEG (95:5)	26 %	5.0
DiChems/DPPC	DiChems:DPPC:PEG (32:63:5)	20 %	5.8
C16Chems	Chems:PEG (95:5)	< 5 %	79
C18:1Chems	Chems:PEG (95:5)	< 5 %	>115
DiChems	DiChems:PEG (95:5)	< 5 %	53
HSPC	HSPC:Chol:PEG (51:44:5)	< 5 %	260
POPC 51	POPC:Chol:PEG (51:44:5)	14 %	130
POPC 80	POPC:Chol:PEG (80:15:5)	37 %	5.9

In vivo Toxicity and Platinum Distribution

  After screening the different formulations for cisplatin release and activity, four formulations were chosen for further study. We were interested in improving upon the HSPC formulation so it was included as a non-leaky control. C18:1Chems was selected as a non-leaky SML formulation, while DiChems/DPPC was picked as a moderately releasing liposome. Finally, the leakiest liposome, C8Chems, was chosen.

  Due to the loading limitations, a max tolerated dose was never established for the HSPC formulation.[5] While we didn't expect to observe any gross toxicity, it was included in the toxicity screen as a comparison to the non-leaky C18:1Chems and leaky C8Chems. All three formulations were dosed at the highest allowable volume
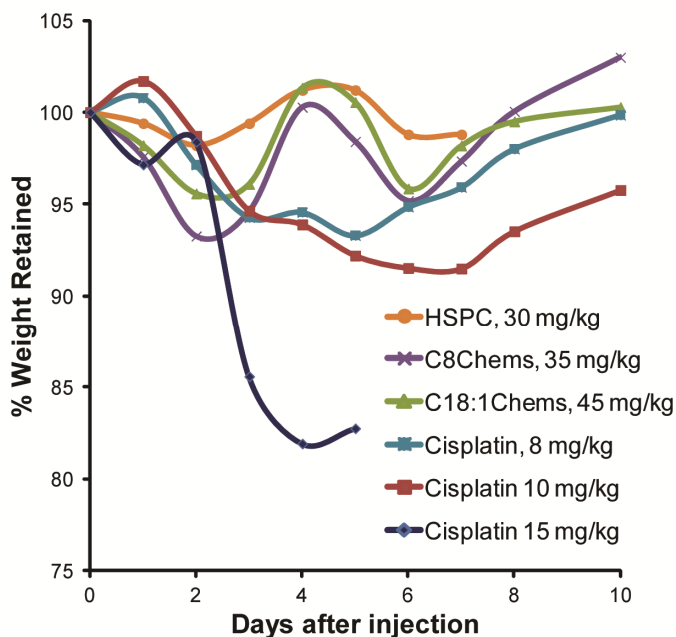

Figure 6.5. Retention of body weight after single injection of cisplatin and cisplatin liposomes in healthy, tumor free mice.

Table 6.3. Pharmacokinetic parameters for HSPC and C8Chems liposomes

PK parameters	HSPC	C8Chems
$t_{1/2, \alpha}$ (hr)	1.31	-
$t_{1/2, \beta}$ (hr)	36.8	20.7
V_1 (g blood)	0.77	1.2
$AUC_{0 \rightarrow \infty}$ (%ID*hr/g blood)	1456	902
k_{el} (1/min)	0.0005	0.0006

< 500 µl and no significant toxicity was observed (Figure 6.5). In comparison, 15 mg cisplatin/kg was lethal to healthy, tumor free Balb/C mice, giving a MTD of 10 mg/kg.

After confirming that the C8Chems prep was well tolerated the pharmacokinetics of this formulation was studied. Mice were dosed with either HSPC, C8Chems, or free cisplatin at 3 mg cisplatin/kg. Blood was collected over 72 hours and analyzed for platinum by ICP.

Cisplatin is rapidly excreted from the body[5] and the blood concentrations were below the Pt detection limit. Given the rapid clearance of small molecules, we anticipate that the platinum detected is encapsulated in liposomes. Likewise, the leaky nature of the C8Chems liposomes could explain why the blood platinum concentration is lower than the HSPC liposomes (Figure 6.6). In general, the liposome circulation time does not differ significantly between the different types of lipids, in part because of the stability and protection of the PEG shell.[29] As shown in Table 6.3, both formulations had elimination phase half-lives greater than 20 hours and favorable area-under-the-curve ($AUC_{0 \rightarrow \infty}$), which is advantageous for increased tumor uptake.
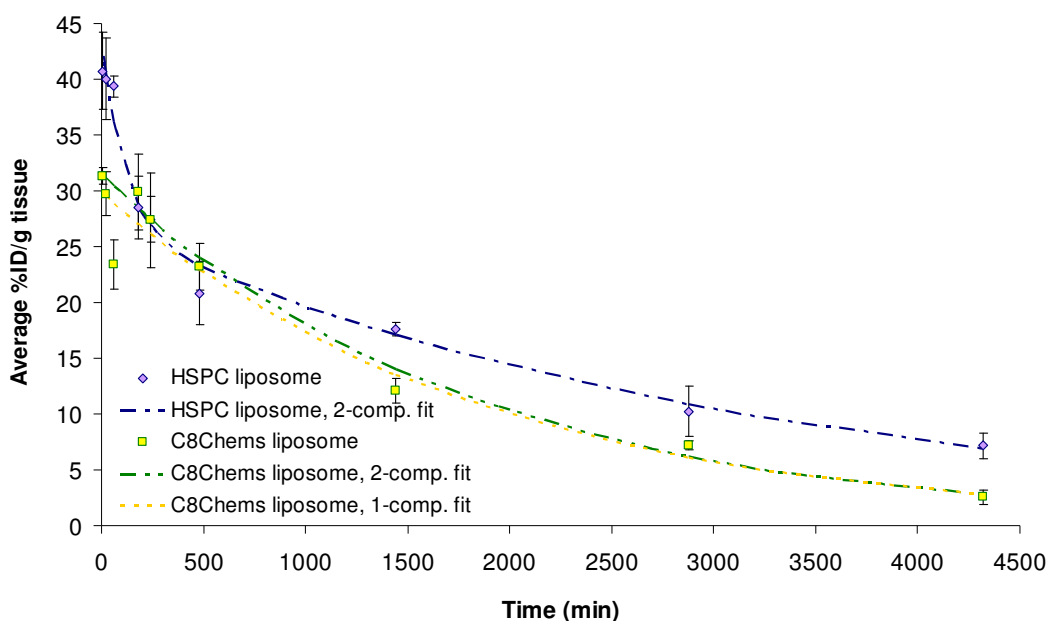

Figure 6.6. Blood circulation of liposomes in healthy, tumor free mice. Blood collected and analyzed for platinum by ICP-AES at 214 nm.

Given the favorable PK parameters, we measured the platinum biodistribution in C26 tumored mice. At 10 days post tumor inoculation, mice were injected with cisplatin, HSPC liposomes or C8Chems liposomes at a 10 mg cisplatin/kg concentration. Blood and tissue were collected after 48 hours, digested with a 70% nitric acid solution, and analyzed for platinum content.

Encapsulation of cisplatin significantly increased platinum concentrations in the blood and tumor tissue, with > 7% of the injected dose accumulating in the tumors after 48 hrs. Liposomes do not undergo significant renal clearance; therefore, the spleen and liver are responsible for liposome removal and have higher Pt accumulation. Our data is consistent with previous distribution studies using the HSPC formulation in these organs. Peak spleen accumulation (25 µg Pt/g tissue) occurred after 96 hours and a 2-fold reduction in Pt levels after 196 hours; therefore, we aren't concerned about long term organ accumulation.[5] The C8Chems formulation provided a huge dose in the tumor and a lower dose in the kidneys. Less than 5% of the Pt dose was retained in the kidney after 48 h, which is an important parameter for reducing nephrotoxicity.
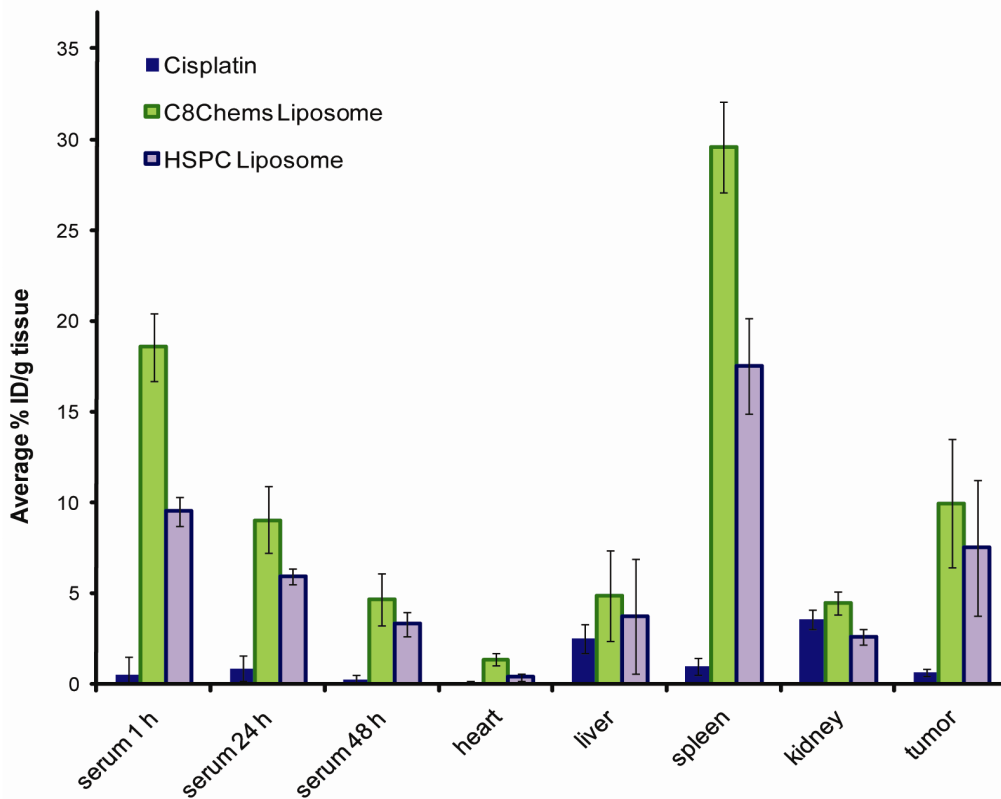

Figure 6.7. Biodistribution in C26 tumored mice (n=4), dosed at 10 mg cisplatin/kg. Blood collected 1 h, 24 h, and 48 h post-injection, and tissue collected at 48 h. One of the four C8Chems tumor samples was excluded from analysis, as an accurate mass could not be determined due to the small size.

Efficacy of Liposomal Cisplatin in C26 Tumor Model

We expected that the fast releasing formulation, which had a low IC_{50} in cell culture and equivalent tumor uptake to the slow releasing formulation, would have superior activity to cisplatin. The antitumor efficacy of four cisplatin liposomal formulations was compared to the free drug. Balb/C mice were tumored subcutaneously with C26 colon carcinoma cells and treated 8 days after inoculation. The treatment groups included PBS, cisplatin (6 mg/kg, once a week for 2 weeks), and liposomes C8Chems, DiChems/DPPC, C18:1Chems, and HSPC at 6 mg cisplatin/kg once a week for 2 weeks. The new dosing schedule, as compared to the single Pt dose used in Chapter 3, improved survival without significantly increasing toxicity. Although weight loss was observed, a blood panel was normal and the mice showed no other signs of

toxicity such as lethargy or ruffled fur. All of the treatment groups had statistically significant survival and tumor regression as compared to PBS. The HSPC formulation, despite the poor cisplatin release, was the only formulation which performed better than cisplatin.
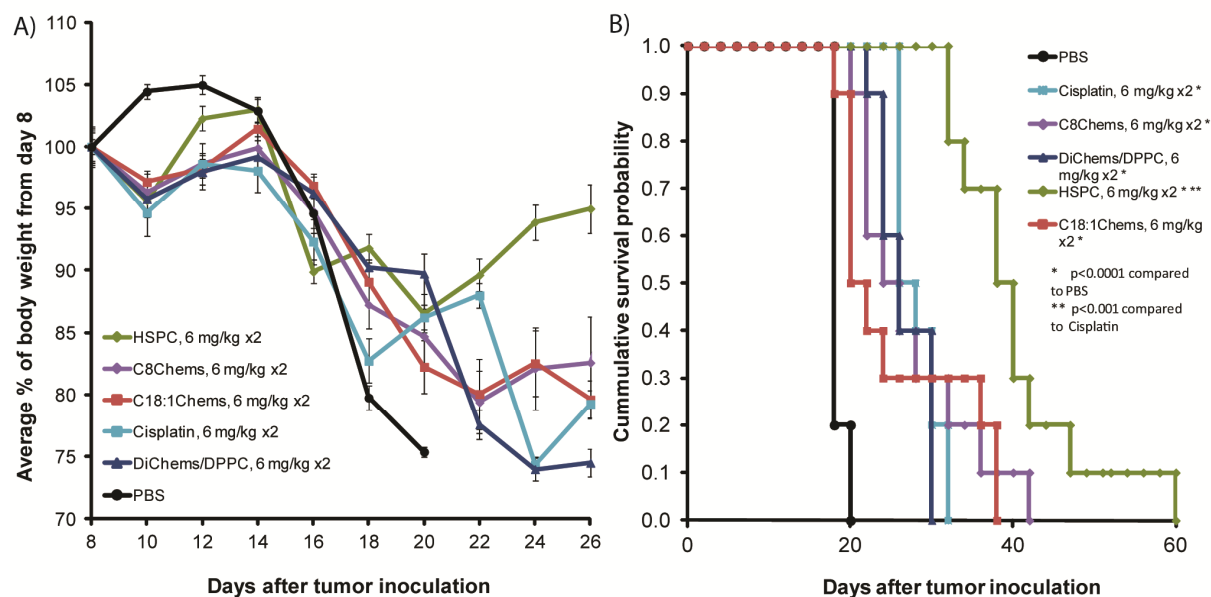

Figure 6.8. A) Average change in body weight from day of injection. B) Survival probability for mice treated with cisplatin and liposomal cisplatin. Mice (n=10) dosed on day 8 and day 15.

Re-designing the Cisplatin formulation

The results of the chemotherapy experiment suggest that the sterol modified lipids may not be the ideal formulation to deliver cisplatin, as neither the leaky nor non-leaky liposomes improved activity. We were interested in exploring why fast releasing formulations did not improve survival over the classic HSPC formulation. In particular, the presence of cholesterol and the type of lipid were of interest. Cholesterol is added to liposomes to stabilize the bilayer during circulation and control content release, but can exchange with other biomembranes causing premature leakage.[30–33] While cholesterol is an important component in liposome formulation, Dos Santos and co-workers found a cholesterol-free formulation improved the pharmacokinetics of an encapsulated antibiotic.[34] Likewise, unsaturated lipids such as POPC can provide more fluidity to a membrane and affect drug release. When these two parameters were combined (Table 6.2), the unsaturated POPC 80 formulation (15% cholesterol) had excellent Pt release and toxicity, while POPC 51 (44 % cholesterol) was more stable and had reduced toxicity. We hypothesized that the cholesterol could be affecting how the liposomes were interacting with the tumor environment and could be facilitating release of Pt from the HSPC formulation, thus improving efficacy.

A second chemotherapy experiment was completed comparing the leaky C8Chems and POPC 80 formulations to the non-leaky HSPC and POPC 51 formulations, with the same 6 mg cisplatin/kg x 2 dose schedule. On day 20, a blood sample was collected and elevated blood urea nitrogen concentration screened for as an indicator of kidney damage and decreased kidney function. As with the previous chemotherapy, the mice exhibited weight loss (Figure 6.9) without the other signs of toxicity or elevated urea levels. All of the formulations had statistically

101

significant tumor regression and increased survival compared to PBS. Interestingly, neither leaky formulation had improved survival as compared to cisplatin despite the favorable Pt release and tumor accumulation, while both non-leaky formulations did significantly better than cisplatin. These results suggest that while the leaky formulations increase the availability of cisplatin, this does not translate to increased cellular uptake. Likewise, the rate of cisplatin release may be too slow to overcome inactivation by glutathione and other nucleophiles.
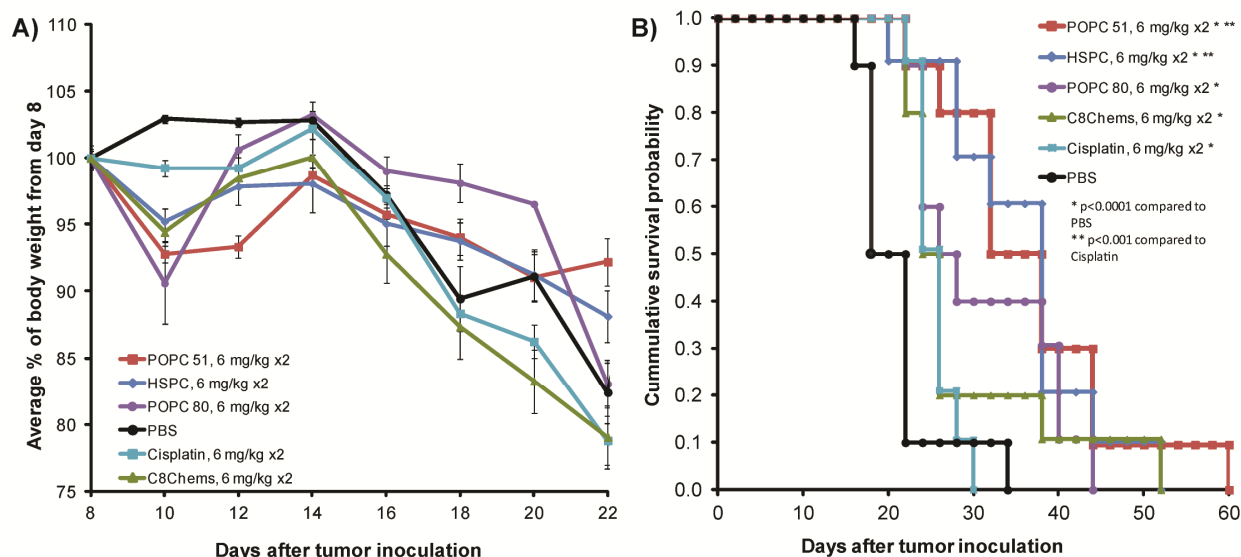

Figure 6.9. A) Average weight change since treatment. B) Survival plot of mice treated with leaky versus non-leaky cisplatin liposomes. Mice (n=10) were dosed on day 8 and 15.

To investigate the intratumoral disposition of platinum from various formulations, a microfluorescence (X-ray fluorescence microscopy, or XFM) experiment was conducted at Argonne National Lab. This technique maps the spatial distribution of multiple elements within a sample and is amenable to both single cells and tissue slices.[35] To aid in the design of new drugs, XFM has been used to better understand the fate of platinates in tumor cells.[36–40] C26 tumors were excised (after 54 h) from mice treated with cisplatin, C8Chems, POPC 80, and HSPC at 10 mg/kg. Ten µm tissue slices were mounted on a thin film for analysis. As expected for the small molecule cisplatin, the Pt concentration was low and was distributed throughout the tumor section. In contrast, the liposomal formulations tended to accumulate along the tumor periphery, often in clusters. Generally these overlay well with the iron map, which is indicative of vasculature. There are subtle differences between the formulations. C8Chems appeared to have the most accumulation along the periphery near the iron, while HSPC had low levels of Pt throughout. POPC 80 had more punctate distribution, suggesting that in this tumor model, leaky liposomes do not increase the amount of platinum in the tumor.

In a separate study, DNA was extracted from tumor tissue (n=3) and the concentration of Pt-DNA adducts quantified by ICP-MS (Table 6.4). Cisplatin had the lowest concentration of bound platinum while HSPC had the highest. In this experiment, the POPC 80 formulation had higher Pt levels than the POPC 51 formulation; however, a broad range of Pt concentrations were measured in the five samples. Taken together, the results support the hypothesis that more stable

liposomal cisplatin improves tumor distribution, but additional imaging and ICP-MS experiments at a variety of time points and tumor sizes are needed to unambiguously confirm that non-leaky formulations are superior to leaky formulations.
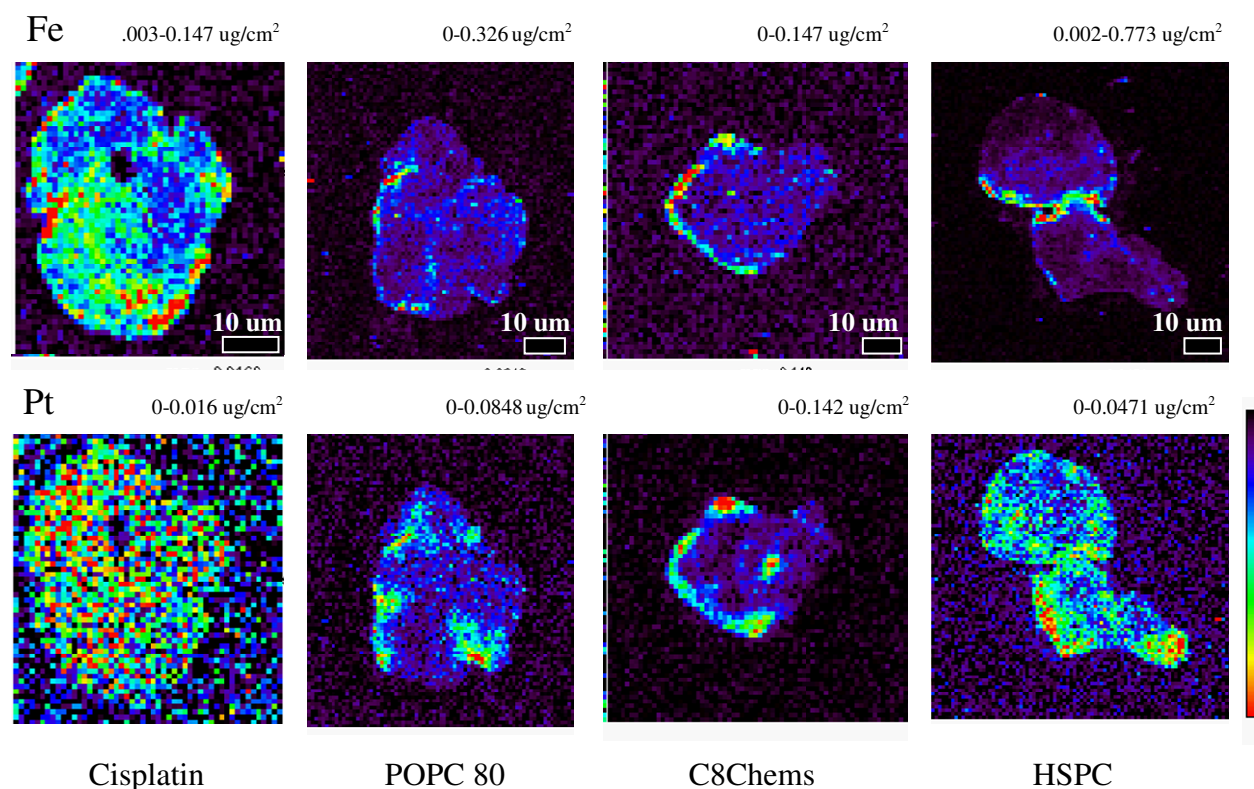

Figure 6.10. Microfluorescence of platinum in C26 tumor. Maximum and minimum threshold values are given which correspond with the rainbow color overlay. Fe maps are used to indicate vasculature.

Table 6.4. Pt-DNA adducts in s.q. C26 tumors, quantified by ICP-MS.

	ng Pt/ug DNA	% Injected Dose (x10⁻³)	% ID/ug DNA (x10⁻⁵)
Cisplatin	0.022 +/- 0.013	0.5 +/- 0.04	1.2 +/- 0.7
C8Chems	0.078 +/- 0.076	3.7 +/- 1.0	3.9 +/- 3.8
POPC 80	0.195 +/- 0.220	2.6 +/- 2.1	10.8 +/- 12.2
POPC 51	0.093+/- 0.052	2.1 +/- 0.7	4.8 +/- 2.3
HSPC	0.221 +/- 0.227	5.1 +/- 0.1	11.8 +/- 12.1

CONCLUSIONS

A number of formulation strategies were explored to improve cisplatin loading in liposomes. While not all techniques were amenable to use with cisplatin, chaotropic agents in particular hold great potential for use with other difficult to solubilize drugs. A variety of different sterol modified lipids were screened to design a liposome capable of releasing cisplatin. C8Chems gave

the best release and toxicity profile and was chosen for *in vivo* studies against the standard HSPC formulation. The liposomes had favorable circulation time and uptake into tumor tissue. A chemotherapy study found that the SML liposomes were efficacious but did not outperform the HSPC formulation. Coupled with the high tumor accumulation, we hypothesize that the platinum is being deactivated upon liposomal release or the liposome could be interacting with macrophages to a greater degree than the tumor cells. Furthermore, a low cholesterol POPC formulation was comparable to C8Chems while POPC 51 worked as well as HSPC. The *in vivo* studies suggest that the C26 tumoral response to Pt varies between tumors; therefore it would be interesting to explore Pt uptake and efficacy in an array of tumor models. While not the formulation outcome predicted, the POPC 51 formulation has the potential to improve the bioavailability of cisplatin in a variety of cancers.

EXPERIMENTAL

Materials. Materials were used as obtained from commercial sources unless otherwise noted. Cisplatin was purchased from Sigma-Aldrich. Lipids were purchased from Avanti Polar Lipids, kindly donated by Dr. Zhaohua Huang, or synthesized as previously described.[41,42] SPEX CertiPrep Ultralene Film (4 µm) was purchased from Fisher Scientific. The platinum ICP standard was purchased from VHG Labs. Chloroform was removed under reduced pressure using a rotary evaporator.

General Liposome Preparation. Prior to liposome formation, lipids were dissolved in chloroform, evaporated to form a thin film, and dried overnight. Lipid mixtures are abbreviated as listed in Table 6.5. Various formulation conditions, as described below, were explored to make liposomes. Following formation, liposomes were extruded through a 200 nm and 100 nm polycarbonate membrane 11 times each at 60°C, held at 60°C for 15 min and then cooled to room temperature. Free cisplatin precipitated and was removed by filtration, and liposomes were dialyzed for 24 hours against HEPES buffer (10 mM HEPES, 150 mM NaCl. pH 7.4). Average liposome diameter and zeta potential were determined by dynamic light scattering measurements (Malvern Instruments Zetasizer Nano ZS).

Table 6.5 Lipid Formulations

Name	Lipids	Molar Ratio
HSPC	HSPC:Chol:m-PEG-DSPE	51:44:5
POPC 51	POPC:Chol:m-PEG-DSPE	51:44:5
POPC 80	POPC:Chol:m-PEG-DSPE	80:15:5
CXChems	$Chems_x$:m-PEG-DSPE, where x= 8, 10, 16, 18:1	95:5
DiChems	DiChems:m-PEG-DSPE	95:5
DiChems/DPPC	DiChems:DPPC:m-PEG-DSPE	32:63:5

Quantification of Platinum in Liposomes. Cisplatin loading in the liposomes was measured by inductively coupled plasma-atomic emission spectroscopy (ICP-AES; Perkin Elmer Optima 7000 DV Optical Emission Spectrometer). Liposomes (50 µl) were diluted to 6 ml with a 5% HNO_3 solution and allowed to stand at room temperature for 1 h. Samples were measured in triplicate for their Pt emission at 214.423 nm.

Ethanol Injection Method.[43] This method was used to prepare liposomes for all *in vitro* and *in vivo* studies. Cisplatin (8.5 mg/ml) was dissolved in 0.9% NaCl at 60°C, while the lipids were

dissolved in ethanol (100 mg/ml) at 60-70°C. With a pre-warmed syringe, the ethanolic mixture (100 µl) was rapidly injected into the cisplatin solution (900 µl) and allowed to stir covered for 1 h at 60°C. Formulation continued as described above. Size: 110-140 nm, Platinum loading:1-1.7 mg cisplatin/ml.

Chaotropic Method.

Urea: At 65°C, lipid thin films were hydrated for 30 min with cisplatin dissolved in 7M Urea (20 mg/ml) and then sonicated for 30 min. Formulation continued as described above. Size: 100-150 nm, Pt loading: 2-4 mg cisplatin/ml.

Guanidinium Chloride: Lipids were dissolved in ethanol and injected into cisplatin-6M Guan HCl (15 mg/ml). Mixture heated at 65°C for 1 h before continuing as described above. Size: 140 nm. Pt: 0.23 mg cisplatin/ml.

DMSO Injection Method.[22] With heating, cisplatin was dissolved in DMSO (20 mg/ml) and the lipids in ethanol. The DMSO-cisplatin solution (350 µl) was either added to the ethanol solution (150 µl) and then injected into 1 ml Hepes or injected with two separate syringes into the HEPES. The solution was stirred for 10 min, extruded and dialyzed to remove free cisplatin and the organics. Size: 100 nm, Pt loading: 0.02 mg cisplatin/ml.

Remote loading Cisplatin.

$(NH_3)_2Pt(OH_2)_2^{2+}$ Synthesis: To a 2 dram vial was added cisplatin (30 mg, 1 eq), AgNO$_3$ (21 mg, 1.9 eq), and 750 ul water. 2% HNO$_3$ was added until the pH < 2.0 was reached (~20 µl). The vial was covered, heated at 70° C overnight, and then cooled to 0° C for filtering. The resulting dinitrato $(NH_3)_2Pt(OH_2)_2^{2+}$ salt was kept covered until use.

Liposome formuation: A thin film of POPC 51 was hydrated with either 300 mM NaCl or 300 mM Malonic Acid (adjusted to pH 7) at 65°C and then sonicated for 10 min. Following extrusion, the liposomes were exchanged into 10% sucrose via dialysis. To load the liposomes with Pt, 300 µl dinitrato salt was added to 1 ml of liposomes and heated at 60°C for 2-24 hr. Liposomes were dialyzed against Hepes and then Hepes/NaCl to remove free Pt. Size: 110-130 nm, Pt loading: Malonic acid-0.03 mg cisplatin/ml, NaCl (2h)- 0.14 mg cisplatin/ml, NaCl (24 h)- 1 mg Cisplatin/ml.

Co-Encapsulation of Cisplatin and Azodicarboxylic dimorpholide (ACM). A thin film of HSPC was hydrated with cisplatin and ACM dissolved in either HEPES or 250 mM Ammonium Sulfate. Liposomes were sonicated for 10 min at 60°C until opalescent. The liposome preparation was passed through a PD-10 column to remove any free drug. The bright orange ACM was separated from the liposomes and did not remain encapsulated. Liposomes were also loaded with either 250 mM Ammonium Sulfate or 250 mM Dextran Sulfate and exchanged into 10% sucrose/5 mM HEPES. ACM remote loading at 65°C was looked at between pH 4.5-6.5 for 1h. After liposome purification on a PD-10 column, no ACM remained encapsulated visually or by HPLC (gradient method, 0% ACN:100% water, 0.05% TFA was ramped to 100% ACN over 20 min at 1 ml/min flow rate).

Platinum Release Experiments. Cisplatin liposomes in 30% FBS were aliquoted into Eppendorf tubes and placed in a 37° C shaker. At various time points over 48 h, a sample was passed through a Sepharose GL-6B column and the liposome fraction collected. Because platinum can interact with serum proteins, it was important to remove both free cisplatin and the serum proteins from the liposomes. The liposome fraction was diluted with 5% HNO$_3$ and the platinum content measured by ICP as previously described.

Toxicity of Cisplatin Liposomes in C26 cells. Cells were seeded onto a 96-well plate at a density of 5.0 x 10^3 cells per well in 100 µl of medium and incubated overnight (37 °C, 5% CO$_2$,

and 80% humidity). An additional 100 µl of new medium (RPMI medium 1640/10% FBS/1% penicillin-streptomycin) containing either cisplatin or cisplatin liposomes with concentrations ranging from 50 nM to 500 µM Pt equivalents was added to the cells. The tests were conducted in replicates of three for each concentration. After incubation for 72 h, 40 µl of media containing thiazolyl blue tetrazolium bromide solution (2.5 mg/mL) was added. The cells were incubated for 2 h, after which time the medium was carefully removed. To the resulting purple crystals was added 200 µl of DMSO, followed by 25 µl of pH 10.5 glycine buffer (0.1 M glycine/0.1 M NaCl). The optical densities at 570 nm and 690 nm (background) were measured on a SpectraMAX M3 microplate reader (Molecular Devices, Sunnyvale, CA). Wells containing cells that received neither liposome nor drug were considered to represent 100% viability. IC$_{50}$ values were obtained from sigmoidal fits of semilogarithmic plots of the percentage of viability versus platinum concentration by using Origin 7 SR4 8.0552 software (OriginLab, Northhampton, MA).

Cisplatin Degradation. Cisplatin was dissolved in 7M Urea/150 mM NaCl, 6M Urea/1M NaCl, or 6M GuCl/150 mM NaCl at 15 mg/ml and heated in the dark at 65° C. At various time points, samples were removed, diluted (1:50), and stored until use. A standard MTT assay in C26 cells was used to assess loss of activity. Cisplatin in PBS represented 100% viability and the chaotropic solutions were the negative control.

Animal and Tumor Models. All animal experiments were performed in compliance with National Institutes of Health guidelines for animal research under a protocol approved by the Committee on Animal Research at the University of California (San Francisco, CA) (UCSF). C26 colon carcinoma cells obtained from the UCSF cell culture facility were cultured in RPMI medium 1640 containing 10% FBS. Female BALB/c mice were obtained from Simonsen Laboratories, Inc. (Gilroy, CA).

Toxicity in Healthy Mice. Female Balb/C mice were injected via tail vein injection with cisplatin or cisplatin liposomes. Mice weights and general health were monitored over 9 days. When gross toxicity was observed, such as loss of greater than 15% of initial body weight, lethargy or ruffled fur, mice were removed from the study.

Pharmacokinetic Analysis in Mice. Six- to eight week-old female Balb/C mice were dosed via tail vein injection with liposomes (3 mg Pt/ml). Blood was collected in heparinized tubes (10 µL heparin (50 mg/mL)) by submandibular bleeds 5, 20, 60, 180, 240, and 480 min post injection and by heart puncture 24, 48, and 72 h post injection. The blood was centrifuged at 5,000 rpm for 3 min, the serum separated, and stored at 4 °C until use. Samples were diluted to 2 ml with 5% HNO$_3$, incubated for 1 h at 40 °C, and then centrifuged to remove insoluble particles. Platinum content was analyzed by ICP.

Biodistribution Study in Tumored Mice. Six- to eight week-old female Balb/C mice were injected in the right hind flank with 3×10^5 C26 cells. Ten days after tumor inoculation, mice were randomized into four groups of four mice each. Mice were injected by means of the tail vein either with cisplatin (10 mg/kg), and Pt liposomes (10 mg/kg) in ~200 µL of PBS. Blood was collected in heparinized tubes by submandibular bleeds 60 min and 24 h after dosing; mice were sacrificed 48 h post-injection. The blood (collected by heart puncture), heart, liver, spleen, kidney, and tumor were collected for analysis. Blood was centrifuged for 5 min at 5,000 rpm to allow for serum removal. Each organ was weighed and 200-300 mg of the collected organs were homogenized with zirconium beads and 250 µL deionized water. The tissue samples were diluted with 583 μL concentrated HNO$_3$ (~70% acid solution) and the serum samples were diluted to 2 mL with 5% HNO$_3$. Samples were gently heated at 40 °C overnight and centrifuged to remove any insoluble particles. Platinum content in each sample was analyzed by ICP.

Chemotherapy Experiment in Tumored Mice. While under anesthesia, female Balb/C mice were shaved, and C26 cells (3 x 10^5 cells in 50 µL) were injected subcutaneously in the right hind flank. At eight days post-tumor implantation, mice were randomly distributed into treatment groups of 10 animals. Mice were injected by means of the tail vein with cisplatin (6 mg/kg once a week for 2 weeks) or cisplatin liposomes (6 mg/kg once a week for 2 weeks) in approximately 200 µL of solution. Five days post-treatment, blood was collected by submandibular bleeds and analyzed for 19 toxicity markers (UC Davis Comparative Pathology Dept). Blood urea nitrogen levels were quantified with Quantichrome Urea Assay Kit (BioAssay Systems, Hayward, CA). Mice were weighed and tumors measured every other day. The tumor volume was estimated by measuring the tumor volume in three dimension with calipers and calculated using the formula tumor volume = length x width x height. Mice were removed from the study when (i) a mouse lost 15% of its initial weight, (ii) any tumor dimension was > 20 mm, or (iii) the mouse was found dead. The mice were followed until day 60 post-tumor inoculation. Statistical analysis was performed using MedCalc 8.2.1.0 for Windows (MedCalc Software, Mariakerke, Belgium). The tumor growth delay was calculated based upon a designated tumor volume of 400 mm^3.

Tissue Sections. While under anesthesia, female Balb/C mice were shaved, and C26 cells (3 x 10^5 cells in 50 µL) were injected subcutaneously in the right hind flank. At ten days post-tumor implantation, mice were injected with cisplatin (10 mg/kg) or cisplatin liposomes (10 mg/kg) labeled with membrane dye DiD. After two days, mice were sacrificed and the tumors collected. Tissue was mounted in O.C.T. embedding compound (Sakura Tissue-TEK) and flash frozen with dry ice cooled isopentane. Using a cryostat, 10 µm tissue samples were cut and transferred to Ultralene film which had been gently secured to a glass slide. Sections were air dried before being transported to Argonne National Lab for X-ray fluorescent microscopy.

X-Ray Fluorescence Microscopy. With the assistance of Dr. Lydia Finney, sections were imaged with the scanning x-ray microprobe at beamline 8-BM-B at the Advanced Photon Source (Argonne, IL). Undulator-generated x-rays of 15-keV incident energy were monochromatized with a double monochromator and focused to a measured spot size of ~ 100 µm pinhole. Tissues were rasterscanned in steps of 0.1 mm and fluorescence spectra were collected for 4-8 s per pixel with a four-element silicon drift detector (Vortex-EX, SII Nanotechnology, CA). Quantitation and image-processing of the x-ray fluorescence (XRF) datasets were performed with MAPS software.[44]

REFERENCES
(1)   Zieske, P. A.; Koberda, M.; Hines, J. L.; Knight, C. C.; Sriram, R.; Raghavan, N. V.; Rabinow, B. E. *Am. J. Hosp. Pharm.* **1991**, *48*, 1500–1506.
(2)   Reedijk, J. *Chem. Comm.* **1996**, 801-806.
(3)   Hirai, M.; Minematsu, H.; Hiramatsu, Y.; Kitagawa, H.; Otani, T.; Iwashita, S.; Kudoh, T.; Chen, L.; Li, Y.; Okada, M.; Salomon, D. S.; Igarashi, K.; Chikuma, M.; Seno, M. *Int. J. Pharm.* **2010**, *391*, 274–283.
(4)   Schroeder, A.; Honen, R.; Turjeman, K.; Gabizon, A.; Kost, J.; Barenholz, Y. *J. Control. Release* **2009**, *137*, 63–68.
(5)   Newman, M. S.; Colbern, G. T.; Working, P. K.; Engbers, C.; Amantea, M. a *Cancer Chemother. Pharmacol.* **1999**, *43*, 1–7.
(6)   Stathopoulos, G. P. *Anticancer Drugs* **2010**, *21*, 732–6.
(7)   Woo, J.; Chiu, G. N. C.; Karlsson, G.; Wasan, E.; Ickenstein, L.; Edwards, K.; Bally, M. B. *Int. J. Pharm.* **2008**, *349*, 38–46.

(8)   Zisman, N.; Dos Santos, N.; Johnstone, S.; Tsang, A.; Bermudes, D.; Mayer, L.; Tardi, P. *Chemoth. Res. Pract.* **2011**, *2011*, 1–7.

(9)   Suzuki, R.; Takizawa, T.; Kuwata, Y.; Mutoh, M.; Ishiguro, N.; Utoguchi, N.; Shinohara, A.; Eriguchi, M.; Yanagie, H.; Maruyama, K. *Int. J. Pharm.* **2008**, *346*, 143–150.

(10)   Tippayamontri, T.; Kotb, R.; Paquette, B.; Sanche, L. *Invest. New Drug* **2011**, *29*, 1321–7.

(11)   Dragovich, T.; Mendelson, D.; Kurtin, S.; Richardson, K.; Von Hoff, D.; Hoos, A. *Cancer Chemother. Pharmacol.* **2006**, *58*, 759–764.

(12)   Han, I.; Jun, M. S.; Kim, M. K.; Kim, J. C.; Sohn, Y. S. *Cancer Sci.* **2002**, *93*, 1244–1249.

(13)   Mori, A.; Wu, S. P.; Han, I.; Khokhar, A. R.; Perez-Soler, R.; Huang, L. *Cancer Chemother. Pharmacol.* **1996**, *37*, 435–444.

(14)   Fantini, M.; Gianni, L.; Santelmo, C.; Drudi, F.; Castellani, C.; Affatato, A.; Nicolini, M.; Ravaioli, A. *Chemoth. Res. Pract.* **2011**, *2011*, 1–7.

(15)   Wheate, N. J.; Walker, S.; Craig, G. E.; Oun, R. *Dalton T.* **2010**, *39*, 8113–27.

(16)   White, S. C.; Lorigan, P.; Margison, G. P.; Margison, J. M.; Martin, F.; Thatcher, N.; Anderson, H.; Ranson, M. *Br. J. Cancer* **2006**, *95*, 822–828.

(17)   Rosenthal, D. I.; Yom, S. S.; Liu, L.; Machtay, M.; Algazy, K.; Weber, R. S.; Weinstein, G. S.; Chalian, A. A.; Miller, L. K.; Rockwell, K.; Tonda, M.; Schnipper, E.; Hershock, D. *Invest. New Drug* **2002**, *20*, 343–349.

(18)   Harrington, K. J.; Lewanski, C. R.; Northcote, A. D.; Whittaker, J.; Wellbank, H.; Vile, R. G.; Peters, A. M.; Stewart, J. S. *Ann. Oncol.* **2001**, *12*, 493–496.

(19)   Meerum Terwogt, J. M.; Groenewegen, G.; Pluim, D.; Maliepaard, M.; Tibben, M. M.; Huisman, A.; ten Bokkel Huinink, W. W.; Schot, M.; Welbank, H.; Voest, E. E.; Beijnen, J. H.; Schellens, J. M. *Cancer Chemother. Pharmacol.* **2002**, *49*, 201–210.

(20)   Zamboni, W. C.; Gervais, A. C.; Egorin, M. J.; Schellens, J. H. M.; Zuhowski, E. G.; Pluim, D.; Joseph, E.; Hamburger, D. R.; Working, P. K.; Colbern, G.; Tonda, M. E.; Potter, D. M.; Eiseman, J. L. *Cancer Chemother. Pharmacol.* **2004**, *53*, 329–336.

(21)   Bandak, S.; Goren, D.; Horowitz, A.; Tzemach, D.; Gabizon, A. *Anticancer Drugs* **1999**, *10*, 911–920.

(22)   Szoka Jr, F. *US Patent 5,567,434* **1996**.

(23)   Sundquist, W. I.; Ahmed, K. J.; Hollis, L. S.; Lippard, S. J. *Inorg. Chem.* **1987**, *26*, 1524–1528.

(24)   Fischer, S. J.; Benson, L. M.; Fauq, A.; Naylor, S.; Windebank, A. J. *Neurotoxicology* **2008**, *29*, 444–452.

(25)   Riviere, K.; Kieler-Ferguson, H. M.; Jerger, K.; Szoka, F. C., Jr *J. Control. Release* **2011**, *153*, 288–296.

(26)   Kosower, E. M.; Kosower, N. S.; Kenety-Londner, H.; Levy, L. *Biochem. Biophys. Res. Co.* **1974**, *59*, 347–351.

(27)   Kosower, N. S.; Kosower, E. M. In *Biothiols Part A Monothiols and Dithiols, Protein Thiols, and Thiyl Radicals*; Academic Press, 1995; Vol. 251, pp. 123–133.

(28)   Haran, G.; Cohen, R.; Bar, L. K.; Barenholz, Y. *Biochim. Biophys. Acta* **1993**, *1151*, 201–215.

(29)   Immordino, M. L.; Dosio, F.; Cattel, L. *Int. J. Nanomedicine* **2006**, *1*, 297–315.

(30)   Phillips, M. C.; Johnson, W. J.; Rothblat, G. H. *Biochim. Biophys. Acta* **1987**, *906*, 223–276.

(31)   Kan, C. C.; Yan, J.; Bittman, R. *Biochemistry* **1992**, *31*, 1866–1874.

(32) Drummond, D. C.; Meyer, O.; Hong, K.; Kirpotin, D. B.; Papahadjopoulos, D. *Pharmacol. Rev.* **1999**, *51*, 691–744.

(33) Hamilton, J. A. *Curr. Opin. Lipidol.* **2003**, *14*, 263–271.

(34) Dos Santos, N.; Mayer, L. D.; Abraham, S. A.; Gallagher, R. C.; Cox, K. A. K.; Tardi, P. G.; Bally, M. B. *Biochim. Biophys. Acta, Biomembr.* **2002**, *1561*, 188–201.

(35) Paunesku, T.; Vogt, S.; Maser, J.; Lai, B.; Woloschak, G. *J. Cell. Biochem.* **2006**, *99*, 1489–1502.

(36) Hall, M. D.; Dillon, C. T.; Zhang, M.; Beale, P.; Cai, Z.; Lai, B.; Stampfl, A. P. J.; Hambley, T. W. *J. Biol. Inorg. Chem.* **2003**, *8*, 726–732.

(37) Hall, M. D.; Alderden, R. A.; Zhang, M.; Beale, P. J.; Cai, Z.; Lai, B.; Stampfl, A. P. J.; Hambley, T. W. *J. Struct. Biol.* **2006**, *155*, 38–44.

(38) Crossley, E. L.; Aitken, J. B.; Vogt, S.; Harris, H. H.; Rendina, L. M. *Aust. J. Chem.* **2011**, *64*, 253–257.

(39) Chen, K. G.; Valencia, J. C.; Lai, B.; Zhang, G.; Paterson, J. K.; Rouzaud, F.; Berens, W.; Wincovitch, S. M.; Garfield, S. H.; Leapman, R. D.; Hearing, V. J.; Gottesman, M. M. *Proc. Natl. Acad. Sci. U.S.A.* **2006**, *103*, 9903–9907.

(40) Shimura, M.; Saito, A.; Matsuyama, S.; Sakuma, T.; Terui, Y.; Ueno, K.; Yumoto, H.; Yamauchi, K.; Yamamura, K.; Mimura, H.; Sano, Y.; Yabashi, M.; Tamasaku, K.; Nishio, K.; Nishino, Y.; Endo, K.; Hatake, K.; Mori, Y.; Ishizaka, Y.; Ishikawa, T. *Cancer Res.* **2005**, *65*, 4998–5002.

(41) Huang, Z.; Szoka, F. C. *J. Am. Chem. Soc.* **2008**, *130*, 15702–15712.

(42) Huang, Z.; Jaafari, M. R.; Szoka, F. C. *Angew. Chem., Int. Ed.* **2009**, *121*, 4210–4213.

(43) Peleg-Shulman, T.; Gibson, D.; Cohen, R.; Abra, R.; Barenholz, Y. *Biochim. Biophys. Acta, Biomembr.* **2001**, *1510*, 278–291.

(44) Vogt, S. *Journal de Physique IV (Proceedings)* **2003**, *104*, 635–638.